

Investigation on Laser Bending of Duplex-2205 Sheet by Applying Forced Cooling

Doctoral Thesis

by

“Ramsingh Yadav”

(2018MEZ0006)



**DEPARTMENT OF MECHANICAL
ENGINEERING
INDIAN INSTITUTE OF TECHNOLOGY
ROPAR**

August 2023

Investigation on Laser Bending of Duplex-2205 Sheet by Applying Forced Cooling

A Thesis Submitted

In Partial Fulfilment of the Requirements
for the Degree of

DOCTOR OF PHILOSOPHY

by

“Ramsingh Yadav”

(2018MEZ0006)



DEPARTMENT OF MECHANICAL
ENGINEERING
**INDIAN INSTITUTE OF TECHNOLOGY
ROPAR**

August 2023

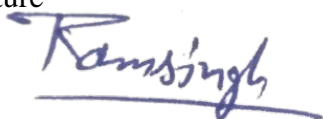
Copyright © “2023” by Indian Institute of Technology Ropar
All Rights Reserved

DEDICATED
TO
MY YOUNGER BROTHER LATE MR. TEJPAL YADAV AND GRANDFATHER
LATE SHRI LADU RAM YADAV

DECLARATION

I declare that this work entitled “**Investigation on Laser Bending of Duplex-2205 Sheet by Applying Forced Cooling**” has not previously been accepted in substance for any degree and is not being simultaneously submitted in candidature for any other degree. This thesis is being submitted in partial fulfilment of the requirements for the degree of PhD in Mechanical Engineering. This thesis is the result of my own independent investigation, except where otherwise stated. I have acknowledged all the other sources by stating the references explicitly. I declare that any idea/data/fact/source stated in my thesis has not been fabricated/falsified/misrepresented. All the principles of academic honesty and integrity have been followed. I understand that any violation of the above will cause disciplinary action by the Institute and can also evoke penal action from the sources which have thus not been properly cited or from whom proper permission has not been taken when needed. I hereby give consent for my thesis, if accepted, to be available online in the Institute’s Open Access repository and for inter-library loan and for the title and abstract to be made available to outside organizations.

Signature



Name: Ramsingh Yadav

Entry Number: 2018MEZ0006

Program: PhD

Department: Department of Mechanical Engineering

Date: 05-08-2023

CERTIFICATE

It is certified that the work contained in the thesis titled **“Investigation on Laser Bending of Duplex-2205 Sheet by Applying Forced Cooling”** by **“Ramsingh Yadav”** has been carried out under my supervision and that this work has not been submitted elsewhere for the award of any degree.

Signature of the Supervisor



Dr. Ravi Kant

Department of Mechanical Engineering

Indian Institute of Technology Ropar

Rupnagar, Punjab 140001

Date: 05-08-2023

ACKNOWLEDGMENTS

Foremost, I am highly indebted to Almighty God, who blessed me with spiritual support and resilience at each and every stage of this work. I would like to express my sincere gratitude to my thesis supervisor, **Dr. Ravi Kant**, Department of Mechanical Engineering, Indian Institute of Technology Ropar, for the valuable inputs, intellectual guidance, and patience throughout this research work. On a personal level, he inspired me to become a hardworking, professional, and passionate individual, which contributed significantly to molding me into an enriched personality. He has always been cordial, attentive, responsible, and supportive throughout all highs and lows during the entire journey of this dissertation. Without his timely help, constructive criticism, positive attitude, continuous support, and painstaking efforts, it would have been impossible to complete this thesis in its present form.

Additionally, I would like to thank my doctoral committee members: Dr. Ekta Singla, Prof. Harpreet Singh, Dr. Chandrakant Nirala, and Dr. Kailash Chandra Jena, for extending their support and guidance throughout this tenure. I would also like to express my thanks and gratitude to Prof. Rajeev Ahuja (Director, Indian Institute of Technology, Ropar), Prof. Sarit K. Das (Ex-Director, Indian Institute of Technology, Ropar), Dr. Prabhat K. Agnihotri (Head, Department of Mechanical Engineering), Dr. Ekta Singla (Ex-Head, Department of Mechanical Engineering), Indian Institute of Technology Ropar, and the Government of India for providing financial, infrastructural, and administrative support to carry out this work. I would like to extend my thanks to the Material Processing Research Laboratory, Central Workshop, Surface Engineering Laboratory, and Central Research Facilities of the Indian Institute of Technology Ropar for providing instruments to carry out the research work.

I am highly obliged and wish to owe my sincere thanks to the technical staff, especially to Mr. Jaswinder Singh, Mr. Girdhari Lal, Mr. Jograj Singh, Mr. Rambeer Singh, Mr. Bhupinder Singh, Mr. Sukhwinder Singh, Mr. Pankaj Thakur, Mr. Amit Kaushal, and all the workshop staff, who helped me in all the possible way during experimental work. The author thanks the library staff, IIT Ropar, for prompt responses and for instantly providing the plagiarism reports.

I am highly grateful to his lab mates Dr. Talwinder Singh Bedi, Dr. Neeraj Deswal, Dr. Avneesh Kumar, Dr. Papiya Bhowmik, Mr. Dhruva Kumar Goyal, Mr. Yadwinder Pal Sharma, Mr. Gidla Vinay, Mr. Sumitkumar Rathor, Mr. Eqbal, Mr. Rahul Nair, Mr. Dhara Singh Meena, Mr. Sachin Kumar, Mr. Narayan Suthar, Mr. Sonu Kadam, Mr. Sandeep Yadav, Mr. Karan Choudhary, Mr. Rohit Yadav, Mr. Altaf, Mr. Harman, Mr. Atirek Swami, Mr. Praveen Jakka, Mr. Sudhanshu Sharma, Mr. Samarth Patel, Mr. Pratik, Mr. Anshul, Mr. Vikas Anand for being such a fantastic team at both professional and personal level. I extend my heartfelt thanks to my friends Mr. Himanshu Markanday, Mr. Sanjeev Yadav, Mr. Vishal Singh, Mr. Yogeshwer Dasari, Mr. Ravi Beniwal, Dr. Navneet Singh, Mr. Saiful Wali Khan, Mr. Rajat Dhiman, Mr. Amandeep Garg, Mr. Arshpreet Singh, Mr. Deepak, Mr. Aman Chander, Mr. Vara Prasad and Mr. Amit Chipa for moral support and camaraderie help during the tenure of this work.

Above all, I am deeply indebted to my Grandparents (Smt. Sedi Devi and Sh. Govind Ram), Parents (Smt. Ganga Devi and Sh. Ramchandra), Sisters (Sajana-Ramesh, Vidya-Kishan, Sohani-Manoj), Brothers (Mukesh Kumar-Ena, Ramprasad-Sayar) for their blessing and encouragement. I want to thank all the loving children of his family (Nikita, Nikhil, Anish, Anushka, Manit, Kashvi, Tanu, Palak, Pari Paridhi, Gunnu, Bittu, Avi, and Baby) for the positive energy and excitement they were giving me every time. I especially thank my wife, Anju Yadav, for her continuous support and caring. My heartfelt gratitude to my brothers, Mr. Mukesh Kumar and Dr. Bholu Ram, for being my inspiration and mentor.

Finally, I dedicate this thesis to my loving younger brother Late Mr. Tejpal Yadav (Montu), and My Grandfather Late Sh. Ladu Ram Yadav.

Ramsingh Yadav

ABSTRACT

This research aimed to enhance the capabilities of laser bending by exploring forced cooling and investigating other performance parameters of the bent specimen. The study focused on the feasibility of laser bending of high-strength dual-phase stainless steel (duplex-2205) and the post-bending effects on material properties. A finite element-based 3D numerical model was developed and experimentally validated for laser bending. Single-scan laser bending was simulated and experimented under natural and forced cooling conditions to analyze the effects of various process parameters. The feasibility of forced cooling was studied using an aluminium alloy. An experimental setup with real-time bend angle and temperature measurement capability was established. Experimental studies were conducted for both single and multi-scan laser bending under different cooling conditions, analyzing the effects of process parameters on bend angles and material properties.

In the pilot study, a 3D numerical model incorporating temperature-dependent material and heat loss by convection and radiation was developed. Experimental validation of the model showed good agreement between numerical and experimental results. Numerical simulations of single-scan laser bending revealed the bending mechanism and the influence of line energy, laser power, and scanning speed on bend angle and edge effects. The mechanical properties of the bent specimens were compared to the base material, showing increased hardness and reduced ductility. Numerical simulations of single-scan laser bending with forced cooling demonstrated significantly increased bend angles at high line energy parameters. A robust experimental setup was developed, and feasibility studies with an aluminium alloy showed reduced coating degradation and increased bend angles with forced cooling.

Forced cooling assisted single-scan laser bending experiments on duplex-2205 revealed reduced maximum temperature and increased cooling rates with forced cooling. The application of forced cooling led to a significant increment (35.2%) in the bend angle on the bottom surface of the sheet. The effectiveness of forced cooling was influenced by process parameters, with lower scanning speed, intermediate beam diameter, and higher laser power being more effective. The forced cooling assisted laser-bent specimens exhibited improved hardness and tensile strength compared to naturally

cooled specimens. The phase distribution showed variations at the upper surface in the scanning region, while the lower surface resembled the base material.

In the forced cooling assisted multi-scan laser bending study at high line energy, experiments were conducted under various process conditions. The forced cooling significantly enhanced bend angles, with a maximum increment of 427% observed. The effect of process parameters exhibited different trends compared to natural cooling. The bend angle per scan increased with the number of scans in forced cooling, reaching a maximum bend angle per scan that was around 300% higher than that achieved in natural cooling. The microstructural analysis revealed the influence of cooling on the ratio of ferrite and austenite phases, resulting in increased hardness and tensile strength but reduced ductility. Corrosion behavior analysis indicated a decreased pitting potential in forced-cooled samples.

For forced cooling assisted multi-scan laser bending at low line energy, experiments were conducted under different cooling conditions. The temperature distribution along the scanning line showed a decrease in average maximum temperature with an increase in laser power. Forced cooling resulted in a reduced heat-affected zone compared to natural cooling. The bend angle achieved in forced cooling was lower than in natural cooling for low line energy parameters but increased with laser power and line energy. The waiting time between successive scans and the number of scans required to achieve the desired bend angle was reduced in forced cooling conditions. The bent specimens exhibited improved tensile strength and hardness, with the forced cooling condition demonstrating the highest values. The microstructure showed increased ferrite content and a more refined grain structure in the forced cooling condition.

This research significantly contributes to advancing laser bending technology by improving bend angles and understanding the effects of forced cooling on material properties. The findings provide valuable insights for improving manufacturing productivity and have the potential to optimize laser bending processes in various industries such as microelectronics, aerospace, and marine, where high deformation with good precision is a prime requirement.

LIST OF PUBLICATIONS

Publications From Thesis

1. **Ramsingh Yadav**, Dhruva Kumar Goyal, and Ravi Kant. "A comprehensive study on the effect of line energy during laser bending of duplex stainless steel." Optics & Laser Technology, 151, 108025 (2022). <https://doi.org/10.1016/j.optlastec.2022.108025>
2. **Ramsingh Yadav**, Dhruva Kumar Goyal, and Ravi Kant. "Enhancing process competency by forced cooling in laser bending process" Journal of Thermal Stresses, 45, 617-629 (2022). <https://doi.org/10.1080/01495739.2022.2103057>
3. **Ramsingh Yadav**, Dhruva Kumar Goyal, and Ravi Kant. "Multi-scan Laser Bending of Duplex Stainless Steel Under Different Cooling Conditions" CIRP: Journal of Manufacturing Science and Technology, 39, 345-358 (2022). <https://doi.org/10.1016/j.cirpj.2022.10.002>
4. **Ramsingh Yadav** and Ravi Kant. "Effectiveness of forced cooling during laser bending of duplex-2205." Materials and Manufacturing Processes, 38, 598-607 (2022). <https://doi.org/10.1080/10426914.2022.2146717>
5. **Ramsingh Yadav** and Ravi Kant. "Improving Bend Angle by Using forced cooling when laser bending Al Sheet" Lasers in Engineering, 55, 75-85 (2023).
6. **Ramsingh Yadav** and Ravi Kant. "Optimization of Cooling Condition and Energy Parameters During Laser Bending of Duplex-2205" Materials and Manufacturing Processes. <https://doi.org/10.1080/10426914.2023.2236191>
7. **Ramsingh Yadav**, Dhruva Kumar Goyal, and Ravi Kant. "How Different Coating Conditions Affect Temperature and Bend Angle when Laser Bending Mild Steel Sheet" Lasers in Engineering, 55, 103-115(2023).
8. **Ramsingh Yadav** and Ravi Kant. "Mechanical, Metallurgical and Corrosion Analysis of Forced Cooling Assisted Laser Bending of Duplex-2205" Journal of Manufacturing Processes, (Submitted).
9. **Ramsingh Yadav** and Ravi Kant. "Underwater Laser Bending of Stainless-steel Sheet" Manufacturing Letters, (Submitted).

Book Chapters

1. **Ramsingh Yadav**, Dhruva Kumar Goyal, and Ravi Kant. "An Experimental Study of Forced Cooling in Single-Scan Laser Bending." In Advances in Forming, Machining and Automation, Springer, Singapore (2022). https://doi.org/10.1007/978-981-19-3866-5_2

Other Publications During Ph.D. Program

1. **Ramsingh Yadav**, Amit Pancharya and Ravi Kant, “Influence of Injection and Holding Pressure on Tribological and Mechanical Behavior of Injection Moulded Thermoplastic.” *Materials Today: Proceedings*, 41, 915-920 (2020). <https://doi.org/10.1016/j.matpr.2020.09.486>
2. Dhruva Kumar Goyal, **Ramsingh Yadav** and Ravi Kant. “An integrated hybrid methodology for estimation of absorptivity and interface temperature in laser transmission welding.” *International Journal of Advanced Manufacturing Technology*, 121, 3771–3786 (2022). <https://doi.org/10.1007/s00170-022-09536-y>
3. Yadwinder Pal Sharma, Balwinder Singh Sidhu, Ravi Kant, **Ramsingh Yadav**. “Enhancing the bend angle and mechanical properties of mild steel using fiber laser bending technique under the influence of electromagnetic force.” *Optics and Lasers in Engineering*, 168, 107631(2023). <https://doi.org/10.1016/j.optlaseng.2023.107631>
4. Dhruva Kumar Goyal, **Ramsingh Yadav** and Ravi Kant. “Laser transmission welding of polycarbonate sheets using electrolytic iron powder absorber.” *Optics & Laser Technology*, 161, 109165 (2023). <https://doi.org/10.1016/j.optlastec.2023.109165>
5. Rahul Nair, Ravi Kant, **Ramsingh Yadav** and H. Gurung. "Experimentally Validated Analytical Modelling of the Laser Bending of Low Carbon Steel Sheets." *Lasers in Engineering*, 53, 253-265 (2022).
6. Dhruva Kumar Goyal, **Ramsingh Yadav** and Ravi Kant. “Study of Temperature Field Considering Gradient Volumetric Heat Absorption in Transparent Sheet During Laser Transmission Welding (LTW).” *Lasers in Engineering*, 53, 215-229 (2022).
7. Rohit Yadav, **Ramsingh Yadav**, Ravi Kant. “Experimental Study on Laser Bending of Mild Steel with Buckling Mechanism” *Optics & Laser Technology*, 167, 109803 (2023). <https://doi.org/10.1016/j.optlastec.2023.109803>
8. Yadwinder Pal Sharma, Balwinder Singh Sidhu, Ravi Kant, **Ramsingh Yadav**. “Improving Bend Angle and Mechanical Properties During Multi-scan Laser Bending of Mild Steel Using Forced Bottom Cooling” *Optics and Laser Technology* (Submitted).

Conferences

1. **Ramsingh Yadav**, Dhruva Kumar Goyal, and Ravi Kant. “Fem Simulations of Laser Bending of Duplex Stainless Steel” 8th International Conference on Advancements and Futuristic Trends in Mechanical and Materials Engineering (AFTMME-2020), Rupnagar, Punjab, India.
2. **Ramsingh Yadav**, Dhruva Kumar Goyal, and Ravi Kant. “Effect of Cooling in Laser Bending of Duplex” 8th International Conference on Advancements and Futuristic Trends in Mechanical and Materials Engineering (AFTMME-2020), Rupnagar, Punjab, India.
3. **Ramsingh Yadav**, Dhruva Kumar Goyal, and Ravi Kant. “An experimental study of forced cooling in single scan laser bending” All India Manufacturing Technology, Design and Research Conference (AIMTDR-2021), Coimbatore, India.
4. **Ramsingh Yadav** and Ravi Kant. “An Experimental study of forced cooling during laser bending process” 9th International Conference Advancements and Futuristic Trends in Mechanical and Materials Engineering (AFTMME-2021), Rupnagar, Punjab, India.
5. **Ramsingh Yadav** and Ravi Kant. “An Experimental study of forced cooling at bottom surface during laser bending of duplex stainless-steel sheet” National Conference on Advanced Research in Engineering, Science and Technology (NCAREST-2022), Mandi Gobindgarh Punjab, India.

CONTENTS

CHAPTER 1	1
INTRODUCTION	1
1.1. Background	1
1.2. Laser Bending.....	2
1.3. History of Laser Bending	3
1.4. Advantages	3
1.5. Limitations	6
1.6. Applications.....	7
1.7. Motivation	8
1.8. Organisation of The Thesis	9
CHAPTER 2	12
LITERATURE REVIEW	12
2.1. Mechanisms of Laser Bending	12
2.1.1. Temperature Gradient Mechanism.....	12
2.1.1.1. Effect of Process Parameters in TGM.....	14
2.1.2. Buckling Mechanism.....	25
2.1.2.1. Effect of Process Parameters in BM	26
2.1.3. Upsetting Mechanism	28
2.1.3.1. Effect of Process Parameters in UM.....	30
2.2. Methods for Improving Laser Bending.....	31
2.2.1. Absorptivity Enhancement by Surface Modifications	31
2.2.2. External Force-assisted Laser Bending	33
2.2.3. Multi-scan Laser Bending.....	36
2.2.4. External Cooling Assisted Laser Bending	41
2.3. Modelling of Laser Bending Process.....	45

2.3.1. Numerical Modelling.....	45
2.3.2. Analytical Modelling.....	47
2.3.3. Soft-computing Modelling.....	49
2.4. Complex Shape Generation.....	51
2.4.1. 3D Laser Bending.....	51
2.4.2. Scanning Strategies	54
2.5. Materials Processed with Laser Bending	58
2.6. Mechanical Properties and Metallurgical Variation in Laser Bending.....	63
2.6.1. Mechanical Properties	63
2.6.2. Metallurgical Analysis.....	66
2.7. Sustainability Aspect of Laser Bending	68
2.8. Applications.....	69
2.9. Challenges Associated with Laser Bending	72
2.9.1. Non-Uniform Bending.....	72
2.9.2. Changes in Material Properties	74
2.9.3. Poor Process control and Repeatability	74
2.9.4. Generation of Residual Stresses	75
2.9.5. Poor Process Efficiency and Productivity	76
2.10. Observations and Conclusions	77
2.11. Research Objectives.....	79
CHAPTER 3	81
PILOT STUDY	81
3.1. FEM based numerical model of laser bending	81
3.1.1. Heat Input	82
3.1.2. Thermal Analysis	82
3.1.3. Mechanical Analysis	83
3.1.4. Model Description.....	84

3.1.5. Input Parameters.....	86
3.1.6. Experimental Validation.....	88
3.2. Exploration of Underlying Bending Mechanism.....	89
3.2.1. Temperature Study	89
3.2.2. Bend Angle Analysis.....	92
3.2.3. Edge Effect.....	94
3.2.4. Mechanical Analysis	95
3.2.5. Relation of temperature variation with bend angle and mechanical properties	98
3.3. Numerical Feasibility Analysis of Forced Cooling Assisted Laser Bending...	100
3.3.1. Effect of cooling on bend angle	100
3.3.2. Impact of cooling on edge effect.....	103
3.3.3. Longitudinal Distortion	104
3.3.4. Effectiveness of forced cooling.....	105
3.4. Experimental Feasibility Exploration of Forced Cooling Assisted Laser Bending	107
3.4.1. Experimental Details	107
3.4.2. Results and Discussions.....	107
3.4.2.1. Temperature Analysis	107
3.4.2.2. Bend Angle Analysis	109
3.4.2.3. Effectiveness of cooling.....	112
3.5. Summary	113
CHAPTER 4	117
EXPERIMENTAL DETAILS OF FORCED COOLING ASSISTED LASER BENDING	117
4.1. Overall Methodology	117
4.2. Worksheet Material.....	118
4.3. Experimental Setup with Cooling Arrangement	119

4.4. Beam Diameter Calculation	121
4.5. Bend angle Measurement	123
4.6. Temperature Measurement	124
4.7. Post-bending Analysis	126
4.7.1. Micro-hardness	126
4.7.2. Tensile Strength	127
4.7.3. Corrosion Analysis	128
4.7.4. Metallurgical Analysis	129
4.7.4.1. Optical Microscopy	129
4.7.4.2. Scanning Electron Microscopy	130
4.7.4.3. Energy Dispersive Spectroscopy	131
4.7.4.4. X-Ray Diffraction	131
4.8. Summary	132
CHAPTER 5	135
FORCED COOLING ASSISTED SINGLE SCAN LASER BENDING	135
5.1. Input Parameters	135
5.2. Temperature Analysis	136
5.3. Bend Angle Analysis	137
5.4. Mechanical and Metallurgical analysis	147
5.5. Optimization	150
5.5.1. Regression Fit Function	150
5.5.2. Process Parameter Optimization using Pareto optimality and Genetic Algorithm	151
5.5.3. Mechanical and metallurgical properties at optimum condition	155
5.6. Summary	156
CHAPTER 6	158
FORCED COOLING ASSISTED MULTI-SCAN LASER BENDING	158

6.1. Multi-Scan Forced Cooling assisted Laser Bending at High Line Energy	158
6.1.1. Bend angle analysis	159
6.1.2. Microstructural Analysis	166
6.1.3. Mechanical Analysis	170
6.1.4. Corrosion Analysis	171
6.2. Multi-Scan Forced Cooling assisted Laser Bending at Low Line Energy	174
6.2.1. Input Parameters.....	174
6.2.2. Temperature analysis	175
6.2.3. Bend angle analysis	179
6.2.4. Mechanical and metallurgical analysis.....	183
6.3. Summary	190
CHAPTER 7	194
CONCLUSION AND FUTURE SCOPE.....	194
7.1. Conclusions	195
7.2. Research Contribution	201
7.3. Future directions of the work	202
APPENDIX	237
REFERENCES	203

LIST OF FIGURES

Figure 1-1. Schematic of the laser bending process.....	3
Figure 2-1: Schematic of temperature gradient mechanism.....	13
Figure 2-2. Slender elliptical beam shaping using a cylindrical lens.....	20
Figure 2-3. Different beam shapes with a constant beam area	21
Figure 2-4. Schematic of buckling mechanism	26
Figure 2-5. Schematic of upsetting mechanism.....	29
Figure 2-6. (a) Worksheet surface and (b) bend angle variation with different combinations of coating thickness and surface roughness.	33
Figure 2-7. Complex shapes formed by forced assisted laser bending (a) design of chair, (b) cube.....	34
Figure 2-8. Bend angle variation with (a) air gap between sheet and electromagnet, (b) current supplied to the electromagnet	35
Figure 2-9. Domination range of different factors influencing the bending rate with number of scans (Edwardson et al., 2010a).....	38
Figure 2-10. Effect of laser power, number of scans, sheet thickness on bend angle and section thickening during multi-scan laser bending.....	39
Figure 2-11. Schematic representation of passive water cooling	43
Figure 2-12. (a) Cooling plate and stainless steel plate before exposure, (b) schematic illustration of the bent sheet, cooling plate and cooling fluid path.	43
Figure 2-13. (a) 3D spoon geometry formed with laser bending (b) spoon after improved surface quality by sandblasting and spray coating.....	52
Figure 2-14. Various complex shapes generated from flat sheet	53
Figure 2-15. (a) Scanning scheme for manufacturing cranial prosthesis and (b) cranial prosthesis manufactured by laser bending.....	55
Figure 2-16: Various scanning strategies for dome shape (a) circular, (b) radial	56
Figure 2-17. Different combinations of scanning lines, number of scans for two different bending lengths (a) 16 mm, (b) 20 mm.....	57
Figure 2-18. Step-by-step shape formation from additively manufactured components shaped by laser bending	70
Figure 2-19. A step-by-step operational sequence on cutting and bending for the formation of cube which contained a functioning electronic circuit	71

Figure 3-1. Worksheet mesh model	85
Figure 3-2. Representation of (a) moving heat flux at the top surface, and (b) forced cooling region at the bottom surface, used in numerical simulations of laser bending	86
Figure 3-3. Laser scanned surface at 250 W laser power (a) 45 J/mm line energy (b) 50 J/mm line energy	89
Figure 3-4. Maximum temperature variation at 250 W laser power and 30 J/mm line energy (a) along the thickness (b) along the scan line	90
Figure 3-5. Maximum temperature variation along the transverse to scan line at (a) different laser powers at 35 J/mm line energy (b) different line energies at 600 W laser power	91
Figure 3-6. Maximum temperature difference between Point A and B with (a) line energy at different laser powers (b) laser power at different line energies	92
Figure 3-7. Bend angle with line energy at different laser powers	92
Figure 3-8. Plastic strain history of Points A and B, For different line energies at 600 W laser power	93
Figure 3-9. The maximum temperature at Point B with line energy at different laser powers	94
Figure 3-10. Edge effect with line energy at different laser powers	95
Figure 3-11. (a) Dimensional schematic of tensile specimen, (b) laser scanned tensile test specimen before the test and (c) after the test	96
Figure 3-12. Stress-strain curves obtained from the tensile test of specimens, scanned at 250 W laser power and different line energies	97
Figure 3-13. Hardness with line energy at 250 W laser power	97
Figure 3-14. Microstructures of duplex stainless steel at different scanning conditions (a) No irradiation (b) irradiation with 30 J/mm line energy (c) irradiation with 50 J/mm line energy	98
Figure 3-15. Effect of maximum temperature on bend angle at different line energies	99
Figure 3-16. Effect of maximum temperature on hardness and breaking strain at 250 W laser power	100
Figure 3-17. Effect of line energy on the bend angle at different cooling conditions.	101
Figure 3-18. (a) Plastic strains at top and bottom surfaces in X-direction at different cooling conditions for 600 W laser power (b) magnified view of the change in strain at the bottom (c) magnified view of the change in strain at the top	102

Figure 3-19. The change in maximum temperature at Point B with line energy (a) for natural cooling condition at different laser powers, and (b) for different cooling conditions at 800 W laser power.....	102
Figure 3-20. (a) Edge effect and maximum variation in temperature gradient along the scan line at different line energy and 600 W laser power. (b) Edge effect and maximum variation in strain gradient along the scan line with laser power at 35 J/mm line energy	103
Figure 3-21. Variation in bend angle along the scanning direction	104
Figure 3-22. Displacement in Z-direction along the scan line at different cooling conditions with (a) laser powers and (b) line energies.....	105
Figure 3-23. The effect of laser power on percentage increase in bend angle at (a) $h = 500 \text{ W/m}^2\text{-K}$, and (b) $h = 1000 \text{ W/m}^2\text{-K}$	106
Figure 3-24. The final plastic strain at Point B with respect to (a) laser power, and (b) line energy	106
Figure 3-25. Percentage increase in bend angle with line energy at (a) $h = 500 \text{ W/m}^2\text{-K}$, and (b) $h = 1000 \text{ W/m}^2\text{-K}$	106
Figure 3-26. Temperature measurement points along the scan line in (a) thermal imaging software (b) schematic	108
Figure 3-27. Variation of $T_{\text{avg.}}$ with number of scans in both the cooling conditions at (a) different laser power and at 1500 mm/min scanning speed, and (b) different scanning speeds and at 700 W laser power.....	108
Figure 3-28. Temperature profile after five scans for 1500 mm/min scanning speed at (a) 400 W, and (b) 700 W laser powers.....	109
Figure 3-29. Variation in bend angle for different cooling conditions with (a) laser power at different scanning speed, and (b) scanning speed at different laser powers.....	110
Figure 3-30. Bend angle in each scan at a laser power of (a) 400 W, and (b) 850 W.	111
Figure 3-31. Bend angle in each scan at a scanning speed of (a) 1000 mm/min, and (b) 2500 mm/min.....	112
Figure 3-32. Percentage increment in bend angle in each scan due to forced cooling (a) for different laser powers at 1500 mm/min scanning speed, and (b) for different scanning speeds at 700 W laser power	112
Figure 4-1. Overall methodology of the study.....	118
Figure 4-2. Graphite coated duplex-2205 sheet specimens.....	119
Figure 4-3. Laser cutting machine	120

Figure 4-4. Experimental setup (a) position of laser head and laser displacement sensor, (b) cooling arrangement	120
Figure 4-5. Schematic of experimental setup with forced cooling (a) front view and (b) side view.....	120
Figure 4-6. Schematic of the laser beam profile [Redrawn with permission].....	121
Figure 4-7. Laser displacement sensor.....	123
Figure 4-8. (a) measurement of distance between spot lights of laser source and laser displacement sensor, (b) schematic for bend angle calculation.....	124
Figure 4-9. Thermal imaging camera.....	125
Figure 4-10. Experimental setup for emissivity estimation by temperature validation with thermocouple.....	125
Figure 4-11. (a) Estimation of emissivity by mapping the temperature profiles of thermal imaging camera and thermocouple, (b) schematic representation of temperature measurement points on top surface.....	126
Figure 4-12. (a) Vicker's microhardness tester (b) dimensions and position from where hardness test specimen is taken	127
Figure 4-13. Micro-tensile testing machine.....	128
Figure 4-14. Dimensions and orientation of tensile test specimen (a) along the scan line and (b) perpendicular to the scan line	128
Figure 4-15. (a) Autolab electro-chemical workstation (b) position of electrodes.....	129
Figure 4-16. Inverted optical microscope.....	130
Figure 4-17. Scanning electron microscopy with energy dispersive spectroscopy attachment.....	131
Figure 4-18. X-Ray diffraction setup	132
Figure 5-1. Irradiated surface temperature at the center of scanning line: (a) $P = 550$ W, $V = 600$ mm/min, (b) $P = 1000$ W, $V = 600$ mm/min, (c) $P = 1000$ W, $V = 1800$ mm/min for both the cooling conditions	136
Figure 5-2. Bend angle vs. laser power at different (a) scanning speed (b) beam diameter (c) sheet thickness and (d) width of the worksheet.....	141
Figure 5-3. Bend angle vs. scanning speed at different (a) laser power, (b) beam diameter, (c) sheet thickness, and (d) width of the worksheet.....	143
Figure 5-4. Bend angle vs. beam diameter at different (a) laser power (b) scanning speed	144

Figure 5-5. Bend angle vs. sheet thickness at different (a) laser power (b) scanning speed	145
Figure 5-6. Bend angle vs. width of the worksheet at different (a) laser power (b) scanning speed	145
Figure 5-7. Bend angle variation with (a) laser power, and (f) scanning speed at different flow rates	146
Figure 5-8. Tensile strength analysis at: (a) different laser powers for $V = 600$ mm/min, and (b) different scanning speeds for $P = 1000$ for both natural and forced cooling conditions	148
Figure 5-9. Hardness in scanning region at both upper and lower surfaces at: (a) different laser powers for $V = 600$ mm/min, and (b) different scanning speeds for $P = 1000$ W	148
Figure 5-10. Microstructural images of (a) base material, (b) scanning region, (c) upper surface in natural condition and (d) upper surface in forced cooling condition, (e) lower surface in natural condition and (f) lower surface in forced cooling condition	149
Figure 5-11. Experimental data on the field of both objective functions.....	152
Figure 5-12. Optimized pareto front.	154
Figure 5-13. Comparison of mechanical properties (a) Tensile (b) hardness and (c) microstructure of the laser bent specimens irradiated with optimum processing condition with respect to the base material.....	156
Figure 6-1. Variation in bend angle with (a) laser power at different scanning speed, (b) scanning speed at different laser power for both the cooling conditions	160
Figure 6-2. The variation in bend angle with beam diameter at various (a) laser power and (b) scanning speed for both the cooling conditions.....	161
Figure 6-3. The variation in bend angle with sheet thickness at various (a) laser powers and (b) scanning speeds for both the cooling conditions	162
Figure 6-4. The variation in bend angle with worksheet width for both the cooling conditions at various (a) laser powers and (b) scanning speeds	162
Figure 6-5. The variation in bend angle with flow rate for both the cooling conditions at various (a) laser powers and (b) scanning speeds.....	163
Figure 6-6. Bend angle per scan at constant laser power of 850 W and different scanning speed of (a) 600 mm/min, (b) 1000 mm/min, (c) 1400 mm/min and (d) 1800 mm/min	164

Figure 6-7. Bend angle per scan at a constant scanning speed of 1000 mm/min and different laser power of (a) 550 W, (b) 700 W, (c) 850 W, and (d) 1000 W	165
Figure 6-8. Optical & SEM images of selected samples (a) Base material (b) N700_600 (c) N550_1000 (d) F700_1800 (e) F550_1000	168
Figure 6-9. EDS mapping and elemental distribution of (a) N700_600 (b) F700_1800	169
Figure 6-10. XRD plot of samples with different conditions	169
Figure 6-11. Mechanical analysis of bent samples (a) hardness (b) tensile strength..	171
Figure 6-12. Potentiodynamic polarization plots of (a) base material (b) N550_1000 (c) N700_600 (d) N700_1800 (e) N1000_1000 (f) F550_1000 (g) F700_600 (h) F700_1800 (i) F1000_1000	172
Figure 6-13. EDS mapping and elemental distribution of N1000_1000 after corrosion test	174
Figure 6-14. $T_{avg.}$ for each scan at various power at 10 J/mm LE for (a) CC1 (b) CC2 (c) CC3	176
Figure 6-15. $T_{avg.}$ for each scan at various power at 15 J/mm LE for (a) CC1 (b) CC2 (c) CC3	176
Figure 6-16. $T_{avg.}$ in each scan at various power at 20 J/mm LE for (a) CC1 (b) CC2 (c) CC3	176
Figure 6-17. $T_{avg.}$ in each scan at various power at 25 J/mm LE for (a) CC1 (b) CC2 (c) CC3	176
Figure 6-18. Temperature distribution in lateral direction to the scan line at 25 J/mm line energy and 750 W laser power: (a) Observation points considered for temperature measurement and temperature distribution in (b) First scan (c) Third scan and (d) Fifth scan for all three cooling conditions	178
Figure 6-19. Temperature distribution along the scan line at 25 J/mm line energy and 750 W laser power: (a) Observation points considered for temperature measurement and temperature distribution during (b) First scan and (c) fifth scan for all three cooling conditions	179
Figure 6-20. Bend angle achieved in each scan at various power and particular line energy of 10 J/mm for (a) CC1 (b) CC2 (c) CC3	180
Figure 6-21. Bend angle achieved in each scan at various power and particular line energy of 15 J/mm for (a) CC1 (b) CC2 (c) CC3	180

Figure 6-22. Bend angle achieved in each scan at various power and particular line energy of 20 J/mm for (a) CC1 (b) CC2 (c) CC3	181
Figure 6-23. Bend angle achieved in each scan at various power and particular line energy of 25 J/mm for (a) CC1 (b) CC2 (c) CC3	181
Figure 6-24. Variation in final bend angle after five scans with laser power at various LE for (a) CC1 (b) CC2 (c) CC3	182
Figure 6-25. HAZ at (a) top surface (b) bottom surface and (c) cross-section of the worksheet in all three cooling conditions at 1000 W power and 25 J/mm LE.....	185
Figure 6-26. Initial and final condition of tensile test specimens (a) along (b) perpendicular to the scan line	185
Figure 6-27. Tensile strength and breaking strain along the scanned direction at 750 W power and (a) 10 J/mm (b) 25 J/mm LE	186
Figure 6-28. Tensile strength and breaking strain perpendicular to the scanned direction at 1000 W power and (a) 10 J/mm (b) 25 J/mm LE.....	187
Figure 6-29. Hardness within the scanned region at (a) top surface, (b) bottom surface for different cooling conditions at 15 J/mm line energy, and 1000 W laser power	187
Figure 6-30. Phase analysis of the (a) initial worksheet, and scanned area of the top surface for (b) CC1, (c) CC2, and (d) CC3 at 15 J/mm line energy and 1000 W laser power.....	188
Figure 6-31. Grain size analysis of the (a) initial worksheet, and scanned area of the top surface for (b) CC1 (c) CC2 and (d) CC3 at 15 J/mm line energy and 1000 W laser power.....	189
Figure 6-32. Microstructure of the bottom surface in (a) CC1 (b) CC2 (c) CC3 at 15 J/mm line energy and 1000 W laser power	189

LIST OF TABLES

Table 1-1. History of the advancements in the field of laser bending	4
Table 3-1. Properties of worksheet material used in numerical simulation of laser bending	84
Table 3-2. Process parameters for numerical simulations of the laser bending process	88
Table 3-3. Comparison of experimental and simulation results at 250 W laser power.	88
Table 4-1. Chemical composition of Duplex-2205 sheets	119
Table 5-1. Input parameters of laser bending experiments.....	136
Table 5-2. Bend angle achieved at different process parameters in both natural and forced cooling conditions	139
Table 5-3. Bend angle variation with respect to variable cooling water flow rate	146
Table 5-4. Results of ANOVA for the regression model of bend angle.	150
Table 5-5. Experimental validation of fit function at random process parameters.	151
Table 5-6. Optimized Pareto front data set.....	153
Table 6-1. Set of process parameters and their calculated line energies	166
Table 6-2. Electro chemical corrosion results in 3.5% NaCl medium	172
Table 6-3. Notation used for three different cooling conditions.....	175
Table 6-4. Scanning speed for different sets of laser power and line energy	175
Table 6-5. Bend angle after five scans and percentage change in bend angle for different cooling conditions	182

LIST OF ABBREVIATIONS

TGM	Temperature Gradient Mechanism
BM	Buckling Mechanism
UM	Upsetting Mechanism
FEM	Finite Element Method
P	Laser Power
V	Laser Scanning Speed
D	Laser Beam Diameter
R	Laser Beam Radius
T	Sheet Thickness
f	Water Flow Rate
w	Width of the Worksheet
η	Absorption Coefficient of Worksheet Surface
$q(r)$	Heat Flux at Radius r
q_c	Convective Heat Loss
q_r	Radiation Heat Loss
ρ	Density of Worksheet Material
T_s	Temperature at Worksheet Surface
T_e	Environmental Temperature
c_p	Specific Heat of Worksheet Material
k	Thermal Conductivity of Worksheet Material
h	Convective Heat Transfer Coefficient
ε	Worksheet Surface Emissivity

σ	Stefan-Boltzmann Constant
$\dot{\epsilon}$	Strain Rate
σ_y	Temperature-Dependent Yield Strength
$\sigma_1, \sigma_2, \text{ and } \sigma_3$	Principal Stresses Along Direction X, Y, Z Axis, Respectively
σ_{eq}	Equivalent Thermal Stress Generated in The Workpiece
MVTG	Maximum Variation in Temperature Gradient Along the Scan Line
MVSG	Maximum Variation in Strain Gradient Along the Scan Line
$T_{avg.}$	Average of the Maximum Temperature of Five Equidistant Points Along the Scan Line
w_o	Beam Waist (Minimum beam radius at the focal point)
H	Stand-off Distance (Distance between beam waist and worksheet surface)
M^2	Beam Quality Factor
λ	Wavelength of Fiber Laser Beam
θ	Half Divergence Angle of Laser Beam
f_1	Focal Length of the Lens
R_L	Laser Beam Radius Before Lens
IR	InfraRed
DAQ	Data Acquisition
SEM	Scanning Electron Microscopy
EDS	Energy Dispersive Spectroscopy
XRD	X-Ray Diffraction
LE	Line Energy

CHAPTER 1

INTRODUCTION

1.1. Background

Forming is one of the prominent manufacturing methods due to its ability to improve mechanical properties, minimize material waste, and achieve high production rates (Klocke, 2008). The process involves reshaping the materials using plastic deformation by applying stresses, such as tensile, compressive, or shear stresses. These stresses are governed by the energy given to the workpiece in the form of mechanical, thermal, or electrical energy. Mechanical energy is commonly used in the processes like rolling, forging, drawing, extrusion, deep drawing, spinning, and embossing (Banabic, 2007). But, forming high-strength and brittle materials using only mechanical energy is difficult; therefore, thermal energy is often used as an assistive method, and it is called hot forming. Thermal energy is not only used to assist mechanical energy but can also cause deformation independently, as in flame bending.

In flame bending, heat is supplied in a narrow region along the bending line of the workpiece using an oxy-propane flame. The heating reduces the yield strength of the material and, due to non-uniform heating, generates thermal stresses (Das and Biswas, 2018; Frank Hanus, 1999). The heated region attempts to expand, but since the adjacent area restricts it, compressive stresses are generated at that particular region (Moshaiov and Latorre, 1985). Due to the compressive stress and decreased yield strength in the heated region, the material undergoes compressive plastic deformation (Hwang et al., 2021). During cooling, the materials on the adjacent side of the heated region attempt to contract in order to restore their original shape. This leads to increased material contraction within the deformed region, resulting in the bending of the worksheet (Hemmati and Shin, 2007). This process is beneficial for job and batch production of large-size products, as large tooling is not required and is also suitable to deform high-strength and brittle materials. Some limitations associated with this process include large heat-affected area, poor controllability, difficulty in automating, and the

requirement of skilled workers (Moshaiov and Vorus, 1987). These limitations can be overcome to a large extent by using laser power as the heat source instead of oxy-propane flame (Scully, 1987).

Laser is a highly focused, monochromatic, and coherent beam having various unique properties such as high energy density, good controllability, less heat-affected area, rapid heating, easy portability and automation, etc., (Dutta Majumdar and Manna, 2011). These properties make it one of the most favorable tools in the automobile, aerospace, electronics, marine, medical, and other manufacturing industries. Nowadays, it is one of the most suitable manufacturing tools in various processes: cutting, welding, machining, surface treatment, polishing, additive manufacturing, and forming (Padmanabham and Bathe, 2018; W. M. Steen, 1997). Laser power can provide a more precise and controllable heat source, resulting in a smaller heat-affected zone, better process control, and easier automation. So, laser power can be used instead of an oxy-propane flame for bending and known as laser bending.

1.2. Laser Bending

In recent years, laser bending gained significant attention because of its advantages over traditional bending processes. It offers high accuracy, fast processing time, good controllability, excellent flexibility, and the ability to produce complex shapes (Dixit et al., 2015). There is no requirement of specific dies and tools for shaping the sheets, making modifying product design more effortless and ultimately reducing the production cost. Because of these qualities, laser bending has become a popular technique in the manufacturing industry, especially in the automotive, aerospace, medical, and electronics sectors (R. Kant et al., 2016).

As shown in the schematic (Figure 1-1), a defocused laser beam is used to fabricate sheet metal components. The sheet is clamped from one edge, and the other edge is free. The laser is irradiated linearly parallel to the free end by moving the worksheet or laser head with the help of a CNC system. It causes localized heating that creates a non-uniform temperature field. This non-uniform temperature distribution causes thermal stresses in the sheet material. The sheet will deform permanently when these thermal stresses exceed the temperature-dependent flow stress. The laser bending process can be used for various materials: metals, alloys, ceramics, plastics, composites, metal

foams, and bimetal sheets (Safari et al., 2020a). The process is used to bend sheets, plates, rods, and pipes. The bending geometry is not limited to straight line bending but curvilinear bending, and 3D complex shapes are also explored.

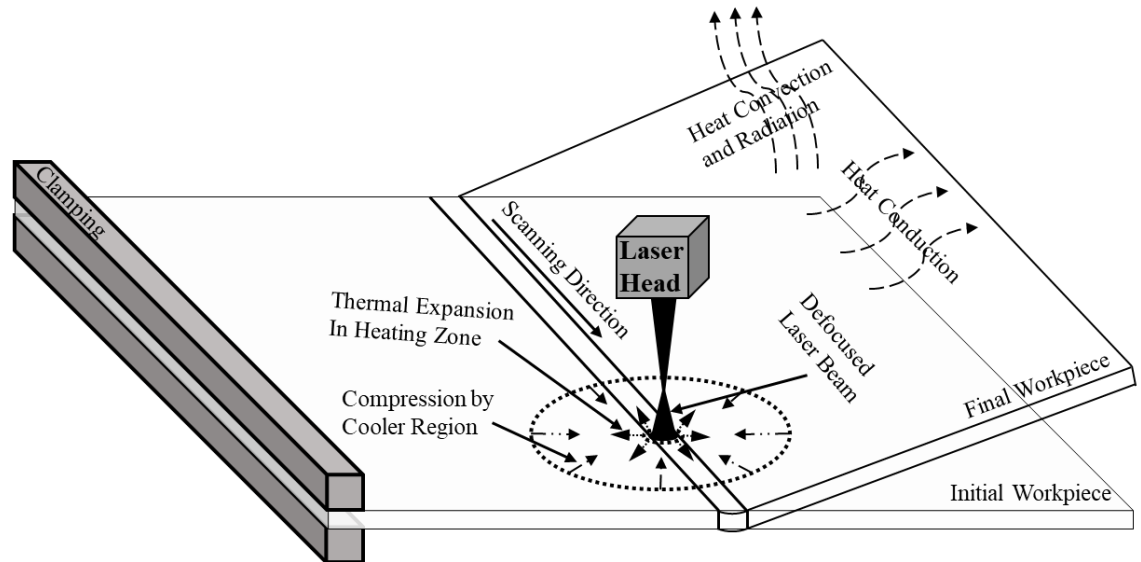


Figure 1-1. Schematic of the laser bending process

1.3. History of Laser Bending

The following table provides an overview of the historical developments in laser bending process. It highlights key studies, their outcomes, and significant contributions made by researchers over the years.

The historical developments in laser bending have showcased remarkable advancements in understanding the process, exploring new materials, predicting bend angles, and optimizing parameters, ultimately paving the way for its practical applications in various industries.

1.4. Advantages

Laser bending offers several advantages over traditional bending methods, including:

Excellent controllability: Laser offers quick and precise control on energy input, which gives good control over the process (Hennige et al., 1997; Steen, 2003)

High precision: Laser bending allows precise control over the bending angle and radius, making it ideal for producing complex shapes (Hennige et al., 1997; J. Widlaszewski, 1997).

Table 1-1. History of the advancements in the field of laser bending

Reference	Study	Outcome
(N. Kitamura, 1983)	High-power laser used for sheet bending for the first time	The sheet can be precisely bent by laser without any external force.
(Deacon, 1984)	Investigated the metallurgical aspect of laser-bent HY-80 steel sheet	Observed grain growth and carbide segregation. Recommended multi-pass bending with low energy parameters instead of a single scan with high energy parameters.
(Biegeleisen, 1986)	Analyzed deflection and residual stresses during laser bending	Developed an algorithm to calculate residual stresses for compound shapes, including cone, sine, saddle, and dish.
(Geiger and Vollertsen, 1993)(Vollertsen, 1994)	Explored the mechanism of laser bending and proposed a two-layer analytical model	The model explained the influence of sheet thickness and thermal expansion coefficient on bending. Based on the temperature distribution, a temperature gradient mechanism was proposed.
(Geiger et al., 1993)	First time used the laser bending process for practical application	Proposed the use of laser bending for straightening car body shells.
(Arnet and Vollertsen, 1995)	Explored the buckling mechanism for the first time	Proposed that convex bending can be achieved by varying process parameters. Discussed three different mechanisms.
(Vollertsen et al., 1995)	Proposed an analytical model to predict the bend angle in the buckling mechanism	Developed an analytical model that can generate a bend angle of 10 degrees in one scan.
(Yau et al., 1996)	Explored laser bending of metal matrix composite sheet for the first time	Successfully bent an Al-based metal matrix composite using laser bending process. Generated a bend angle of 80 degrees in 200 scans.
(Hsiao, 1997; Hsiao et al., 1997)	Conducted the first finite element modeling of the laser bending process	Developed a finite element thermo-mechanical model for laser bending process
(Thomson and Pridham, 1997a)	Applied a feedback control system with laser bending process for the first time	Formulated process design principles for different shapes, including dome, V-bend saddle, using a feedback control system.
(Mucha et al., 1997)	Investigated laser bending of thick sheet	Developed an analytical model for thick sheet laser bending.
(Hennige, 2000) (Edwardson et al., 2001)	Used laser bending for 3D shape generation for the first time	Investigated different scanning strategies for spherical dome shape formation.
(Chen et al., 2002; Cheng and Lin, 2000)	Used neural networks for the first time to predict the bend angle	The bend angle prediction using neural network was in good agreement with experiments.
(Li and Yao, 2001)	Explored laser bending of tubes	Investigated the mechanism of tube bending and developed an analytical model for bend angle prediction.
(Cheng and Yao, 2001)	Explored cooling effects in laser bending for the first time	Applied forced air cooling and investigated the bend angle, total forming time, and material properties with and without cooling. Reported a significant reduction in total forming time with cooling, although it slightly reduced ductility.
(Bao and Yao, 2001a)	First dedicated study on edge effect	Analyzed the edge effect for TGM and buckling mechanisms. Discussed the variation in edge effect with process parameters and proposed an analytical model for edge effect prediction.
(Hao and Li, 2003a, 2003b)	Conducted EFM and analytical analysis on laser tube bending	Analyzed laser tube bending using EFM analysis.
(Chen et al., 2004)	Explored curvature bending for the first time	Investigated strain and deformation behavior along the length and width of the worksheet.
(Guan et al., 2005)	Investigated the influence of material properties on laser bending	Found that the bend angle reduces with an increase in Young's modulus, yield strength, density, thermal conductivity, and specific heat, while it increases with the thermal expansion coefficient.
(Edwardson et al., 2006)	Conducted a dedicated study on the geometrical influence on laser bending during multi-scan	Observed that in multi-scan bending, the beam shape's geometry changed due to bending, which reduced the bend angle. Clamping with a v-block gave better results than cantilever clamping.
(Birnbaum et al., 2007)	Investigated the effect of clamping of the sheet	Found that clamping has no significant effect on the bend angle.
(Shen et al., 2007)	Attempted laser bending with variable scanning speed to reduce the edge effect	Observed a significant reduction in the edge effect by varying the scanning speed.
(Shen et al., 2008)	Explored laser bending of bilayer systems of metal-ceramic	Developed an analytical model for bend angle prediction in a bilayer plate of aluminum alloy and silicon carbide ceramic. The model showed good agreement with simulation results.

(Wu et al., 2009)	Attempted laser bending of brittle materials	Experimentally explored laser bending of single crystal silicon, borosilicate glass, and Al ₂ O ₃ ceramic.
(Guglielmotti et al., 2009; Quadrini et al., 2010)	Explored laser bending of metal foam for the first time	Found laser bending to be a feasible solution for bending aluminum foam without affecting the surface integrity of the foam.
(Roohi et al., 2012)	Explored external force-assisted laser bending	Found that external force assistance significantly increased the bend angle.
(Xu et al., 2015)	Explored the effect of preloading in laser bending	The preloading helps in the formation of complex curved shapes
(R. Kant and Joshi, 2016)	Explored the laser bending of magnesium alloy sheet.	Laser bending can be a prominent tool for forming of magnesium alloy.
(Folkersma et al., 2016c)	Attempted the alignment of optical fibers using laser bending process	The laser bending process found to be a significant tool for precise alignment.
(Froend et al., 2017)	Explored the laser bending of dissimilar titanium welded joints	Found that laser bending is suitable for the straightening of the welded joints.
(Thomsen et al., 2018)	Investigated the impact of cooling on edge effect	Reported that cooling has no significant impact on edge effect during laser bending
(Seyedkashi et al., 2018)	Analysed the feasibility of underwater laser bending for the first time	Laser bending can be used for underwater deformation
(Abedi and Gollo, 2019)	Investigated the effect of surface roughness and coating thickness on laser bending process	Results revealed that the surface roughness has positive effect in laser bending whereas coating thickness should be optimized for higher bend angle
(Kotobi et al., 2019)	Experimental and numerical analysis of steel-titanium bimetal sheets were performed for laser bending	Results showed that bimetal sheets can be formed precisely using laser bending process
(Safari et al., 2020b)	Attempted to generate complex saddle shaped surfaces using laser bending process	Laser bending found to be a significant process for generation of complex 3D surfaces

Negligible spring back: The deformation that occurred in this process is majorly plastic, results in negligible spring back. Which again offers good dimensional accuracy and precision (Yocom et al., 2018).

Low tooling costs: Laser bending does not require expensive dies or tooling, making it a cost-effective process (Yocom et al., 2018).

Fast setup time: As no specific tooling arrangement is required, it can be set up quickly and reduce production lead times.

High flexibility: As tools and dies are not required, it is easy to alter the product design. It gives more flexibility to produce complex shapes that are difficult to achieve with conventional methods (Lazarus and Smith, 2017).

Reduced material waste: Laser bending can be used to produce components with minimal scrap material, reducing material waste and lowering costs. It also reduces the material used in dies for different product designs.

Process hard-to-form materials: Hard and brittle materials which are very difficult to form with conventional forming processes can be formed easily.

Low heat-affected area: Laser is a highly focused tool that offers less heat-affected area, which makes the process suitable for heat-sensitive materials as well.

Easy automation: The process can be easily programmable, which leads to easy automation.

Forming in inaccessible areas: The easy transportation of laser beams through fiber cables and mirrors offers the potential for forming in inaccessible areas.

1.5. Limitations

Material limitation: Materials with highly reflective surfaces cannot be processed with laser bending.

Production limitation: The process is limited to small bend angles, and multiple scans are required for large deformations. The process is slow than the conventional processes for mass production.

Quality limitation: Excessive heating may cause melting and material degradation; material properties may deteriorate.

Capital cost: Higher capital investment is required in comparison to conventional machine tools.

1.6. Applications

This technology has found a wide range of applications across various industries, some of which include:

Automotive industry: Laser bending is commonly used in the automotive industry to shape metal parts for car bodies, such as door frames, fenders, and hood panels. It offers an efficient and precise way to create complex curves and shapes (Geiger et al., 1993; Magee et al., 1998a).

Aerospace industry: In the aerospace industry, laser bending is used to shape and form parts for aircraft and spacecraft. It is particularly useful for creating complex shapes and contours that are difficult to achieve with traditional methods (Blake, 1996) (Siqueira et al., 2016).

Medical industry: Laser bending is used in the medical industry to create custom orthodontic devices, such as dental braces and aligners. It can also be used to create medical implants and prosthetics (Cook et al., 2016).

Electronics industry: Laser bending is used to shape and form metal components for electronic devices, such as smartphones and tablets. It can create precise shapes and features that are required for these devices (Yau et al., 1998) (Magee et al., 1998a) (Seyedkashi et al., 2016).

Jewelry industry: Laser bending is used in the jewelry industry to create intricate and delicate designs. It allows jewelers to create unique shapes and patterns that would be difficult or impossible to achieve with traditional methods (Silve and Zhao, 2004; Silve, 2006).

Rapid Prototyping: Laser bending is a prominent tool for rapid prototyping because of its ability to form near-net shapes with excellent precision and controllability (Blake, 1996; Pridham and Thomson, 1994; Thomson and Pridham, 1997b).

Art industry: Laser bending is used in the art industry to create sculptures and other works of art. It allows artists to create complex shapes and forms that would be difficult or impossible to achieve with traditional methods (Dearden and Edwardson, 2003).

Alignment and adjustment: This process is very much precise and cost-effective for fitting and maintenance of parts. It can be used for straightening and other shape correction in body parts of sheet metal (Blake, 1996; Blake et al., 1997; Geiger et al., 1993; Hoving, 1997; Olowinsky et al., 1998).

Overall, laser bending offers a range of benefits, including precision, speed, and versatility. As such, it will likely find increasing use across various industries in the future.

1.7. Motivation

Duplex-2205 is a member of the stainless-steel family that consists of a two-phase microstructure, i.e., ferrite and austenite (Tathgir et al., 2020, 2019). The material possesses high mechanical strength, corrosive resistance, fatigue resistance, wear resistance, good weld-ability, and superplastic behavior (Ghosh et al., 2019; Kim et al., 2015). These properties make it suitable for chemical storage, marine chemical tankers, railway wagons, pressure vessels, heat exchangers, condensers in chemical industries, coastal works, oil and gas industries pipelines, and large structures like bridges, tunnels, and architectures (Davidson and Singamneni, 2016; Davidson et al., 2021). However, hot working is not preferred for duplex-2205 because of the alteration in properties (Faccoli and Roberti, 2013; Pramanik et al., 2018; Tehovnik et al., 2016). A large spring back is observed during conventional forming and requires more powerful machines, as its strength is almost twice of the austenite steel, and the ductility is lower than the austenite (Nomani et al., 2017).

The laser bending process is an advanced manufacturing technique that offers the potential for precise bending of difficult-to-form materials with minimal springback and a small heat-affected area. From this perspective, laser bending has the potential to be a suitable method for bending duplex stainless steel. This has encouraged the investigation of laser bending for this material. Additionally, it is interesting to examine the mechanical and metallurgical properties of duplex stainless steel after laser bending.

Although laser bending offers many merits, like excellent controllability, good flexibility, high precision, etc., over conventional processes, it is limited to small bend angles. Literature reports that laser bending explored for a range of materials: titanium alloys (Wang et al., 2015), magnesium alloy (Ravi Kant and Joshi, 2016a; Nath et al.,

2021), aluminum alloys (Siqueira et al., 2016), mild steel (Lawrence et al., 2001), stainless steel (Li and Wang, 2019a), ceramics (Xu et al., 2013), composites, etc. These studies investigated various aspects: bend angle, edge effect, the effect of process parameters, material behaviour, complex shape generation, mechanism, etc. The bend angle achieved in these studies was observed to be limited to 0.1 to 3 degrees per scan. Many researchers attempted multi-scan laser bending in order to generate a high bend angle, but the material degradation and reduction in the temperature gradient in successive scans are the major problems associated with it. A longer cooling time was provided between the scans to resolve these problems, which resulted in reduced process efficiency and longer production time (Lambiase et al., 2011).

Several researchers recommended forced cooling to overcome the above-mentioned problems associated with natural cooling in multi-scan laser bending. Most of these studies are focused on reducing the waiting time during multi-scan laser bending by applying forced cooling. However, forced cooling is yet to be explored as a tool to improve the bend angle by increasing the temperature gradient. Additionally, limited work is reported on the experimental analysis of the effect of forced cooling during the laser bending process. This gap in knowledge has motivated further exploration of forced cooling at the bottom surface as a tool to enhance the bend angle, and it is called forced cooling assisted laser bending. Additionally, it is interesting to investigate the material behavior during laser bending with forced cooling.

1.8. Organisation of The Thesis

Chapter 1 presented an overview of the laser bending process and its base principle. The advantages, limitations, and industries where the process has possible applications are discussed. Further, the motivation to conduct research in the area of laser bending of duplex stainless steel is also described.

Chapter 2 presents a comprehensive literature review in the field of laser bending. The current status of technology is discussed in terms of bending mechanisms, multi-scan laser bending, assisted laser bending, scanning strategies, modelling, materials exploration, mechanical and metallurgical aspect, applications, and challenges for the process. The critical observations of the above-mentioned aspects are summarized from the literature review, and the research objectives are stated at the end of the chapter.

Chapter 3 presents the pilot study carried out to assess the feasibility and understand the mechanism of laser bending. This chapter includes a numerical investigation of the laser bending process, aiming to analyze the bending behavior of the sheet under different process parameters and gain insights into the underlying mechanism governing the observed bending behavior. Moreover, the numerical analysis examines the feasibility of forced cooling assisted laser bending, providing a comprehensive understanding of the bending behavior and the associated underlying mechanism. Additionally, experimental tests on aluminum alloy sheets were conducted to evaluate the feasibility of forced cooling in laser bending.

Chapter 4 describes the methodology, materials, and experimental details of the forced cooling assisted laser bending process. The chapter provides a comprehensive overview of the experimental setup, highlighting the various instruments employed and their respective roles throughout the study.

Chapter 5 presents forced cooling assisted single scan laser bending. It investigates the bending behavior under natural and forced cooling conditions. The impact of process parameters on bending behavior is analyzed for both cooling conditions. Additionally, the study explores the post-bending effects on mechanical and metallurgical properties. Furthermore, the process parameters are optimized for single-scan laser bending to achieve the maximum bend angle while minimizing energy consumption.

Chapter 6 presents forced cooling assisted multi-scan laser bending. The chapter investigates the influence of process parameters on the bending behavior under both natural and forced cooling conditions. A comparative analysis is conducted to assess the differences between the two cooling approaches. Moreover, the mechanical, metallurgical, and corrosion properties of the bent specimens are examined for both cooling conditions.

Chapter 7 presents the key findings and conclusions derived from the present research work. The potential for future work in this particular field is also discussed in this chapter.

CHAPTER 2

LITERATURE REVIEW

This chapter provides an in-depth analysis of the state-of-the-art laser bending process. It explores the various mechanisms underlying the process and examines the influence of different process parameters on these mechanisms. Additionally, the chapter discusses proposed methods to enhance the technology, showcasing its capacity to form complex 3D shapes and the precise techniques employed for achieving them. Moreover, the chapter discusses the materials investigated to form by this process and highlights any changes in their properties. The sustainability aspects of the laser bending process are also covered, adding a valuable perspective to the overall exploration of this topic. It also addresses the diverse applications of the process and discusses its inherent limitations.

2.1. Mechanisms of Laser Bending

First of all, Geiger and Vollertsen (Geiger and Vollertsen, 1993) explored the mechanism behind laser bending. They reported that the bending is occurred because of the thermal stresses generated due to laser heating. The thermal expansion coefficient and thickness of the worksheet are the most significant factors for the bending. There are three kinds of mechanisms of laser bending given by Vollertsen (Vollertsen, 1994). These three mechanisms are named as temperature gradient mechanism (TGM), buckling mechanism (BM), and upsetting mechanism (UM). These mechanisms are dependent on the laser energy parameters and the work geometry. These mechanisms are responsible for deformation separately or in combination.

2.1.1. Temperature Gradient Mechanism

TGM is the most commonly used mechanism due to its good controllability. As its name suggests, it depends on the steep temperature gradient across the sheet thickness. To generate this temperature gradient, the beam diameter is kept similar to the sheet

thickness, and the scanning speed is set to be high. When dealing with materials of high thermal conductivity, it is necessary to choose an even higher scanning speed.

The process starts with laser heating along the bending line (Figure 2-1(a)) and generates intense heating at the laser-material interaction region. This localized intense heating led to the thermal expansion of the heated region, resulting in counter bending (bending away from the laser source) of the worksheet, as shown in Figure 2-1(b). The adjacent cooler region restricts this thermal expansion and develops compressive stresses in the heated and tensile stresses in the cooler region (Figure 2-1(c)). Furthermore, the flow strength of the heated region decreases due to high temperature. As soon as the flow strength falls down than the compressive stresses, compressive plastic strain takes place (Imhan et al., 2018b). This compressive strain continues until the heating stops.

The cooling starts as soon as the laser passes from that point. Due to this cooling, the heated material begins to shrink. Since the heated surface was under compressive strain during the heating phase, the shrinkage in the top surface is more as compared to the non-heated surface. This difference in shrinkage (compressive plastic strain) between the upper and lower surfaces causes the sheet to bend towards the laser source (Dearden and Edwardson, 2003), as shown in Figure 2-1(d).

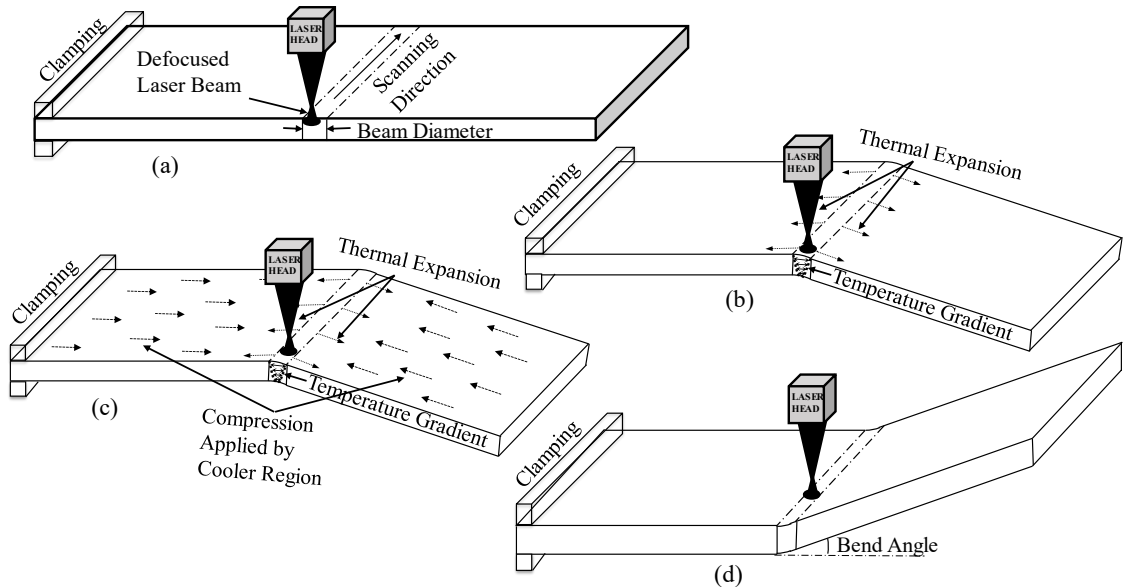


Figure 2-1: Schematic of temperature gradient mechanism

Bucher et al. (Bucher et al., 2018b, 2017) proposed the modified temperature gradient mechanism (MTGM) for laser bending of metal foam. According to MTGM, bending

occurs due to the irreversible plastic deformation of foam cells. They reported that the cell walls had broken, and densified in the scanning region due to the compressive stresses. They also explored the bending of metal foam (AlSI10) sandwiched with two face-sheets of AW 5005. They observed that the bending of face-sheets occurred due to TGM (for smaller diameter) and UM (for larger diameter), but the metal foam was bent due to MTGM (Bucher et al., 2018a).

2.1.1.1. Effect of Process Parameters in TGM

Laser bending is a highly controllable and flexible process that allows for precise deformation of materials. Various parameters, including energy parameters, material properties, the shape and size of the workpiece, and numerous other factors influence the process. Geiger et al. (Geiger et al., 1993) initially categorized these factors into three main categories: energy, material, and geometry. As technology advances, additional factors have been identified and incorporated into the understanding of laser bending. This section provides an in-depth discussion of the critical process parameters significantly impacting the laser bending process.

Laser Power

The laser power plays a critical role in determining the effectiveness and efficiency of the laser bending process. It directly influences the temperature rise in the material, thereby controlling the resulting deformation. Previous studies have explored the relationship between laser power and bend angle for various materials and configurations, providing insights into the impact of laser power on the bending process. Yau et al. (Yau et al., 1996) studied the effect of the energy parameters for the first time on bend angle during laser bending of Al-based metal matrix composite. They combined laser power and beam diameter into a single term known as power density (obtained by dividing laser power by beam area), while scanning speed was considered an independent parameter. They concluded that the bend angle enhances with the power density and reduces with scanning speed. In another study, they reported that the bend angle increases with laser power however, at too high laser powers, it becomes nearly constant because of the reduction in temperature gradient (Yau et al., 1998). Chen et al. (Chan et al., 2000) studied the laser bending of stainless steel sheets and found that the bend angle increased with the laser power until it reached a certain threshold, beyond

which it remained constant. The researchers reported that there is a minimum required heat input for bending, and any excess heat input did not contribute to further enhancement of the bend angle. Seyedkashi et al. (Seyedkashi et al., 2016) explored the effect of laser power on the laser bending of metal composite (steel and copper). They reported that the bend angle after 40 scans increased upto 94% with a 25% increment in laser power. Kant and Joshi (Ravi Kant and Joshi, 2016b, 2016a) analyzed the effect of laser power during the bending of magnesium M1A alloy. They reported that the bend angle increased with laser power at higher scanning speed, but if the scanning speed was low, it started reducing after attaining a peak. Maji et al. (Maji et al., 2016) investigated the laser bending of AISI 304 steel sheet and analyzed the influence of laser power on bend angle. They found that although the bend angle increased with laser power, the rate of increment was not constant and decreased with increasing laser power. However, they also discovered that a larger beam diameter and higher scanning speed could maintain the rate of increment in the bend angle with laser power. Fetene et al. (Fetene et al., 2018a) reported that the bend angle initially showed a significant increase with laser power. However, beyond a certain threshold, the angle remained almost constant.

The literature highlights the significant influence of laser power on the laser bending process. The bend angle generally increases with laser power; however, the rate of increment may vary depending on factors such as material composition, scanning speed, and beam diameter. At excessively high laser powers, the bend angle tends to reach saturation due to a reduction in the temperature gradient. It is essential to carefully optimize the laser power to achieve desired bending outcomes according to the specific characteristics and requirements of the material being processed.

Scanning Speed

Scanning speed plays a crucial role in the laser bending process, impacting heating rate, heat distribution, accuracy, quality, efficiency, and material properties. Various studies have investigated the influence of scanning speed on the bend angle and its relationship with other process parameters. Pridham et al. (Pridham and Thomson, 1994) attempted to make a prototype by laser bending, and for that, they considered two different scanning speeds remaining the other factors constant. The results showed that the number of passes required to achieve a bend angle of 90 degrees was reduced to 200 from 700 by reducing the scanning speed from 50 mm/s to 25 mm/s. Yau et al. (Yau et

al., 1998, 1996) investigated the effect of scanning speed and reported that bend angle reduces with an increase in scanning speed. Magee et al. (Magee et al., 1998b, 1997) studied the influence of scanning speed at constant laser power and constant line energy during laser bending of Ti alloy and Al alloy. They reported that for Ti alloy the bend angle is maximum at an optimum value of scanning speed in both constant power and line energy conditions. Whereas, for Al alloy due to high thermal conductivity the bend angle continuously decreased with scanning speed. Cook et al. (Cook et al., 2016) reported that the bend angle decreases with an increase in scanning speed; however, the rate of decrement reduces with an increase in laser power. Seyedkashi et al. (Seyedkashi et al., 2016) examined the effect of scanning speed during laser bending of a steel-copper composite sheet and reported that the bend angle was reduced to 35% by increasing the scanning speed by 200%.

Kant and Joshi (Ravi Kant and Joshi, 2016b, 2016a) reported that at low laser power, the bend angle decreased with increasing scanning speed. However, at high laser power, the bend angle first increased and then decreased after reaching a peak with increasing scanning speed. They also found that the rate of decrease in the bend angle increased with an increase in the beam diameter. The authors explained that this behavior was due to the reduction in available energy with an increase in scanning speed and a reduction in energy density with an increase in beam diameter. Ghoreishi and Mahmoodi (Ghoreishi and Mahmoodi, 2022) explored the bending of a copper-aluminium bi-metal sheet with varying thicknesses and analyzed the effect of process parameters. They found that the bend angle increased with an increase in scanning speed. This is due to the reduction in temperature gradient at low scanning speeds, as both materials have high thermal conductivity.

Overall, the scanning speed has a notable impact on the laser bending process, affecting the resulting bend angle and the overall efficiency of the process. Optimal scanning speed values may differ depending on the material being bent, interaction between scanning speed, and other parameters like laser power and beam diameter.

Beam Diameter

The beam diameter is a critical parameter in the laser bending process, as it directly influences the energy density, heat distribution, bend angle, and bending radius. Studies

have investigated the effect of beam diameter on the bending characteristics of different materials and composite sheets. Hennige et al. (Hennige et al., 1997) reported that the bending radius increase with an increase in beam diameter. Seyedkashi et al. (Seyedkashi et al., 2016) investigated the effect of beam diameter during laser bending of metal composite (steel and copper). They reported that the bend angle was reduced by 30% with increasing the beam diameter by 80%. Kant and Joshi (Ravi Kant and Joshi, 2016b, 2016a) investigated the influence of beam diameter on bend angle at different scanning speed and powers. They discovered that the bend angle decreased as the beam diameter increased, which they attributed to a reduction in energy density. They also noted that the beam diameter had a more pronounced effect on the bend angle at high scanning speeds and low laser powers, which may be due to a further reduction in available energy. Maji et al. (Maji et al., 2016) found that an optimum value for beam diameter existed to achieve maximum bend angle. They also noted that this optimum value was dependent on other factors, such as laser power and scanning speed. The optimum value of beam diameter was higher for high laser power and low scanning speed, and vice versa. Bucher et al. (Bucher et al., 2018a) attempted the laser bending of metal foam sandwiched sheets and reported that for these sheets, the bend angle increased with an increase in beam diameter.

In general, the beam diameter significantly affects the laser bending process, influencing the resulting bend angle and bending radius. Increasing the beam diameter generally reduces the bend angle, attributed to a decrease in energy density. However, the optimal beam diameter for achieving the maximum bend angle depends on various factors, such as laser power, scanning speed, and the nature of the material or composite being bent.

Line Energy

Line energy is the energy given to the per unit length of the scanning line. It can be calculated by taking the ratio of laser power to scanning speed. It plays a significant role in governing the heat input and subsequent deformation of the sheet. Various studies have explored the influence of line energy on the bending characteristics, mechanical properties, and microstructural changes of different materials. Yau et al. (Yau et al., 1998) studied the effect of line energy during the bending of a thin sheet (0.25 mm) and reported that 0.14 J/mm is the minimum line energy required to cause the deformation for that particular worksheet. The bend angle found to increase with line energy

significantly upto 1 J/mm, after that, the rate of increment reduces and then becomes almost constant.

Akinlabi and Shukla (Akinlabi and Shukla, 2016) investigated the mechanical and microstructural changes in laser-bent steel sheets with respect to line energy. They reported that the yield strength and hardness of the formed sheet were improved, whereas ductility and grain size were reduced. These changes were found to be more prominent at high-line energies. Mjali and Botes (Mjali and Botes, 2018) investigated the influence of line energy in the laser bending process and reported that line energy is an important factor in the laser bending process. Although, other factors i.e., heat flux, beam, interaction time, and temperature gradient, also significantly affect the process even at constant line energy. They observed that the higher line energy led to a reduction in mechanical properties and surface condition. Paramasivan et al. (Paramasivan et al., 2018a) reported that the bend angle increased with line energy. However, when the line energy was held constant, the bend angle was found to be higher at high laser power and scanning speed.

Line energy is a critical parameter in laser bending, influencing the deformation process and resulting bend angle. A minimum line energy threshold is required for sheet deformation, and an increase in line energy generally leads to an increase in the bend angle. However, high line energies can affect the mechanical properties, surface condition, and microstructure of the formed sheet. Understanding the complex relationship between line energy and various process factors is crucial for effectively optimizing laser bending operations and achieving the desired bending characteristics.

Duty Cycle and Pulse Duration

The duty cycle and pulse duration are crucial parameters in laser bending processes, as they directly impact the thermal energy delivered to the material. The duty cycle represents the ratio of pulse on time to the total time, while the pulse duration refers to the duration of each laser pulse. Understanding the effect of duty cycle and pulse duration on the bending behavior is essential for controlling the deformation process and achieving desired bend angles. Pridham et al. (Pridham and Thomson, 1994) studied the effect of pulse ratio (pulse on time/Total time) on bend angle during laser bending and found that bend angle increased with an increase in pulse ratio. Yoshioka et al.

(Yoshioka et al., 1998) explored the laser bending of metal wire and foil with a pulsed YAG laser and studied the effect of pulse duration, energy, and stand of distance. They reported that the bend angle has increased with an increase in pulse duration upto 6 ms, but a further increase in pulse duration led to excessive melting resulted in low bend angle. Similar trend was observed with laser beam energy whereas it got reversed with stand of distance. Chen et al. (Chen et al., 1998a) attempted the microscale bending of stainless-steel sheets using a pulsed laser with constant pulse duration and variable laser pulse energy. They reported that the bend angle increased with an increase in pulse energy.

Chen and Xu (Chen and Xu, 1999) compared the laser bending with continuous wave and pulse lasers and found that continuous laser gave a higher bend angle, whereas pulse laser provided high precision. Maji et al. (Maji, 2019a) analyzed the micro-forming of thin sheets using a pulse laser in a steady state. They exposed the laser beam on two different shape worksheets, rectangular and circular, and observed the deformation occurred at different process conditions i.e., laser power, pulse duration, and beam diameter. It was found that deformation increased with laser power and pulse on time and reduced with beam diameter for single pulse forming. Whereas, for multiple pulses, smaller pulse time led to higher deformation because of high temperature gradient generation.

The literature review reveals that the duty cycle and pulse duration significantly influenced the bend angle and precision in laser bending. Higher pulse ratios increase the bend angle, while excessive melting resulting from longer pulse durations can lead to reduced bend angles. Continuous-wave lasers tend to provide higher bend angles, whereas pulse lasers offer higher precision. The deformation behavior under different process conditions, such as laser power, pulse duration, and beam diameter, demonstrates the intricate relationship between these parameters and the resulting deformation. The optimization of duty cycle and pulse duration is vital for achieving the desired bending outcomes and controlling the thermal energy input during the laser bending process.

Beam Shape

The beam shape is an important factor in laser bending processes, influencing the distribution of thermal energy and heat absorption characteristics of the material. Various studies have explored the effect of beam shape on the bend angle and edge effects during laser bending. Understanding the influence of beam width, inclination angle, and aspect ratio on the bending behavior is crucial for optimizing the process and achieving desired deformation outcomes. Chen et al. (Chen et al., 1998a) studied the laser bending of stainless steel using a pulsed laser of slender elliptical shape (like a line) using a cylindrical lens, as shown in Figure 2-2. The beam covers the whole width of the sheet (0.8 mm), as the beam length is 1.55 mm. The laser beam width varied between 29.2 to 87.3 μm , and the effect of beam width on bend angle was analyzed. The results showed that the bend angle reduces with an increase in beam width.

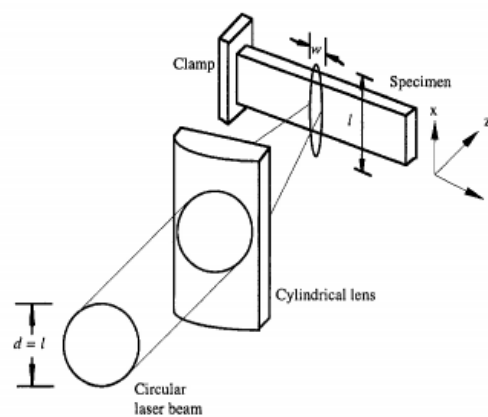


Figure 2-2. Slender elliptical beam shaping using a cylindrical lens

Cook et al. (Cook et al., 2016) studied the effect of inclination angle on the absorption of a graphite-coated steel sheet surface. They reported that the absorptivity increases from 0 to 10° of inclination, then returns to its original value between 10 to 20° and remains nearly constant up to 50°. However, further inclination of the sheet drastically reduces the absorptance. Fauzi et al. (Fauzi et al., 2019) investigated the influence of beam shape on bend angle and edge effect. They examined six different beam shapes (Figure 2-3) of the same beam area, which gave the constant power intensity for all beam shapes. They found that a diamond-shaped beam gave the highest bend angle but with a large variation in bend angle along the scan line (edge effect). The triangular beam also produces a similar bend angle with relatively less edge effect. The study

proposed that the triangular-shaped beam was more significant than the conventional circular-shaped beam in order to get a high bend angle with a lower edge effect. They also analyzed the effect of the aspect ratio (width/height) of the triangular beam and reported that the bend angle increased with the aspect ratio upto a threshold value i.e., 1.05. They also concluded from this study that beam width had more impact on bending as compared to length.

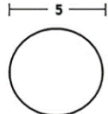
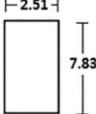



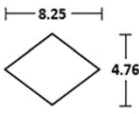
	Circular	Rectangle	Triangle	House	Diamond	Diamond Transverse
Beam Profile						
Aspect Ratio	1	0.32	1.15	0.60	0.58	1.73

Figure 2-3. Different beam shapes with a constant beam area

Literature shows that beam shape plays a significant role in laser bending. The bend angle is found to decrease with an increase in beam width, indicating the importance of controlling the width of the laser beam. The inclination angle of the sheet surface affects the absorptivity, with an optimum range providing higher absorptance values. Different beam shapes, such as circular, rectangular, diamond, elliptical and triangular, offer varying levels of bend angles and edge effects. The triangular beam shape shows promise in achieving high bend angles with reduced edge effects compared to conventional circular beams. The aspect ratio of the triangular beam also influences the bend angle, with an increase in aspect ratio leading to higher bend angles up to a certain threshold. Overall, selecting an appropriate beam shape and optimizing its width is critical for achieving desired bend angles and minimizing edge effects in laser bending processes.

Material Properties

As laser bending is a thermo-mechanical process, the deformation is occurred because of the thermal stresses induced due to laser heating. The material properties play a significant role in the generation of thermal stresses and the deformation of the sheet. Guan et al. (Guan et al., 2005) conducted a study to investigate the influence of various material properties on the laser bending process. They examined the effects of thermal conductivity, specific heat, yield strength, density, thermal expansion coefficient, and

Young's modulus by varying one material property at a time while keeping others constant during numerical simulations. As the thermal conductivity increased, the bend angle decreased due to a reduction in the temperature gradient. The specific heat showed an inverse relationship with the bend angle. A higher specific heat resulted in a lower maximum temperature, leading to higher flow strength and reducing the bend angle. It was also observed that yield strength, density, and Young's modulus had inverse effects on the bend angle. As these material properties increased, the material exhibited a greater capacity to resist deformation, resulting in a reduction in the bend angle. Interestingly, the thermal expansion coefficient showed a positive correlation with the bend angle. An increased thermal expansion coefficient led to higher compressive stresses, which enhanced the bend angle during the laser bending process. These findings emphasize the significant impact of material properties on the laser bending process, providing valuable insights for further optimization and control of this thermo-mechanical forming technique.

Worksheet Geometry

Worksheet geometry is a critical factor that affects the laser bending process, influencing the resulting bend angle, deformation behavior, and overall quality of the bent parts. The dimensions, shape, and orientation of the worksheet can significantly impact the distribution of temperature, stress, and strain during laser bending. Various studies have investigated the impact of worksheet geometry on laser bending, providing insights into the relationship between geometric parameters and bending behavior. For the first time, Geiger et al. (Geiger et al., 1996) investigated the effect of worksheet geometry in the laser bending process in order to explore the bending of microparts. They have studied the effect of sheet thickness keeping the other parameters constant and found that the bend angle increased with reducing sheet thickness, but at lower sheet thickness, it may reduce due to low-temperature gradient. Further reduction in sheet thickness led to increasing the bend angle again because the mechanism involved in the bending had changed; the bending occurred because of the buckling mechanism. Fetene et al. (Fetene et al., 2018a) investigated the laser bending of high-strength steel AH36 and analyzed the influence of worksheet size on the deformation of the worksheet. Their findings revealed that larger width worksheets resulted in a higher bend angle, whereas

thicker sheets experienced a decrease in bend angle. Moreover, the rate of reduction in bend angle reduced as the thickness of the sheet increased further.

Parmasivan et al. (Paramasivan et al., 2017) attempted to laser bend a stainless steel sheet with a rectangular cut at its center. They reported that the dimensions of the cut perpendicular to the scan line did not affect the bend angle, while the dimensions of the cut along the scanning line had a significant effect on the bend angle. They found that the bend angle decreased with the increasing length of the cut along the scan line, while the maximum temperature on the surface was independent of the cut dimensions. Navarrete and Celentano (Navarrete et al., 2018; Navarrete and Celentano, 2018) investigated the impact of worksheet geometry on the laser bending of AISI 304 sheets in three different shapes: circular, ring, and rectangular. The scanning paths for circular and ring-shaped sheets were concentric circles, while for rectangular sheets, it was linear. They observed a noticeable spring-back effect in the curved sheets, but it was negligible in the rectangular sheets. Additionally, they found that the deformation did not align with the plastic strain developed for different worksheet geometries. Based on that, they concluded that worksheet geometry significantly influenced plastic deformation.

The literature highlights the significant influence of geometric parameters on the bend angle and deformation behavior. It has been observed that reducing sheet thickness generally leads to an increase in the bend angle, although at extremely low thicknesses, the bend angle may reduce due to reduced temperature gradient. Additionally, the presence of cuts along the scanning line can substantially affect the bend angle, with longer cuts resulting in decreased bending. Furthermore, the width of the worksheet has been found to positively impact the bend angle, while thicker sheets tend to experience a decrease in the bend angle. The shape of the worksheet, whether circular, ring-shaped, or rectangular, also affects the deformation behavior, with different worksheet geometries leading to varying degrees of spring-back and plastic deformation. Overall, these findings emphasize the significance of worksheet geometry in the laser bending process and provide insights for optimizing the process parameters to achieve desired bending outcomes.

Worksheet Clamping

The effect of worksheet clamping in laser bending has been a subject of interest in various studies. Researchers have investigated different clamping conditions to understand their influence on the bending process. Birnbaum et al. (Birnbaum et al., 2007) explored the influence of clamping during laser bending. They considered two different clamping conditions: in the first one, the sheet was clamped with one of its ends (cantilever), whereas in another the sheet was just laying on flat surface (no clamp). The results showed that there was no significant effect of clamping condition on bend angle, but it affected the bend angle variation along the scan line. The bend angle variation was found to be higher in cantilever clamping as compared to no clamp condition. They also investigated the effect of the thermal conductivity of the clamp. They reported that a highly conductive clamp work as heat sink and increase the cooling rate in scanning region. But, it did not affect the bend angle in single scan bending because during plastic deformation the temperature of scanning region was same for both the insulated and conductive clamps.

Edwardson et al. (Edwardson et al., 2006) also attempted to investigate the effect of clamping conditions and considered two clamp conditions: cantilever and V-block. It was observed that the bend angle was equal for both the conditions upto the first 15 scans; after that V-block gave marginally higher bending. A significant change in bend angle per scan was observed after 25 scans. The rate of increase in bend angle per scan was higher in V-block condition as compared to cantilever. They reported that it might be caused due to the change in beam area in the cantilever condition, whereas it was more uniform in V-block condition. Kant and Joshi (Kant and Joshi, 2012) analysed the different clamping conditions: clamping whole edge, clamping with two corner points of an edge, clamping with one point at the center of an edge and no clamping. They reported that although the bend angle was slightly higher in case of one point center clamping but the cantilever clamping along whole edge gave best uniformity in the bend angle along the scanning direction.

The literature suggests that clamping conditions have an impact on the variation of bend angles along the scan line during laser bending. The thermal properties of the clamping can also affect the temperature and cooling rates, although it not affected the bend angle in single scan bending but can be significant in multi-scan bending. While the overall

bend angle may not be significantly affected by clamping, the choice of clamping condition can influence the uniformity of bending and the rate of increase in bend angle per scan.

2.1.2. Buckling Mechanism

As the laser bending process provides flexibility in controlling various parameters, certain conditions need to be met in order to observe the buckling mechanism. This occurs when the beam diameter is much higher than the sheet thickness, and the scanning speed is slow enough to maintain an almost uniform temperature throughout the sheet thickness (Vollertsen et al., 1995). Materials with high thermal conductivity are more likely to exhibit this phenomenon.

The process starts with the heating with a large diameter laser beam moving at slow scanning speed which leads to almost uniform temperature along the thickness. This heating leads to thermal expansion, which is restricted by the surrounding material and results in compressive stresses in the heated region. The flow stress of the central high-temperature region of the beam reduces. This decreased flow strength of that large heated area and high compressive stresses in that particular area led to a buckle in that region. The direction of this buckling depends on the pre-bending of the sheet and the residual stresses, which start relaxing during this heating process. The height of the buckle increases due to the thermal expansion of the material on further heating. Plastic strain is developed at the center of this buckle because of its very low flow strength due to high temperature. Whereas elasto-plastic strain is developed at the outer region of the laser beam area because of relatively higher flow stress as the temperature is lower in this portion, as shown in Figure 2-4. As the laser moves across the width of the sheet, the buckle is generated in the same direction as the initial buckling along the whole width. After irradiation along the whole bending edge, elastic strains are relaxed, and only plastic strains remain in the sheet. This plastic strain is responsible for the development of the bending angle. The bending angle generated by this mechanism is around 1 to 15 degrees which is very large compared to the temperature gradient mechanism.

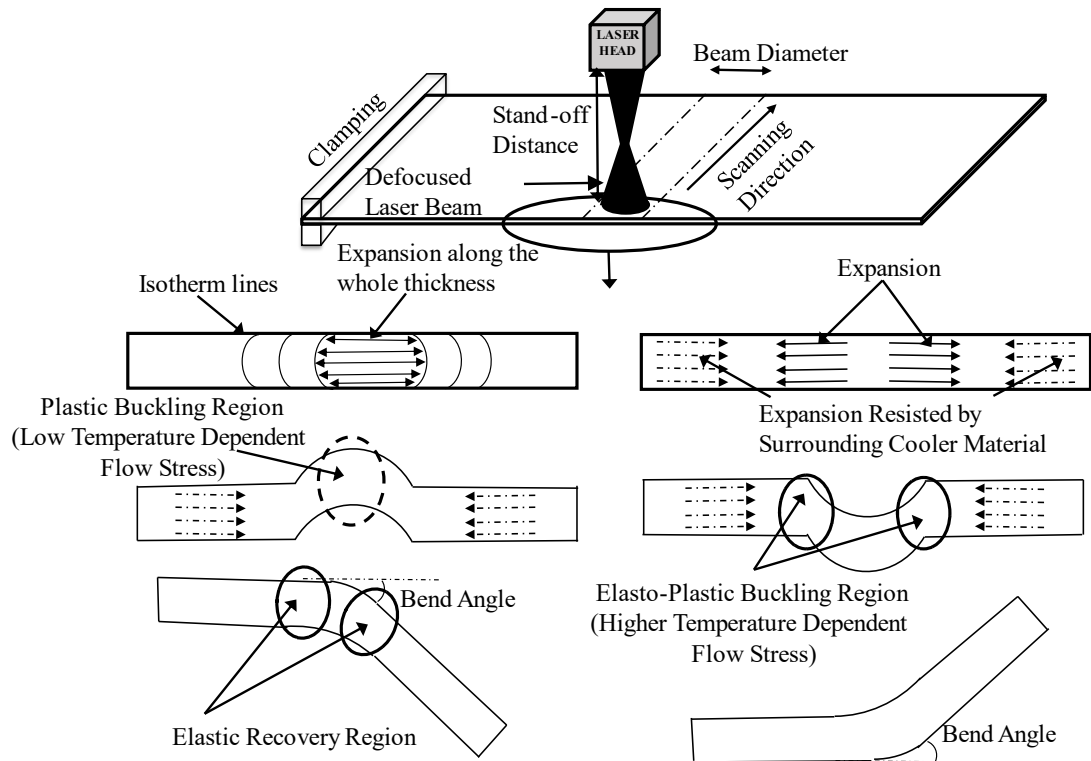


Figure 2-4. Schematic of buckling mechanism

The buckling mechanism has a limitation in controlling the direction of bending, as the bending can occur either towards or away from the laser beam. It is dependent on the pre-bending of the sheet and the residual stresses. The pre-bending can occur arbitrarily due to handling the worksheet or storing the worksheet in folds which develops the uncertainty in the bending direction. Pre-bending can be produced intentionally by temperature gradient mechanism to control this uncertainty, as TGM always develops a positive bending. This positive bending is worked as a pre-bending for the buckling mechanism.

2.1.2.1. Effect of Process Parameters in BM

Various researchers have investigated the buckling mechanisms and effects on different process parameters on this mechanism. First, Arnet and Vollertsen (Arnet and Vollertsen, 1995) explored this mechanism experimentally and reported that bending can be possible in both directions: towards and away from the laser source. Geiger et al. (Geiger et al., 1996) explored the laser bending process for forming microparts and reported that the process is significantly effective for microparts. In their study, they reduced the sheet thickness keeping the other parameters constant, and found that at low thickness, the bend angle may reduce due to low-temperature gradient. Further reduction

in sheet thickness led to increasing the bend angle again because the mechanism involved in the bending had changed, and the bending occurred because of the buckling mechanism. Magee et al. (Magee et al., 1998b, 1997) reported that for low thermal conductivity material (Titanium alloy), the temperature gradient mechanism is responsible for bending even at a high beam diameter to thickness ratio. Whereas, for high thermal conductive material (Aluminium alloy), the bending mechanism changes from temperature gradient to buckling by reducing the scanning speed, especially at high beam diameter to thickness ratio. Similarly, Chen and Xu (Chen and Xu, 2001) also observed during the bending of 100 μm thin stainless steel sheet that at low scanning speed the mechanism involved in bending of sheet was change from TGM to BM. Chakraborty et al. (Chakraborty et al., 2016) attempted to create a bowl shape using a stationary laser beam with varying beam diameter and laser exposure time. They observed that the material bent towards the laser source when using a small diameter laser beam, while with a large diameter beam (ten times the sheet thickness), it bent away from the laser source. They attributed this behavior to the activation of the buckling mechanism at higher beam diameter-to-thickness ratios.

Li and Yao (Li and Yao, 2000) attempted to control the bending direction during laser bending with the buckling mechanism by changing the start point of the scan from the edge to the center of the worksheet. They reported that initial convex bending due to temperature difference between top and bottom surfaces remains in the sheet if the scan started from the center and it works as pre-bending for further deformation. They observed that the convex bending increased with laser power and reduced with scanning speed. Guo et al. (Guo et al., 2020) applied preloading to control the bending direction in the buckling mechanism and developed an analytical model for predicting bend angle under preloading conditions. Jamil et al. (Jamil et al., 2011) explored the effect of laser beam shape during laser bending with the buckling mechanism. They took a beam of constant area with different aspect ratios and compared the results with the conventional circular-shaped beam. They reported that the bend angle increased with the longer beam dimension in the scanning direction. Hsieh and Lin (Hsieh and Lin, 2005a, 2005b) explored the laser bending of tube with the buckling mechanism with and without the axial preload. They numerically analyzed the temperature and stress distribution, and deformation of the tube. They reported that the tube bend due to the thermal expansion

of the heated surface, and this deformation increased with the increase in preload magnitude.

Hu et al. (Hu et al., 2002) studied the laser bending by buckling mechanism and examined the effect of various process parameters on the bending angle as well as the bending direction. They observed that the bending direction dependent not only on the pre-bending and stress condition of the sheet but also on the process parameters. They reported that the bending direction changed from concave to convex by increasing the scanning speed. Furthermore, it was also dependent on other parameters, including laser power, beam diameter, sheet thickness, and worksheet material. For thin sheets, the bend angle varied from concave to convex and then became zero on further increase in scanning speed at small beam diameters. Whereas, at large beam diameters, the bend angle varied from convex to concave with an increase in scanning speed. For thick sheets, it was difficult to achieve convex bending. Chen et al. (Chen et al., 2008) examined the influence of various process parameters, including worksheet thickness, scanning speed, laser power, line energy, beam width, and sheet thickness. They observed that the bend angle increased with laser power, line energy, scan speed, and the ratio of beam width to sheet thickness, while it decreased with an increase in sheet thickness. They reported that the mechanism involved in the bending of the sheet was a buckling mechanism if the width-to-sheet thickness ratio was more than 4. If it was less than 2, both TGM and BM mechanisms may have taken place. Liu et al. (Liu et al., 2010) attempted to generate the negative laser bending of steel foil and examine the effect of process parameters. They gave pre-bending to the sheet away from the laser source to control the bending direction. The bend angle increased with the pre-bending displacement for buckling-dominated parameters, but for TGM-dominated parameters, the pre-bending reduced the bend angle. The negative bending reduced with an increase in the scanning speed. High laser power was recommended for the negative bending with a moderate beam diameter.

2.1.3. Upsetting Mechanism

This mechanism becomes apparent when the beam diameter is approximately equal to the sheet thickness and the scanning speed is sufficiently low to achieve a uniform temperature distribution across the sheet thickness. High thermal conductivity materials facilitate the attain uniform temperature across the sheet thickness. All the necessary

conditions for this mechanism are identical to those of the buckling mechanism, except for the beam diameter, which is smaller in this case.

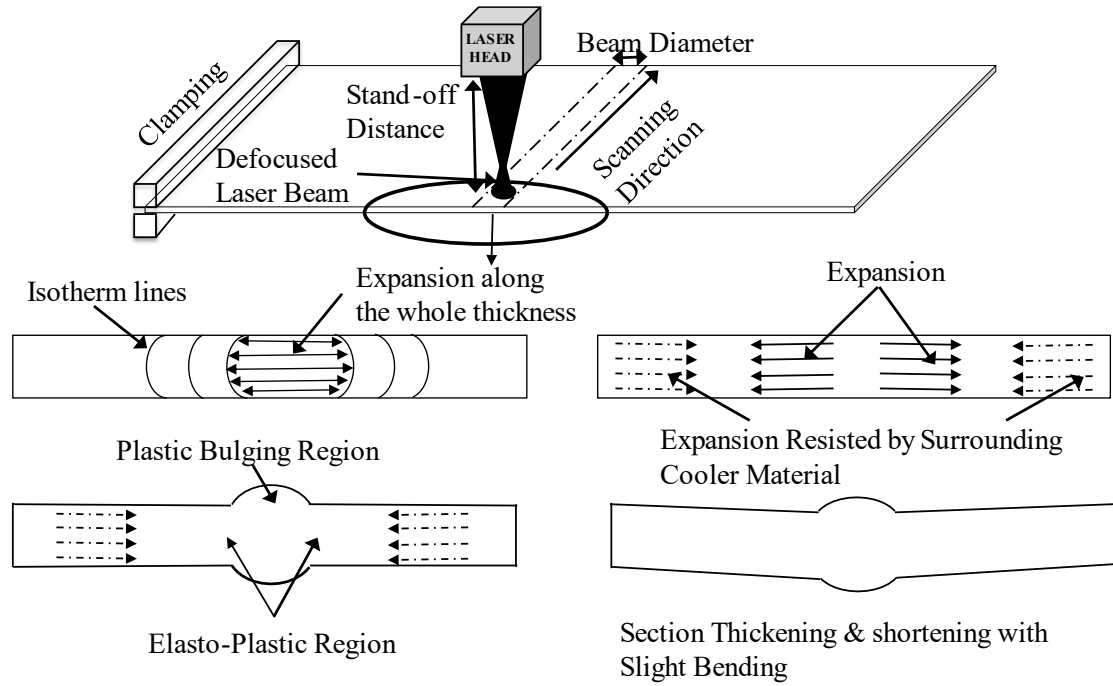


Figure 2-5. Schematic of upsetting mechanism

The process starts with laser scanning at low scanning speed, which generates almost uniform temperature throughout the thickness. As the temperature increases thermal expansion takes place, and the flow strength of the heated region also decreases. The thermal expansion is restricted by surrounding cooler material and develops compressive stress in the heated region, whereas tensile stresses in the cooler region. Unlike the buckling mechanism, this results in a bulge formation in the heated region due to the high stiffness of the geometry caused by the small beam diameter (Bachmann et al., 2020). The reduced flow strength at the center of the bulge leads to plastic deformation, while the outer region exhibits elastoplastic behavior due to its relatively higher flow strength. As the laser is passed the particular point, cooling starts, and the material starts to recover the elastic deformation. The elasto-plastic region contracts and shortens the length of the sheet (K. Paramasivan, S. Das, 2019). Overall, this mechanism results in the thickening and shortening of the sheet. A stepwise schematic of the mechanism is shown in Figure 2-5.

During TGM the plastic deformation occurs on the top surface only, whereas in the upsetting mechanism, it is on both top and bottom surfaces due to uniform temperature.

In UM, the bottom surface also gets sufficient heat to deform plastically. But the plastic deformation at the top surface is higher than that of bottom because it is impossible to achieve zero temperature gradient along the sheet thickness (Shi et al., 2012b). The difference in plastic strain between the top and bottom surface lead to small bending, and the plastic strain at both the surfaces lead to shortening and thickening. This combined effect of TGM and UM is called coupling mechanism (Shen, 2008). Shi et al. (Shi et al., 2006) explored the parametric ranges for domination of particular mechanism. They observed that TGM dominates if the diameter to thickness ratio is upto than 3, in the range of 3 to 4.5 coupling mechanism is dominated, upsetting mechanism dominates in the range of 4.5 to 6, and for getting buckling, this ratio should be more than 10. The highest line energy is required to achieve UM followed by coupling mechanism due to low scanning speed for uniform temperature.

2.1.3.1. Effect of Process Parameters in UM

Jamil et al. (Che Jamil et al., 2011) conducted a numerical study on the laser bending of SS304 sheets and tubes, considering a range of process parameters such as laser power, beam diameter, and sheet thickness. They also examined the mechanism involved in the sheet-forming process. The authors reported that for low sheet thicknesses (0.5 and 0.9 mm), the deformation occurred due to a buckling mechanism at 800 W laser power and a 16 mm beam diameter. In contrast, for thicker sheets (1.5 and 2 mm), the observed deformation occurred in the plane of the sheet, possibly due to upsetting, with small bending. The bending of the tube was attributed to the shortening and thickening of the heated region of the tube. Shi et al. (Shi et al., 2012a) attempted to minimize the bending that occurred along with the plane strain during the upsetting mechanism. They explored different heating strategies with varying process parameters. It was also observed that the smaller beam diameter and high laser power led to an increase in the temperature gradient and resulted in higher bending. They reported that the bending can be reduced significantly by simultaneous heating at the top and bottom surfaces. Conventionally, a large diameter beam with low scanning speed was used for upsetting, but while simultaneous heating smaller diameter with high speed can be used. Chakraborty et al. (Chakraborty et al., 2013) studied the effect of the Fourier number on the coupling mechanism and found that the bending reduced with the increase in Fourier number, whereas thickening increased. In another study, they also reported that both bending and

thickening increased with the beam diameter (Chakraborty et al., 2015). Maji et al. (Maji et al., 2018)(Maji, 2019b) developed a neuro-fuzzy interface-based model to predict the bending and thickening that occurs in the coupling mechanism. They conducted multi-objective optimization and reported that the bending was higher compared to thickening for parameters that resulted in lower values of the Fourier number.

2.2. Methods for Improving Laser Bending

As discussed in the previous section, the temperature gradient mechanism offers excellent controllability over the process, giving precise and accurate bending without any external force and tools. Forming of hard-to-form material and forming in inaccessible areas can be done. The mechanism is limited to job and batch-type production but not suitable for mass production because of the small bend angle. Furthermore, the mechanism is not suitable for thin sheets of high thermal conductive materials because it is difficult to generate high-temperature gradient. Many researchers proposed different techniques to get higher bend angles like: multi-scan laser bending, laser bending with cooling, external force-assisted laser bending, and absorptivity enhancement.

2.2.1. Absorptivity Enhancement by Surface Modifications

In order to enhance the bend angle and productivity of the laser bending process, researchers have explored the concept of absorptivity enhancement through surface modification. By improving the absorptivity of the worksheet surface, researchers aim to increase the available energy for deformation without altering the input energy. The surface condition of a material plays a crucial role in laser material processing, including laser bending. The surface condition can significantly influence the absorption and reflection of laser energy, thereby impacting the efficiency and quality of the laser bending process. Various investigation has been done to understand the effects of surface condition, surface roughness, coatings, and oxide layers on absorptivity. Kant et al. (Kant et al., 2016) examined the influence of absorptivity on laser bending. They observed that the absorptivity significantly affected the temperature and stress-strain distribution, which resulted in a notable effect on the bend angle and edge effect. They reported that the bend angle increased nonlinearly with an increase in absorptivity, whereas the edge effect was found to be reduced. The study concluded that the laser

bending process is highly influenced by absorptivity, which is highly sensitive to the surface condition of the worksheet.

Fetene et al. (Fetene et al., 2017b) investigated the laser bending of aluminium and mild sheet for three different surface conditions i.e., friction stir processed, cement coated and unprocessed. They reported that the friction stir processing increased the surface roughness, resulting in higher absorptivity. The bend angle of the friction stir processed aluminum sheet was higher than the unprocessed sheet, but lower than the cement-coated sheets. In contrast, the bend angle of the cement-coated and friction stir processed mild steel sheets was nearly the same for higher number of scans and significantly higher than the unprocessed mild steel sheet. Imhan et al. (Imhan et al., 2018a) attempted to improve the material absorption by laser heat treatment. They observed that an oxide layer was formed on the surface due to laser heat treatment. The absorptivity of the material surface improved due to this oxide laser significantly. Abedi and Gollo (Abedi and Gollo, 2019) investigated the effect of Cr_2O_3 coating thickness and surface roughness of the SS304 worksheet on the laser bending process. Different combinations of coating thickness and surface roughness are shown in Figure 2-6. They reported that the surface absorptivity and bend angle increased with an increase in the surface roughness (from $R_a = 0.04$ to 1.9) and Cr_2O_3 coating thickness (from 0 to $6 \mu\text{m}$). They also optimized both the surface roughness and the thickness of the Cr_2O_3 layer. They reported that the optimum values were $1.9 \mu\text{m}$ for surface roughness and $1.7 \mu\text{m}$ for coating thickness. At these values, the absorption increased from 38% to 99.86% , and the bend angle increased from 3.43° to 7.71° . Rattan et al. (Rattan et al., 2020) explored lime as a coating material for the laser bending of plain carbon steel and observed that the bend angle improved compared to the bare sheet. However, they found that the bend angle decreased with increasing coating thickness.

The literature on surface conditions in laser bending demonstrates the significant influence of surface properties on the bending process. The absorptivity of the worksheet surface has been found to have a nonlinear relationship with the bend angle, with higher absorptivity resulting in increased bend angles and reduced edge effects. Surface treatments such as friction stir processing and laser heat treatment can improve absorptivity and enhance bending performance. Coatings, such as Cr_2O_3 and lime, have also been investigated, showing varying effects on the bend angle depending on their

thickness. Surface roughness is another crucial factor, where an optimal range of roughness values can lead to improved absorption and bend angle. These findings emphasize the significance of surface conditions in the laser bending process to attain the desired bending outcomes and improve process efficiency.

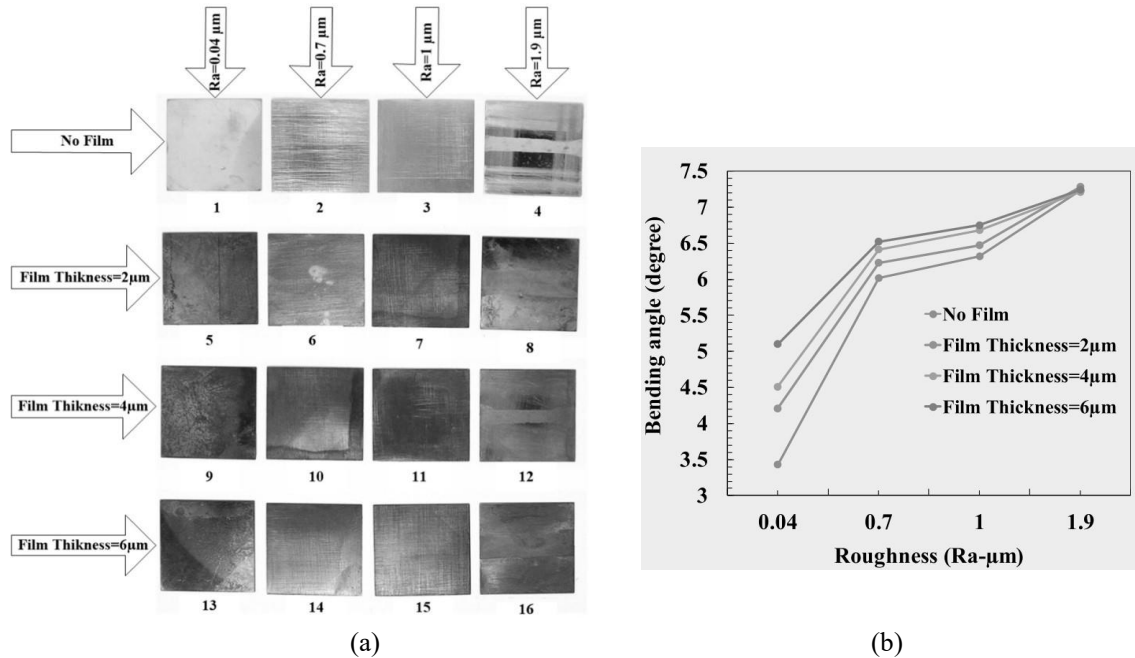


Figure 2-6. (a) Worksheet surface and (b) bend angle variation with different combinations of coating thickness and surface roughness.

2.2.2. External Force-assisted Laser Bending

Forced-assisted laser bending is a technique that aims to increase the bend angle in the laser bending process. In addition to laser energy, external forces are applied to the material to enhance deformation, especially in the case of difficult-to-form materials like thick plates. The application of external mechanical force allows for greater control over the final shape of the bend (Mucha et al., 2016). This section discusses various studies that have utilized external forces, such as mechanical load, pressure assistance, magnetic or electromagnetic force, and preloading, to achieve higher bend angles, reduced spring-back, and improved material properties.

Roohi et al. (Roohi et al., 2012) applied external mechanical force during the laser bending of Al-5005 aluminium alloy to gain a bend angle upto 90° . They observed that the bend angle increased by nearly 40% with the application of external force. Kant et al. (Kant and Joshi, 2013) applied a mechanical load at the free end of the worksheet,

which is moving along the laser beam. They reported that the compressive stresses at the top surface and tensile stresses at the bottom surface increased due to mechanical load and resulted in a higher bend angle and it increased with an increase in mechanical load. Although, the edge effect and spring back effect were also found to be increased with the mechanical loading. Gisario et al. (Gisario et al., 2017, 2016a) attempted laser-assisted external force bending to achieve a high bend angle with a sharp fillet radius and negligible spring-back. They were able to achieve a bend angle of up to 140° with a fillet radius of less than 2 mm, and the spring-back was reduced by up to 30 times. The 3D complex shapes made by forced-assisted laser bending are shown in Figure 2-7.

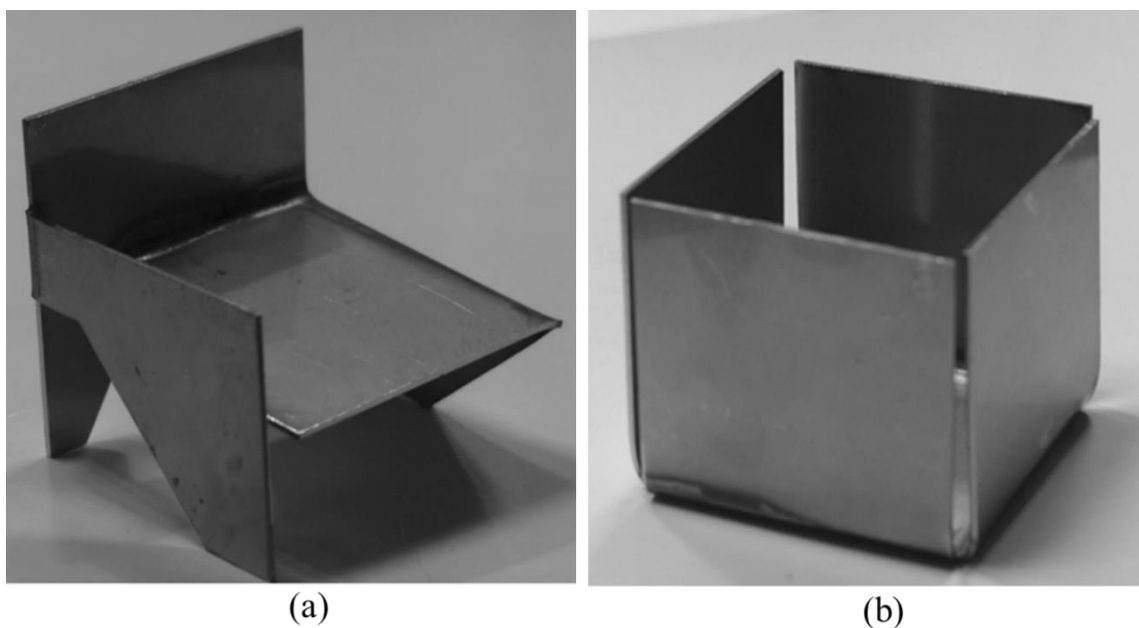


Figure 2-7. Complex shapes formed by forced assisted laser bending (a) design of chair, (b) cube

Shi et al. (Shi et al., 2016) attempted to reduce the variation in bend angle along the scanning direction by applying an assisted force at the free edge. They applied three different loads (uniform line load, two-point loads of the same magnitude, and two-point loads of different magnitudes) one by one and analyzed the optimum loading condition for minimum bend angle variation. They reported that applying two unequal loads at the two corners of the free edge resulted in the minimum variation in bend angle. Widłaszewski et al. (Widłaszewski et al., 2022, 2021) conducted a study on the force-assisted laser bending of Inconel beams and found that it led to a significant increase in deformation, enabling the achievement of convex bending.

Lang et al. (Lang et al., 2017) investigated the influence of preloading on laser bending of metal sheets and reported that the bend angle increased exponentially with an increase in preload amount. Guo et al. (Y. Guo et al., 2021a, 2021b, 2021c) investigated the pressure-assisted laser bending and developed an analytical model for prediction of bend angle. They reported that the pressure assistance enhanced the bend angle and offered more control over the process (bending direction). In another study, Guo et al. (J. Guo et al., 2021) proposed a novel technique for bending of aluminium high-stiffened structures by laser-assisted four-point bending method. In this process, the structure was initially subjected to a mechanical force at four points, inducing elastic strain energy. Subsequently, laser application converted this elastic strain energy into plastic strain energy. The results demonstrated that the use of laser significantly reduced spring-back, while mechanical bending facilitated high deformation during laser bending. Therefore, the laser-assisted four-point bending method yielded considerably higher deformation with minimal springback.

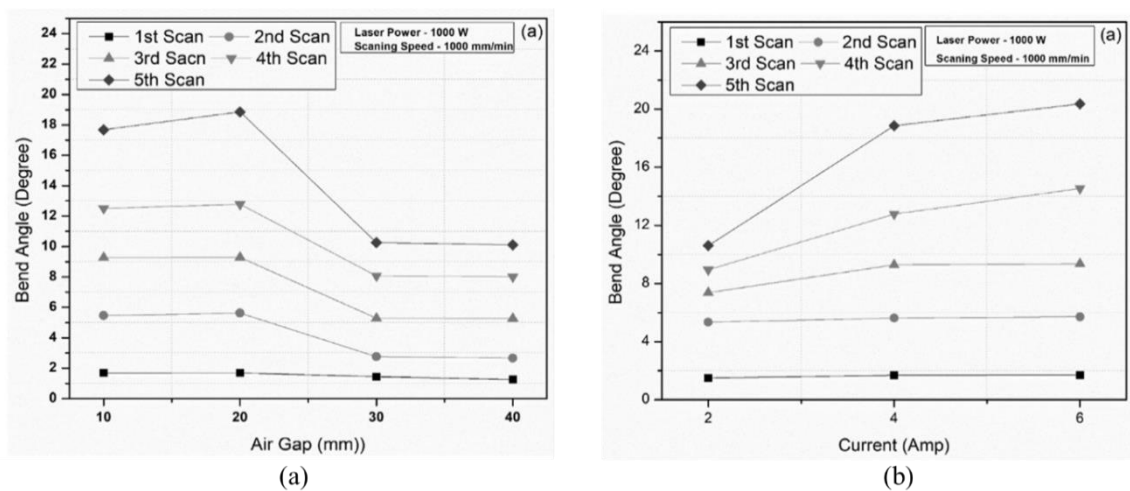


Figure 2-8. Bend angle variation with (a) air gap between sheet and electromagnet, (b) current supplied to the electromagnet

Fetene et al. (Fetene et al., 2017a) applied external force with the help of a magnet in both directions: towards and away from the laser source. They reported that the bend angle was enhanced due to magnetic force if the direction of bending and direction of force were the same. The edge effect was also found to be reduced especially at low scanning speed when the free end of the sheet came in physical contact with the magnet. Dutta et al. (Dutta et al., 2018) got similar results for laser bending assisted with electromagnetic force. Sharma et al. (Sharma et al., 2023) also investigated the electromagnetic force-assisted laser bending with varying the current supplied to the

electromagnet and the gap between the worksheet and electromagnet. They reported that the electromagnetic force increased the bend angle significantly, and it further increased with the current supplied to the electromagnet (Figure 2-8). However, it requires an optimum air gap between the worksheet and the electromagnet.

The literature on external force-assisted laser bending highlights its effectiveness in achieving high bend angles, sharp fillet radii, and reduced spring-back. The application of external forces, such as laser-assisted external force bending, preloading, pressure assistance, and electromagnetic force, has shown significant improvements in bend angles, surface quality, and deformation capabilities. These approaches have been applied to a variety of materials, including thick plates, Inconel beams, and high-stiffened structures. The combination of mechanical force and laser energy has proven to be advantageous, enabling the conversion of elastic strain energy into plastic strain energy and facilitating higher deformations with minimal spring-back. These findings highlight the potential of external force-assisted laser bending as a valuable technique for achieving desired bend shapes and improved material properties in various applications.

2.2.3. Multi-scan Laser Bending

Multi-scan laser bending is a technique used to increase the bend angle during the laser bending process. In this method, the laser beam is scanned multiple times over the desired bending region, leading to enhanced deformation and greater bend angles. Various research studies have examined the impact of the number of scans on bending behaviour, considering factors such as bend angle, bending radius, surface roughness, microhardness, grain size, and edge effect. Magee et al. (Magee et al., 1998b, 1997) reported that a high bend angle can be achieved by multiple scans, but the rate of bend angle reduces with the number of scans due to thickening in the scanning region. Gisario et al. (Gisario et al., 2016a) investigated the effect of the number of scans on the bend angle and bending radius during external force-assisted laser bending. They reported that the bend angle increased with the number of scans while the bending radius continuously decreased.

Seyedkashi et al. (Seyedkashi et al., 2016) reported in their study of laser bending of metal composite sheets that the bend angle increased with the number of scans, but the

rate of increment was not linear; it decreased with an increase in the number of scans. It might be because of the degradation of graphite coating, preheating and change in beam shape. Kant and Joshi (Ravi Kant and Joshi, 2016b) also reported a similar trend in the bending of M1A. However, they provided a different perspective by utilizing numerical simulation. They observed that with each scan, the temperature increased, which reduced the restriction provided by the cooler material to thermal expansion, resulting in lower thermal stresses. Edwardson et al. (Edwardson et al., 2010b, 2007) reported that there may be a number of possible reasons for the non-uniform increment in bend angle with the number of scans. These factors include strain hardening, thermal effects, coating degradation, section thickening, and geometrical effects. Thermal effects involve an increase in available energy for deformation but also a reduction in temperature gradient. Section thickening refers to the thickening in the irradiation region, which increases the sheet stiffness. Coating degradation reduces absorptivity, while strain hardening increases resistance to deformation. Geometrical effects cover the changes in the shape of the laser beam and the interaction area with the worksheet as the bend angle increases. These factors dominated in different ranges of the number of scans as shown in Figure 2-9. Maji et al. (Maji et al., 2016) reported that the bend angle increased with number of scans and this effect was more pronounced at high laser power, low scanning speed and smaller beam diameter. Das and Biswas (Das and Biswas, 2017) optimized the process parameters (sheet thickness, scanning speed, number of passes, and laser power) to obtain the maximum bend angle. They reported that among these process parameters, the number of passes was the most significant, followed by sheet thickness, laser power, and scanning speed.

Chan et al. (Chan and Liang, 2000) investigated the laser bending of Al6013/SiC_p aluminium matrix composite sheet and analysed the effect of process parameters with the number of scans. They reported that the bend angle increased with the number of scans, but the bend angle increment per scan was dependent on the laser power and scanning speed. The bend angle increased with a higher rate at high laser power and low scanning speed. Marya and Edwards (Marya and Edwards, 2000) examined the effect of various factors, including laser power, sheet thickness, and number of scans, on bend angle as well as thickening of the sheet. They reported that the bend angle increased with laser power, reached maximum and then decreased, and this variation was not affected by the number of scans (Figure 2-10(a)). It was observed that the bend angle

increased with the number of scans, but the rate of the bend angle increment varied with laser power. As Figure 2-10(a) shows a low bend angle at low as well as high laser power, the slope of the bend angle to the number of scan plots is highly sensitive to laser power. Whereas, for intermediate laser power where bend angle is high, the laser power did not affect the rate of bend angle Figure 2-10(b). The beam diameter also significantly affected the bend angle increment in per scan. For high thickness sheet the bend angle per scan was higher upto initial 10 scans whereas after 10 scans it was higher for low thickness sheet (Figure 2-10(c)). They reported that this variation in bend angle per scan is because of the thickening of the sheet, as the sheet thickening also varied with the number of scans as shown in Figure 2-10(d).

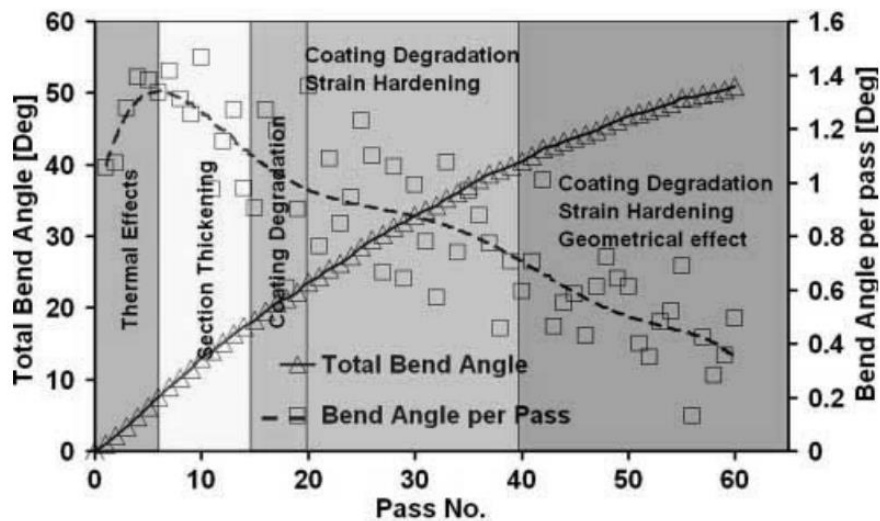


Figure 2-9. Domination range of different factors influencing the bending rate with number of scans (Edwardson et al., 2010a)

Chen and Liang (Chan and Liang, 2001) observed during the laser bending of Ti3-Al-based intermetallic alloy that the bend angle increased with the number of scans, but the slope of the plot is different for different laser powers. They analyzed that for low laser power, the slope of the bend angle-number of scan curve reduced, whereas for high laser power, it was linear. They reported that strain hardening on the lower layer of the sheet was responsible for the decrement in the slope of the bend angle plot, whereas recrystallization of the lower layer may lead to linear increment in bend angle with the number of scans which occurred at high laser power. Lawrence et al. (Lawrence et al., 2001) attempted laser bending of a mild steel sheet with high-power diode laser for 40 scans. They reported that the bend angle increased linearly with the number of scans for different laser power and scan speeds, whereas the slope of these lines increased with

laser power and reduced with scanning speed. Bellisario and Quadrini (Bellisario and Quadrini, 2012) also observed a similar trend in aluminium alloy sheets. Majumdar et al. (Majumdar et al., 2004) studied the effect of scanning speed during multi-scan laser bending of stainless-steel sheets. They reported that the bend angle increased with the number of scans with different rates of bend angle per scan at different scanning speeds. The rate of bend angle per scan reduced with the number of scans at low scanning speed, whereas at high scanning speed, it increased with the number of scans. This variation might be due to the reduction in temperature gradient at low scanning speed during multi-scan, whereas for high scanning speed, it increased the available energy, which was not enough at high scanning speed.

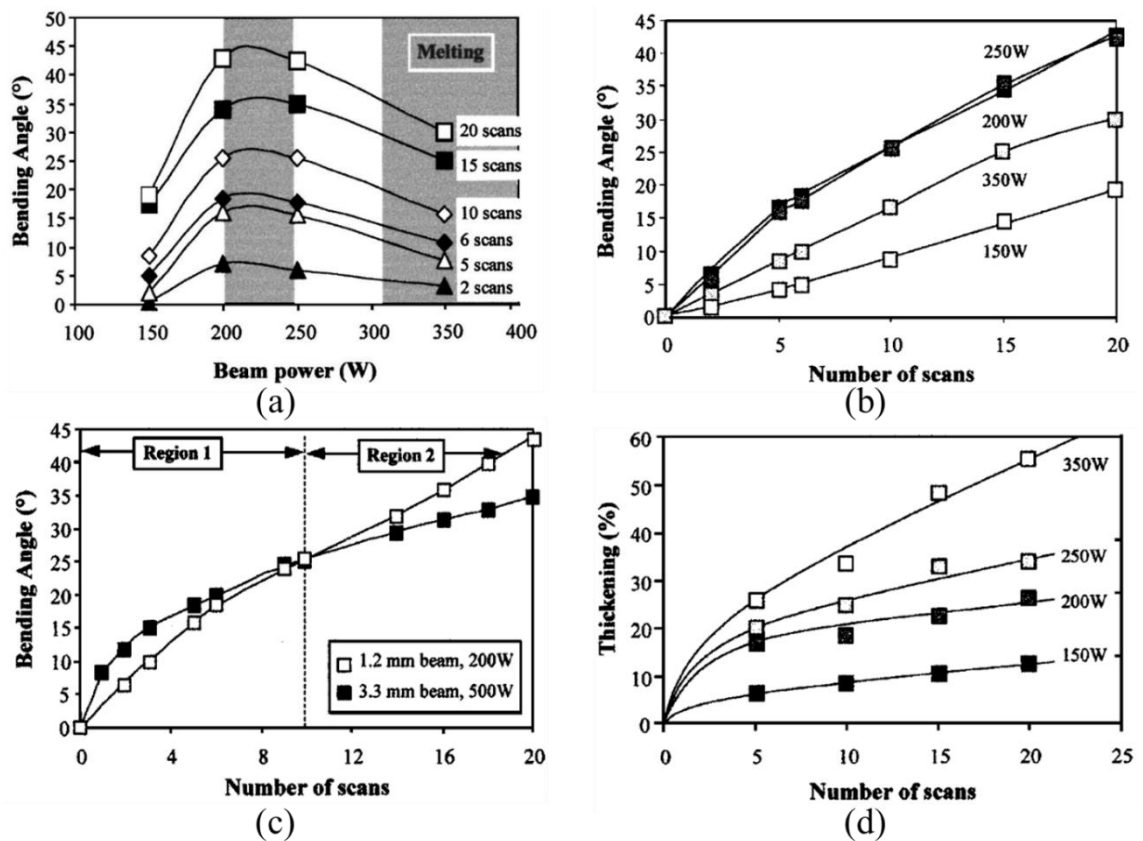


Figure 2-10. Effect of laser power, number of scans, sheet thickness on bend angle and section thickening during multi-scan laser bending

Lubiano et al. (Lubiano et al., 2000) investigated the laser bending of thin sheets (0.5 mm) of three different materials 304 stainless steel, 1100 aluminium alloy, and 1010 steel sheets with 20 laser irradiations on each sheet. They reported that the bend angle increased with the number of scans for all three sheets, but the increment in bend angle per scan was different. The bend angle per scan reduced at a higher number of scans for

aluminium and steel sheets, where it was constant for stainless steel. It was because the high thermal diffusivity of aluminium and steel rapidly conducted the heat supplied and resulted in low-temperature gradient, whereas for stainless steel sheets the temperature gradient was maintained even at a high number of scans. Edwardson et al. (Edwardson et al., 2005, 2003) attempted the bending of metal laminate composites, varying the number of laminate layers and fiber orientations. They reported that the bend angle increased with the number of scans for all the varying conditions, but the bend angle rate per scan was significantly influenced by these conditions. The bend angle rate per scan was reduced with the increase in number of laminate layers. The bend angle rate found to be maximum when the bending line is parallel to the reinforced fibers and it was minimum for the perpendicular orientation of fibers with bending line. Wu et al. (Wu et al., 2010a) investigated the effect of sheet thickness (100 to 300 μm) during multi-scan laser bending of silicon sheet. The bend angle reduced with an increase in sheet thickness, whereas it increased with the number of scans. For low sheet thickness the rate of bend angle per scan was higher for initial scans and it reduced with number of scans whereas for thicker sheets the bend angle per scan rate was higher for later scans.

Kotobi and Honarpisheh (Kotobi and Honarpisheh, 2017) studied the effect of the number of scans on bend angle, surface roughness, and microhardness in the scanning region. They found that the bend angle and surface roughness increased with the number of scans, whereas the microhardness in the scanning region increased initially and then became nearly constant. Fetene et al. (Fetene et al., 2018a) reported that the grain size was also affected by the number of scans. They found that the grain size became finer with an increase in the number of scans. Zhang et al. (Zhang et al., 2019) conducted a study on the edge effect in multi-scan laser bending of DP980 steel sheets. They observed that the edge effect decreased as the number of scans increased. Furthermore, they proposed a new scanning strategy to mitigate the edge effect. According to that strategy, the scanning process began from one edge, moved up to 10 mm along the scanning path, returned to the starting point, then continued moving along the scan line upto the opposite edge. Subsequently, the laser moved back upto 10 mm along the scan line and again proceeded to the opposite edge. This novel scanning strategy resulted in a reduction of the edge effect by up to 20%.

The number of scans in multi-scan laser bending has been found to be a critical parameter for achieving enhanced bend angles and improving the productivity of the process. The number of scans significantly influences the bend angle and other bending characteristics in laser bending. The relationship between the number of scans and the bending angle is influenced by factors such as graphite coating degradation, preheating, beam shape changes, temperature increase, thermal stresses, laser power, scanning speed, and beam diameter. Additionally, the number of scans affects surface roughness, microhardness, grain size, and the edge effect. Although multi-scan laser bending can achieve a high bend angle, it is limited by longer cooling times between consecutive scans, which leads to low productivity. Additionally, excessive melting during the process can result in alterations in material properties and surface degradation.

2.2.4. External Cooling Assisted Laser Bending

The application of cooling was proposed to overcome the limitations of multi-scan laser bending by reducing the cooling time and excessive melting. Cooling conditions play a vital role in laser bending, affecting factors such as energy availability, material properties, and production rate. The type of cooling, cooling time between scans, and cooling method applied to the worksheet surface all contribute to the bend angle, productivity, mechanical properties, and microstructure of the material. Optimizing the cooling conditions is crucial for achieving desired bending outcomes in terms of bend angle, production time, and material properties. This section discusses the role of cooling in increasing the bend angle and its implications for the productivity of the laser bending process. Yau et al. (Yau et al., 1998) investigated the effect of holding time (cooling time) between the two consecutive scans and reported that the bend angle reduces with longer holding time because of the higher heat loss. Seyedkashi et al. (Seyedkashi et al., 2016) analyzed the effect of cooling time between the scans during the bending of three-layer steel-copper-steel composite. They reported that the bend angle increased with an increase in cooling time, although this also increased the bending duration. Therefore, it needs to be optimized to achieve a higher bend angle in the minimum time and with minimum energy consumption.

Cheng and Yao (Cheng and Yao, 2001) explored forced cooling during laser bending for the first time. They applied high-pressure air in the laser heating area at bottom surface with the help of a moving air jet. They reported that forced cooling helped to

maintain the temperature gradient during multi-scan laser bending specially at low laser power and scanning speed. The bend angle increased due to forced cooling at low power and scanning speed condition. The pressure of cooling air also affected the bend angle as it increased with air pressure for high power and speed, whereas it reduced for low power and speed due to excessive heat loss. They also reported that the forced cooling showed adverse effects during the laser bending with buckling mechanism because of increased flow strength and tendency to generate non-uniform temperature along the sheet thickness. Shen et al. (Shen et al., 2011) attempted to reduce the cooling time between the successive scans by a moving boundary condition of cooling during the numerical study. They analyzed three different cooling conditions, including cooling at the top only, cooling at the bottom only, and cooling at both the top and bottom surfaces. In all these cases, the cooling moved behind the laser beam. They observed that the bend angle slightly increased in cooling conditions, especially for the cooling at both surfaces. Lambiase et al. (Lambiase et al., 2013) investigated the effect of passive water cooling in the laser bending process. The worksheet was positioned like 90% of the sheet thickness was submerged in water, as shown in Figure 2-11. They reported that passive water cooling significantly reduced the cooling time between the scan without much affecting the bend angle, and it also reduced the chances of surface oxidation. They also investigated the productivity of the multi-scan laser bending process. The process parameters and cooling conditions were optimized to minimize the production time to produce a particular bend angle (Lambiase et al., 2016). Interestingly, they found that the process parameters which gave maximum bend angle did not necessarily result in higher productivity. This was because the cooling time between scans played a critical role in process productivity, leading to different optimal parameters for maximum productivity and maximum bend angle.

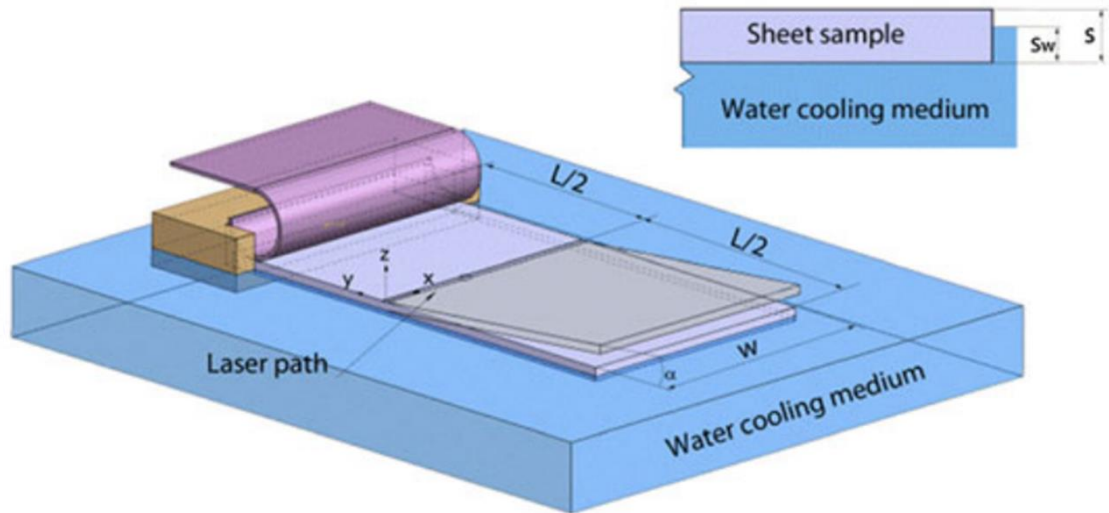


Figure 2-11. Schematic representation of passive water cooling

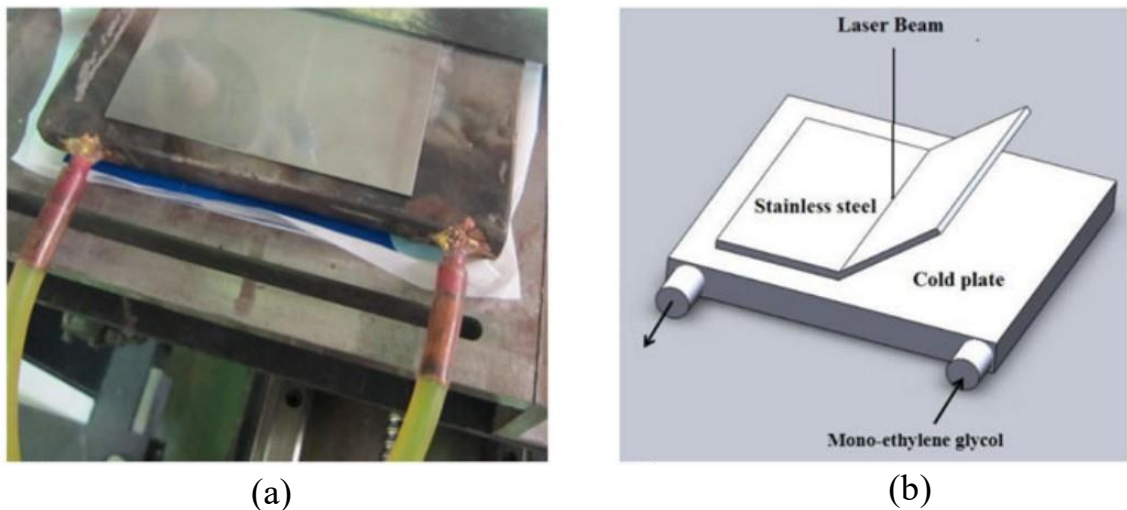


Figure 2-12. (a) Cooling plate and stainless steel plate before exposure, (b) schematic illustration of the bent sheet, cooling plate and cooling fluid path.

Chinizadeh and Kiahosseini (Chinizadeh and Kiahosseini, 2017) studied the influence of natural and forced cooling on laser bending, mechanical properties, and microstructure of AISI316. They used a cold plate with a circulation of cold fluid at 0°C placed below the worksheet, as shown in Figure 2-12 . The authors reported that forced cooling significantly improved the bend angle for a high number of passes but not for a smaller number of passes. They also observed that the hardness decreased during natural cooling, whereas it increased during forced cooling. This was attributed to the grain size, which increased during natural cooling and decreased during forced cooling. Thomsen et al. (Thomsen et al., 2018) applied the forced air cooling with four different heat transfer coefficients in order to investigate the effect of cooling on the edge effect.

However, they observed that the forced cooling did not influence the edge effect, and it remained unchanged.

Paramasivan et al. (Paramasivan et al., 2018b) applied forced cooling at the bottom surface of the worksheet in order to increase the bend angle. They analyzed the influence of the area and shape of cooling applied at the bottom surface. Three different cooling conditions are investigated numerically i.e., circular jet moving along with laser beam, strip along the whole width of the worksheet, and complete bottom surface of the worksheet. It was observed that the bend angle was almost equal in the last two cases and slightly lower in the first case, but it is significantly higher than the natural cooling condition. They also optimized the cooling diameter for moving circular cooling and reported that the bend angle increased with the cooling diameter, but it became ineffective after a limit. Khandandel et al. (Khandandel et al., 2021) investigated the influence of forced cooling in the laser bending of steel tubes by applying forced water cooling at different offsets to the laser heating. The results showed that forced cooling significantly reduced the processing time. However, the application of forced cooling near the heating area increased residual stresses and formed intergranular precipitation, which could potentially cause stress corrosion cracking. These residual stresses were reduced with an increase in cooling offset, thereby reducing the possibility of corrosion cracking.

The literature on cooling conditions in laser bending highlights the importance of optimizing cooling parameters to achieve desired bend angles, productivity, and material properties. Passive water cooling has shown promising results by reducing cooling time and minimizing surface oxidation. It is also observed that the forced cooling at bottom surface not only reduced the cooling time and surface degradation but also significantly increased the temperature gradient and resulted in higher bend angle. The cooling conditions, such as natural cooling, forced cooling, and underwater cooling, have demonstrated varying effects on bend angles, mechanical properties, and microstructure. Additionally, the impact of cooling conditions on edge effects and residual stresses has been studied, with mixed findings regarding their influence. Overall, the literature emphasizes the need to carefully control and optimize cooling conditions to achieve desired bend angles, productivity, and material properties in laser bending processes.

2.3. Modelling of Laser Bending Process

2.3.1. Numerical Modelling

Numerical modelling plays a crucial role in the study of laser bending by providing a means to simulate and predict the bending behavior of materials under various process parameters. These models utilize mathematical and computational techniques to simulate the thermal and mechanical phenomena that occur during laser bending, allowing researchers to gain insights into the underlying mechanisms and optimize the process. Vollertsen et al. developed the FDM and FEM models for laser bending and got the temperature distribution and bend angle. The model was limited to material properties independent of temperature. Hsiao et al. (Hsiao, 1997; Hsiao et al., 1997) developed the numerical model for the laser bending of Low-carbon steel, HY-80, HSLA steel, aluminium alloy, titanium alloy, and Inconel alloys. They measured the out-of-plane transient displacement of the plate and predicted the metal movement while laser heating, and determined the required heating pattern to achieve a predefined shape. They explained the bending mechanism with thermal stress distribution and analyzed the effect of process parameters. Kermanidis et al. (Th. B. Kermanidis, An. K. Kyrsanidi, 1997) developed a numerical model for laser bending using ANSYS code. They incorporated the temperature-dependent thermal (Conductivity, specific heat), physical (density), and mechanical properties (young's modulus, poisson ratio) by linear interpolation. The model was found to be in good agreement with the experimental results.

Odumodu and Das (Odumodu and Das, 1997) developed a numerical model by considering the Gaussian surface heat flux and double-ellipsoid power density model. The heat distribution equation is given in Equation 2-1. Where Q is the power supplied, a, b and c are the semi-axis of the ellipsoid, and x_0, y_0 , and z_0 are the start point in X, Y, and Z directions. The convective and radiative boundary conditions were incorporated by Equation 2-2. Where, h is the effective heat transfer coefficient, T is the temperature in Kelvin, ε is emissivity, and K (0.00241 to 22.72) is constant for hydrodynamic and temperature of an impinging jet.

$$q = \frac{6\sqrt{3}Q}{abc\sqrt{\pi}} e^{-3(\frac{x-x_0}{a})^2} e^{-3(\frac{y-y_0}{b})^2} e^{-3(\frac{z-z_0}{c})^2} \quad 2-1$$

$$h = K\epsilon T^{1.61} \quad 2-2$$

Ji and Wu (Ji and Wu, 1998) developed a numerical model based on the simplified mathematical model in which thermo-mechanical coupling is neglected and analysed the laser heating process only. They validated the computed FEM results with FDM and analysed that the temperature of upper and lower surfaces was increased with laser power but decreased with an increase in scanning speed and sheet thickness. Tong (Tong, 1998) performed a numerical study on the laser bending of titanium alloy using the finite element method. He used two separate codes, TOPAZ3D and LS-NIKE3D, for thermal and mechanical analysis, respectively. He predicted the surface peak temperature and bend angle using these codes for two thicknesses of titanium sheets. Shen et al. (Shen et al., 2018a, 2018b) developed a numerical model based on the minimum energy principle, including optimization to determine the strain distribution required for the target shape. Based on that strain distribution, the scanning path was planned to convert a singly curved sheet into a doubly curved sheet and vice versa Castillo et al. (Castillo et al., 2018) numerically characterized the effect of strain rate in laser bending. They reported that a strain-independent plastic model could not predict the deformation adequately, especially at high maximum temperatures. They proposed a strain rate-dependent viscoplastic model including a stress-dependent viscosity law and found that the model-predicted bend angle was in good agreement with that of the experimental, even at high maximum temperatures.

Bucher et al. (Bucher et al., 2016) conducted a numerical study on the laser bending of closed-cell Al-foam, developing three different geometry models (equivalent solid, Kelvin-cell, and voxel model) for predicting temperature and heat flow. They validated these models with experiments and reported that the equivalent solid model was the simplest and fastest but had the highest error compared to the experiments. On the other hand, the voxel model gave the best prediction with minimum error, but it was complex and took longer computation time. Kumar and Dixit (Kumar and Dixit, 2018) developed a numerical model to estimate the hardness of a laser-bent worksheet. The model incorporated factors such as strain hardening, phase transformation, and cooling rate.

The results of the model were found to be in good correlation with experimental findings of Vickers hardness.

Numerical modelling has emerged as a powerful tool in the field of laser bending, offering researchers the ability to simulate and analyze the bending process in a virtual environment. These models provide insights into the temperature distribution, bend angle, and other critical parameters, enabling process optimization and a deeper understanding of the underlying physics. By reviewing the literature on numerical modelling in laser bending, researchers can identify trends, limitations, and potential areas for further investigation, leading to advancements in this important manufacturing process.

2.3.2. Analytical Modelling

Analytical modelling plays a significant role in understanding and predicting the bending behavior of materials during laser bending processes. By formulating mathematical equations and utilizing fundamental principles, analytical models provide a simplified yet effective approach to estimating the bend angle, deformation, and other important parameters associated with laser bending. First of all, Geiger and Vollertsen (Geiger and Vollertsen, 1993) explored the mechanism behind laser bending and gave a two-layer model for the prediction of bend angle (Equation 3) and reported that the thermal expansion and worksheet thickness are the most significant factor. After that, Vollertsen et al. (Vollertsen et al., 1995) gave the first analytical model for the buckling mechanism and predicted the bend angle for the same, given in Equation 4. Mucha et al. (Mucha et al., 1997) developed an analytical model for bend angle prediction. They reported that the bend angle was dependent on the shape of the plastically deformed zone. The model was experimentally validated, and it found that the predicted data is in good agreement with the experimental. Dovc et al. (Dovč et al., 1999) proposed an analytical model for optimizing the deformation of circular plates using pulsed laser beams. They reported that the depth of plastic deformation was reduced with an increase in laser pulse radius, and the permanent deformation at the centre increased with laser pulse energy upto a limit and then started decreasing. Geiger and Huber (Geiger, and Huber, 1999) proposed a model to predict the contraction, which helps in alignment and adjustment applications.

Hao and Li (Hao and Li, 2003b) proposed an analytical model for tube bending, in which laser scanned the top half of the tube periphery. The bend angle was calculated by taking the strain difference between the scanned and unscanned regions. Imhan et al. (Imhan et al., 2017) improved the analytical model discussed above by including the temperature-dependent properties of the material and reduced the error significantly. Gou et al. (Gou et al., 2018) presented a thermal-microstructure-mechanical model that integrates thermal, mechanical, and microstructural aspects during the laser bending process. They developed this model using a temperature-controlled mixed hardening law and kinetic transformation model. The resulting model was able to accurately predict the mechanical deformation (bending) as well as the microstructural distribution in the laser-scanned worksheet. They also proposed another model for prediction of bend angle under preloading (Guo et al., 2020). Li and Wang (Li and Wang, 2019b) developed an analytical model to estimate the bending angle of laminated sheets made of stainless steel and carbon steel. They established temperature distribution equations for both material layers and estimated plastic deformation based on the recrystallization temperature of each material. The average compressive stress in the plastic zone of both materials was then calculated using the integral method. Finally, the model was further developed by optimizing the average compressive stresses and the depth of the plastic zone using mechanical equilibrium. The model was found to be in good agreement with experimental results, with an average error of 9.95%.

Mulay et al. (Mulay et al., 2020) proposed an analytical model for the prediction of bend angle. The model was based on the comparison of strain energy stored in laser irradiated area due to thermal stresses and the strain energy associated with the reactive bending moment of the sheet. The model was experimentally validated and found well aligned with an average error of 13.06%. They applied a similar approach to multi-scan laser bending and proposed an analytical model specifically for multi-scan bending as well (Mulay et al., 2021). Ye et al. (Ye et al., 2021) also derived a new analytical model for the prediction of deformation that was based on internal force balance and energy transformation. Nath and Yadav (Nath and Yadav, 2022) proposed an analytical model for estimating the temperature and bend angle. The temperature model is based on the 3D heat distribution equation, considering conduction and convection losses, and it has been validated with experimental results. Once the temperature distribution was

validated, the strain on the top and bottom surfaces was calculated. The bend angle was then predicted based on the difference between these strains.

Researchers have continuously improved and refined analytical models to enhance their accuracy and applicability. Some models have incorporated additional factors such as microstructural changes, mechanical properties, and strain energy considerations to capture the complex behavior of materials during laser bending. Analytical modelling in laser bending has also been extended to specific applications, such as tube bending and laminated sheet bending, where specialized models have been proposed to cater to the unique characteristics of these geometries. By reviewing the existing literature on analytical modelling, researchers can identify the strengths, limitations, and potential areas for further development in this important field of study.

2.3.3. Soft-computing Modelling

As discussed in the previous section, the deformation behavior of the material in the laser bending process on various process parameters makes it challenging to predict and control the final shape accurately. Soft computing is a promising tool for managing these process parameters and predicting the deformation with high accuracy. Soft computing methods, including artificial neural networks, fuzzy logic, and genetic algorithms, can be used to create models that can learn from past data and optimize the process parameters for better bending accuracy. The laser bending process can be made more efficient, cost-effective, and accurate with the integration of soft computing and leading to improved manufacturing quality and increased productivity.

Shimizu (Shimizu, 1997) proposed an algorithm to determine the heating process parameters for a given set of scanning lines to produce the predefined shape. They optimized those parameters and validated them experimentally. Giannini and Guarino (Giannini and Guarino, 2016) developed a numerical model based on fuzzy logic to describe uncertainty. The model characterized the residual bending for different parameter combinations and selected process parameters and uncertainties related to the model. This model facilitated the selection of the best operational parameters with minimal uncertainty. Esfahani et al. (Esfahani et al., 2016) applied a genetic algorithm and ANFIS to optimize the mesh density of the finite element model used for laser bending in a circular path. They found that increasing mesh density improved the

accuracy of the model, but after a limit, the accuracy did not improve much, although the computational time increased drastically. The researchers optimized the mesh density to achieve satisfactory accuracy with minimal computational time to balance accuracy and computational efficiency. Jovic et al. (Jović et al., 2017) determined the influence of process parameters using ANFIS and predicted the process parameters for maximum bending and thickening of the shaped surface. Maji et al. (Maji, 2019b; Maji et al., 2018) developed an adaptive ANFIS based model for the prediction of bending as well as thickening of the sheet. The model predictions were in good correlation with the experiments for both forward (deformation) and backward (process parameters) predictions. They also analyzed the influence of Fourier number in laser bending and reported that it is one of the key factors for the process.

Lambiase et al. (Lambiase et al., 2016) used artificial neural network techniques to optimize the process condition for maximum productivity. The ANN model was trained with experiments performed for various scanning speeds, number of scans, laser power, and cooling medium. They reported that the optimum parameters for maximum bend angle and maximum productivity are different because the cooling time between consecutive scans significantly affected the productivity. Fetene et al. (Fetene et al., 2018c) constructed an artificial neural network using an experimentally validated finite element model to generate additional data for training a radial basis function neural network. The resulting radial basis function neural network was utilized to predict the range of bend angles and was further validated, showing good agreement with the observed data. Safari and Joudaki (Safari and Joudaki, 2018) also predicted the bend angle for tailor machine blank using the artificial neural network with an accuracy of 1.1%. Other researchers also proposed the fuzzy based models and ANN for the prediction of bend angle as well as process parameter for predefined band angle (Nejati et al., 2018) (Ponticelli et al., 2018) (Safari and Joudaki, 2018) (Gisario et al., 2020) (Maji et al., 2020) (Keshtiara et al., 2021).

In the literature review of laser bending, several soft computing modelling approaches have been proposed to address the challenges in predicting and controlling the deformation behavior. Researchers have applied algorithms, such as genetic algorithms, fuzzy logic, and artificial neural networks, to optimize process parameters for achieving predefined shapes, considering uncertainties, and maximizing productivity. These

models utilize past experimental data to train and optimize the parameters, enabling accurate predictions of the bend angle and other relevant factors. The integration of soft computing with laser bending opens up opportunities for further advancements and optimizations in this field of study.

2.4. Complex Shape Generation

2.4.1. 3D Laser Bending

3D laser bending is a process that enables the formation of complex three-dimensional shapes by selectively irradiating a metal sheet with a laser beam. This technique has gained significant attention due to its ability to produce intricate geometries with high precision and efficiency. Researchers have explored various aspects of the process, including the influence of laser exposure time, scanning parameters, sheet thickness, laser power, scan speed, and scanning curve height on the deformation behavior and final shape achieved. Analytical models, numerical simulations, and experimental investigations have been conducted to better understand the underlying mechanisms and optimize the process parameters for specific bending requirements.

Chakraborty et al. (Chakraborty et al., 2016) shaped a circular blank into a bowl shape by directing a stationary laser beam at its center. They noted that the degree of deformation increased with longer laser exposure times. Shahabad et al. (Shahabad et al., 2017a, 2017b) investigated the parametric influence on the dome shape formed with laser bending. They reported that the height of the dome increased with line energy, heat flux, and laser power, whereas, it reduced with sheet thickness, beam diameter, and scan speed. Based on the numerical output they obtained an equation to predict the dome height which found to be in good agreement with experimental results.

Kant and Joshi (Kant and Joshi, 2018) attempted curvilinear bending to generate 3D complex shapes and investigate the effect of the arc height of the curved scan. They observed that bending did not occur along the scanning line; instead, the sheet was bent parallel but with an offset outside the scan line. The curve height of the scanning line significantly influenced the bending offset, bend angle, and edge effect. The bending offset increased with curve height, whereas the bend angle reduced with curve height at high power and low scan speed but increased for low power and high speed. The edge

effect was found to be reduced up to a limit but increased drastically with further increases in curve height, possibly due to warping at the free edge. Wang et al. (Wang et al., 2020) also conducted an investigation on the curvature bending of metal laminated composite plates, where it was observed that the sheet exhibited double curvature deformation. The study revealed that the bend angle increased with laser power up to 700 W and remained constant thereafter. Additionally, the bend angle decreased with an increase in scanning speed at low laser powers, while it increased at high laser power. Gisario et al. (Gisario et al., 2016b) developed a 3D complex geometry (spoon) using a high-power diode laser. The study reported that the scanning pattern significantly affects the bend angle, and scanning at an optimum distance from the worksheet edge results in a higher bend angle due to less heat accumulation at the edge. Figure 2-13 shows the spoon shape formed by laser bending and the finished product after sand blasting and spray coating.

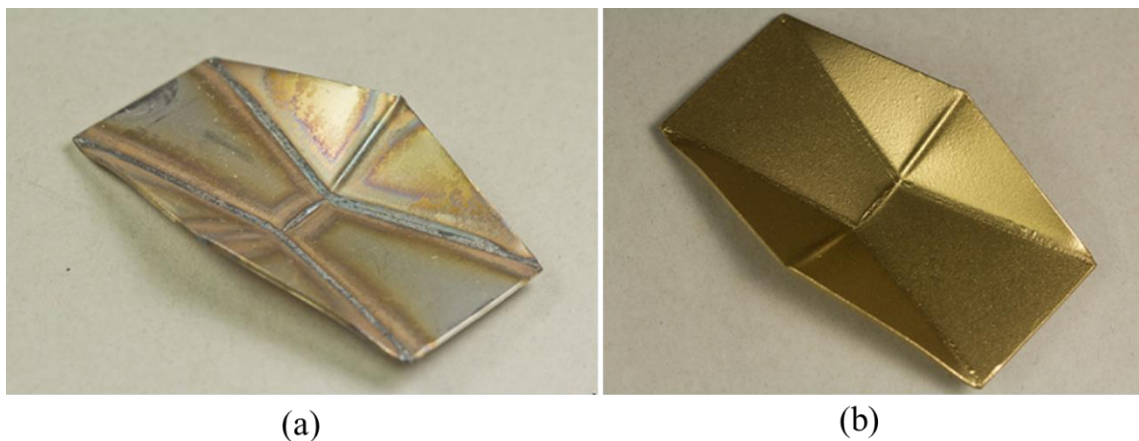


Figure 2-13. (a) 3D spoon geometry formed with laser bending (b) spoon after improved surface quality by sandblasting and spray coating

Safari and Mostaan (Safari and Mostaan, 2016) attempted to form a cylindrical surface of a particular radius of curvature by laser bending process. The worksheet was irradiated along simple linear lines parallel to each other. They developed an analytical model for the prediction of the number of scanning lines required to form a cylindrical surface of a specific radius of curvature. Abolhasani et al. (Abolhasani et al., 2019a, 2019b) attempted to create a 3D shape by using a double raster scanning approach. According to this approach, laser irradiated along multiple lines near the two long edges of the worksheet. The effect of scanning line length, beam diameter and the gap between the lines were investigated, and observed that the deformation increased with an increase in the gap between scanning lines for constant beam diameter. Whereas, the total plastic

strain reduced with an increase in beam diameter and a decrease in the gap between scan lines which resulted in lower deformation. Lazarus and Smith (Lazarus and Smith, 2018, 2017) explored the formation of 3D complex shapes from flat sheets by using laser cutting and bending simultaneously (Figure 2-14). Many other researchers also developed different 3D shapes using laser bending process (Hao et al., 2021) (Kaglyak et al., 2021) (Wang et al., 2022a) (Wang et al., 2022b).

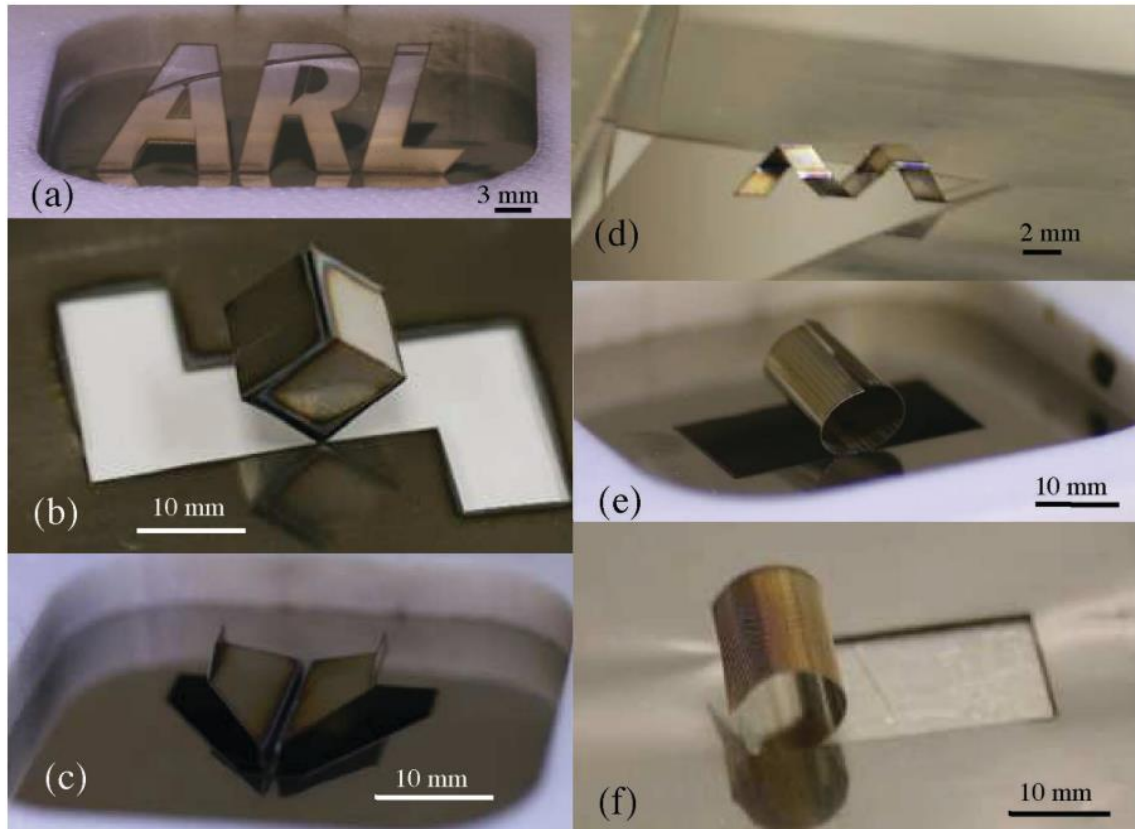


Figure 2-14. Various complex shapes generated from flat sheet

The literature on 3D laser bending demonstrates the feasibility and versatility of this technique for shaping metal sheets into complex three-dimensional geometries. Researchers have successfully achieved various desired shapes by optimizing process parameters and understanding the interplay between laser energy, scanning patterns, and material behavior. The studies highlight the importance of parameters such as laser power, scanning speed, curve height, beam diameter, and the gap between scanning lines in controlling the deformation and achieving the desired shape characteristics. Overall, the literature underscores the significance of ongoing research and development in 3D laser bending to further enhance process efficiency, control, and application versatility. Continued advancements in this field have the potential to revolutionize

manufacturing capabilities and open new possibilities for the production of complex three-dimensional components.

2.4.2. Scanning Strategies

Scanning strategies play a crucial role in the laser bending process as it determine the shape and characteristics of the final product. Researchers have investigated various scanning strategies to optimize the deformation behavior, control the shape, and improve the uniformity of the bent sheet. Hennige et al. (Hennige et al., 1997) reported that multiple scans are required to get high deformation, but the radius of curvature is also varying with the number of scans and scanning strategy. They attempted two scanning strategies in order to generate a bend angle of 30°. First approach, multiple passes along a scanning line and then move to the next one, and second approach, multiple passes along with different scanning lines placed at a particular distance from each other. The radius of curvature increased with the increase in distance between scanning lines, and the required number of scans was reduced to generate a pre-defined bend angle. Magee et al. (Magee et al., 1998c) developed a demonstrator system for the laser bending of large aluminium alloy sheets. They have attempted to form a large rectangular flat sheet into a cylinder of 900 mm radius. During this demonstration, they found that the scanning pattern, starting point of scan, direction of scan, clamping location of the worksheet, and energy input significantly affect the final geometry and dimension of the product. They found that the same scanning scheme for multiple scans leads to distortions in the sheet, and to avoid that, it needs to alter the above-mentioned variables.

Chakraborty et al. (Chakraborty et al., 2016) attempted to form a bowl shape by directing a stationary laser beam toward the center of a circular blank. They reported that the resulting shape was more symmetrical than those formed using moving laser irradiations. Cook et al. (Cook et al., 2016) attempted to form a cranial prosthesis with laser bending and compare it with the desired shape, which was taken from a CT scan of human skull. In that process, first, they observed the effect of parameters (power and scan speed) on the bend angle and determined the strain field by straightening the desired shape. Based on the strain field and parametric influence, they decided the scanning path and parameters. The scanning path is taken radially with a spacing of 1.5 mm between the scans, as shown in Figure 2-15. Gao et al. (Gao et al., 2017, 2016)

conducted a similar study on the development of ship hull shapes using a laser bending process. They deformed the initial shape into the desired shape using a virtual press in numerical simulation and extracted the strain-displacement field. Based on this data, they determined the scanning scheme, energy parameters such as laser power, and scanning speed required for achieving the desired shape.

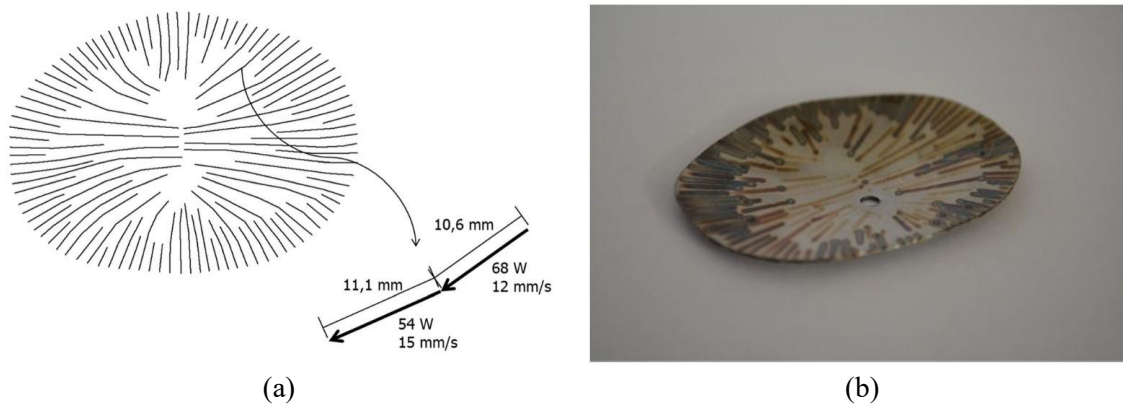


Figure 2-15. (a) Scanning scheme for manufacturing cranial prosthesis and (b) cranial prosthesis manufactured by laser bending

Dehghan et al. (Dehghan et al., 2016) attempted two different scanning strategies, radial-circular and spiral, to form a dome shape. They observed that the formed shape and stress distribution were more uniform with spiral scanning compared to radial-circular scanning. This was attributed to the fact that the bending direction during the two perpendicular radial scans was opposite, resulting in non-uniform deformation in radial-circular scanning. Yang et al. (Yang et al., 2004) explored two other scanning schemes, namely, cross spider and radial lines, on different-shaped sheets, including square, rectangular, and circular. They reported that the spider scanning pattern transforms all shapes into a dome shape, while radial scanning transforms the rectangular sheet into a saddle shape. They also observed that the dome shape formed by the circular sheet is more symmetrical than that of the square. Tavakoli et al. (Tavakoli et al., 2017a, 2017b) optimized scanning schemes for two different patterns: circular and radial, to obtain a uniform shape. They explored various scanning schemes for circular irradiation, such as clockwise (CW) or anti-clockwise (ACW), continuous and discontinuous scanning, starting from the same point or with an angular step (as shown in Figure 2-16(a)). They found that continuous CW and ACW scanning with an angular step of 180° gave better uniformity to the dome shape. Similarly, for the radial

scanning pattern, they used various schemes, such as diagonal scan or radial scan, radial scan in converging or diverging direction, radial scan crossing the center or not, with or without a 30° angular step while moving to the next scan (Figure 2-16(b)). They reported that the radial converging scan without crossing the center with a 30° angular step was the best optimum for achieving high deformation and uniform shape. In continuation of these studies, Tavalkoli et al. (Tavakoli et al., 2018) compared the circular and hexagonal scanning paths with 180° step to the start point and 30° rotation of hexagon in successive paths. They observed that the dome height achieved in hexagonal scanning was twice that of in circular case, although the edge distortion was also increased marginally. Chakraborty et al. (Chakraborty et al., 2018) investigated the mechanism behind the forming of bowl shape by radial laser scans. They revealed that the bending occurred because of two phenomena, the first is thickening along the scan line due to shrinkage, and the second one is localized buckling in the scanning region.

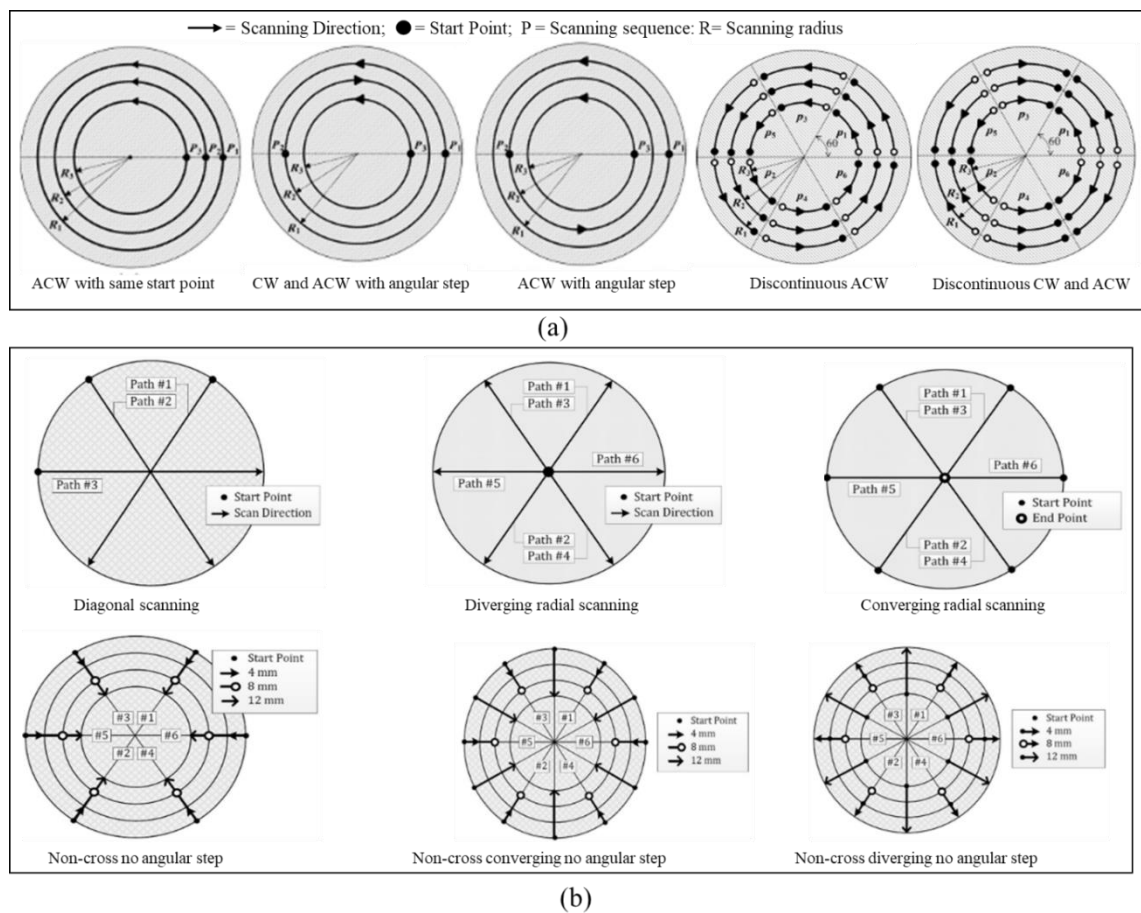


Figure 2-16: Various scanning strategies for dome shape (a) circular, (b) radial

Shen et al. (Shen et al., 2018a, 2018b) developed a numerical model for optimizing the scanning path and process parameters based on the difference between the strain

distribution of the target and initial sheet. They utilized the nonlinear deformation theory based on the minimum energy principle to optimize in-plane and out-of-plane strains, allowing the deformation of a singly curved sheet to a doubly curved sheet and vice versa. Thomsen et al. (Thomsen et al., 2019b) conducted a study on the total bend angle achieved and the smoothness of the bending curvature for various combinations of scanning lines (3, 5, 9, 15, 45) and scanning passes (15, 9, 5, 3, 1) while maintaining a constant total number of scans (45) in two different bending lengths (16 mm and 20 mm), as shown in Figure 2-17. The authors observed that higher numbers of scanning lines resulted in greater bend angles and improved smoothness for both bending lengths. Additionally, they found that longer bending lengths (20 mm) produced higher bend angles and smoother bending curvatures than shorter lengths (16 mm). Safari (Safari, 2022) compared the linear and curved scanning schemes and reported that linear scanning provided a higher bending angle with greater uniformity compared to the curved scanning scheme. Many other studies were also available in the literature which showed the influence of scanning schemes and proposed different scanning schemes to achieve a predefined target shape (Luo et al., 2020) (Khandandel et al., 2020) (Ye et al., 2020) (Safari et al., 2020b) (Safari et al., 2021) (Wang et al., 2021a).

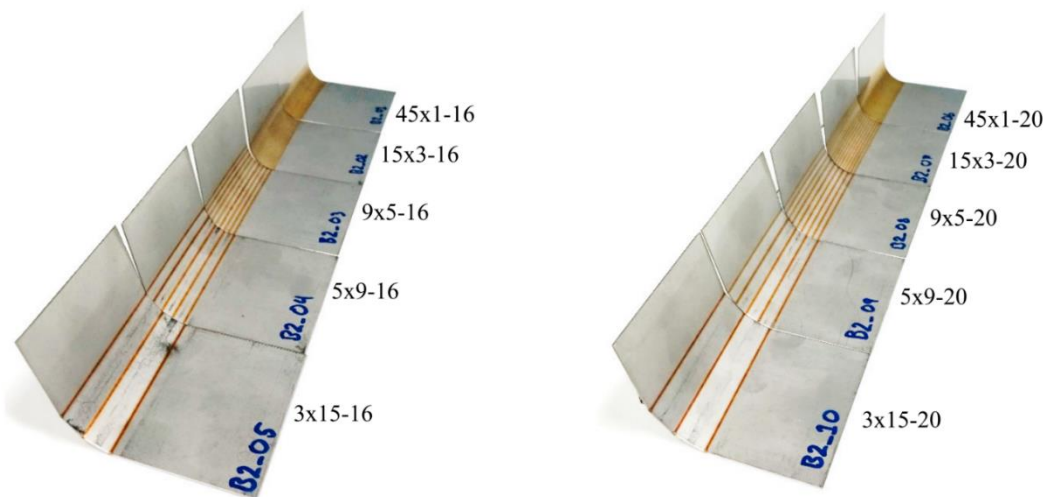


Figure 2-17. Different combinations of scanning lines, number of scans for two different bending lengths (a) 16 mm, (b) 20 mm

Researchers have investigated various scanning patterns and demonstrated their influence on the shape, bend angle, radius of curvature, symmetry, stress distribution, and overall quality of the bent sheet. The studies emphasize the importance of optimizing scanning parameters and considering factors such as scanning path,

direction, spacing, clamping location, and energy input to obtain the desired shape and minimize distortions. The continuous exploration of scanning patterns, optimization techniques, and process parameters will contribute to the development of advanced laser bending technologies and their wider application in industries such as aerospace, automotive, and manufacturing.

2.5. Materials Processed with Laser Bending

Laser bending has emerged as a promising technique for shaping various materials due to its ability to induce localized plastic deformation without the need for traditional mechanical tools or dies. This literature review focuses on the specific material processing using laser bending, exploring its applications, process parameters, and resulting effects on different materials. The reviewed literature covers a wide range of materials, including steel, living organisms, titanium, composites, aluminium alloys, ceramics, metal foam, magnesium alloys, superalloys, Inconel, and bi-metal sheets.

Steel: Steel, being a widely used material in automotive and construction industries, has been extensively investigated for laser bending. Geiger et al. (Geiger et al., 1993) suggested that laser bending is an efficient tool for straightening the car body shell made of steel (St14). Pridham and Thomson (Pridham and Thomson, 1994) made cubical prototypes of mild steel and SS304 by laser bending. Chen et al. (Chen et al., 1998a) studied the microscale laser bending of stainless steel using a pulsed laser. Castillo et al. (Castillo et al., 2018) examined the effect of strain rate during the laser bending of stainless steel sheets. They found that the strain rate-dependent viscoplastic model gives better agreement with experimental results than the rate-independent plastic model, especially for high-line energy parameters. Gisario et al. (Gisario et al., 2016b) generated a 3D spoon shape of stainless steel (AISI304) using high-power diode laser. They reported that the scanning at an optimum distance from the worksheet edge results in a higher bend angle due to less heat accumulation at the edge. Lambiase et al. (Lambiase et al., 2016) analyzed the productivity of multi-scan laser bending of AISI304. They conducted experiments to investigate the effects of various process conditions, including the number of scans, laser power, scanning speed, and cooling conditions. They trained an artificial neural network with those experimental results and determined the optimal process conditions for achieving the required bend angle with minimal processing time. Maji et al. (Maji et al., 2016) investigated the influence of

energy and geometry parameters on bend angle during multi-scan laser bending of AISI 304. They observed that the bend angle increased with laser power, number of scan and worksheet width, whereas reduced with the scanning speed. Chinizadeh and Kiahosseini (Chinizadeh and Kiahosseini, 2017) explored the laser bending of AISI316 under two different cooling conditions: natural cooling and forced cooling. They applied forced cooling using a cold plate (with a circulation of cold fluid at 0°C) placed below the worksheet. The authors analysed the bend angle, mechanical properties and microstructure in both the cooling conditions.

Titanium: Arcella et al. (Arcella et al., 1995) explored the laser bending of titanium for the first time and reported that laser bending could be a potential tool for forming titanium. Magee et al. (Magee et al., 1998b, 1997) explored the laser bending of Ti alloy and studied the influence of energy parameters on bend angle. They reported that due to the low thermal conductivity of the material temperature gradient mechanism dominated in laser bending. Tong (Tong, 1998) estimated the top surface temperature and bend angle for titanium plates of two different thicknesses using a finite element-based numerical model. Gisario et al. (Gisario et al., 2016a) attempted to bend a titanium alloy using external force-assisted laser bending and achieved an angle of 80-140° with a fillet radius of less than 2 mm. They were also able to control the spring-back up to 10 times that of mechanical bending. Froend et al. (Froend et al., 2017) attempted to bend a t-joint welded dissimilar titanium alloys (Ti-6Al-4V and cp-Ti) to compensate the deformation occurred during welding. Mjali et al. (Mjali et al., 2017) compared laser bending and mechanical bending in terms of hardness and microstructure of bent titanium sheets. They found that mechanical bending did not change the microstructure, and the hardness was also comparable to the unprocessed worksheet, whereas laser bending increased the hardness as well as grain size.

Composite: The investigation of composite materials for laser bending applications has garnered significant attention, encompassing both metal matrix composites and fiber-metal laminates. Yau et al. (Yau et al., 1996) explored the laser bending of metal matrix composite for the first time. They bent the Al-based metal matrix composite sheet by 80° in 200 scans without affecting the microstructure. Seyedkashi et al. (Seyedkashi et al., 2016) attempted the laser bending of steel-copper composite and compared it with that of steel (SUS430) and copper (C11000). They found that the copper sheet bent to

around 3°, steel to 45°, and the steel-copper composite sheet bent to nearly 10° after 20 scans. Gisario and Barletta (Gisario et al., 2020; Gisario and Barletta, 2018) explored the laser bending of fiber-metal laminates (FMLs) composite and observed that laser bending could be a viable option for the shaping of FMLs. They investigated the parametric influence on the bending of FMLs and also discussed the issues associated with the bending of FMLs, like; delamination. Liu et al. (Liu et al., 2018) conducted laser bending experiments on Cu-Ni laminated composite sheets and concluded that bending accuracy in the range of microns could be achieved without delamination. However, they also observed surface roughening in the formed region, which increased with higher laser energy supplied to the composite sheet. Li and Wang (Li and Wang, 2019a) investigated the laser bending of multilayer laminated sheets of stainless steel and carbon steel and compared with the stainless-steel sheet of the same thickness. They reported that the heat flowed in the thickness direction is less in laminated sheet as compared to stainless steel sheet due to the interfacial resistance between material layers. The depth of the plastic zone was less in laminated sheets, resulting in a lower bend angle as compared to stainless steel sheets.

Aluminium alloy: Magee et al. (Magee et al., 1998b, 1997) explored the laser bending of aluminium alloy and studied the influence of energy parameters on bend angle. They reported that the high thermal conductivity of the material leads to a low bend angle due to low-temperature gradient. The bending mechanism involved in bending Al alloy changed from temperature gradient to buckling at low scanning speed and high beam diameter to thickness ratio because of low-temperature gradient and stiffness. Ramos et al. (Ramos et al., 1998) examined the microstructure of laser bent aluminium alloy (AA2024) sheets. They introduced a term called accumulated energy density (AED) to quantify the energy supplied to the worksheet. They reported that below 25 J/mm² of AED the sub-grains were formed, and partial recrystallization occurred of aluminium alloy. In contrast, complete recrystallization and elongated crystal structure were observed between 25 to 133 J/mm² of AED. Fusion took place at a higher value of AED (133 to 25 J/mm²). Gisario et al. (Gisario et al., 2016) attempted to bend an aluminium alloy using external force-assisted laser bending and achieved an angle of 90-140° with a fillet radius of less than 2 mm. They were also able to control the spring-back up to 30 times that of mechanical bending. Siqueira et al. (Siqueira et al., 2016) investigated the laser bending of high-strength aluminium alloy AA6013-T4. They reported that for

maximum bend angle the melting should not exceed 38% of the sheet thickness. Roohi et al. (Roohi et al., 2017) explored the laser bending of the Al6061-T6 aluminum alloy and investigated the effect of process parameters. They found that the number of scans and laser power had a direct relationship with the bend angle. However, the bend angle was more sensitive to the number of scans than the laser power. On the other hand, they observed an inverse relationship between sheet thickness and scan speed. Furthermore, the bend angle was more sensitive to sheet thickness than scan speed.

Metal foam: Metal foam has emerged as a fascinating domain within materials science, offering a unique combination of mechanical properties and lightweight characteristics that render them promising candidates for various engineering applications (Changdar and Chakraborty, 2021). Their intricate cellular structures and high surface-area-to-volume ratios present novel challenges and opportunities in shaping and deformation techniques. Bucher et al. (Bucher et al., 2019a, 2019b, 2016; Bucher and Yao, 2018) attempted the laser bending of closed-cell aluminium foam and analyzed the thermal aspects of three different geometric models (equivalent solid, Kelvin-cell, and voxel model). They validated their findings through experiments and reported that although the voxel model was computationally intensive, it best predicted the temperature and heat flow. They also explored the bending of metal foam (AlSi10) with two facesheets of AW 5005 (sandwiched metal foam) and reported that the kelvin sandwich model gave better predictions in comparison to the equivalent model (Bucher et al., 2018a). Roohi et al. (Roohi et al., 2018) investigated the influence of energy parameters during the bending of closed-cell aluminum foam. It was observed that the bend angle increased with laser power and number of scans and reduced with scanning speed and beam diameter. Zhang et al. (Zhang et al., 2018) also investigated the closed-cell foam and reported similar observations. In another study, Zhang et al. (Zhang et al., 2022; Zhang and Yao, 2022) conducted a study on the energy absorption behavior and mechanical strength of laser-formed metal foam. Their findings revealed that the cells within the laser-formed specimen experienced crushing, resulting in a reduction in the energy absorption capacity compared to the as-received metal foam. It was also observed that the fatigue performance of the metal foam increased for low loads, whereas, for high load, the fatigue strength got reduced.

Magnesium alloy: Kant and Joshi (Ravi Kant and Joshi, 2016b, 2016a) explored the laser bending of magnesium M1A alloy and analyzed the effect of process parameters on bend angle, edge effect, and mechanical properties. Nath et al. (Nath et al., 2021) also investigated the bending of AM30 Magnesium alloy numerically. They studied the single as well as multi-scan laser bending and analyzed the bend angle and edge effect. They reported that the bend angle increased and the edge effect reduced in multi-scan bending.

Superalloy: Li et al. (Li et al., 2016) studied the microstructural changes that occurred in K465 Nickel-based superalloy due to the laser bending. They observed that grain boundary liquation occurred, and liquid film appeared with the increase in temperature. Yoshigai et al. (Yoshigai et al., 2016) examined the mechanical properties of a Ni-based superalloy and reported that the tensile strength had improved, but the elongation and fatigue strength had decreased after laser bending.

Inconel: Hembram et al. (Hembram et al., 2016) optimized the process parameters for the laser bending of Inconel-625. They reported that the bend angle increased with laser power and beam diameter and reduced with scanning speed.

Bi-metal sheet: Gollo and Kalkhoran (Gollo and Kalkhoran, 2017) explored the laser bending of bi-layer metal sheet (Fe/Al) and investigated the post-bending effect on mechanical, chemical, and metallurgical behaviour. They reported that laser bending was the suitable process for the bending of bi-layer metal sheets without degrading the material properties. Kotobi and Honarpisheh (Kotobi et al., 2019; Kotobi and Honarpisheh, 2018) conducted a study on the laser bending of a bimetallic sheet (steel-titanium) produced by explosive welding. They investigated the effect of energy parameters on residual stresses and bend angle variation. Their observations revealed that both the bend angle and residual stresses increased with an increase in laser power and number of scans, and decreased with an increase in scanning speed. Sharma et al. (Sharma et al., 2018) attempted the laser bending of the Nickel-Titanium sheet and observed a similar effect of energy parameters on bend angle. Nejad et al. (Masoudi Nejad et al., 2021) investigated the laser bending of aluminium-copper bimetal sheets and optimized the process parameters. Their findings indicated that the bend angle increased with laser power and decreased with scanning speed. Additionally, the bend angle initially increased and then decreased with beam diameter.

Ceramics: Chen et al. (Chen et al., 1998b) explored the laser bending of ceramics ($\text{Al}_2\text{O}_3/\text{TiC}$) using a pulsed Nd:YLF laser beam and achieved the microscale bending. Wu et al. (Wu et al., 2010b) attempted to bend different brittle materials such as Al_2O_3 , borosilicate glass, and mono-crystalline silicon. They discovered that by maintaining the substrates at elevated temperatures, they were able to prevent brittle fracture. Interestingly, the bending direction varied among the materials. For Al_2O_3 and monocrystalline silicon, bending occurred in the direction of the laser source. Whereas, for borosilicate glass, the bending took place in towards as well as away from the laser source.

Cheng et al. (Cheng et al., 2018) explored the laser bending of pseudorotaxane crystals using lasers of two different wavelengths. They reported that it could bend in opposite directions using different wavelengths without any decay. This bending occurred by Π - Π interaction between trans-azobenzene groups.

Overall, laser bending offers a versatile approach to shaping various materials, eliminating the need for conventional mechanical tools and dies. The reviewed literature highlights the effectiveness of laser bending in processing specific materials, providing insights into process parameters, bending mechanisms, microstructural changes, and optimal conditions for achieving desired bend angles. Further investigations and advancements in laser bending technology are expected to expand its applications and enhance its effectiveness in shaping a wide range of materials.

2.6. Mechanical Properties and Metallurgical Variation in Laser Bending

2.6.1. Mechanical Properties

It is essential to examine the mechanical properties of laser-formed parts to evaluate the suitability and performance of components produced through laser bending. This literature review explores the mechanical properties of laser-formed parts, including hardness, tensile strength, elongation, and surface quality. Arcella et al. (Arcella et al., 1995) explored the laser bending of titanium, and characterized the material properties. They found that the mechanical properties of the formed part are better than the ASTM specifications for C-2 titanium. Mahar et al. (Maher et al., 1998) examined the post-

bending effect on the hardness of titanium, steel, Inconel 718, and aluminium alloy and found that the hardness had enhanced for titanium, steel, and aluminium alloy however, for Inconel 718, it was unaltered.

Akinlabi and Shukla (Akinlabi and Shukla, 2016) performed the tensile test, micro Vickers hardness, and analyzed the residual stresses of laser-formed steel sheet and compared with parent material. The study revealed an 18% improvement in the yield strength of the bent sheet and a 40% increase in hardness was observed. Furthermore, the residual stresses were observed to have changed from compressive to tensile. Kurp et al. (Kurp et al., 2016) analyzed the mechanical properties and microstructure of laser-formed construction bars. They reported that the tensile strength and hardness were improved while the elongation was reduced. They also reported that martensite had been formed up to the depth of 450 to 600 μm and that the ferrite and pearlite structures were found to be refined. Maji et al. (Maji et al., 2016) investigated the variation in hardness in the irradiated region of a laser-bent stainless steel sheet. They observed that the hardness decreased while moving away from the center of the irradiated line. Furthermore, they found that the hardness varied in the thickness direction and decreased as the distance from the irradiated surface increased. Fetene et al. (Fetene et al., 2018a) investigated the mechanical properties of AH36 steel sheet that underwent laser bending. They observed an improvement in hardness within the scanning region, which decreased as the distance from the center line of the scan increased. Additionally, they found that the flexural strength of the bent sheet increased with the amount of energy provided to the sheet.

Abazari et al. (Abazari et al., 2017) investigated the mechanical properties of a laser-formed steel-copper-steel laminate composite. They found that the elongation reduced up to 30 passes, then increased for further irradiations. Similarly, fatigue life and microhardness improved in the initial scans but were reduced in the later scans. It may be due to martensite formation in the heat-affected zone (HAZ) during the initial scans, which later converted into ferrite. Gollo and Kalkhoran (Gollo and Kalkhoran, 2017) examined the chemical and mechanical behaviour after the laser bending of bi-layer sheet (Fe/Al). They found that the corrosion resistance, and tensile strength of laser bent sheet had increased with the number of scans, whereas ductility had decreased. Seyedkashi et al. (Seyedkashi et al., 2019) characterized the mechanical and

microstructural behaviour of laser-bent the stainless steel and copper-cladded sheet. There was no significant change observed in microhardness and microstructure of copper and steel layers whereas tensile and fatigue strength was found to be improved after multiple passes. Wang et al. (Wang et al., 2021b) examined the material properties of laser-formed stainless steel-carbon steel-stainless steel laminated composites sheet. The results indicated that the ultimate tensile strength of the composite increased from 562 to 582 MPa, while the yield strength improved from 395 to 455 MPa. Additionally, the microhardness of the top stainless-steel sheet exhibited a variation from 245 to 229 Hv, whereas the bottom stainless-steel sheet showed a change from 232 to 243 Hv.

Chinizadeh and Kiahosseini (Chinizadeh and Kiahosseini, 2017) investigated the influence of natural and forced cooling on the mechanical properties of AISI316. They reported that the hardness decreased during natural cooling, whereas it increased during forced cooling. This was attributed to the grain size, which increased during natural cooling and decreased during forced cooling. Sala et al. (Sala et al., 2022) investigated the surface quality of a laser-formed titanium alloy and analyzed the effect of process parameters on the surface quality. It was observed that the surface roughness increased after laser bending, and micro-cracks were also observed near the laser-processed surface. The number of micro-cracks increased with laser power density, the number of scans, and the overlap.

The literature review reveals that laser bending has a significant impact on the mechanical properties of formed parts. The findings suggest that laser-formed parts can exhibit improved mechanical properties compared to their initial states. This includes enhanced hardness, tensile strength, and yield strength in materials such as titanium, steel, aluminum alloy, and laminated composites. However, certain materials, like Inconel 718, may not experience significant changes in their mechanical properties after laser bending. Surface quality, as indicated by roughness and the presence of micro-cracks, is another crucial aspect that affects the overall performance and durability of laser-formed components. Overall, the literature highlights the importance of considering the mechanical properties of laser-formed parts, enabling informed design decisions, and ensuring the suitability and reliability of laser-formed components for diverse applications.

2.6.2. Metallurgical Analysis

Comprehensive knowledge of the metallurgical changes in laser-formed parts is essential for evaluating their structural integrity, mechanical properties, and overall performance. This literature review focuses on examining the metallurgical alterations and microstructural evolution in materials subjected to laser bending. Yau et al. (Yau et al., 1996) investigated the microstructure of Al-based metal matrix composite before and after the laser bending and found that there is no such variation in the microstructure. Magee et al. (Magee et al., 1998c) examined the metallurgical changes in laser-bent titanium alloy (Ti6Al4V) and found that acicular plates of martensite and retained β phase have formed in heat affected zone. Furthermore, these formations decreased while moving away from the center line and increased with an increase in line energy. Maher et al. (Maher et al., 1998) investigated the metallurgical alteration after laser bending of titanium, steel, Inconel 718, and aluminium alloy. They reported that α' martensite appeared in titanium, a fine microstructure was observed due to re-austenization followed by complete martensitic transformation in steel and elongated grains were observed in HAZ of Al2219, whereas no such changes were observed in Inconel 718. Fidler et al. (Fidler et al., 2019, 2018, 2017) examined the microstructural transformation of α -titanium after laser bending and mechanical bending. They found that multiple microstructural changes occurred in the material like: β to α transformation, recovery, slip, grain fragmentation, and grain boundary slide. They also reported that laser bending was more beneficial for fatigue life as compared to mechanical bending. Akinlabi and Akinlabi (Akinlabi and Akinlabi, 2017a, 2017b) investigated the microstructural changes in titanium alloy (Ti-6Al-4V) consisting of both alpha and beta phases in equiaxed and acicular form. It was found that the beta phase was present in globular form in the matrix of the alpha phase after forming, and the grain size also got fine. They also investigated the corrosion behaviour of laser formed titanium alloy and observed that best corrosion resistance was offered by parent material (Akinlabi et al., 2018).

Kurp et al. (Kurp et al., 2016) examined the microstructure of laser-bent construction bars and observed that martensite had been formed up to the depth of 450 to 600 μm , and ferrite and pearlite structures were found to be refined after bending. Gou et al. (Gou et al., 2018) predicted the mechanical and microstructural changes in laser-irradiated

DP590 dual-phase (ferrite-martensite) steel sheets using a thermal-microstructural-mechanical model. They found that the yield strength of the material improved upto 10% after five scans. This could be attributed to the transformation of ferrite into austenite during heating, followed by a conversion from austenite to martensite during cooling. Raza et al. (Raza et al., 2021) investigated the microstructural behavior of stainless steel during multi-pass laser bending, focusing on achieving varying depths of melting. The selection of specific process parameters aimed to ensure controlled melting depths. The results revealed the presence of equiaxed cellular grains within the melted region, while dendritic grains were observed in the region of interaction between the melted material and the solid substrate.

Akinlabi and Shukla (Akinlabi and Shukla, 2016) analyzed the microstructural evolution of laser-bent steel sheets and discovered that the grain size was 60% smaller compared to the parent material. Fetene et al. (Fetene et al., 2017b) investigated the laser bending of friction stir processed aluminum and mild steel sheets and compared them with cement-coated and unprocessed sheets. They found that the grain size of the friction stir processed sheet decreased after laser bending, resulting in increased hardness of both aluminum and mild steel sheets. Additionally, they reported that the hardness decreased linearly from the top to the bottom surface. Moore et al. (Ramos-Moore et al., 2021) investigated the microstructural changes during laser bending of stainless steel, interstitial free steel, and aluminium alloy. They observed grain growth and melting in the high-temperature regions.

Based on the reviewed literature, laser bending induces significant metallurgical changes and microstructural evolution in various materials. These changes include the formation of acicular plates of martensite, retained β phase, and α' martensite, as well as grain refinement and variations in grain size. The depth and extent of these metallurgical changes depend on factors such as laser energy, line energy, heat-affected zone, and material composition. Additionally, the presence of equiaxed cellular grains, dendritic grains, and grain growth in high-temperature regions was observed during laser bending. These metallurgical changes have implications for the mechanical properties, corrosion resistance, and fatigue life of laser-formed parts. Further research is necessary to gain a deeper understanding of these changes and their implications for the design and manufacturing of laser-formed components.

2.7. Sustainability Aspect of Laser Bending

Laser bending involves the controlled application of laser energy to induce plastic deformation in metal sheets, resulting in the desired shape without requiring extensive tooling or complex setups. This section explores various studies that highlight the sustainability benefits of laser bending, including reduced energy consumption, minimized material waste, improved accuracy, and environmental friendliness. Laser bending requires less energy compared to traditional bending processes, as it only heats a small area of the metal sheet, thereby reducing energy consumption and minimizing environmental impact. Additionally, laser bending reduces material waste by minimizing the need for complex tooling and reducing the number of steps involved in the manufacturing process.

Geiger et al. (Geiger et al., 1993) reported that the shape correction for a car body shell is 15 times more than its welding time and proposed laser bending for the straightening of car body shells distorted during the welding operation. It reduced the shape correction time and saved the loading-unloading time as welding and straightening could be performed at the same workstation. They also proposed closed-loop straightening, which offered good accuracy and precision and produced net shape car body shells. Geiger (Geiger, 1994) proposed the application of laser bending along with other laser materials processing like laser cutting, joining, heat treatment etc. This practice offered lower lead time as multiple operations were performed at a single station, which reduced loading and unloading time, reduced the floor area as less number of stations were required, reduced the cost and material associated with fixtures and other arrangements, and also led to efficient use of laser equipment.

Hennige et al. (Hennige et al., 1997) worked on the accuracy of laser bending; they developed a closed-loop system to control the process. They gave two strategies for close loop control; in the first one, without changing the laser parameters, they just increased the number of scans until the difference between required and achieved bend angle was less than half of the angle achieved in the last scan. In the second strategy, the laser power was changed according to the difference between the required and achieved bend angle. Results showed that they achieved an accuracy of $\pm 0.8^\circ$ and $\pm 0.2^\circ$ with the first and second strategies, respectively. This accuracy of the process makes it free of secondary operation and shape corrections and makes a sustainable option for

metal forming. Ding et al. (Ding et al., 2016) developed a laser-based measurement system for quantifying the deformation during laser bending. This system could measure deformations with an accuracy of up to 0.03 mm, which enabled precise and reliable measurements of deformation and ultimately improved product quality.

Folkersma et al. (Folkersma et al., 2016b, 2016c, 2016a) attempted the alignment of optical fibers placed in a microtube using laser bending. They successfully positioned the fibers with an accuracy of 0.1 μm and proposed laser bending as an efficient tool for micro-level alignment. They reported that this process can avoid the risk of misalignment after assembly. It also reduced the assembly complications as assembly accuracy can be relaxed upto 10 μm and make the process cost effective. Akinlabi and Akinlabi (Akinlabi and Akinlabi, 2018) reported that laser bending is a sustainable manufacturing process due to its non-contact nature and lack of toxic fumes, making it environmentally friendly and safe for all manufacturing applications. Additionally, laser bending enables complex configurations to be made, and the system can be automated, reducing the need for human intervention. These benefits make laser bending a viable and sustainable manufacturing option, contributing to the modernization and improvement of manufacturing processes.

The reviewed literature highlights the sustainability benefits of laser bending as a manufacturing process. The reduced energy consumption, minimal material waste, and decreased reliance on complex tooling make laser bending an environmentally friendly option. The ability to achieve high accuracy and precision in bending, along with the potential for automation, further enhances its sustainability. The applications of laser bending in car body straightening, shipbuilding, pipe and tube bending, optical fiber alignment, and more demonstrate its versatility and potential for widespread adoption. Overall, laser bending proves to be a sustainable manufacturing process that contributes to the advancement and improvement of modern manufacturing practices.

2.8. Applications

The application of laser bending has garnered significant attention across various industries due to its potential for the efficient shaping and forming of a wide range of materials. This literature review aims to explore the extensive research conducted in this field, highlighting the diverse applications and benefits of laser bending. The reviewed

studies encompass a broad spectrum of disciplines, including automotive manufacturing, biomedical engineering, aerospace, electronics, and rapid prototyping. Magee et al. (Magee et al., 1998a) reported that laser bending could be used for shipbuilding, pipe and tube bending, form dish and spherical shapes, rapid prototyping, flexible straightening of car body shells, adjustment and alignment of electrical and electronic components, tensioning the saw blades and forming in space.

Geiger et al. (Geiger et al., 1993) proposed the laser straightening of car body shells, distorted during the welding operation. They reported that more than 75% of the time of manufacturing a part is consumed in correction works; using laser bending process this time can be reduced significantly. Pridham and Thomson (Pridham and Thomson, 1994) suggested that laser bending can be a significant tool for prototyping and making a cubical prototype. Bachmann et al. (Bachmann et al., 2020) suggested that laser bending has the potential to be used for rapid-prototyping for metal 3D printing and lightweight metallic structure manufacturing. Geiger (Geiger, 1994) suggested to use the laser bending with other laser material processes like: laser cutting, joining, material property modification etc., which benefits in terms of reducing lead time, tooling cost, and efficient use of laser equipment. Gudur and Simhambhatla (Gudur and Simhambhatla, 2022) explored laser bending to shape additive manufactured parts. They successfully developed complex geometries that were difficult to achieve through additive manufacturing, including sharp bends, converging overhangs, multiple overhang features, and twisted profiles, as shown in Figure 2-18.

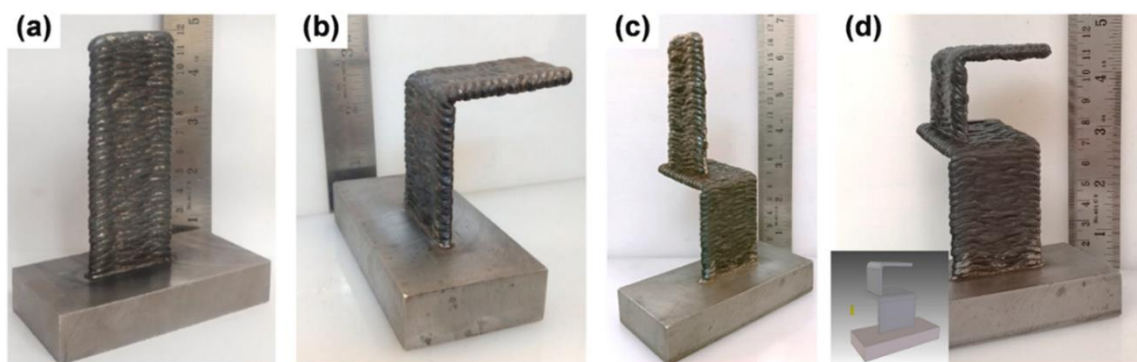


Figure 2-18. Step-by-step shape formation from additively manufactured components shaped by laser bending

Sobol et al. (E. Sobol, V. Bagratashvili, A. Omel'chenko, 1994) explored the laser bending in living organisms. They shaped the nasal cartilage successfully using a pulse and continuous both lasers. Cook et al. (Cook et al., 2016) attempted to manufacture a

cranial prosthesis with laser bending process and achieved a near-net shape with an error of 0.2 mm.

Magee et al. (Magee et al., 1997) explored the bending of aerospace materials (Ti alloy and Al alloy) and opened a new field of application for the process. Yau et al. (Yau et al., 1998) investigated the bending behaviour of thin steel alloy strips, which were used in the electronic integrated circuit leadframes. Olowinsky et al. (Olowinsky et al., 1998) reported that laser bending was used for the adjustment of relays and audio heads for electromagnetic tape decks. Bachmann et al. (Bachmann et al., 2022) employed laser bending to transform a 2D-printed circuit board into a 3D structure. They employed high laser power for cutting and low laser power for localized bending of the component, as shown in Figure 2-19. In the case of highly reflective materials, they initially oxidized the surface through laser exposure before proceeding with cutting or bending operations.

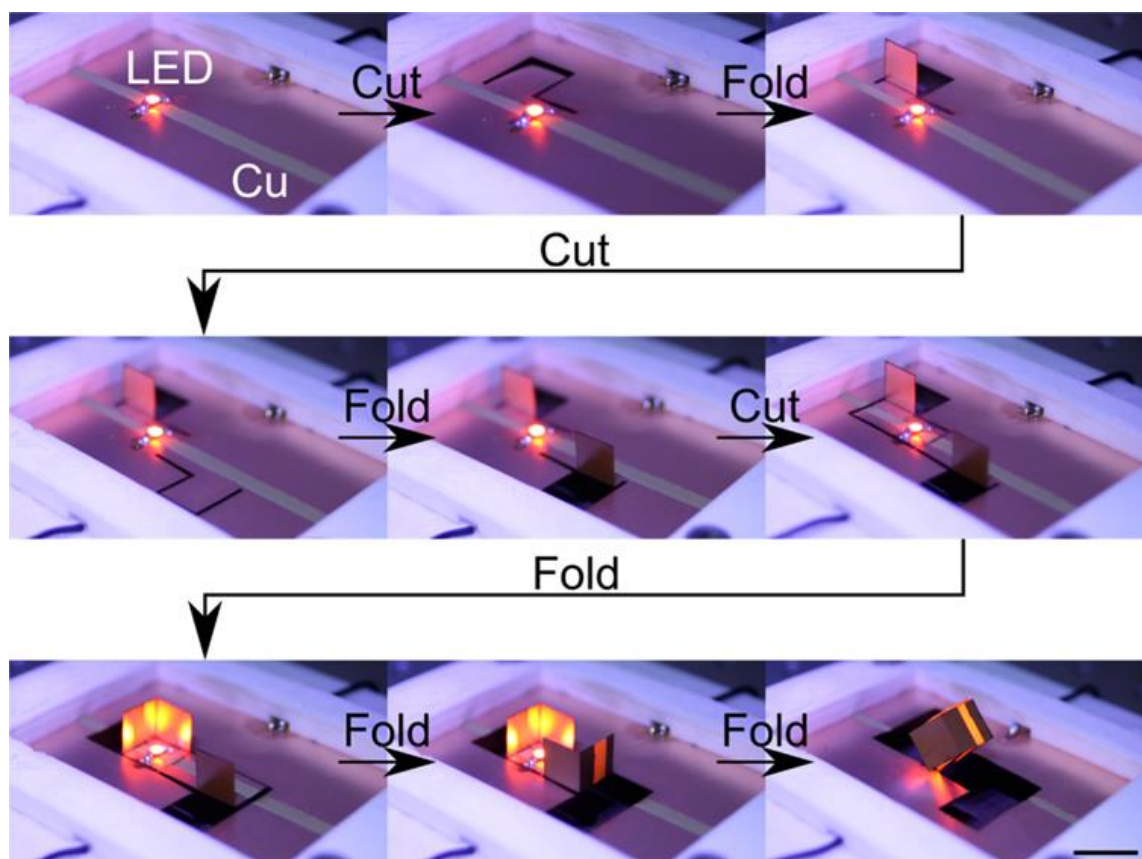


Figure 2-19. A step-by-step operational sequence on cutting and bending for the formation of cube which contained a functioning electronic circuit

Folkersma et al. (Folkersma et al., 2016a, 2016c, 2016b) explored the bending of microtube containing optical fibers for alignment. They succeeded in aligning the optical fiber to the accuracy of 0.1 μm . Smith et al. (Smith et al., 2018) attempted to

fabricate an antenna using the laser bending technique and reported that the dimensional accuracy was superior, and the design modifications were considerably easier compared to the conventional process. Woizeschke et al. (Woizeschke et al., 2018) employed laser bending for edge locking in the hemming process and observed that this process can achieve edge bending without any cracks. Fang et al. (Fang et al., 2022) proposed laser bending as a viable technique for adjusting pipe assembly. They successfully reduced the misalignment from 7.086° to 0.154° , effectively aligning the pipes for welding purposes. Ames et al. (Ames et al., 2023) attempted the formation of flexible mechanisms using the laser bending process. These mechanisms can be used in switch binary systems and for actuating mechanical parts.

The reviewed literature demonstrates the wide-ranging applications of laser bending across multiple industries. From automotive and aerospace manufacturing to medical and electronic sectors, laser bending has shown its potential in reducing lead time, improving dimensional accuracy, and enabling the fabrication of complex geometries. Further research and development in this field will uncover new opportunities and refine the existing techniques.

2.9. Challenges Associated with Laser Bending

The laser bending process presents several challenges that need to be addressed for the successful implementation of the technology. These challenges include non-uniform deformation, alteration of material properties, poor process control and repeatability, residual stresses, poor productivity, and process efficiency.

2.9.1. Non-Uniform Bending

Laser bending is a promising technique for achieving precise deformations in various materials. However, one of the challenges encountered in laser bending is the non-uniform deformation along the scan line, commonly known as the edge effect. This phenomenon poses a significant obstacle to achieving consistent and accurate bending results. Understanding and mitigating the edge effect is crucial for improving the overall quality and reliability of laser bending processes. Bao and Yao (Bao and Yao, 2001a) examined the factors contributing to the occurrence of the edge effect. They found that non-uniform heating along the scan line, caused by variations in material availability,

was responsible for this effect. The researchers observed a curvature in the bending edge, which they attributed to differential contraction between the top and bottom surfaces in the scanning direction. Specifically, they reported that the curvature was concave for BM and convex for TGM. Shen and Hu (Shen and Hu, 2013) attempted to reduce the edge effect by providing extra material at the beginning and end of the scan. This extra material helped in maintaining uniform temperature along the scan line and resulted in reduced edge effect. Jha et al. (Jha et al., 2008) reported that the edge effect was not limited to a unidirectional variation in bend angle; rather, it could exhibit multi-curvature. The researchers observed that the edge effect, or multi-curvature, was significantly influenced by the combination of laser power and scanning speed. Moreover, they found that the edge effect could be reduced by increasing the number of scans. Zahrani and Marasi (Zahrani and Marasi, 2013) studied the effect of number of scan, scan speed, beam diameter, and laser power on the edge effect. They observed that the edge effect increased with scanning speed and beam diameter, and the beam diameter was more significant. Whereas, it reduced with an increase in laser power and number of scans.

Shen et al. (Shen et al., 2010) made an effort to minimize the edge effect through the implementation of various scanning schemes: constant velocity, accelerating velocity, decelerating velocity, a combination of accelerating-decelerating velocity, and a combination of accelerating-decelerating velocity with a staircase pattern. The results indicated that the combination of accelerating-decelerating velocity with a staircase pattern significantly reduced the edge effect. Shi et al. (Shi et al., 2016) explored the reduction of the edge effect by applying an external assisting force. They reported that the application of two unequal forces on the extreme ends of the free edge resulted in a reduction of the edge effect. Overall, the edge effect poses a significant challenge in laser bending, leading to non-uniform deformation along the scan line. However, through extensive research and experimentation, various techniques have been proposed to address and reduce the edge effect. These include adding extra material at the ends of the scan line, optimizing laser power and scanning speed, increasing the number of scans, implementing specific scanning schemes, and applying external assisting forces. By incorporating these methods, researchers have made positive steps to minimize the edge effect and improve the overall quality of laser bending processes.

2.9.2. Changes in Material Properties

Some materials are highly sensitive to heat and show complex thermal and mechanical behaviours such as phase changes, recrystallization, or softening. So, it is essential to understand the material behavior under laser-induced thermal stresses to get the desired deformation with desired material properties. Knupfer and Moore (Knupfer and Moore, 2010) investigated the mechanical and metallurgical changes in laser formed low carbon steel and aluminium alloy. It was observed that the hardness and tensile strength of low-carbon steel got increased; however, the ductility reduced. The hardness was increased with an increase in the number of scans and reduced with the depth from the irradiated surface. These changes might be attributed to the dissolution of carbon in pearlite and the formation of bainite. On the other hand, the hardness and tensile strength of aluminium alloy reduced along with a reduction in ductility also. These changes were more pronounced at higher line energy due to the generation of significantly higher temperature than the recrystallization temperature of the material. Els-Botes et al. (Els-Botes et al., 2005) examined the potential of the laser bending process for manufacturing automotive wheels and investigated its effect on fatigue strength. They found that laser bending could be a viable option for manufacturing automotive wheels. The fatigue strength of the laser-bent specimen was better than the conventional manufacturing process, although it was lesser than the un-deformed material. The hardness also found to be improved because of formation of bainite and the development of a needle-like grain structure near the top surface of the material. Overall, these findings contribute to the understanding of laser bending and its potential benefits in achieving desired deformations with improved material properties.

2.9.3. Poor Process control and Repeatability

As discussed in earlier sections, there are a number of factors for which the laser bending process is highly sensitive. Precisely controlling these parameters poses a significant challenge, demanding the development of robust control strategies and real-time monitoring techniques. Many studies in the literature have addressed this issue and proposed various approaches to enhance the controllability and repeatability of laser bending. Thomson and Pridham (Thomson and Pridham, 1998, 1997a, 1997b) suggested the feedback closed-loop control system for better controllability of the process and achieved good repeatability. They controlled the number of scans required

to get predefined deformation by using the close loop system. Hennige et al. (Hennige et al., 1997) proposed the closed-loop control system and improved the process accuracy upto $\pm 0.2^\circ$ at an angle of 10° . Thomsen et al. (Thomsen et al., 2017) gave a method to calculate the error between target geometry and achieved geometry, which could be useful for 2D feedback control. The method was based on the comparison of the second derivative of the target and actual geometries. They reported that the method could help in reducing the planning time and complexity of error calculation. Thomsen et al. (Thomsen et al., 2019a) attempted to form three different shapes: V-bend, dome, and saddle, using a feedback loop. The strain distribution of the flat worksheet and the target worksheet was compared, and based on the required strain field, scanning paths were determined. The process parameters were selected according to the mechanism required for particular shape. The results indicated that the V-bend exhibited the closest agreement with the target shape, the saddle shape achieved a near net shape with some error, while the dome shape required further improvements to reach the target shape. Overall, these studies emphasize the efforts undertaken to overcome challenges in process control and repeatability in laser bending. Through the implementation of feedback control systems, error calculation methods, and careful selection of process parameters, researchers have made significant progress towards ensuring reliable and consistent bending outcomes.

2.9.4. Generation of Residual Stresses

Laser bending is a promising technique for shaping metal sheets due to its precision and efficiency. However, the generation of residual stresses during the process poses a significant challenge. Residual stresses can have a substantial impact on the final shape and dimensional accuracy of the bent component. Understanding the nature and distribution of these residual stresses is crucial for optimizing the laser bending process. Cho et al. (Cho et al., 2004) analyzed the residual stresses and strains with regard to varying factors such as the number of scans and the time interval between scans. The study revealed the presence of high tensile stresses within the laser-irradiated region, while compressive residual stresses of low magnitude were observed away from the laser-irradiated line. Furthermore, the residual strain increased as the number of scans increased. In contrast, the cooling time did not exhibit a significant influence on the residual strain. However, it was noted that the width of the heat-affected area decreased

with longer cooling times. Mjali et al. (Mjali et al., 2018) examined the residual stresses and fatigue strength of laser and mechanical-formed titanium alloy sheet and compared with the base material. It was found that the residual stresses in laser formed sheets were more tensile in nature compared to mechanical, resulting in lower fatigue strength. Kotobi et al. (Kotobi et al., 2019; Kotobi and Honarpisheh, 2018) investigated the residual stresses through the steel-titanium bimetal sheet and analyzed the effect of various process parameters. They reported that the maximum compressive stresses were generated at the interface of the metals, whereas maximum tensile stresses were developed at the bottom surface. It was observed that the residual stresses were increased with laser power and the number of scans, whereas decreased with scanning speed, beam diameter and sheet thickness. The studies highlighted the complex nature of residual stresses and their dependence on factors such as the number of scans, cooling time, laser power, scanning speed, beam diameter, and sheet thickness. Based on the findings from these studies, strategies to mitigate the detrimental effects of residual stresses can be developed and enhance the overall performance of laser bending processes.

2.9.5. Poor Process Efficiency and Productivity

Laser bending is a relatively slow process because of the low deformation compared to traditional forming methods. Increasing the process efficiency and productivity while maintaining quality is a challenge. Improving the laser power and scanning strategies, optimizing the heating and cooling rates, and forced assisted bending are some approaches to address this challenge. Majumdar et al. (Majumdar et al., 2004) investigated the relationship between bend angle and process parameters, such as the number of scans, scanning speed, sheet thickness, and laser power. They reported that the bend angle could vary from 0.5° to 70° by altering these parameters. The bend angle increased with an increase in the number of scans and laser power, while it decreased with higher scanning speeds and sheet thickness. Cheng et al. (Cheng and Yao, 2001) explored the effect of forced cooling during multi-scan laser bending. They reported that the forced cooling significantly reduced the waiting time required between two scan and resulted in higher productivity. Kant and Joshi (Kant and Joshi, 2013) attempted to enhance the process efficiency by applying and moving a mechanical load to assist in laser bending. They discovered that the bend angle was significantly improved and

further increased with an increase in the mechanical load. Despite its relatively slow nature, laser bending holds great potential for efficient and productive metal forming. The findings of the discussed literature emphasize the potential for improving process efficiency and productivity in laser bending, offering promising opportunities for future developments in the field.

2.10. Observations and Conclusions

The extensive literature review on the laser bending process has provided valuable insights into various aspects of this manufacturing technique. The review covered mechanisms of laser bending, process parameters, empirical modeling, complex 3D shape generation, scanning strategies, sustainability aspects, challenges, materials processed, and mechanical properties and metallurgical variations.

The review explored the mechanisms of laser bending, including the temperature gradient mechanism, buckling mechanism, and upsetting mechanism. Although, these mechanisms are complex and sensitive to the worksheet material and laser energy parameters. The literature provided a comprehensive understanding of the fundamental principles that underlie the bending process. It became evident that these mechanisms play a crucial role in facilitating the deformation of materials during laser bending, thereby shaping the final bent products.

The influence of process parameters on laser bending was extensively examined, including energy parameters such as laser power, scanning speed, beam diameter, line energy, number of scans, duty cycle, pulse duration, and beam shape. Material parameters, including material properties, worksheet geometry, surface condition and coating, were also found to significantly impact the bending behavior. Furthermore, the importance of cooling condition and external force assistance in laser bending process are also highlighted. It was suggested that the forced cooling and external force assistance has potential to significantly enhanced the process efficiency and productivity. Although, the process offers excellent controllability with fine tuning of these process parameters, but the number of parameters increased the complexity of the process. Optimizing the process parameters for desired deformation is challenging due to the interdependence of each parameter on the others. Therefore, further exploration is needed to optimize these process parameters.

Empirical modeling techniques, such as numerical, analytical, and soft-computing modelling, were discussed as valuable tools for predicting and optimizing the laser bending process. These modeling approaches enable process optimization and parameter selection to enhance efficiency and productivity. The exploration of complex 3D shape generation and different scanning strategies provides insights into the effects of scanning paths, ultimately offers precise and intricate bending outcomes.

The review further examined the sustainability aspect of laser bending, considering features such as automation, control, correction, and environmental friendliness. Moreover, the challenges associated with laser bending, including non-uniform deformation, alteration of material properties, process control and repeatability, residual stresses, productivity, and process efficiency, were thoroughly identified and discussed. These challenges present significant opportunities for further research aimed at exploring innovative ideas to overcome them. Notably, forced cooling has been suggested as a potential avenue for enhancing process productivity, but further exploration is required to fully realize its benefits and potential applications.

The literature review extensively investigated the application of laser bending to a wide range of materials, including steels, titanium alloys, aluminum alloys, bi-metal sheets, composite materials, metal foams, Inconel, ceramics, and super alloys. The findings indicate that the laser bending process is suitable for an extensive variety of materials, although further exploration is needed for materials having complex structures.

Moreover, the literature review examined the mechanical properties and metallurgical variations associated with laser bending. The understanding of changes in mechanical properties, such as residual stresses, hardness, fatigue and tensile strength, is crucial for ensuring desired performance and reliability of laser-bent components. The metallurgical analyses of the deformed materials also showed the changes in metallurgical characteristics. It is important to note that these mechanical and metallurgical changes will be particularly prominent in heat-sensitive materials. Therefore, there is a need for further exploration of laser bending processes applied to heat-sensitive materials in order to understand and evaluate their mechanical, metallurgical, and chemical properties. This will contribute to expanding the applicability of laser bending and optimizing the process for a broader range of materials.

The review also discussed applications of laser bending in industries such as automobile, aerospace, shipbuilding, microelectronics, and medical, highlighting its use in shape corrections, alignment, and fitting. Overall, the literature review serves as a comprehensive resource for understanding the complexities of laser bending, and it provides valuable directions for further research and development to enhance the productivity, efficiency, and applicability of laser bending for complex heat-sensitive materials in diverse manufacturing sectors.

2.11. Research Objectives

In the current study, a comprehensive review of the reported research work on the laser bending process has been carried out. The objectives of the proposed research work have been derived from the research gaps in the published literature. The overall objective of the present study is to study the effect of cooling on laser bending of duplex-2205. The specific objectives of the proposed research are as follows:

- To Design and development of experimental setup for forced cooling assisted laser bending.
- To conduct Feasibility analysis and exploration of underlying mechanism for forced cooling assisted laser bending by numerical simulation.
- To analyse the effect of forced cooling during single scan laser bending of duplex-2205 sheet.
- To analyse the effect of forced cooling during multi-scan laser bending of duplex-2205 sheet.

CHAPTER 3

PILOT STUDY

This chapter focuses on identifying the parametric range and exploring the feasibility and understanding of forced cooling assisted laser bending of duplex stainless steel. The laser bending process is highly sensitive to various parameters, leading to the need for extensive experimental analysis that can be costly, time-consuming, and prone to errors. Furthermore, obtaining in-situ information regarding the bending mechanism, bend angle increment, temperature profile, and stress-strain histories during physical experiments presents significant challenges. However, recent advancements in high-speed processing computers and user-friendly solvers have provided a cost-effective and time-efficient approach through numerical simulations to enhance our fundamental understanding of these processes. In this chapter, we develop a finite element method (FEM) based numerical model for laser bending to identify the parametric range, gain insights into the bending mechanism, and explore the feasibility of forced cooling. Additionally, a small-scale experimental study is conducted as a pilot study to test the feasibility of the proposed approach.

3.1. FEM based numerical model of laser bending

Laser bending is a thermo-mechanical process that involves the use of a high-intensity laser beam to induce thermal stresses in a workpiece, resulting in plastic deformation and bending. The numerical model aims to predict the temperature distribution, stress-strain distribution, bend angle, and edge effect during the laser bending process. The FEM solver Abaqus is utilized to develop the numerical model, taking into account various governing equations, boundary conditions, and assumptions.

Assumptions:

- Workpiece material is isotropic and homogeneous.
- Energy associated with plastic deformation is neglected.

- Effect of Bauschinger's effect and strain hardening is not considered as the bending takes place at high temperature.
- Steady-state thermal conditions at the beginning of the laser bending process.
- Effect of workpiece weight and residual stresses are negligible in comparison with induced thermal stresses.
- Gaussian distribution is followed by the laser beam for the heat flux inside the beam diameter.

3.1.1. Heat Input

The heat input given to the worksheet is provided by a moving heat flux by using the DFLUX subroutine (Appendix 3.1). The heat flux is assumed to follow Gaussian distribution inside the laser beam diameter. The heat flux distribution along the irradiated path, when the laser is moving in the Y-direction with a speed of V, is formulated by Equation 3-1 (Kant et al., 2015):

$$q(r) = \frac{2\eta P}{\pi R^2} \exp\left(\frac{-2(x^2 + (y - Vt)^2)}{R^2}\right) \quad 3-1$$

where $q(r)$ is heat flux at the radius of r , P is laser power, V is scan speed, t is time, η (= 0.375) is the absorption coefficient, and R (= 2 mm) is laser beam radius.

3.1.2. Thermal Analysis

The temperature distribution in a medium can be obtained from the law of conservation of thermal energy (also called the general form of heat diffusion), as given by Equation 3-2,

$$\rho c_p \frac{\partial T}{\partial t} = \frac{\partial}{\partial x} \left(k \frac{\partial T}{\partial x} \right) + \frac{\partial}{\partial y} \left(k \frac{\partial T}{\partial y} \right) + \frac{\partial}{\partial z} \left(k \frac{\partial T}{\partial z} \right) \quad 3-2$$

where, $k \frac{\partial T}{\partial x}$, $k \frac{\partial T}{\partial y}$ and $k \frac{\partial T}{\partial z}$ are the rate of heat transfer per unit area at the x, y, and z coordinates, ρ ($= 7800 \text{ kg/m}^3$) is workpiece material density, k is the temperature dependent thermal conductivity given in Table 3-1 (Xavier et al., 2015), T is the temperature, t is the time, c_p ($= 500 \text{ J/kg-}^\circ\text{C}$) is the specific heat (Xavier et al., 2015), $\rho c_p \frac{\partial T}{\partial t}$ is the rate of change of thermal energy. The latent heat of fusion is $30 \text{ kJ/kg-}^\circ\text{C}$ and the liquidus and solidus temperatures are 1465°C and 1410°C , respectively.

Convection and radiation heat losses account for the thermal boundary conditions. The convection heat loss is determined using Equation 3-3,

$$q_c = h(T_s - T_e) \quad 3-3$$

Where h ($=25 \text{ W/m}^2\text{-}^\circ\text{C}$) is the convective heat transfer coefficient (Ravi Kant and Joshi, 2016b), T_s is the workpiece temperature, and T_e ($= 20^\circ\text{C}$) is the environmental temperature.

The radiation heat loss is calculated using Equation 3-4,

$$q_r = \epsilon \sigma (T_s^4 - T_e^4) \quad 3-4$$

Where $\sigma = 5.67 \times 10^{-8} \text{ W/m}^2\text{-}^\circ\text{C}^4$ is the Stefan-Boltzmann constant, and ϵ ($= 0.6$) (Xavier et al., 2015) is the workpiece surface emissivity.

3.1.3. Mechanical Analysis

Laser-induced temperature gradients are responsible for the thermal stresses, leading to the deformation in the workpiece. The total strain and strain rate are calculated as a sum of elastic, plastic, and thermal strains, as given in Equation 3-5. The elastic strain rate is described by Hook's law considering Young's modulus of 200 GPa . The thermal strain is estimated by considering the coefficient of thermal expansion as $13 \mu\text{m/m}^\circ\text{C}$. The plasticity was obtained by von-mises yield criteria as given in Equation 3-6,

$$\dot{\epsilon}_{total} = \dot{\epsilon}_{elastic} + \dot{\epsilon}_{plastic} + \dot{\epsilon}_{thermal} \quad 3-5$$

$$\sigma_{eq} = \left[\frac{1}{2} \{ (\sigma_1 - \sigma_2)^2 + (\sigma_2 - \sigma_3)^2 + (\sigma_3 - \sigma_1)^2 \} \right]^{1/2} = \sigma_y \quad 3-6$$

where σ_y is the temperature dependent yield strength shown in Table 3-1 (Tavares et al., 2012; Tehovnik et al., 2016); σ_1 , σ_2 , and σ_3 are the principal stresses along direction X, Y, Z axis respectively; σ_{eq} is the equivalent thermal stress generated in the workpiece. The Von-Mises criterion indicates that when $\sigma_{eq} \geq \sigma_y$, then the plasticity starts. The workpiece is clamped at one side to avoid free body movement, which is modeled by applying zero displacements and zero rotation to the fixed edges.

3.1.4. Model Description

Numerical simulations are performed using FEM solver ABAQUS 6.18 on duplex stainless-steel sheets of size 100 mm \times 50 mm \times 2 mm. The worksheet material is considered isotropic, homogeneous, and free from residual stresses. The temperature dependent thermal and mechanical properties of the worksheet material (as listed in Table 3-1) with linear interpolation between two consecutive values are used to execute the simulations (Tavares et al., 2012; Tehovnik et al., 2016; Xavier et al., 2015). The properties are assumed to remain constant when the temperature exceeds the maximum defined temperature. The worksheet is clamped as a cantilever, and its weight is neglected. It is discretized with eight-node brick element (C3D8T) with an element size of 0.5 mm \times 0.5 mm \times 0.5 mm in the heated region, as shown in Figure 3-1. The effect of Bauschinger's effect, strain hardening, and creep are neglected, and the total strain is taken as the sum of elastic, plastic, and thermal strain.

Table 3-1. Properties of worksheet material used in numerical simulation of laser bending

Temperature (°C)	Yield Strength (MPa)	Thermal Conductivity (W/m-K)	Density (kg/m ³)	Young's Modulus (GPa)	Thermal Expansion Coefficient ($\mu\text{m/m-K}$)	Latent Heat (kJ/kg-K)	Specific Heat (J/kg-K)
20	570	16	7800	184	13	30	470
100	500	17.25		175	13		505
200	440	18.5		165	13.5		540
400	350	21		133	14		610
600	270	21		114	14.5		680
800	170	21		96	15		750
1000	55			79			750
1200	15						

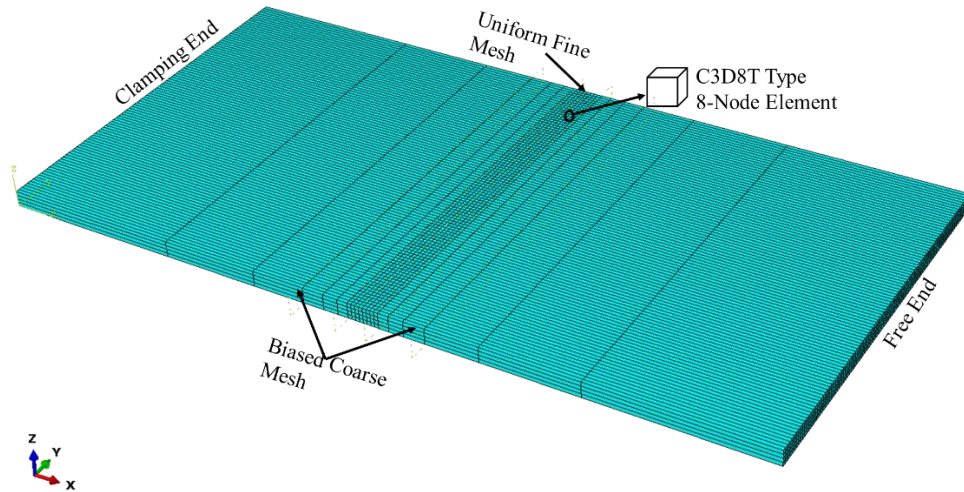


Figure 3-1. Worksheet mesh model

The energy associated with plastic deformation and microstructural changes are neglected in comparison with the laser heat input. The forced cooling is applied during laser irradiation and continued for 20 s after irradiation is completed on the surface opposite the laser source (bottom surface). It covers a 4 mm wide area throughout the width of the worksheet, as shown in Figure 3-2. The simulations are conducted for three different cooling conditions i.e. natural cooling and forced cooling with the heat transfer coefficient values of 500 W/m²-K and 1000 W/m²-K (Lambiase et al., 2013). These high values of heat transfer coefficients can be obtained by applying forced water cooling using a series of nozzles throughout the width of the worksheet. The value of heat transfer coefficient can be controlled by varying the cooling fluid flow rate. The natural cooling condition is assumed by considering the heat loss due to air convection and radiation. The heat transfer coefficient for air is taken as 25 W/m²-K (Ravi Kant and Joshi, 2016b), and emissivity for radiation is taken 0.2 with an atmospheric temperature of 20 °C. The minimum and maximum increments in time and maximum increment in temperature for a single step are taken as 1×10^{-5} s, 0.1 s, and 30 °C, respectively.

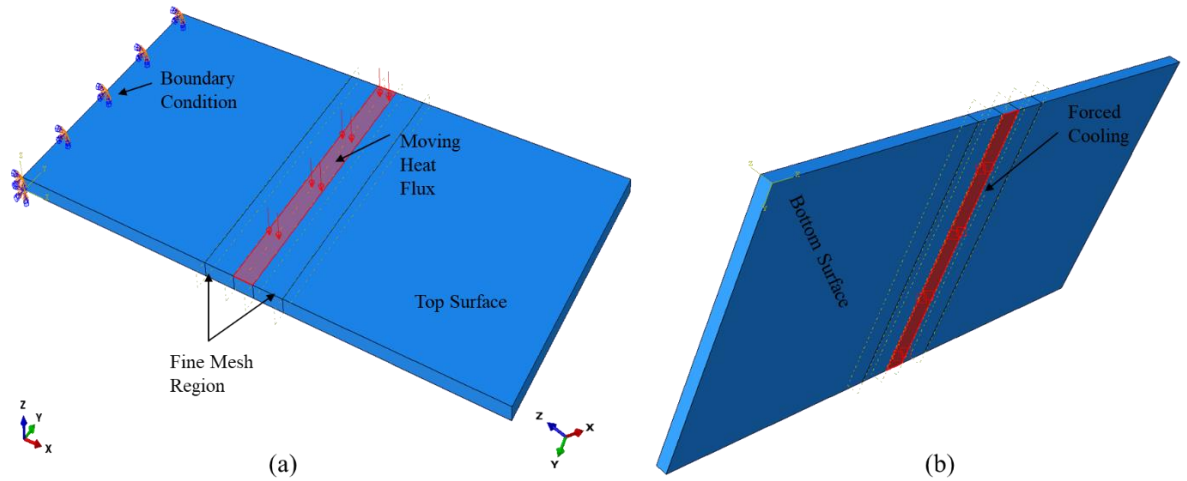


Figure 3-2. Representation of (a) moving heat flux at the top surface, and (b) forced cooling region at the bottom surface, used in numerical simulations of laser bending

The numerical model is validated with the experimental results for natural cooling conditions. The validated model is used to investigate the effect of forced cooling on the laser bending process, where only the value of the heat transfer coefficient is modified, and all other parameters are kept the same. The developed model is used to investigate the effect of forced cooling on temperature distribution, stress-strain distribution, bend angle, and edge effect.

3.1.5. Input Parameters

The numerical simulations are carried out for natural and forced cooling conditions at different line energies (25 – 60 J/mm) and laser powers (250 – 1000 W), as shown in

Table 3-2. Line energy is defined as the energy supplied per unit length to the scan line. The beam diameter is kept constant throughout the numerical study. The respective scanning speed for a particular line energy and laser power can be calculated by using Equation 3-7. All these input parameters (laser power, scanning speed, beam diameter, beam shape, heat flux distribution, and position of the scanning line) are defined by using a DEFLUX subroutine given in Appendix 3.1.

$$\textbf{Scanning Speed} \left(\frac{\text{mm}}{\text{s}} \right) = \frac{\textbf{Laser Power (W)}}{\textbf{Line Energy} \left(\frac{\text{J}}{\text{mm}} \right)} \quad 3-7$$

Table 3-2. Process parameters for numerical simulations of the laser bending process

Case	Cooling Condition	Line Energy (J/mm)	Laser Power (W)
1	Natural Cooling ($h = 25 \text{ W/m}^2\text{-K}$)	25, 30, 35, 40, 45, 50, 55, 60	250, 400, 600, 800, 1000
2	Forced Cooling ($h = 500 \text{ W/m}^2\text{-K}$)	25, 30, 35, 40, 45, 50, 55, 60	250, 400, 600, 800, 1000
3	Forced Cooling ($h = 1000 \text{ W/m}^2\text{-K}$)	25, 30, 35, 40, 45, 50, 55, 60	250, 400, 600, 800, 1000

3.1.6. Experimental Validation

The developed model is validated by conducting experiments on duplex stainless steel (AISI-2205) sheet of dimension $100 \text{ mm} \times 50 \text{ mm} \times 2 \text{ mm}$. The absorptivity of the irradiated area is enhanced by applying graphite coating in the irradiation region. The experimental setup is explained in Chapter 4. Each set of experiments is repeated three times, and the average value is considered for process outcome. As laser bending is a thermo-mechanical process, the developed numerical model is validated with both thermal (temperature) and mechanical (bend angle) outcomes. The variation in experimental values is presented by the coefficient of variation (CV), and it is calculated as a ratio of the standard deviation to the average value.

Table 3-3. Comparison of experimental and simulation results at 250 W laser power

Line Energy	Bend Angle				Maximum Temperature			
	Θ_E	% CV	Θ_S	% Error	T_E	% CV	T_S	% Error
25	0.873	5.19	0.870	-0.31	1271.11	11.09	1223.52	-3.74
30	1.037	7.38	1.095	5.55	1327.6	13.96	1296.46	-2.35
35	1.297	3.95	1.308	0.86	1397.63	8.55	1360.95	-2.62
40	1.403	2.99	1.497	6.72	1428.85	7.44	1406.11	-1.59
45	1.657	5.83	1.645	-0.7	1489.14	5.74	1467.78	-1.43
50	2.014	2.38	1.75	-13.09	1605.68	6.80	1519.23	-5.38
<p>* Θ_E = Average bend angle obtained from experiments Θ_S = Bend angle obtained from simulation results T_E = Maximum temperature recorded experimentally T_S = Maximum temperature obtained from simulation results</p>								

The experimental results are found to be in good agreement with the numerical results in terms of bend angle and temperature of the top surface, as shown in Table 3-3. The average error between numerical and experimental results is found to be 4.54% with a maximum error of 13.09% at 50 J/mm line energy. The higher error at 50 J/mm line energy is a result of the melting of the worksheet, which led to the uncontrolled metal flow in the heated region, which is not incorporated in the numerical simulations. Figure 3-3 shows the laser-scanned surfaces with 45 and 50 J/mm line energy at 250 W laser power. It is observed that a minor melting has occurred at 45 J/mm line energy; however, a significant melting can be observed at 50 J/mm line energy. The temperature in the numerical model is validated with experiments by taking the average of five maximum temperatures along the scan line. The maximum temperature at the top surface obtained from the numerical and experimental results are in good agreement with an average error of 5.38%.

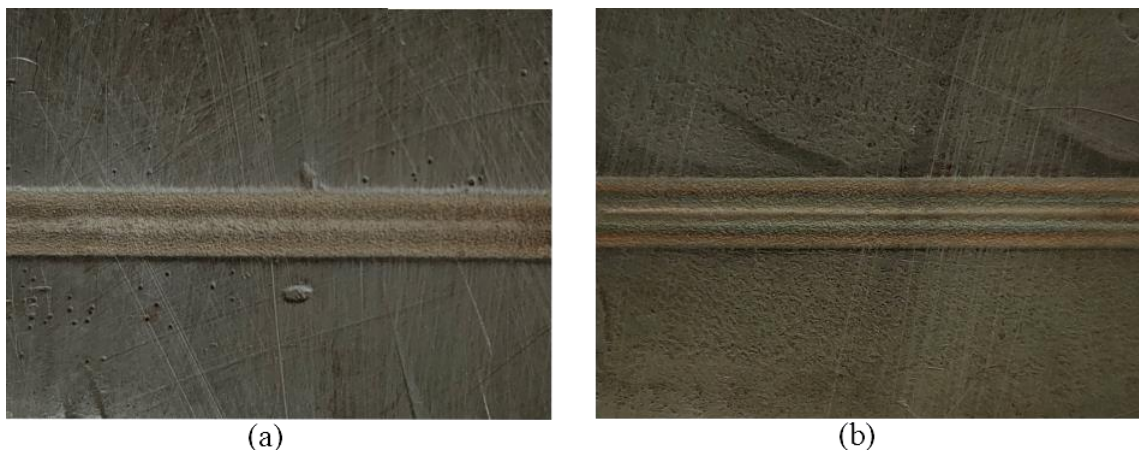


Figure 3-3. Laser scanned surface at 250 W laser power (a) 45 J/mm line energy (b) 50 J/mm line energy

3.2. Exploration of Underlying Bending Mechanism

Numerical Simulations have been carried out for a deep understanding of the process by exploring the temperature and stress-strain distributions and the effect of process parameters, i.e., laser power and scanning velocity, on bend angle and edge effect.

3.2.1. Temperature Study

The temperature distribution along all three axes of the workpiece is discussed in this section. The temperature gradient along the thickness is the principal cause of bending in the temperature gradient mechanism. Figure 3-4(a) shows the variation of maximum

temperature along the thickness of the workpiece at the starting, center, and end of the scan line. It is observed that the maximum temperature decreases polynomially (4th order) along with the thickness. It is also observed that there is a significant difference in the maximum temperature at the start, center, and end of the scan line. It is because of changes in preheating temperature and thermal constraints.

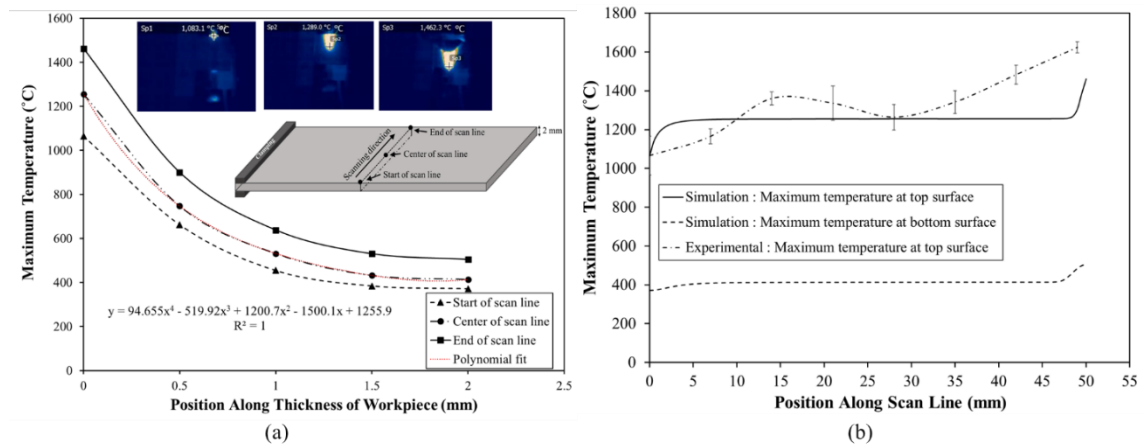


Figure 3-4. Maximum temperature variation at 250 W laser power and 30 J/mm line energy (a) along the thickness (b) along the scan line

The maximum temperature along the scan line at the top (scanned) and bottom (opposite to scanned) surface is shown in Figure 3-4(b). The maximum temperature is nearly constant along the scan line except at the extreme positions where it varies at a high rate. The geometrical and thermal conditions are different at the beginning and end of the irradiation. The maximum temperature increases as the laser beam irradiates over the workpiece becomes almost constant along the scanning path, and increases significantly near the end. There is no heat conduction at the extreme ends, leading to heat accumulation at that point which results in the heat sink effect.

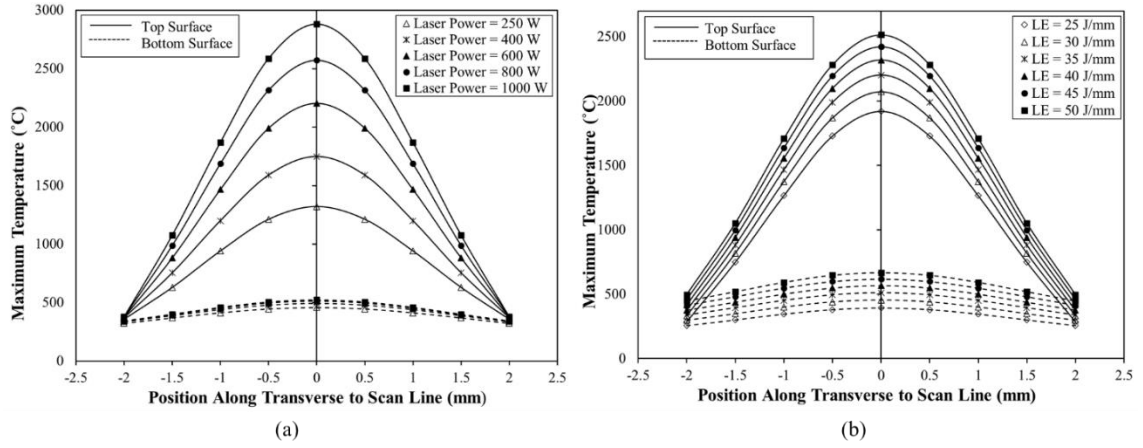


Figure 3-5. Maximum temperature variation along the transverse to scan line at (a) different laser powers at 35 J/mm line energy (b) different line energies at 600 W laser power

The variation of the maximum temperature along the transverse direction to laser scan and in the region of beam diameter at the top and bottom surfaces are shown in Figure 3-5(a) and (b). The centerline of the scan is referred as zero position, and variation is shown up to the radius of the beam on both sides. It is observed that the temperature profile follows Gaussian distribution along the beam diameter. For a specific temperature, the temperature distribution inside a beam diameter becomes wider with the increase in laser power, which leads to a larger bend angle. Furthermore, at particular line energy, the maximum temperature at the top surface increases significantly with an increase in laser power. However, the increase in temperature at the bottom surface is marginal. The variation in maximum temperature at the top and bottom surfaces is comparable when line energy is increased at a constant laser power, as shown in Figure 3-5(b). Therefore, the temperature gradient is increased more significantly with laser power than the line energy, as shown in Figure 3-6(a) and (b), respectively.

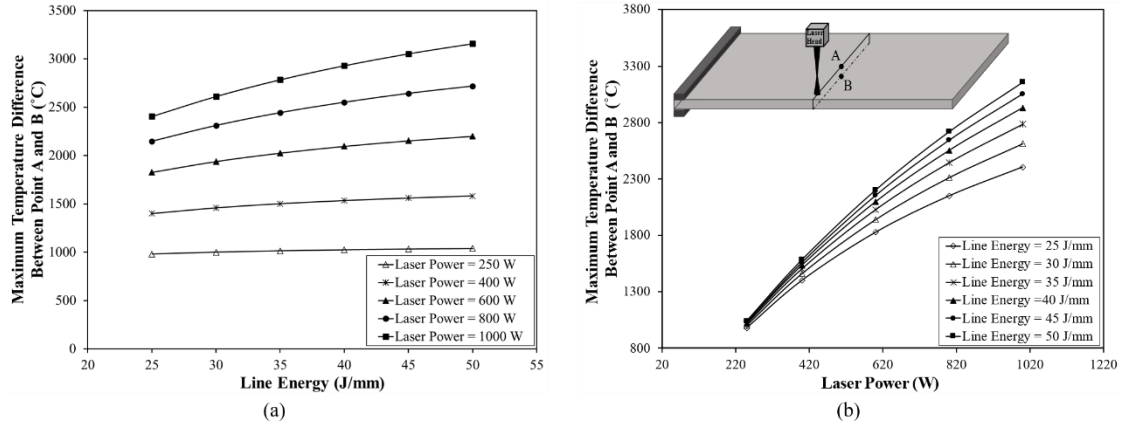


Figure 3-6. Maximum temperature difference between Point A and B with (a) line energy at different laser powers (b) laser power at different line energies

3.2.2. Bend Angle Analysis

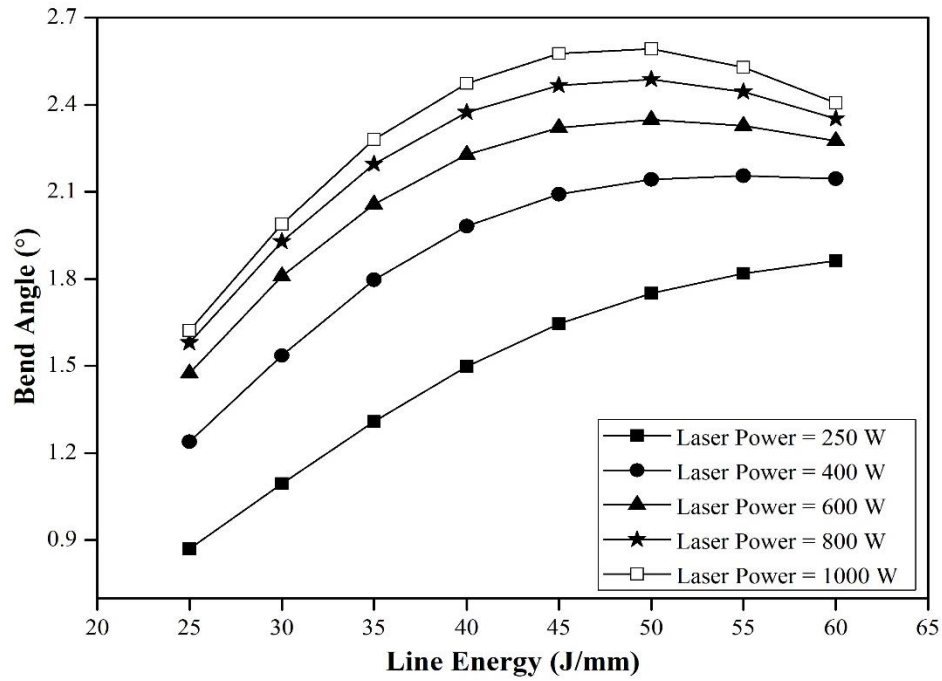


Figure 3-7. Bend angle with line energy at different laser powers

At low laser powers, it is observed that the bend angle increases with an increase in the line energy. However, the increment rate continuously decreases, and the bend angle varies marginally at higher line energies, as shown in Figure 3-7. On the contrary, the bend angle first increases, attains a peak, and then decreases with line energy at high laser powers. In TGM, bending occurs due to the difference between plastic strain at the top and bottom surfaces (Ravi Kant and Joshi, 2016a). When the line energy increases, the maximum temperatures of both Point A and B increase, leading to an increase in

compressive strain at both Points A and B. The tensile strain at Point B decreases due to the generation of compressive stresses at the bottom surface. Up to line energy of 40 J/mm, this decrease in tensile strain is insignificant compared to the increase in compressive strain at the top surface, as shown in Figure 3-8. The net difference between the top and bottom plastic strains increases, which leads to a larger bend angle (Ravi Kant and Joshi, 2016b). The further increase in line energy leads to a decrease in the net difference in the plastic strain, which decreases the bend angle. Figure 3-7 also shows that the bend angle increases with the increase in laser power; however, the increment rate decreases. It is because, at constant line energy, the scanning speed also increases with laser power which increases the temperature gradient. The scanning speed should also be optimized because, at a very high scanning speed, the bend angle starts decreasing because of the reduction in laser-worksheet interaction time.

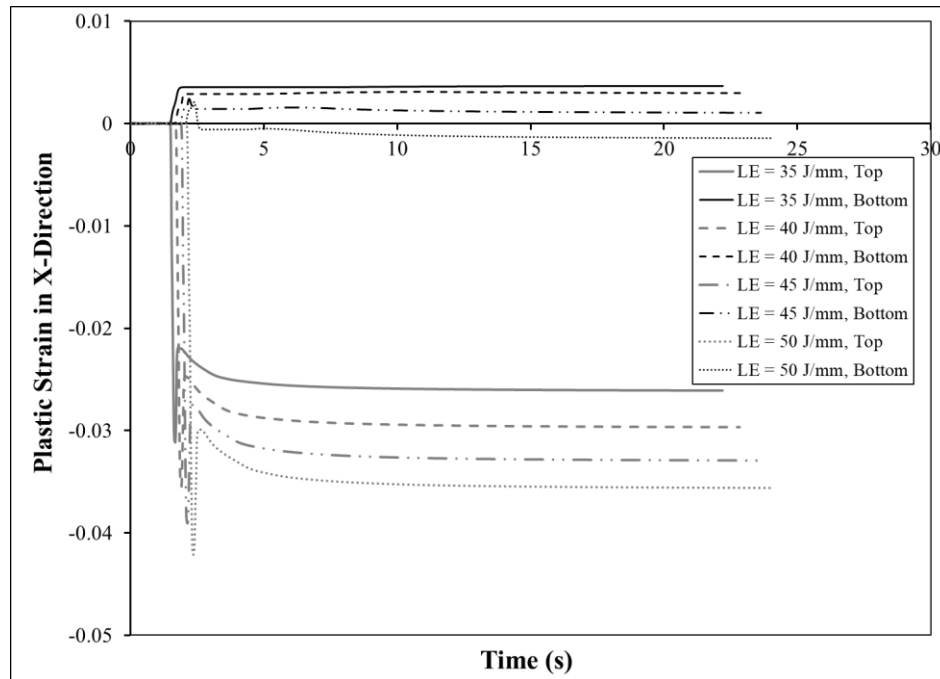


Figure 3-8. Plastic strain history of Points A and B, For different line energies at 600 W laser power

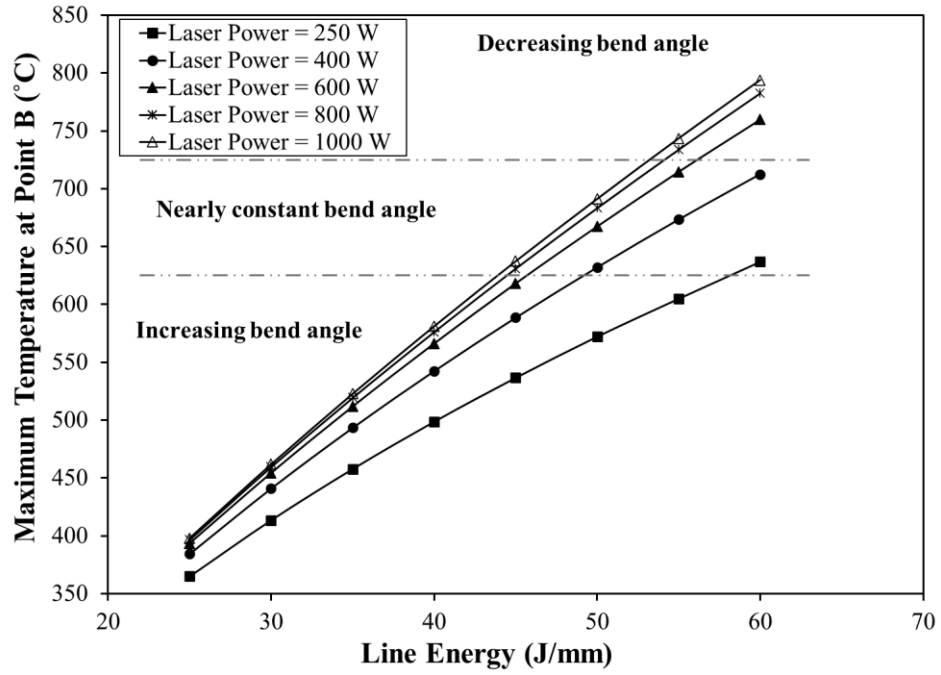


Figure 3-9. The maximum temperature at Point B with line energy at different laser powers

It is also observed that when the maximum temperature at Point B reaches above 625 °C, the bend angle changes marginally, and the further increase in temperature (above 725 °C) leads to a decrease in bend angle, as shown in Figure 3-9. It is because, above 625 °C temperature, the change in the plastic strain at Point A and B is almost equal and leads to a nearly constant bend angle. As soon as the temperature exceeds over 725 °C, the change in the plastic strain at B is more significant than A, which tries to bend the sheet away from the laser source. The net difference in plastic strain decreases and leads to a decrease in bend angle.

3.2.3. Edge Effect

The edge effect shows the variation in the bend angle along the scanning path. It occurs as a result of non-uniform temperature distribution and material constraint along the scanning line (Bao and Yao, 2001b; Shi et al., 2016). The bend angle is measured at three different points along the scan width to quantify the edge effect and is calculated by the following expression (Equation 3-8) (Esmail Ghadiri Zahrani, 2013),

$$\text{Edge Effect} = \frac{\theta_{\max} - \theta_{\min}}{\theta_{\text{avg}}} \quad 3-8$$

where, Θ_{\max} , Θ_{\min} , and Θ_{avg} are the maximum, minimum, and the average of bend angles along the scan line (width), respectively.

The edge effect is mainly generated because of the uneven energy distribution along the width. It is observed that the edge effect increases with an increase in line energy at all the laser powers and it increases with laser power at different line energies, as shown in Figure 3-10. It is because the laser beam is focused on a very small area, due to which a large amount of energy is supplied in a small area, resulting in an uneven distribution of heat with the increase in laser power. It causes more variation in the temperature and plastic strain gradient along the scan line. The edge effect increases with scanning speed at constant line energy because heat distribution is more uniform at lower scanning speed.

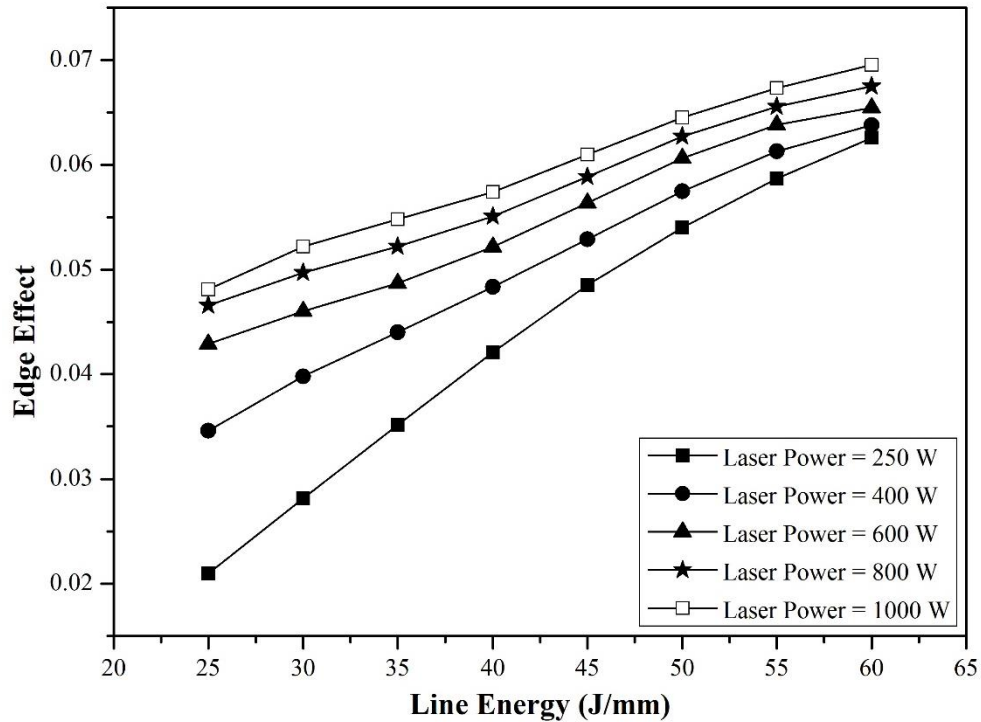


Figure 3-10. Edge effect with line energy at different laser powers

3.2.4. Mechanical Analysis

The effect of laser scanning on mechanical properties is analyzed by conducting micro-tensile and microhardness tests. The specimens are cut along the scan line from the laser-scanned workpieces for the tensile testing, as shown in Figure 3-11 (Ravi Kant and Joshi, 2016a). The tensile tests are performed on a micro-tensile testing machine with a load cell of 10 kN and an elongation rate of 8 $\mu\text{m/s}$. The stress-strain curves for base

material and laser-bent specimens at different line energies are shown in Figure 3-12. It is observed that the ultimate strength of the laser-bent specimens is almost equal to the base material, whereas the ductility of the laser-scanned specimens is reduced. It is also observed that the ductility decreases with an increase in the line energy. The hardness is measured in the laser-scanned region at a load of 500 g and a dwell time of 10 s. The hardness of the base material varies between 259 to 267 HV in 15 observations, and the average (263 HV) is considered as the hardness of the base material. Similarly, the number of indents is taken on each laser-scanned specimen along the scan line, and the average is calculated for particular specimens. It is found that the hardness of scanned specimens is greater than that of the base material, and it increases with an increase in line energy, as shown in Figure 3-13. A similar trend was observed in other studies for SS316 (Majumdar et al., 2004), mild steel (Fetene et al., 2018b; Thomson and Pridham, 2001) and aluminium alloy (Merklein et al., 2001).

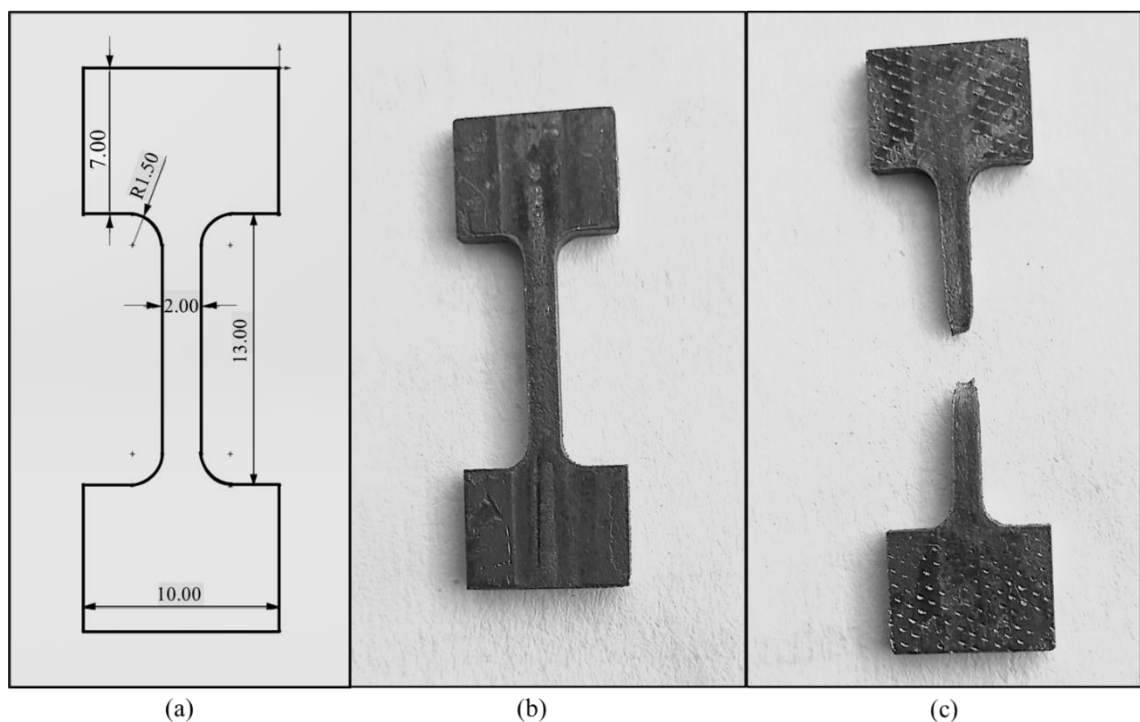


Figure 3-11. (a) Dimensional schematic of tensile specimen, (b) laser scanned tensile test specimen before the test and (c) after the test

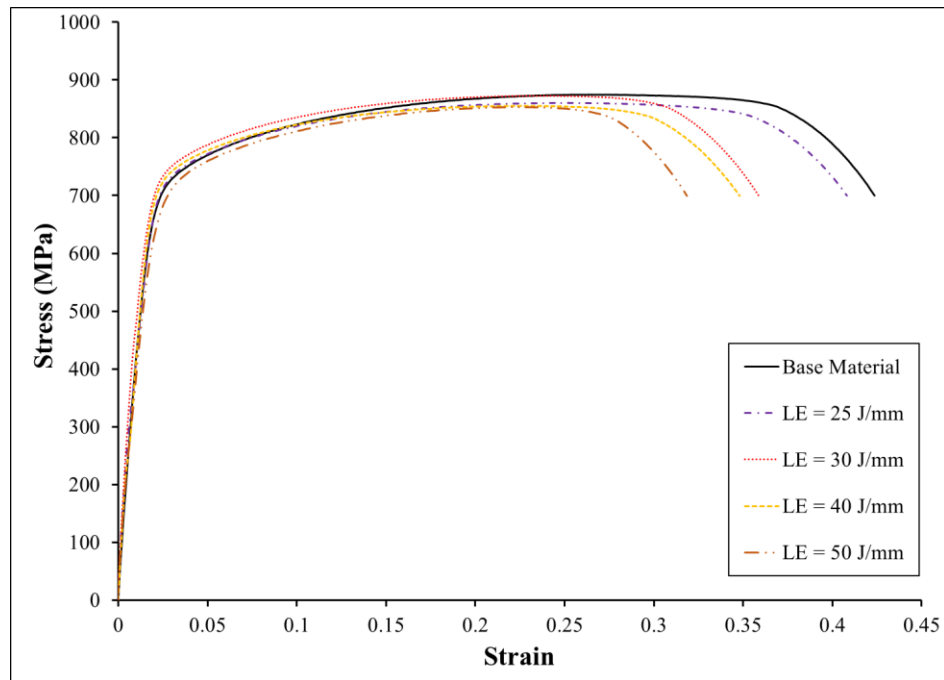


Figure 3-12. Stress-strain curves obtained from the tensile test of specimens, scanned at 250 W laser power and different line energies

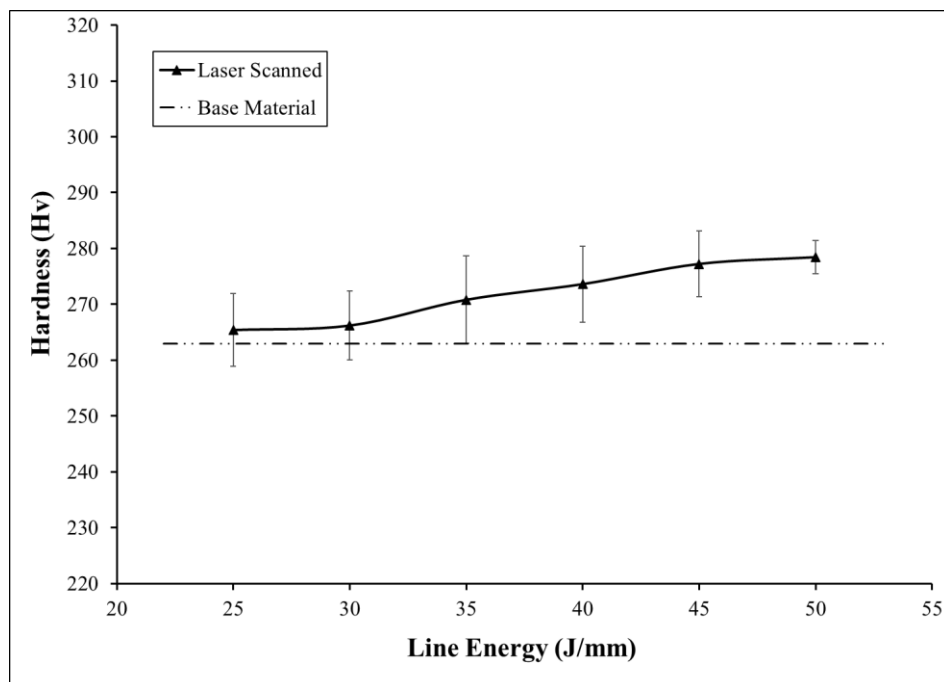


Figure 3-13. Hardness with line energy at 250 W laser power

Microstructural analysis has been done to investigate the possible reasons for variation in mechanical properties. Duplex stainless steel consists of two phases α -ferrite (dark) and γ -austenite (bright), as shown in Figure 3-14(a). Duplex is a heat-sensitive material because during hot working ferrite undergoes dynamic recovery (Choudhary et al., 2013), leading to developing subgrains (Tehovnik et al., 2011), and austenite undergoes

a high degree of strain hardening and the grain recrystallization (Jorge et al., 2011). It is also aggressive to form intermetallic precipitations because of high Cr and Mo and higher diffusion rate in ferrite (Tehovnik et al., 2016). Figure 3-14(b) shows the subgrain formation in the ferrite phase and the formation of the σ -phase because of the laser heating with 30 J/mm line energy. The σ -phase can be formed by eutectoid decomposition of ferrite ($\alpha \rightarrow \sigma + \gamma$) or σ formation from austenite ($\gamma_1 \rightarrow \sigma + \gamma_2$) (Pohl et al., 2007). It is observed that the proportion of the sigma phase (white) increases and ferrite (dark) decreases with an increase in line energy, as shown in Figure 3-14(c). The sigma phase is harder and brittle in nature, leading to decreased ductility and increased hardness.

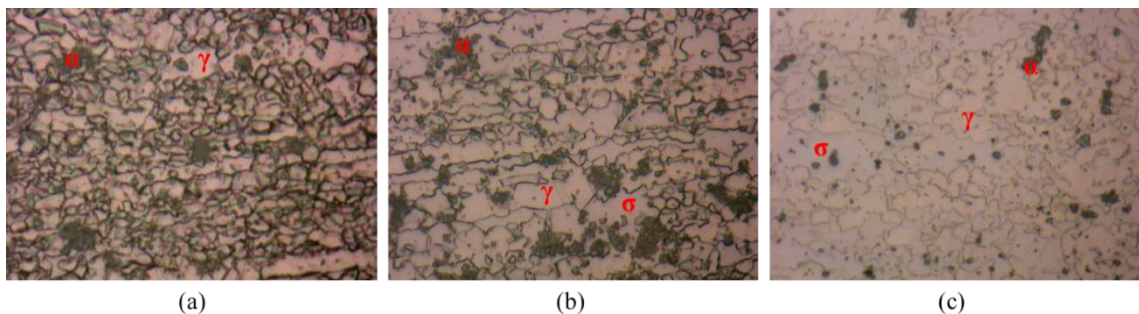


Figure 3-14. Microstructures of duplex stainless steel at different scanning conditions (a) No irradiation (b) irradiation with 30 J/mm line energy (c) irradiation with 50 J/mm line energy

3.2.5. Relation of temperature variation with bend angle and mechanical properties

In this section, the variation of bend angle and mechanical properties are studied with respect to the temperature. Figure 3-15 shows that the bend angle increases with increase in maximum temperature at Points A and B. It is observed that at particular line energy, the rate of increase in bend angle decreases with a increase in temperature at Point A, as shown in Figure 3-15(a). At particular line energy, the maximum temperature at A is increased by increasing the laser power, which further increases the scanning speed to maintain the constant line energy. Initially, the increase in scanning speed increases the temperature gradient, which leads to a drastic increase in bend angle. The further increase in scanning speed leads to lower interaction time which reduces the rate of increase. It is also observed that the bend angle starts decreasing with line energy at high temperatures. It is because the scanning speed is lower at high line energies, which

significantly increases the temperature at B, as shown in Figure 3-15(b). It leads to the generation of compressive plastic strain at B, which tries to bend the sheet away from the laser source.

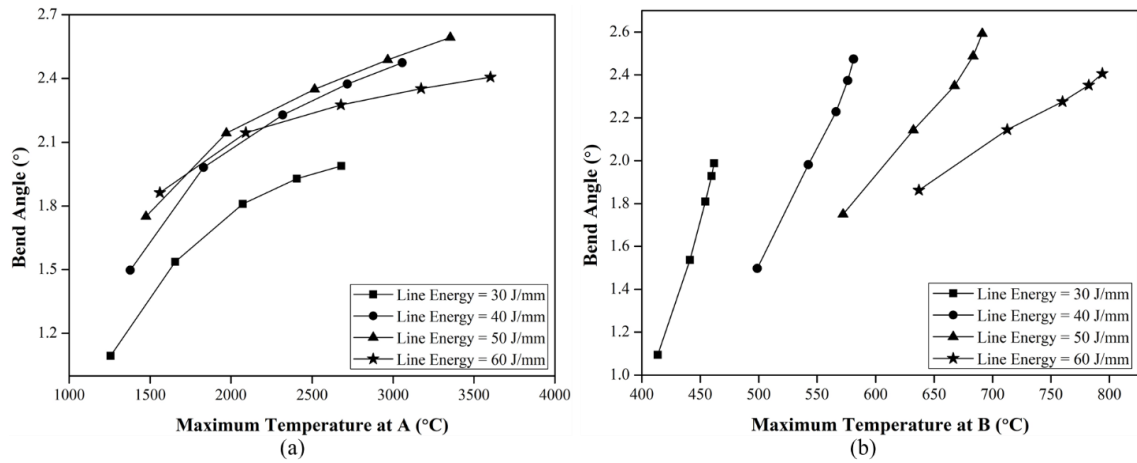


Figure 3-15. Effect of maximum temperature on bend angle at different line energies

Figure 3-16 shows that the hardness increases with temperature at Point A, whereas the breaking strain decreases. It is because of the formation of σ precipitation which is hard and brittle in nature. At a particular laser power, the temperature is increased by decreasing the scanning speed, which further increases the laser-worksheet interaction time, leading to a coarser sigma phase. Santos et al. (Dos Santos and Magnabosco, 2016) also reported that coarse grains in the sigma phase are formed at higher temperatures and longer heating time.

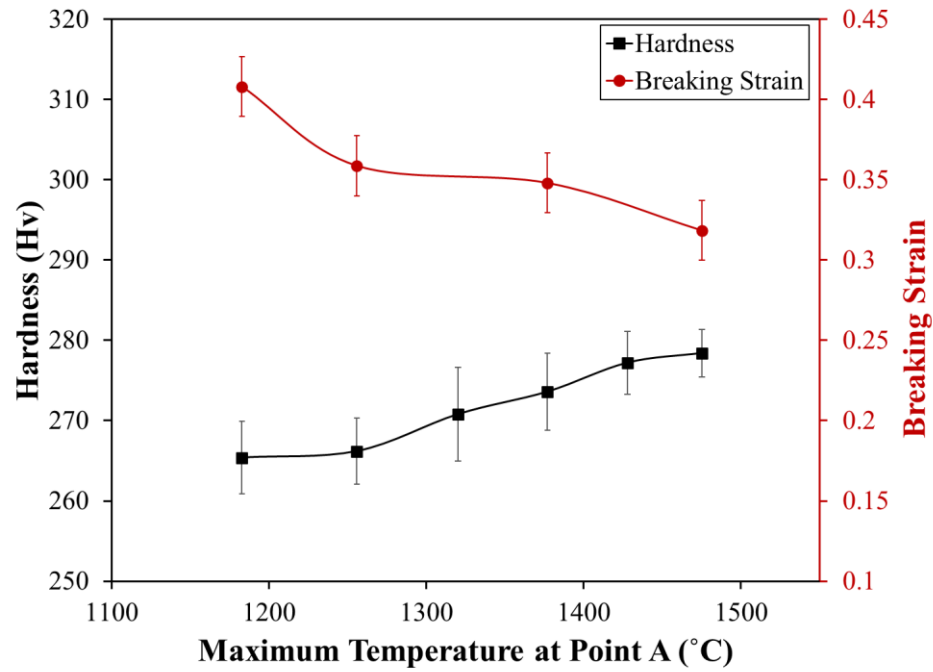


Figure 3-16. Effect of maximum temperature on hardness and breaking strain at 250 W laser power

3.3. Numerical Feasibility Analysis of Forced Cooling Assisted Laser Bending

3.3.1. Effect of cooling on bend angle

The effect of line energy on bend angle for natural and forced cooling condition is shown in Figure 3-17. It is observed that the bend angle increases with an increase in line energy, attains a peak, and starts decreasing at higher line energies for almost all laser powers. It is because the net difference between plastic deformation at top and bottom surfaces starts decreasing at higher line energies.

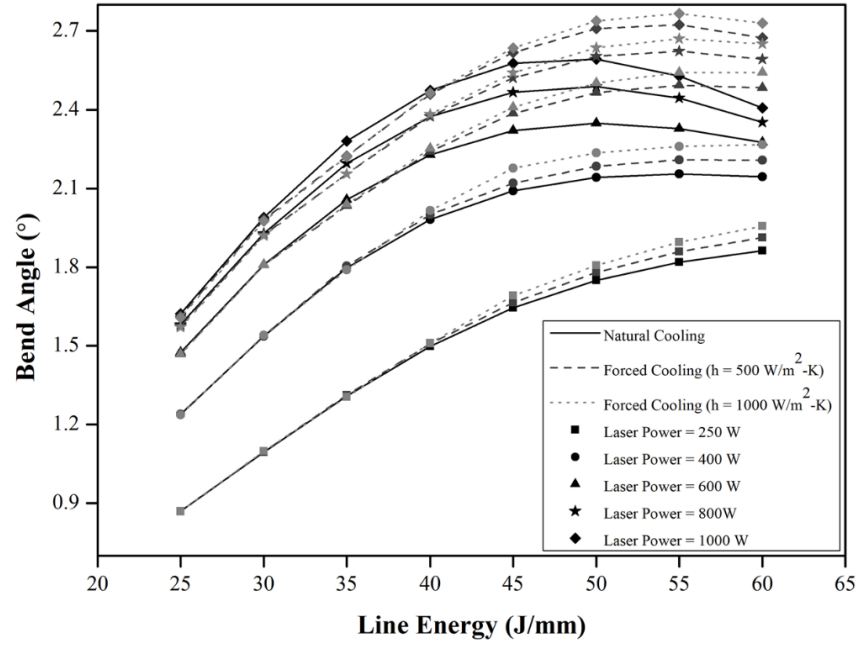


Figure 3-17. Effect of line energy on the bend angle at different cooling conditions.

The change in bend angle with line energy shows a similar trend for natural and forced cooling conditions. However, the bend angle is higher in forced cooling for most of the parametric conditions. The reason behind this is the increment in temperature gradient and the reduction in maximum temperature at the bottom surface (Cheng and Yao, 2001), which leads to the increment of compressive plastic strain at the top and reduction in the compressive strain at the bottom surface, as shown in Figure 3-18. The increase in the plastic strain gradient between the top and bottom surfaces leads to a higher bend angle. Furthermore, bottom cooling reduces the bend angle marginally at low line energy. It is because the forced cooling decreases the peak temperature further, which is already less at low line energy. It is also observed that the peak of maximum bend angle is shifted towards the higher line energies at a particular laser power for the forced cooling conditions.

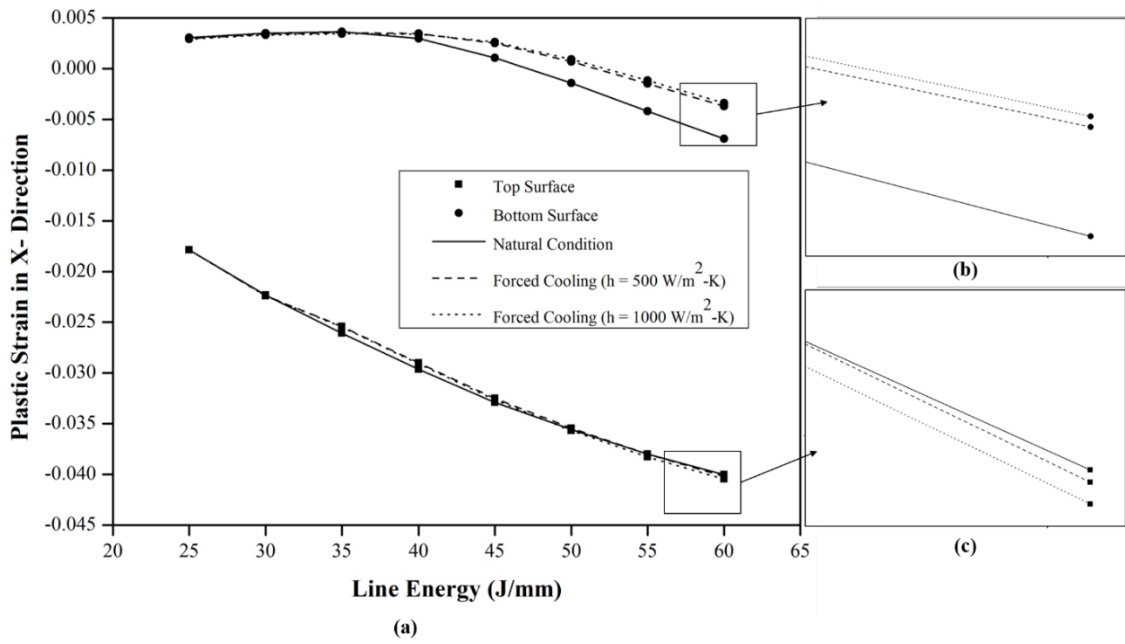


Figure 3-18. (a) Plastic strains at top and bottom surfaces in X-direction at different cooling conditions for 600 W laser power (b) magnified view of the change in strain at the bottom (c) magnified view of the change in strain at the top

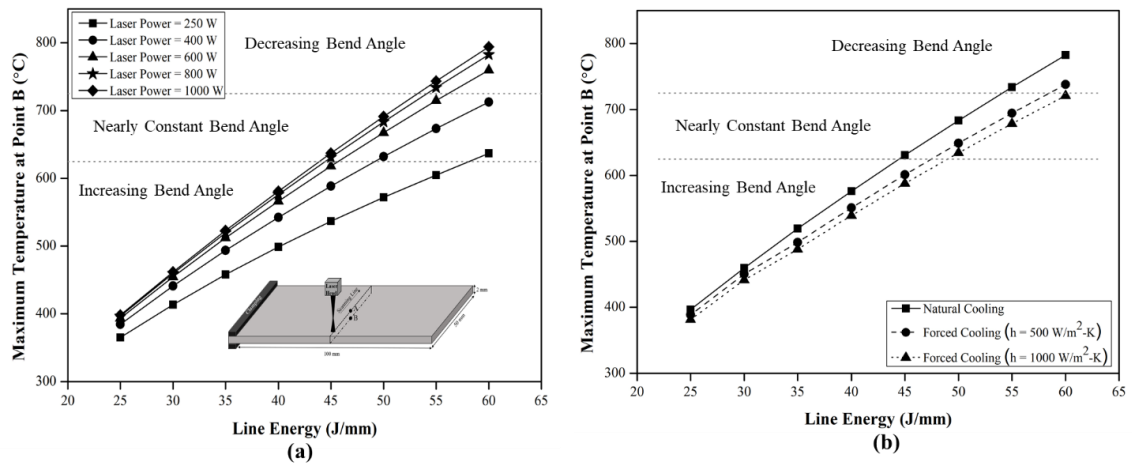


Figure 3-19. The change in maximum temperature at Point B with line energy (a) for natural cooling condition at different laser powers, and (b) for different cooling conditions at 800 W laser power

The maximum temperature both at the top and bottom surfaces increases with line energy. Figure 3-19(a) indicates that when the maximum temperature at the bottom surface reaches the range of 625 °C to 725 °C, the bend angle becomes almost constant with line energy for a particular laser power. The bend angle decreases after 725 °C because the developed compressive plastic strain at the bottom surface starts to dominate. A decrease in the plastic strain gradient between the top and bottom surfaces reduces the bend angle. It is observed that the maximum temperature at the bottom

surface decreases due to the application of forced cooling. Figure 3-19(b) shows that the maximum temperature at the bottom surface can be controlled below 725 °C using forced cooling at the bottom surface with a high convective heat transfer coefficient ($h = 1000 \text{ W/m}^2\text{-K}$) for 800 W laser power and 55 and 60 J/mm line energies, which was above 725 °C in natural cooling condition.

3.3.2. Impact of cooling on edge effect

Figure 3-20(a) shows the effect of line energy on the edge effect for different cooling conditions. It is observed that the edge effect increases with an increase in line energy for all cooling conditions. Moreover, the forced cooling does not show any considerable change in the edge effect at low line energies but increases at higher line energies. It is because, with the increase in line energy, the net temperature variation along the scanning line increases, as shown in Figure 3-20(a). The maximum variation in temperature gradient (MVTG) is taken as the difference between the maximum and minimum temperature gradient along the scan line.

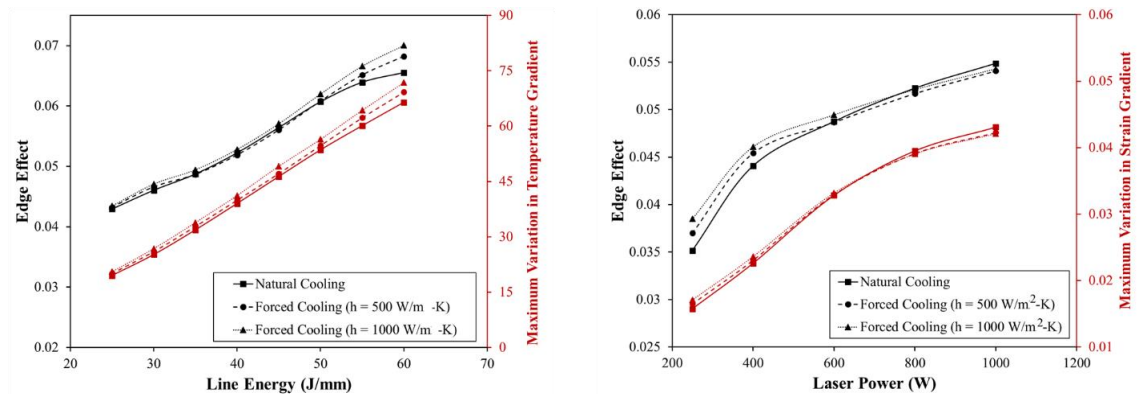


Figure 3-20. (a) Edge effect and maximum variation in temperature gradient along the scan line at different line energy and 600 W laser power. (b) Edge effect and maximum variation in strain gradient along the scan line with laser power at 35 J/mm line energy

Furthermore, the impact of laser power on the edge effect at various cooling conditions is analyzed. Figure 3-20(b) shows that the edge effect increases with laser power for all cooling conditions. It can also be depicted that the magnitude of edge effect is higher for forced cooling conditions at lower laser powers. It is because the maximum variation in strain gradient (MVSG) along the scan line increases with laser power, as shown in Figure 3-20(b). The MVSG is taken as the difference between the maximum and minimum strain gradient along the scan line. As the difference in plastic strain between

the top and bottom surfaces is responsible for the bending of the sheet. Therefore, the variation of plastic strain gradient along the scan line will cause the edge effect. Moreover, the edge effect with forced cooling is limited to less than 7 percent.

Figure 3-21 shows the variation in bend angle along the scanning direction at different line energies. It is observed that the bend angle continuously increases in the scanning direction. It is because the bending of the sheet at the starting of the scan is restricted by the unbent part of the sheet, which is yet to be scanned, whereas, moving ahead on the scan line, the bending is supported by the bent part of the sheet.

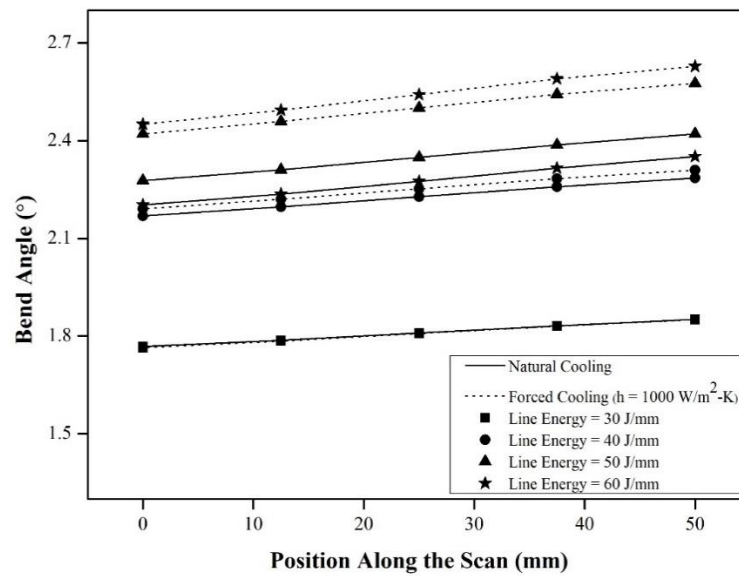


Figure 3-21. Variation in bend angle along the scanning direction

3.3.3. Longitudinal Distortion

Laser irradiation leads to an axial bending with little variation along the scanning line due to edge effect. A slight distortion is observed in the longitudinal direction as well. The longitudinal distortion is usually very small and mostly ignored by the researchers. It occurs as a result of plastic deformation in all the direction by irradiating beam. The longitudinal distortion is represented by the displacement along the scanning line in the direction of the laser head. The longitudinal distortion is not uniform along the scan line due to the uneven temperature and stress distribution in the longitudinal direction.

Figure 3-22(a) and (b) show the effect of different cooling conditions on longitudinal distortion at various laser powers and line energies, respectively. The distortion in

natural cooling condition, continuously decreases along the scan length due to less cooler material in the forward direction and high temperature of already scanned region. For forced cooling conditions, at high laser powers, the distortion decreases upto the middle of the scan line, then it starts increasing in the negative direction. Whereas, at low laser power, no significant effect of the cooling condition is observed on the distortion, and it continuously decreases. Similar effects of forced cooling are also observed at high line energies, but no notable change is observed at low line energies.

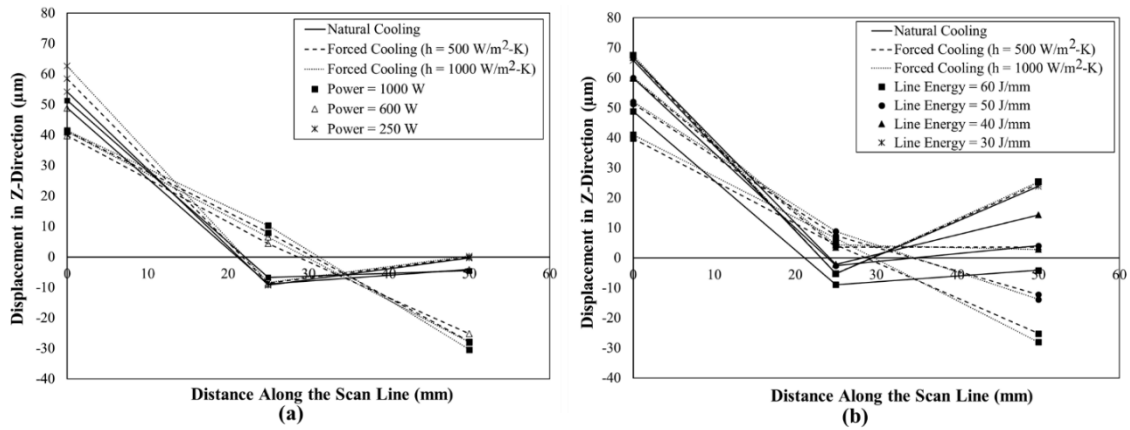


Figure 3-22. Displacement in Z-direction along the scan line at different cooling conditions with (a) laser powers and (b) line energies

3.3.4. Effectiveness of forced cooling

As per the above discussion, forced bottom cooling shows a diverse effect with different processing parameters. Therefore, the parameters need to be optimized to get the higher bend angle. Figure 3-23(a) and (b) show the percentage increment in bend angle with laser power at constant line energy for both the forced cooling conditions i.e., $h = 500 \text{ W/m}^2\text{-K}$ and $h = 1000 \text{ W/m}^2\text{-K}$, respectively. It can be deduced from Figure 3-23(a) and (b) that, at low line energy, laser power has an adverse impact on the bend angle due to forced cooling. It is because the energy required for plastic deformation at the bottom surface is optimum in the case of natural cooling conditions, which get reduced in forced cooling, resulting in the reduction of bend angle. At higher line energy and laser power, generated compressive plastic strain is high (as shown in Figure 3-24 (a)), because the energy available is higher than the required for maximum bend angle. The magnitude of induced strain at the bottom surface of the worksheet will be reduced due to the effect of forced cooling, which leads to the increment in the strain gradient, thus increasing the bend angle.

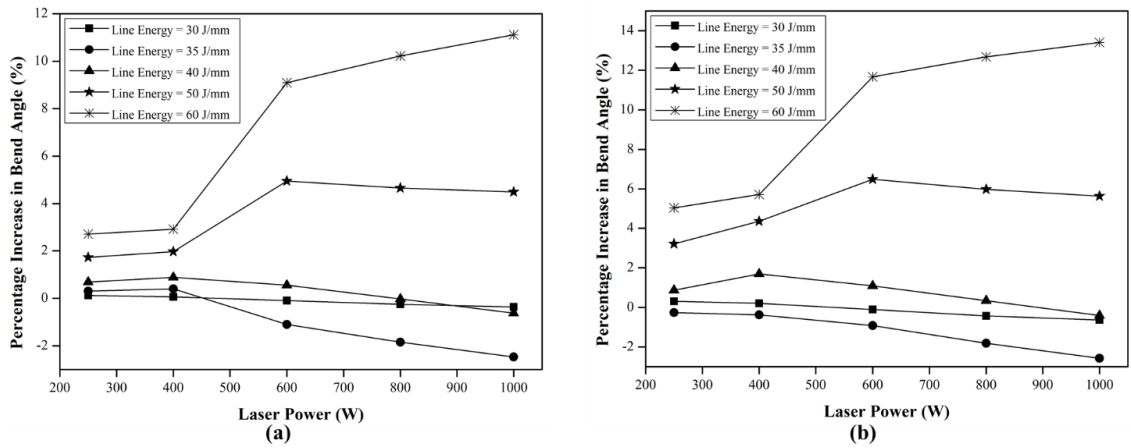


Figure 3-23. The effect of laser power on percentage increase in bend angle at (a) $h = 500 \text{ W/m}^2\text{-K}$, and (b) $h = 1000 \text{ W/m}^2\text{-K}$

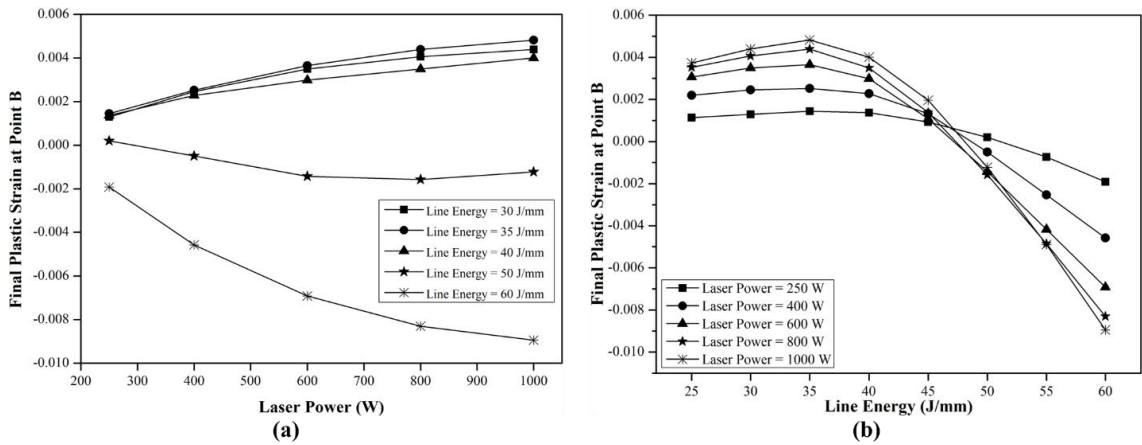


Figure 3-24. The final plastic strain at Point B with respect to (a) laser power, and (b) line energy

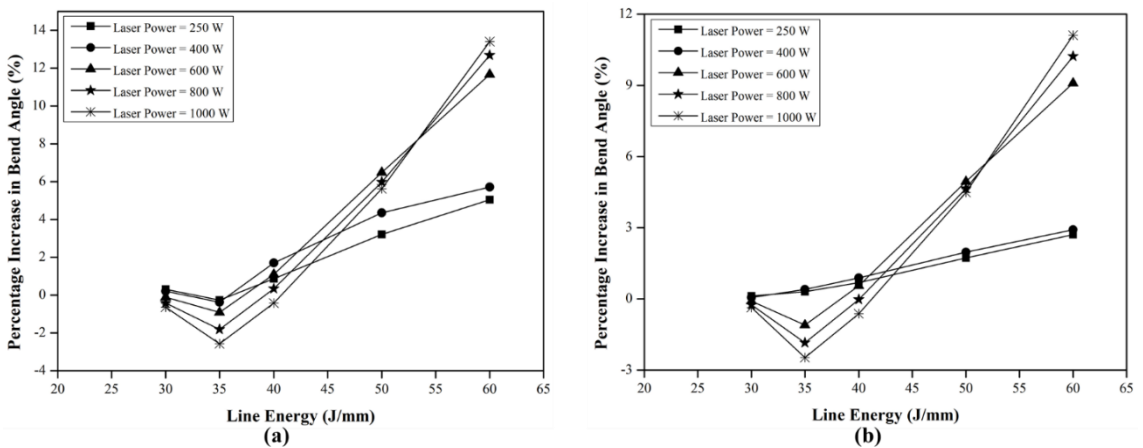


Figure 3-25. Percentage increase in bend angle with line energy at (a) $h = 500 \text{ W/m}^2\text{-K}$, and (b) $h = 1000 \text{ W/m}^2\text{-K}$

Figure 3-25(a) and (b) show that the percentage increment in bend angle with the line energy at constant laser power. The percentage increase in bend angle is increased for

all line energies except for 35 J/mm. Figure 3-24(b) shows that, at point B, with the increase in line energy, the nature of plastic strain is changing from tensile to compressive, which is adverse for higher bend angles. But due to forced cooling, the reduction in the compressive strain at the bottom surface is observed, which leads to the higher bend angle. The plastic strain gradient between the top and bottom surfaces is optimum at 35 J/mm line energy for natural cooling, hence forced cooling is unfavourable for this particular condition.

3.4. Experimental Feasibility Exploration of Forced Cooling Assisted Laser Bending

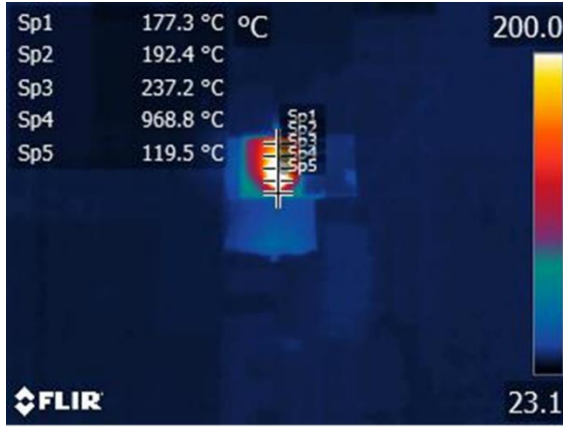
3.4.1. Experimental Details

The laser bending experiments were performed on an aluminium sheet of 60 mm length, 30 mm width, and 2 mm thickness. Aluminium has high reflectivity to the laser, so graphite coating is applied to improve the absorptivity of the worksheet surface. The experimental setup used is discussed in detail in Chapter 4. The experiments were performed for a range of laser power (400–850 W) and scanning speed (1000-2500 mm/min) with a constant beam diameter of 4 mm.

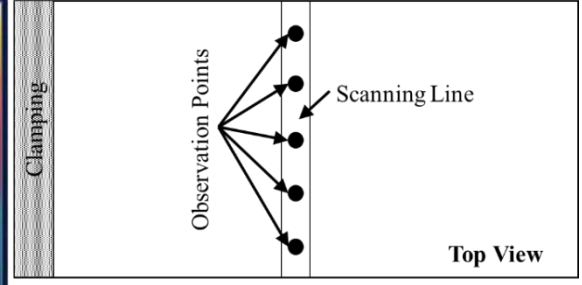
3.4.2. Results and Discussions

3.4.2.1. Temperature Analysis

In this study, the temperature of the scanning region is analyzed experimentally. The temperature is measured by taking an average of the maximum temperature of five equidistant points along the scan line shown in Figure 3-26. Each experiment is repeated thrice, and the average of three trials is considered as the top surface temperature for that particular parameter, and it is represented by T_{avg} .

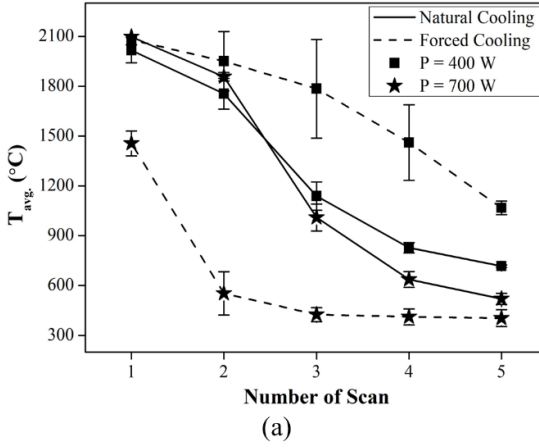


(a)

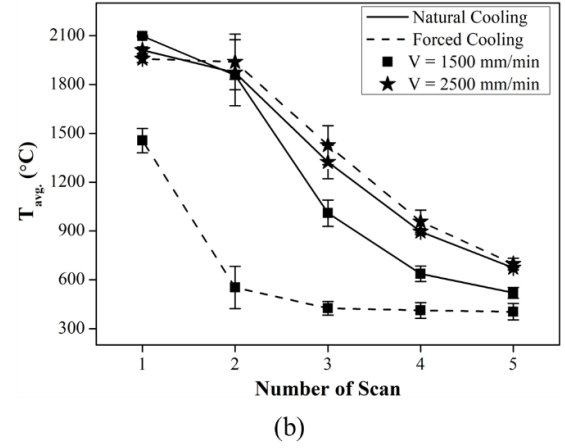


(b)

Figure 3-26. Temperature measurement points along the scan line in (a) thermal imaging software (b) schematic



(a)



(b)

Figure 3-27. Variation of T_{avg} with number of scans in both the cooling conditions at (a) different laser power and at 1500 mm/min scanning speed, and (b) different scanning speeds and at 700 W laser power

Figure 3-27 shows the temperature variation in both the cooling conditions with each scan at different sets of scanning speed and laser power. It is observed that the T_{avg} decreases with the number of scans due to coating degradation. At a constant scanning speed of 1500 mm/min, the T_{avg} is compared for two different laser powers of 400 W and 700 W (Figure 3-27(a)). It is found that in the natural cooling condition, the temperature is higher in the case of 700 W up to two scans due to higher energy. Whereas, at higher scans, T_{avg} is higher for 400 W laser power because of the less coating degradation at low laser power, as shown in Figure 3-28. In forced cooling condition, at low laser power, the temperature is found to be increased because the cooling led to less coating degradation and resulted in higher absorptivity. Whereas, at high laser power, the coating degradation is taken place in forced cooling condition, and

it further reduces the temperature, which leads to a significant reduction in $T_{avg.}$. Figure 3-27(b) shows the $T_{avg.}$ for two different scanning speeds at a constant laser power of 700 W. In natural cooling condition, the $T_{avg.}$ is higher at low scanning speed up to two scans because of higher line energy. However, for a higher number of scans, the $T_{avg.}$ is found to be increased with scanning speed because of the less coating degradation. The forced cooling is not effective at higher scanning speed, whereas at low scanning speed, the temperature is reduced significantly because of the excessive heat loss due to the higher thermal conductivity of the worksheet.

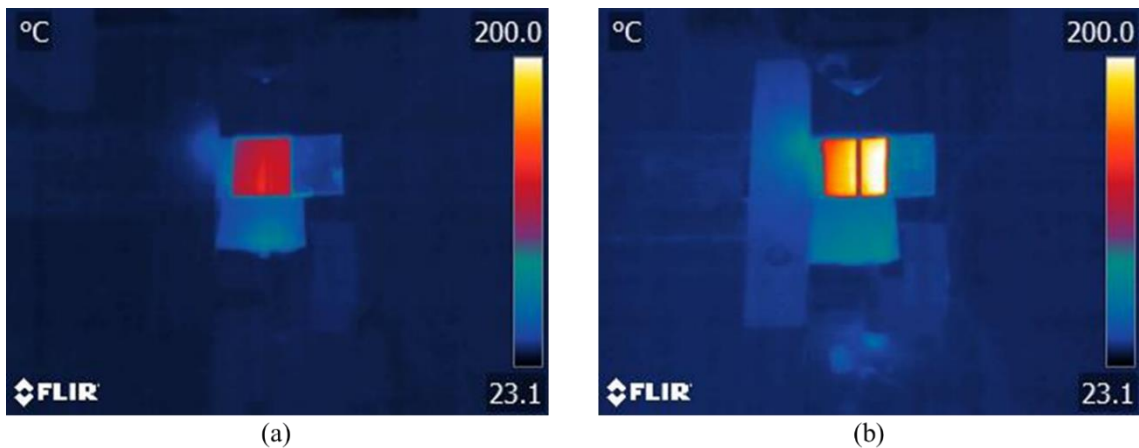


Figure 3-28. Temperature profile after five scans for 1500 mm/min scanning speed at (a) 400 W, and (b) 700 W laser powers

3.4.2.2. Bend Angle Analysis

This section discusses the change in bend angle with different laser power and scanning speed for both natural and forced cooling conditions. Figure 3-29(a) shows that the bend angle is increased with laser power, attained peak and then decreased at high laser powers for all the scanning speeds. However, in natural cooling condition, for lower scanning speed, the maximum bend angle is achieved at lower laser powers; and with an increase in scanning speed, the maximum bend angle shifts to higher laser power. The forced cooling has increased the bend angle for most of the parametric conditions except for the higher scanning speed and low laser powers. It is because the energy available at low laser power and higher scanning speed is less, which is further carried away by the forced cooling. At low laser power, the bend angle is decreased with an increase in scanning speed, whereas at higher laser power it is found to be increased (Figure 3-29(b)). It is because the higher scanning speed, increases the temperature gradient at a higher laser power whereas at low laser power it reduces the available

energy. The forced cooling further reduces the energy available at low laser power and results in a reduction in bend angle, whereas at high laser power it enhances the temperature gradient and results in the increased bend angle. It is also observed that the worksheet breaks into two parts due to excessive melting at low scanning speed (1000 mm/min) and higher laser power (850 W), in natural cooling condition. Whereas, in forced cooling condition, this melting is reduced significantly, and a bend angle of nearly 8 degrees is generated.

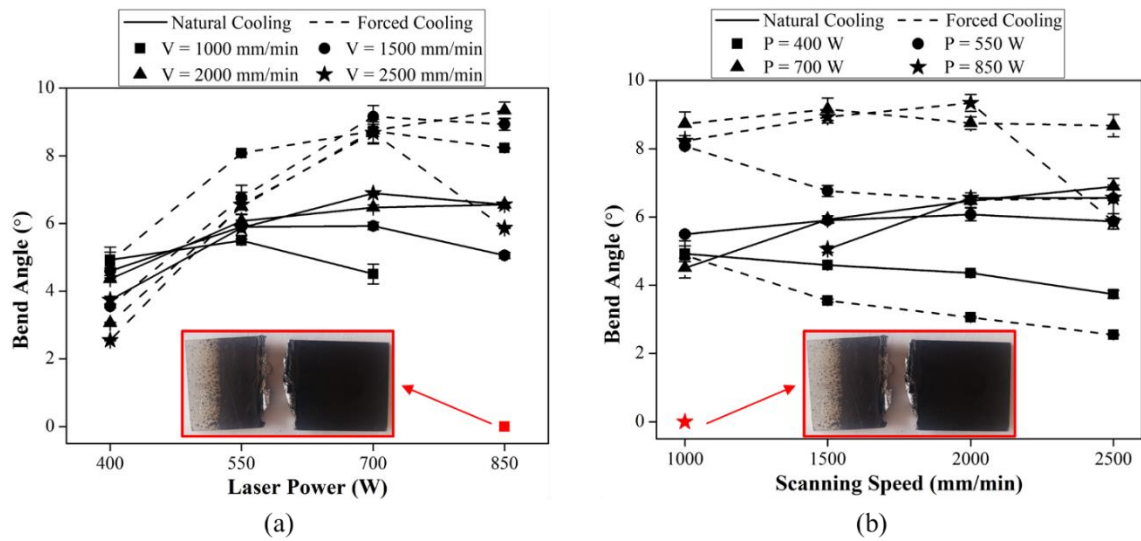


Figure 3-29. Variation in bend angle for different cooling conditions with (a) laser power at different scanning speed, and (b) scanning speed at different laser powers

Figure 3-30 shows the bend angle in each scan at different laser power and scanning speeds in both cooling conditions. At low laser power, the bend angle per scan is increased with the number of scans in natural cooling condition. It may be because of the increase in the available energy due to the retention of heat from the previous scan. Whereas, in forced cooling, the heat is lost by convection and leads to an almost constant bend angle per scan (Figure 3-30(a)). On the contrary, at low scanning speed and high laser power, the bend angle per scan is decreased due to the reduction in temperature gradient with each scan in natural cooling condition (Figure 3-30(b)). Whereas at higher scanning speed, it is slightly increased with the number of scans because the energy available is less, and it increases with each scan due to retention of heat and results in a decrease in flow strength of the worksheet material. In forced cooling condition, the bend angle per scan increased due to increased temperature gradient, but the rate of increment is decreased with the number of scans and finally stabilized. It may be because the heat is carried away by forced cooling, leading to higher flow strength.

Similarly, the variation of bend angle in each scan at different laser powers for a particular scanning speed is shown in Figure 3-31. At low scanning speed, the temperature gradient is decreased in each scan, but at the same time, flow strength is also decreased, resulting in an almost constant bend angle per scan in natural cooling condition. Whereas, at higher scanning speed, the bend angle is increased with the number of scans at both low and high laser powers. It may be due to lower interaction time, and with the number of scans, it increased due to the heat carry-forward from the previous scan. On the other hand, in forced cooling condition, the bend angle at low laser powers is almost constant with the number of scans, whereas it is found to be increased at high laser power. At low laser powers, although the forced cooling enhances the temperature gradient, significant heat loss also occurs, which leads to an almost similar bend angle during the natural cooling condition. However, at high scanning speed, a reduction in bend angle is also observed due to the domination of heat loss. On the other hand, at high laser powers, the forced cooling significantly enhances the bend angle by generating a steep temperature gradient, and it is more significant at lower scanning speeds.

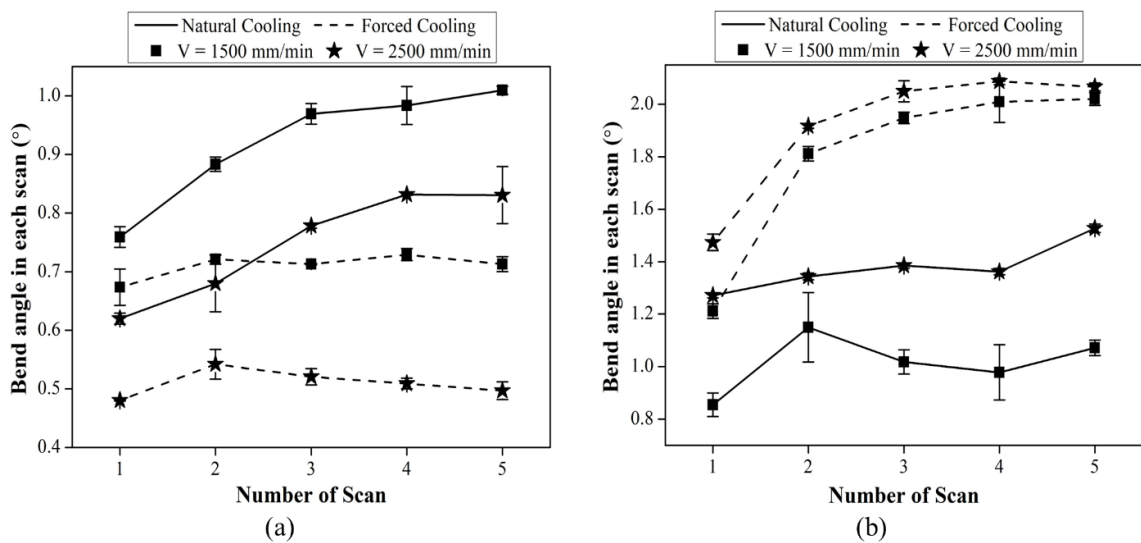


Figure 3-30. Bend angle in each scan at a laser power of (a) 400 W, and (b) 850 W

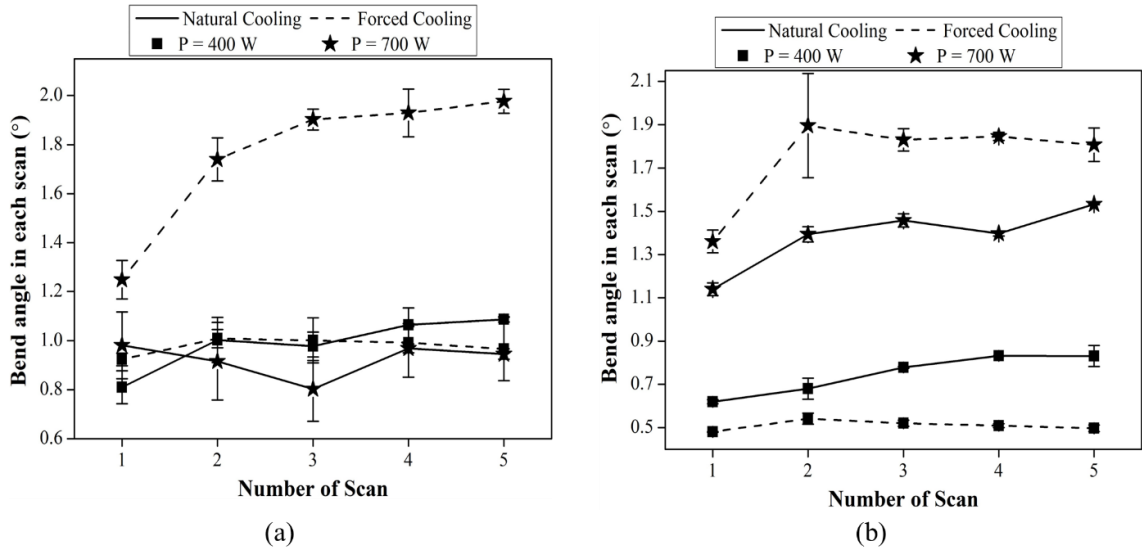


Figure 3-31. Bend angle in each scan at a scanning speed of (a) 1000 mm/min, and (b) 2500 mm/min

3.4.2.3. *Effectiveness of cooling*

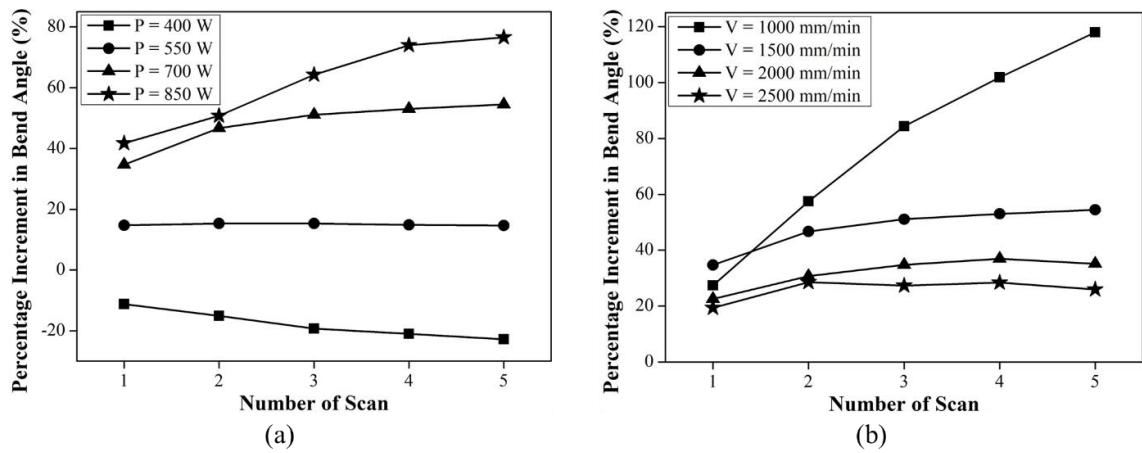


Figure 3-32. Percentage increment in bend angle in each scan due to forced cooling (a) for different laser powers at 1500 mm/min scanning speed, and (b) for different scanning speeds at 700 W laser power

In this section, the effectiveness of forced cooling is analyzed by taking the percentage increment in bend angle due to forced cooling at different laser power and scanning speed. It is observed from Figure 3-32(a) that forced cooling is more effective at higher laser powers, and it negatively affects at low laser power (400 W). Similarly, for a particular laser power, it is found that forced cooling is more effective at a lower scanning speed. It is because the temperature gradient across the sheet thickness is less at high laser power and low scanning speed in natural cooling condition, which is significantly increased in forced cooling condition. It is also observed that at high laser

power and lower scanning speeds, the effectiveness of forced cooling is more at a higher number of scans. In contrast, it becomes almost constant after initial few scans for low laser power and high scanning speed. It is because the increment in temperature gradient is more dominant, and the flow strength of the material is also reduced due to the availability of enough energy at high laser power and low scanning speed, and it increases with the number of scans. Whereas at low laser power and high scanning speeds, the energy absorption per unit length is low, and forced cooling further reduces the energy. Even at a higher number of scans, the heat loss is more dominant over enhancement in the temperature gradient, leading to low effectiveness of forced cooling.

3.5. Summary

This chapter presented the initial feasibility analysis, and identification of the parametric range of the forced cooling assisted laser bending process. The study was initiated with the numerical analysis of the process to understand the underlying mechanism of laser bending for both natural and forced cooling conditions. A numerical model was developed and experimentally validated for the same. Then the feasibility of the forced cooling assisted laser bending was analyzed using the same model. Furthermore, the experimental feasibility of the proposed approach was also tested.

In the first stage of the study, a 3-D non-linear FEM-based numerical model was developed and validated for laser bending of duplex stainless steel sheets. A set of experiments were performed to record the temperature distribution using a thermal imaging camera and the bend angle using a laser displacement sensor. The recorded data was used to validate the numerical model thermally as well as mechanically, and the results were found to be in good agreement with the numerical results.

In the second stage of the study, the temperature distribution, bend angle, edge effect, mechanical properties, and microstructural characterization were investigated for laser bending of duplex stainless steel. The important outcomes of the study were-

- The temperature distributions along and lateral to the scan line and along the thickness of the sheet were analyzed. This temperature study provided a better insight into the bending process and the effect of process parameters.

- The effect of line energy, laser power, and scanning speed on the bend angle and edge effect had been studied. It was observed from the results that at low laser powers, initially, the bend angle increased with line energy and became nearly constant at high line energies. However, for a range of higher laser powers, first, it increased, attained peak, and then decreased at high line energies.
- The bend angle increased with laser power and scanning speed at constant line energy, but at a decreasing rate. It is also observed that the edge effect increased with an increase in laser power and scanning speed at constant line energy.
- Tensile and hardness testing of bent specimens had also been performed to investigate the effect of line energy on mechanical properties. It was found that the hardness of the laser-scanned specimens increased, and the ductility decreased with line energy, whereas no considerable changes were found in the ultimate strength. It was observed from microstructural analysis that the formation of sigma phase precipitation was responsible for the change in mechanical properties.
- The relationship between the temperature, bend angle, and mechanical properties was also analyzed, and found that brittleness and hardness increased with an increase in the maximum temperature at the top surface.

In the third stage of the study, feasibility of the forced cooling assisted laser bending was examined through numerical simulation. The effect of forced cooling at two different heat transfer coefficients, 500 and 1000 W/m²-K, was analyzed for bend angle and edge effect. The effect of forced cooling on the bending mechanism was discussed in detail. It was observed from the results that-

- The bend angle could be increased upto 11.11% and 13.41% by applying forced cooling at the bottom surface with a heat transfer coefficient of 500 W/m²-K and 1000 W/m²-K, respectively. It was also observed that the forced cooling controls the worksheet melting upto a certain limit.
- The study indicated that for a particular laser power, the peak of the bend angle shifted towards higher line energy after the implication of forced cooling as compared to natural cooling.

- There was no significant effect of forced cooling on the edge effect at low line energies, but the edge effect increased at high-line energies. A significant increase in bend angle was observed due to the application of forced cooling at high line energy and laser power, but at the same time, the edge effect also increased.
- Results indicated that the effect of cooling increased with laser power for high line energies, but for low line energies, it decreased with laser power. Forced cooling showed an adverse effect on the bend angle at low line energies and high laser powers. It was challenging to obtain a specific value for heat transfer coefficient, which was in line with the physical experiments and might be the future direction of the work.

In the fourth stage of the study, feasibility of the forced cooling assisted laser bending was examined through experiments. The study was focused on the effectiveness of forced cooling at the bottom surface of the aluminium alloy sheet during laser bending. The temperature and bend angle were compared in natural and forced cooling conditions. The effect of process parameters (laser power and scanning speed) on the effectiveness of forced cooling was also analyzed. The results showed that-

- The temperature of the scanned surface decreased with the number of scans due to coating degradation for both the conditions. The forced cooling reduced the coating degradation upto some extent at low laser powers and resulted in an increase in temperature.
- The forced cooling increased the bend angle for most of the parametric conditions except at low laser power and higher scanning speed. The material degradation and excessive melting were reduced with the application of forced cooling condition.
- The bend angle was found to be increased, attained a peak, and then decreased with laser power, whereas it decreased with scanning speed in both the cooling conditions.
- At low laser power, the bend angle per scan was found to be increased with the number of scans in natural cooling condition, whereas in forced cooling

condition it was nearly constant. In contrast, at high laser power, it was almost constant in natural cooling condition and increased in forced cooling condition. The forced cooling was found to be more effective at high laser power, low scanning speed, and a higher number of scans.

CHAPTER 4

EXPERIMENTAL DETAILS OF FORCED COOLING ASSISTED LASER BENDING

This chapter aims to provide comprehensive information about the methodology of the study, including the worksheet material, experimental setup, cooling arrangement, bend angle measurement, and post-bending analyses. Furthermore, it gives a complete overview of the instruments utilized throughout the study and discusses their roles and contributions. Overall, it gives a complete overview of the experimental procedure conducted in this investigation.

4.1. Overall Methodology

This section gives a step-by-step overview of the present work, shown in Figure 4-1. The study starts with the selection of a range of process parameters and feasibility test of forced cooling assisted laser bending of duplex stainless steel (AISI-2205) with the help of numerical simulations. The experimental studies are performed based on these parameters for both natural and forced cooling conditions. The effect of the forced cooling condition is investigated on bending angle, and material properties (mechanical, metallurgical, chemical) are investigated and compared with that of natural cooling condition. Furthermore, the process parameters are optimized for single as well as multi-scan laser bending to get the maximum bend angle.

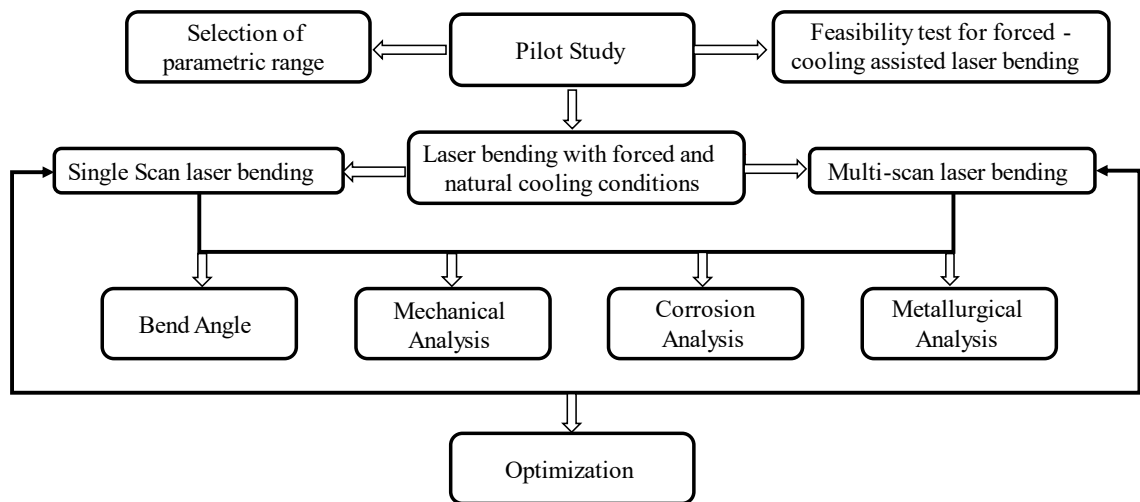


Figure 4-1. Overall methodology of the study

4.2. Worksheet Material

This study is carried out with duplex stainless steel (Grade: 2205) sheet, which is supplied by Padmawati steel & engg. Co., Mumbai, India. Most of the investigations are done on 2 mm thickness sheet with the length and width of 60 mm and 30 mm respectively. Although, for analyzing the effect of sheet geometry, sheets of different thicknesses (1.5, 2 and 3 mm) are used with varying worksheet widths (30, 40, and 50 mm). These sheets of different dimensions are cut with the fiber laser cutting machine, which gives good dimensional accuracy with fine cutting. All the cut worksheets are coated with the graphite spray coating in order to improve the absorptivity, as shown in Figure 4-2. The chemical composition of the material was tested by Laxmi PMI testing service, Mumbai, India, and given in Table 4-1. The test report of the duplex stainless steel sheet is given in Appendix 4.1.



Figure 4-2. Graphite coated duplex-2205 sheet specimens

Table 4-1. Chemical composition of Duplex-2205 sheets

Element	Ni	Cr	Mn	Mo	C	N	Fe
Weight Percentage	5.06	22.15	1.50	3.09	0.03	0.15	68.02

4.3. Experimental Setup with Cooling Arrangement

The laser bending experiments are performed on a high-power laser cutting machine (Model: L3015; Make: ABRO Technologies Pvt. Ltd), shown in Figure 4-3. It consists of a fiber laser source (Model: MFSC-1000W; Make: MAX Photonics Co., Ltd.) of maximum power 1 kW and wavelength of 1075 ± 5 nm. The specifications of the laser cutting machine and fiber laser source are given in the Appendix 4.2 and 4.3, respectively. A clamping arrangement is prepared to hold the worksheet as a cantilever. The laser is irradiated along the width of the worksheet at a predefined straight line near the center of the worksheet length. The CNC can control the scanning speed of the laser, and the beam diameter of the laser beam can be adjusted by varying the height of the laser head from worksheet surface.



Figure 4-3. Laser cutting machine

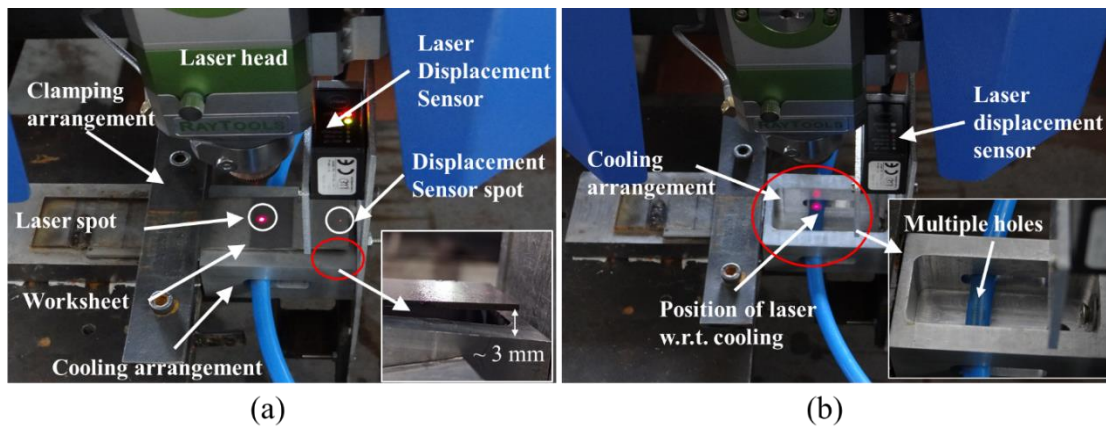


Figure 4-4. Experimental setup (a) position of laser head and laser displacement sensor, (b) cooling arrangement

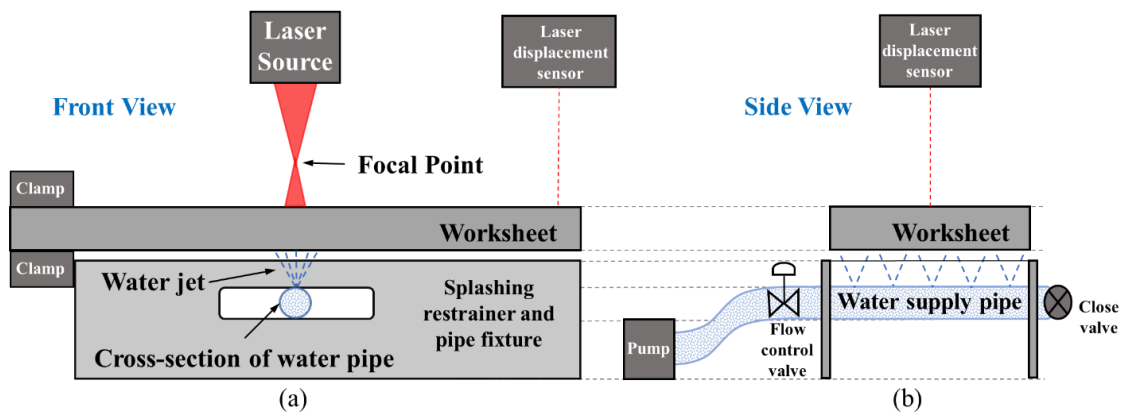


Figure 4-5. Schematic of experimental setup with forced cooling (a) front view and (b) side view

The forced water cooling at the bottom surface (opposite to laser irradiation) is applied throughout the width of the worksheet by a multi-nozzle arrangement. This multi-nozzle arrangement is developed by creating multiple holes of 0.75 mm diameter on a 7 mm diameter pipe using a CO₂ laser cutting machine. The holes are uniformly distributed throughout the width of the worksheet, with a 0.75 mm distance between successive holes. This pipe is placed in a small container that is opened only from one side to avoid water splashing on the top surface (laser irradiating) of the worksheet, as shown in Figure 4-4(b). A small gap between the container and the free end of the worksheet is provided to avoid hindrance during counter bending of the worksheet, shown in inset of Figure 4-4(a). A flow control valve is installed to control the flow rate of water supplied by the pump. The detailed schematic of the experimental setup with the forced cooling arrangement is shown in Figure 4-5.

4.4. Beam Diameter Calculation

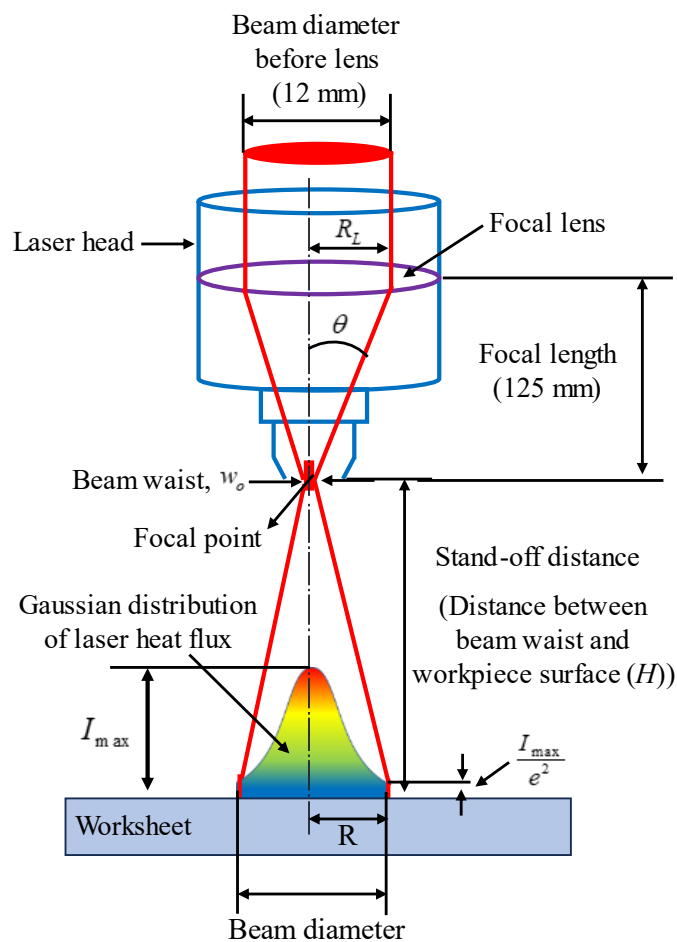


Figure 4-6. Schematic of the laser beam profile [Redrawn with permission]

The laser beam was assumed to be circular with Gaussian distribution of heat flux. The laser beam diameter is adjusted by varying the distance between the focal point and the worksheet surface (H). A schematic of the laser beam profile passing through the focusing lens is presented in Figure 4-6.

The laser beam diameter was calculated via a mathematical model (Kant, 2016) based on the standard beam propagation equations. The beam radius (R) is calculated, according to the Equation 4-1 (Sun, 1998).

$$R = w_o \left[1 + \left(\frac{M^2 \lambda H}{\pi w_o^2} \right)^2 \right]^{1/2} \quad 4-1$$

where w_o is the minimum beam radius at the focal point known as laser beam waist, λ is the wavelength of the fiber laser beam (1080 nm), M^2 is the beam quality factor (1.3). For a perfect Gaussian beam, its value is equal to one; however, it always has a greater value in actual conditions.

According to Sun (Sun, 1998), the half divergence angle (θ) is written as given in Equation 4-2.

$$\theta = \frac{M^2 \lambda}{\pi w_o} \quad 4-2$$

After multiplying the focal length (f_l) on both sides, we got the expression given in Equation 4-3

$$f_l \theta = \frac{M^2 \lambda f_l}{\pi w_o} \quad 4-3$$

where f_l is the focal length of the lens which is 125 mm. The laser beam radius (R_L) can be written as Equation 4-4

$$R_L = f_l \theta \quad 4-4$$

Inserting Equation 4-4 into Equation 4-3, the equation can be expressed as-

$$w_0 = \frac{M^2 \lambda f_l}{\pi R_L} \quad 4-5$$

Equation 4-5 was used to calculate w_0 and it was found to be 0.00931 mm. This value of the beam waist is utilized in Equation 4-1 to determine the required height between the focal point and worksheet surface, considering the desired beam diameter.

4.5. Bend angle Measurement

The bend angle is measured with the help of a laser displacement sensor (Model: ILD1320-50; Make: Micro-Epsilon Ltd.), shown in Figure 4-7. It has an accuracy of 5 μm and a 2 kHz sampling rate. The specifications of the laser displacement sensor are given in Appendix 4.4. The sensor is placed at the free end of the worksheet with a small offset to the edge. It is because, while bending, the laser beam of the sensor may go out of the sheet surface. Once the sensor is fixed, the distance between the spotlight of laser source and the laser displacement sensor is measured and keep it constant for all experiments, as shown in Figure 4-8(a). The sensor gives the displacement of the free end in the Z-direction along with time. The bend angle is calculated by using cosine rule with the help of measured displacement at the free end and the distance between the laser source and displacement sensor, as shown in Figure 4-8(b).

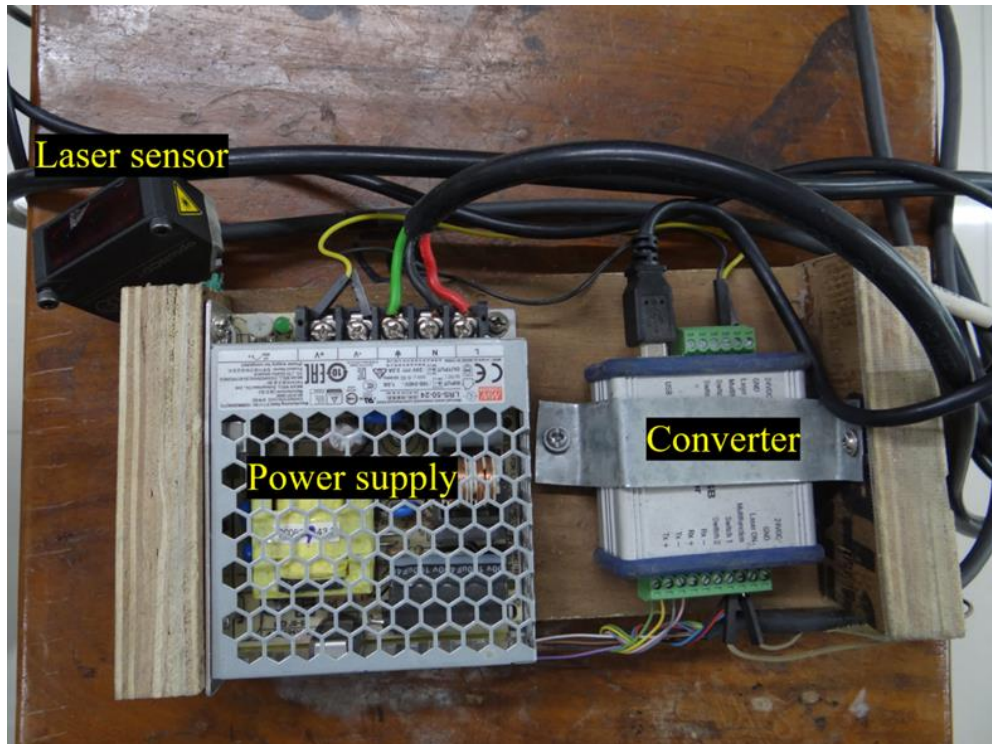


Figure 4-7. Laser displacement sensor

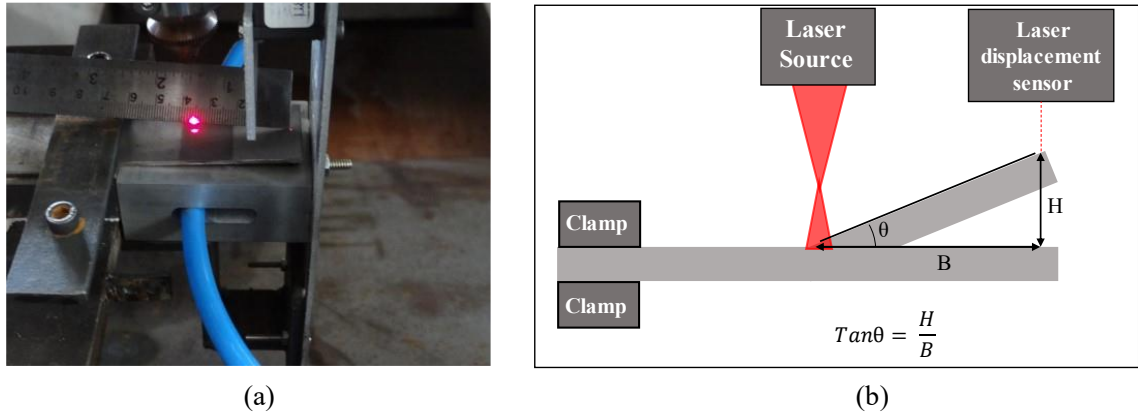


Figure 4-8. (a) measurement of distance between spot lights of laser source and laser displacement sensor, (b) schematic for bend angle calculation

4.6. Temperature Measurement

A thermal imaging camera shown in Figure 4-9 (Model: A315; Make: FLIR Systems Inc.) with a maximum range of 2000 °C at an imaging frequency of 60 Hz is used to measure the temperature of the top surface. The specifications of the thermal imaging camera are given in Appendix 4.5. The emissivity used for the temperature measurement is estimated by comparing the temperature measurements of the IR camera with the measurements taken with the thermocouple and data acquisition (DAQ) system, as shown in Figure 4-10. Similar methodology to estimate emissivity has also been reported in the literature (Goyal et al., 2022a). The thermocouple is placed 5 mm away from the scanning line (shown in the inset of Figure 4-10) to avoid direct interaction with the laser beam. Then the emissivity is estimated by mapping the temperature profiles of thermocouple with IR camera at different emissivities. It is found that the temperature profile by thermocouple correlates well with IR camera at 0.9 emissivity during multiple scans, as shown in Figure 4-11(a). The emissivity is not significantly varied with number of scans; therefore, during all five scans, the emissivity is considered 0.9 for the temperature measurements. Based on this temperature measurement, the maximum temperature at the top surface in each scan and temperature distribution along and lateral direction to the scan line are analyzed. The maximum temperature at the top surface is obtained by taking the average of five different points along the scan line, as shown in the schematic (Figure 4-11(b)). Three repetitions have been carried out, and further, an average of these repetitions is taken as the average maximum temperature at the top surface (T_{avg}).



Figure 4-9. Thermal imaging camera

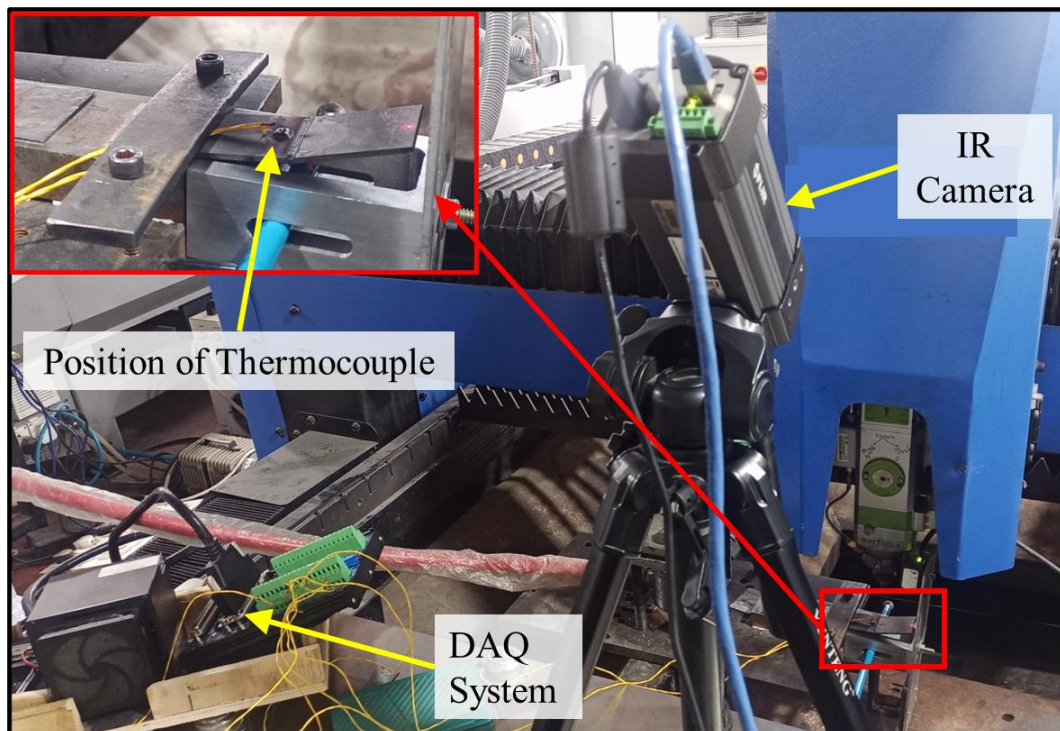


Figure 4-10. Experimental setup for emissivity estimation by temperature validation with thermocouple

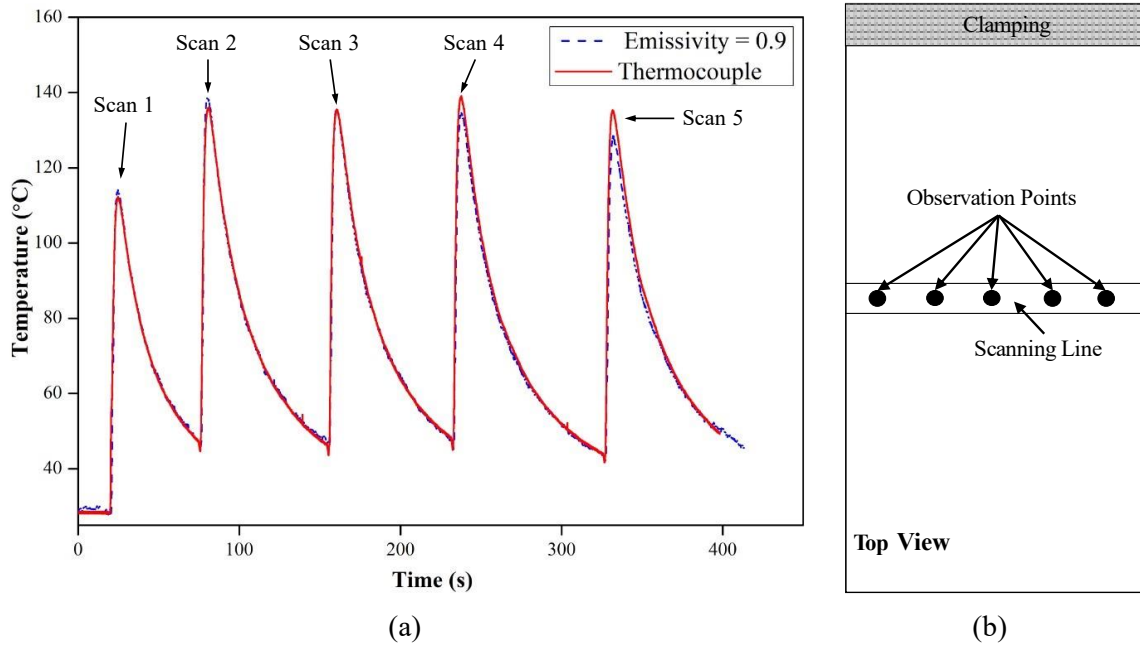


Figure 4-11. (a) Estimation of emissivity by mapping the temperature profiles of thermal imaging camera and thermocouple, (b) schematic representation of temperature measurement points on top surface

4.7. Post-bending Analysis

4.7.1. Micro-hardness

The hardness of the bent specimen is measured with a Vicker's microhardness tester (Model: 402MVD; Make: Wilson), shown in Figure 4-12(a). The specifications of the microhardness tester are given in Appendix 4.6. The specimen for hardness measurement is taken from the scanning region, as shown in Figure 4-12(b), with the help of laser cutting machine. The laser cutting machine has a metal detector sensor that auto-adjusts the height of the cutting nozzle and helps to cut the bent specimens precisely. The hardness is measured at both the top and bottom surfaces after polishing the specimens with polishing papers. The hardness is tested at 16 different locations of each specimen for reasonable data. The two different loads for which tests are performed are 500 g and 300 g, and the dwell time of indentation is kept at 10 s.

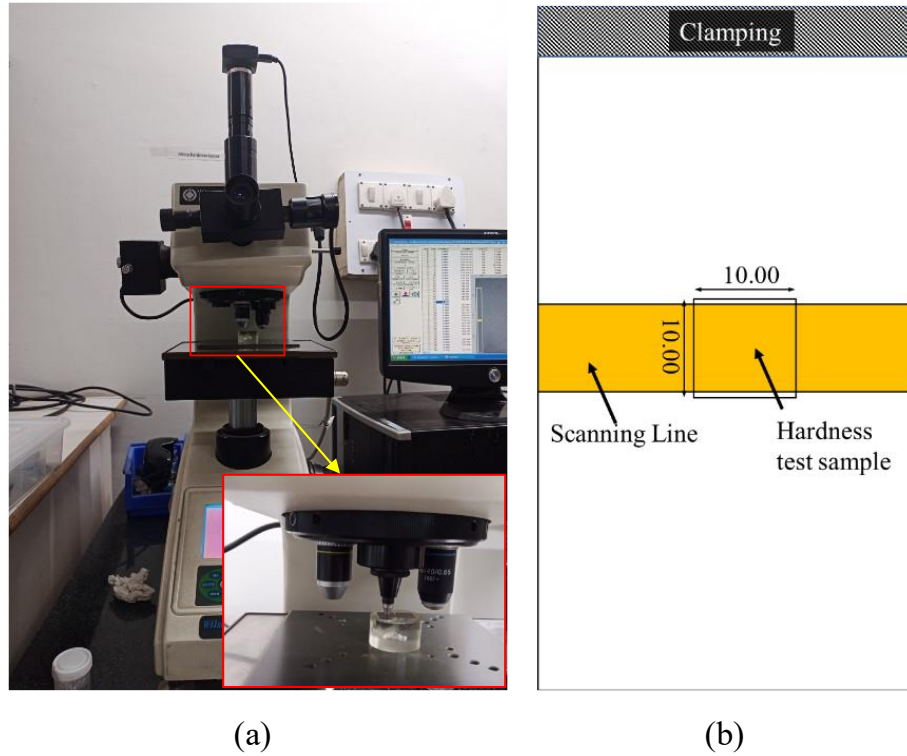


Figure 4-12. (a) Vicker's microhardness tester (b) dimensions and position from where hardness test specimen is taken

4.7.2. Tensile Strength

The tensile testing is conducted on a micro-tensile testing machine shown in Figure 4-13, having the capacity upto 10 kN with the strain rate of 8 $\mu\text{m/s}$. The tensile tests are performed in both along and perpendicular to the scanning line and for both the cooling conditions, as shown in Figure 4-14. These specimens are cut with the laser cutting machine, having a metal detector sensor which auto adjust the height of the cutting nozzle and helps to cut the bent sheet precisely.

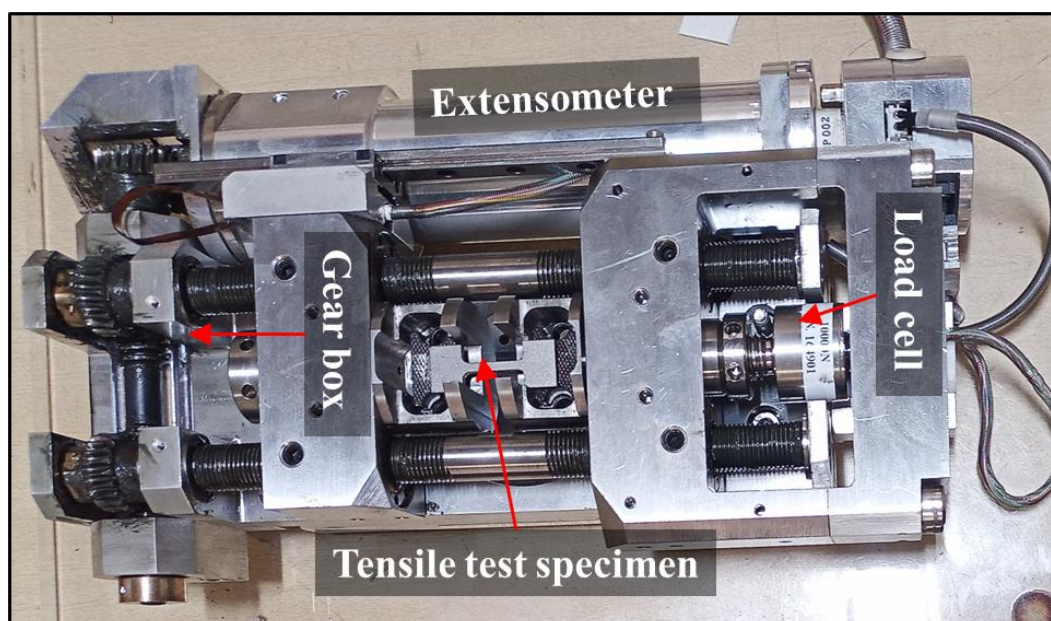


Figure 4-13. Micro-tensile testing machine

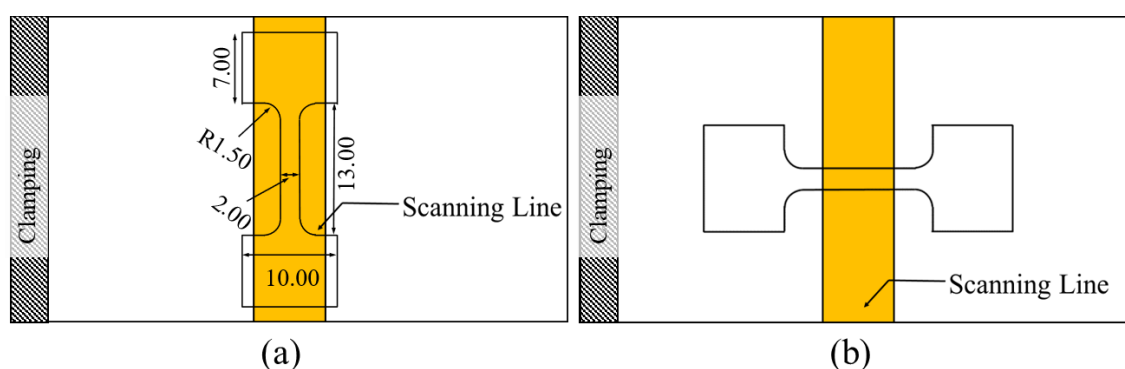


Figure 4-14. Dimensions and orientation of tensile test specimen (a) along the scan line and (b) perpendicular to the scan line

4.7.3. Corrosion Analysis

The corrosion behavior of the laser bent specimens (bent with both forced and natural cooling) is analyzed by the electrochemical corrosion tests with Autolab electrochemical workstation shown in Figure 4-15. The specifications of the autolab electrochemical workstation are given in Appendix 4.7. The potentiodynamic polarization data and Tafel plot is analyzed by the Nova 2.1 software. A three-electrode cell is utilized to conduct the electrochemical corrosion tests, as shown in Figure 4-15 (b). The laser-bent specimen, taken from the scanning region (similar to the hardness specimen, as shown in Figure 4-12(b)), serves as the working electrode. A platinum wire is used as the counter electrode, and Ag/AgCl is used as the reference electrode. A 3.5 wt% NaCl solution is employed as the corrosive medium. The exposed area of the bent

specimen is 1 cm², while the remaining area is painted. Open-circuit potential tests are conducted for 1800 seconds to stabilize the voltage before proceeding with the polarization experiments. The potentiodynamic scans are performed within a voltage range of -1 V to 1 V, with a scan rate of 1 mV/s.

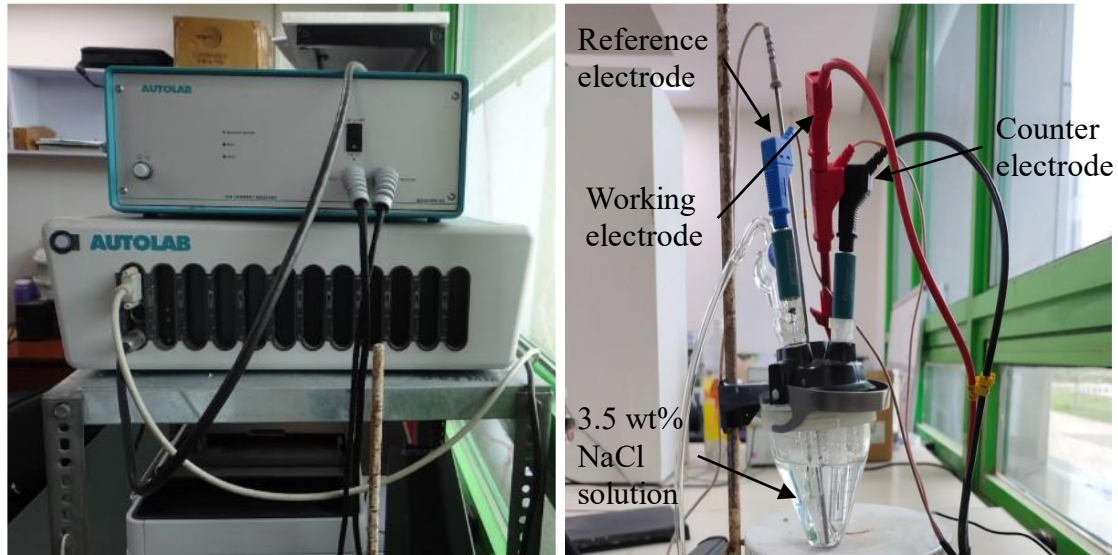


Figure 4-15. (a) Autolab electro-chemical workstation (b) position of electrodes

4.7.4. Metallurgical Analysis

4.7.4.1. *Optical Microscopy*

The metallurgical behaviour of the duplex stainless steel specimens before and after laser bending with forced as well as natural cooling is analyzed. The specimens for this analysis are taken from the central region of the scanning line, like hardness specimens, shown in Figure 4-12(b). These specimens are polished with silicon carbide polishing papers of grit size range of 400 to 4000, and then alumina paste of 1 micron particle size is used for final polishing. The polished specimens are etched with two different etchants, and microstructural images are taken with an inverted optical microscope (model: GX53, make: Olympus) shown in Figure 4-16. The specifications of the optical microscope are given in Appendix 4.8. These two etchants are Beraha's solution (85 ml distilled water, 15 ml HCl, and 1g K₂S₂O₅) and Aqua regia (1 HNO₃ + 3 HCl). Beraha's solution is used as an etchant to differentiate between the phases (ferrite and austenite), whereas Aqua regia is used to see the grain structures of both phases. Furthermore, to measure the grain size, a line is drawn on a microscopic image, and the image processing software is used to measure the length and number of intersections of

grain boundaries with the line. The ratio of the length of the line and the number of intersections is considered as grain size.



Figure 4-16. Inverted optical microscope

4.7.4.2. Scanning Electron Microscopy

Scanning electron microscopy (SEM) (model JSM-6610LV, make JEOL) shown in Figure 4-17 is used for further investigating the microstructure laser bent specimens for both natural and forced cooling. Additionally, the surface morphology of these bent specimens before and after the corrosion testing is also analyzed. The specifications of the SEM are given in Appendix 4.9.



Figure 4-17. Scanning electron microscopy with energy dispersive spectroscopy attachment

4.7.4.3. Energy Dispersive Spectroscopy

The elemental distribution is also investigated in the scanning region for both the cooling conditions before and after the corrosion testing. Energy Dispersive spectroscopy (EDS) (attachment of SEM) is used for analyzing the elemental distribution.

4.7.4.4. X-Ray Diffraction

An X-Ray diffraction (XRD) (model: X'Pert PRO, make: PANalytical) is used to examine the phase distribution in both the cooling conditions before and after the corrosion test. The XRD setup is shown in Figure 4-18, and the specifications are given in Appendix 4.10.



Figure 4-18. X-Ray diffraction setup

4.8. Summary

This chapter provides a comprehensive description of the methodology and experimental details used in the study. It includes the step-by-step process followed in the investigation, material, experimental setup, measurement of performance parameters, and the details of the measuring instruments. The summary of the chapter is as-

- The chapter begins by outlining the overall methodology, which involves selecting process parameters and testing the feasibility of forced cooling assisted laser bending through numerical simulations. Then experimental investigation on both single and multi-scan forced cooling assisted laser bending.
- The chapter discusses the worksheet material used in the study, which is duplex stainless steel (Grade: 2205). It provides details about the dimensions and coating of the worksheet material. The chemical composition of the material is also presented.

- The experimental setup is described, which involves the description of a high-power laser cutting machine equipped with a fiber laser source. The clamping arrangement for holding the worksheet as a cantilever is explained, along with the laser irradiation and scanning process. The cooling arrangement, involving forced water cooling applied to the bottom surface of the worksheet, is also discussed in detail.
- The measurement of the bend angle using a laser displacement sensor is explained. The calculation of beam diameter is presented, considering the Gaussian distribution of heat flux and the laser beam profile passing through the focal lens.
- Temperature measurement methods are described, including the use of a thermal imaging camera to measure the temperature of the top surface. The estimation of emissivity for temperature measurement is explained through a comparison with thermocouple data.
- The chapter also covers the post-bending analysis techniques employed in the study. These include micro-hardness testing, tensile strength testing performed in different orientations, corrosion analysis using electrochemical tests, metallurgical analysis through optical microscopy, scanning electron microscopy (SEM), energy-dispersive spectroscopy (EDS), and X-Ray diffraction (XRD).

Overall, this chapter provides a detailed account of the experimental procedure, including the materials used, experimental setup, measurement techniques, and post-bending analyses, giving a comprehensive understanding of the methodology employed in the study.

CHAPTER 5

FORCED COOLING ASSISTED SINGLE SCAN LASER

BENDING

This chapter includes the experimental investigation of forced cooling assisted single-scan laser bending. The primary focus is to analyze the effects of cooling conditions and various process parameters on key performance indicators, such as temperature distribution, bend angle, and mechanical and metallurgical properties. The objective is to evaluate the effectiveness of forced cooling in improving the laser bending process. The chapter also includes the optimization of process parameters for obtaining a higher bend angle at a minimum possible energy input. The summary of experimental and optimization results is given in the last section of the chapter.

5.1. Input Parameters

The laser bending experiments were performed for different sets of process parameters to investigate their influence on the bend angle. These process parameters and their ranges of variation are given in

Table 5-1. Moreover, experiments at each parameter are repeated three times to obtain

Parameters	Values
Flow rate (f)	0 (Natural Cooling), 0.5, 0.85 L/min (Forced Cooling)
Laser Power (P)	550, 700, 850, 1000 W
Worksheet Width (w)	30, 40, 50 mm
Sheet Thickness (T)	1.5, 2, 3 mm
Beam Diameter (D)	4, 6, 8 mm
Scanning Speed (V)	600, 1000, 1400, 1800 mm/min

reasonable data. The forced cooling referred to a constant value of water flow rate of 0.85 L/min, except during the study that specifically examined the effect of flow rate.

Table 5-1. Input parameters of laser bending experiments

Parameters	Values
Flow rate (f)	0 (Natural Cooling), 0.5, 0.85 L/min (Forced Cooling)
Laser Power (P)	550, 700, 850, 1000 W
Worksheet Width (w)	30, 40, 50 mm
Sheet Thickness (T)	1.5, 2, 3 mm
Beam Diameter (D)	4, 6, 8 mm
Scanning Speed (V)	600, 1000, 1400, 1800 mm/min

5.2. Temperature Analysis

Figure 5-1 shows the temperature profile of the center of the scan line with respect to time for different process parameters in both cooling conditions. It is observed that for constant scanning speed, the maximum temperature is increased and the cooling rate is decreased with increase in laser power, as shown in Figure 5-1(a) & (b). On the other hand, for constant laser power, the maximum temperature reduces, and cooling rate increases with increase in scanning speed, as shown in Figure 5-1 (b) and (c). It may be because of the lower laser-worksheet interaction time. It is also found that the maximum temperature is reduced and cooling rate is increased in forced cooling condition in comparison to natural cooling. Furthermore, the forced cooling is more significant at higher laser power and low scanning speed in terms of reducing the maximum temperature and increasing the cooling rate.

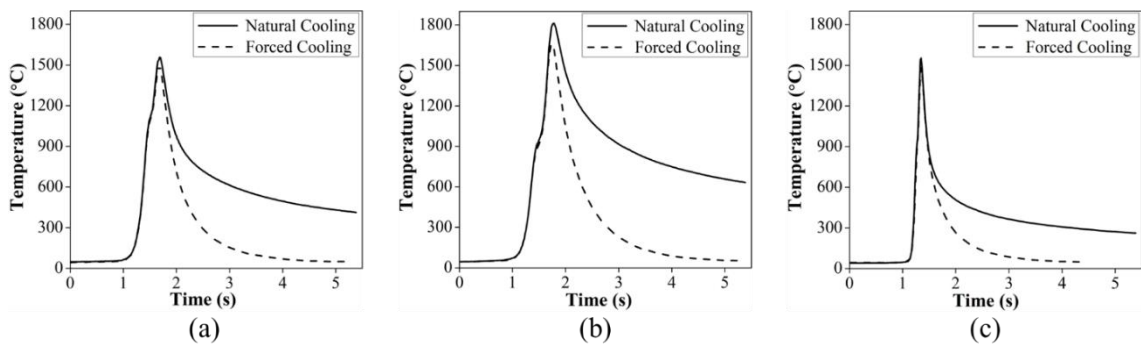


Figure 5-1. Irradiated surface temperature at the center of scanning line: (a) $P = 550$ W, $V = 600$ mm/min, (b) $P = 1000$ W, $V = 600$ mm/min, (c) $P = 1000$ W, $V = 1800$ mm/min for both the cooling conditions

5.3. Bend Angle Analysis

The bend angle achieved at different combinations of process parameters including laser power (P), scanning speed and (V), beam diameter (D), sheet thickness (T), and worksheet width (w) and the percentage increment in bend angle in forced cooling to natural cooling conditions is shown in

Table 5-2. The influence of scanning speed, beam diameter, laser power, thickness, and width of the worksheet on the bend angle is discussed in natural and forced cooling conditions.

Table 5-2. Bend angle achieved at different process parameters in both natural and forced cooling conditions

<i>P</i> (W)	<i>V</i> (mm/min)	<i>D</i> (mm)	<i>T</i> (mm)	<i>w</i> (mm)	Bend angle (°)		% Increment in bend angle
					Natural cooling	Forced cooling	
550	600	4	2	30	2.62	3.18	21.37
	1000				2.40	2.60	8.33
	1400				1.97	2.02	2.54
	1800				1.50	1.54	2.67
700	600	4	2	30	2.59	3.20	23.55
	1000				2.63	2.85	8.37
	1400				2.26	2.44	7.96
	1800				1.92	1.86	-3.12
850	600	4	2	30	2.30	3.06	33.04
	1000				2.82	3.06	8.51
	1400				2.53	2.67	5.53
	1800				2.10	2.07	-1.43
1000	600	4	2	30	2.01	3.11	54.73
	1000				3.04	3.30	8.55
	1400				2.80	2.81	0.36
	1800				2.45	2.43	-0.82
700	600	6	2	30	2.24	3.62	61.61
	1000				2.47	3.18	28.74
	1400				1.81	2.14	18.23
	1800				1.31	1.53	16.79
700	600	8	2	30	2.52	3.53	40.08
	1000				1.54	2.19	42.21
	1400				0.94	1.40	48.94
	1800				0.72	0.80	11.11
550	1000	6	2	30	1.20	1.98	65.00
700					2.47	3.18	28.74
850					3.01	3.85	27.91
1000					2.93	4.11	40.27
550	1000	8	2	30	0.95	1.08	13.68
700					1.54	2.19	42.21
850					2.60	3.26	25.38
1000					3.24	3.61	11.42
700	600	4	1.5	30	0.77	3.69	379.22
	1000				3.21	4.43	38.01
	1400				3.16	3.63	14.87
	1800				2.93	3.43	17.06

700	600	4	3	30	1.84	2.15	16.85
	1000				1.56	1.29	-17.31
	1400				1.03	0.98	-4.85
	1800				0.96	0.61	-36.46
550	1000	4	1.5	30	2.95	3.63	23.05
700					3.21	4.43	38.01
850					2.68	4.37	63.06
1000					0.79	4.24	1
550	1000	4	3	30	1.18	1.13	-4.24
700					1.56	1.29	-17.31
850					1.58	1.63	3.16
1000					1.74	2.01	15.52
550	600	4	2	40	2.47	4.08	65.18
	1000				2.70	3.19	18.15
	1400				2.31	2.68	16.02
	1800				1.99	2.15	8.04
550	600	4	2	50	2.25	4.63	105.78
	1000				2.70	3.74	38.52
	1400				2.87	2.68	-6.62
	1800				2.89	2.56	-11.42
550	1000	4	2	40	2.25	3.02	34.22
700					2.70	3.19	18.15
850					2.87	4.08	42.16
1000					2.89	4.26	47.40
550	1000	4	2	50	2.24	3.07	37.05
700					2.71	3.74	38.01
850					3.16	4.09	29.43
1000					3.39	4.88	43.95

The bend angle in natural cooling condition is decreased with laser power, whereas it is almost constant in the forced cooling condition for low scanning speed, as shown in Figure 5-2(a). In contrast, at high scanning speed, bend angle is increased with laser power in both the cooling conditions. The bend angle is increased with higher rate at a larger beam diameter in comparison to a low diameter (Figure 5-2(b)). Figure 5-2(c) shows the change in bend angle with laser power for the sheets of various thicknesses. It is found that initially the bend angle is increased marginally and then decreased drastically with laser power in both the cooling conditions for low thickness sheets. Instead, for thick sheets, it is increased with laser power. Furthermore, for different widths of the worksheet, the bend angle is increased with laser power in both the cooling

conditions. Moreover, the increment in bend angle is higher in larger width worksheets, especially in forced cooling conditions, as shown in Figure 5-2(d). In general, the bend angle increased by forced cooling is effective at higher laser power at all different parametric conditions. It is because in natural cooling condition at higher laser power, compressive plastic deformation is increased at the lower surface. It tends to bend the sheet in opposite direction and results in reduction in the bend angle. Forced cooling at the lower surface reduces the chances of compressive plastic deformation at the lower surface and results in higher bend angle.

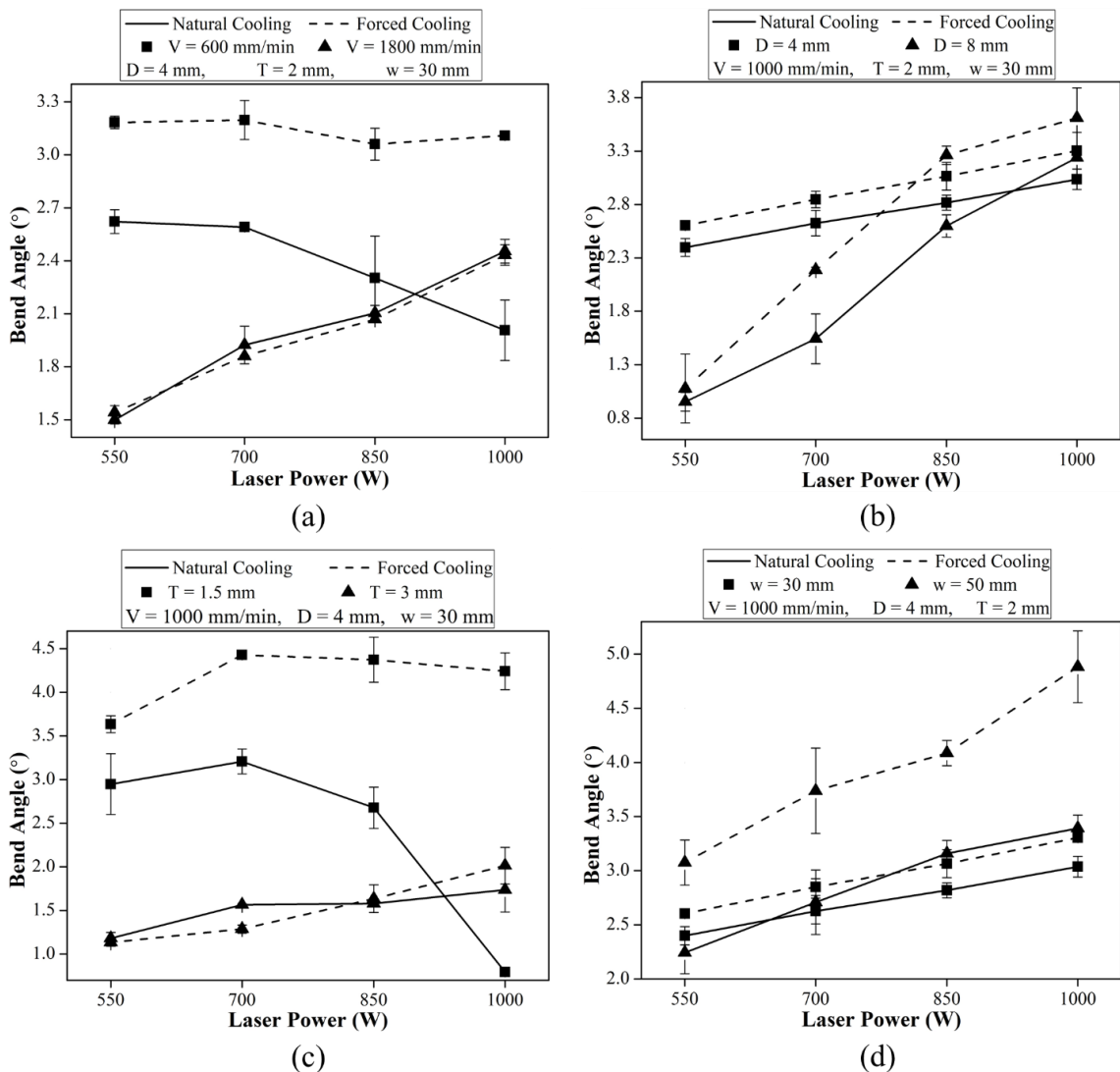


Figure 5-2. Bend angle vs. laser power at different (a) scanning speed (b) beam diameter (c) sheet thickness and (d) width of the worksheet

Figure 5-3 (a) shows that the bend angle is decreased at low laser power, whereas at high laser power, it initially increases, reaches to peak, and then reduces with scanning speed. A similar trend is observed in both natural as well as forced cooling conditions.

For different diameter laser beams, the bend angle decreased with scanning speed for both the cooling conditions. The bend angle is decreased with a higher rate in the condition of larger beam diameter in both natural and forced cooling conditions, as shown in Figure 5-3(b). Figure 5-3(c) shows that the bend angle is first increased for a low thickness sheet and then decreased with scanning speed in both the cooling conditions. In contrast, it is decreased with scanning speed for higher thickness sheets. In the natural cooling condition, the bend angle is decreased with the increment in scanning speed for smaller width of the worksheet, whereas for the large width worksheet, it is increased (Figure 5-3(d)). The bend angle is decreased with scanning speed in forced cooling condition for both the worksheet widths. Overall, the forced cooling significantly increases the bend angle at low scanning speed for all different process parameters. It is because, at low scanning speed, the laser-worksheet interaction time is increased, which leads to a reduction in temperature gradient. It increases the chances of compressive plastic deformation at the lower surface, resulting in a smaller bend angle in natural cooling condition. The temperature gradient is increased in forced cooling condition (Yadav et al., 2022a). It reduces the chances of generating compressive deformation at the lower surface, leading to a higher bend angle.

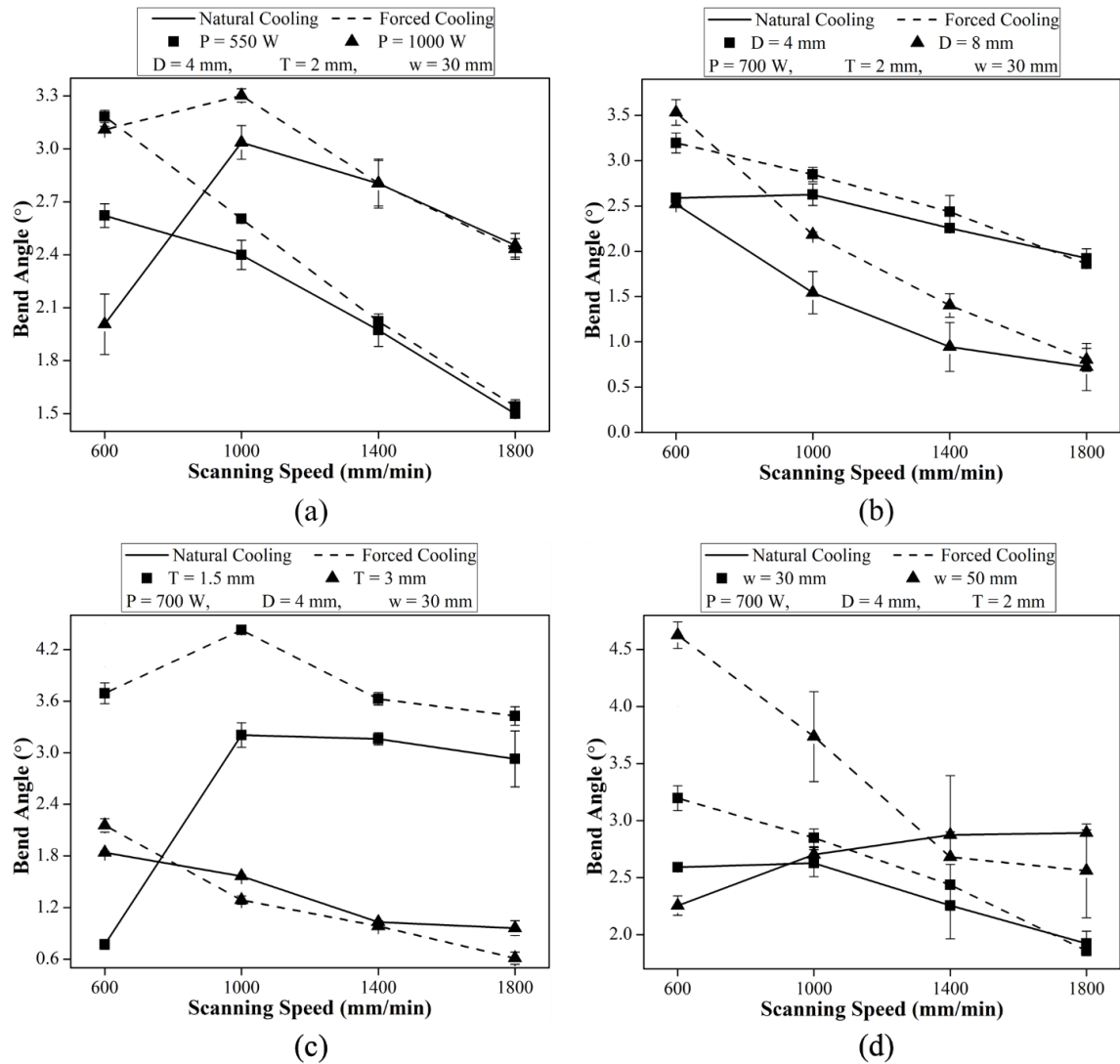


Figure 5-3. Bend angle vs. scanning speed at different (a) laser power, (b) beam diameter, (c) sheet thickness, and (d) width of the worksheet

The bend angle is decreased with beam diameter in both the cooling conditions for low laser power (Figure 5-4 (a)). Whereas at high laser power, it slightly decreases and then increases with beam diameter for natural cooling condition. In forced cooling condition, the angle first increases with beam diameter and then reduces. Figure 5-4(b) shows the influence of beam diameter on bend angle for different scanning speeds. Initially, the bend angle is decreased and then increased with the increment in beam diameter at low scanning speed, in natural cooling condition. In forced cooling condition, it is increased with beam diameter and becomes almost constant. Whereas, at higher scanning speed, the bend angle is decreased with the beam diameter in both the cooling conditions. Overall, the forced cooling is effective at intermediate beam diameter. It may be because, at lower beam diameter, the plastic zone is small, and forced cooling further

reduces the plastic zone. The larger beam diameter reduces the energy density, and forced cooling further reduces the energy by increasing convection heat transfer.

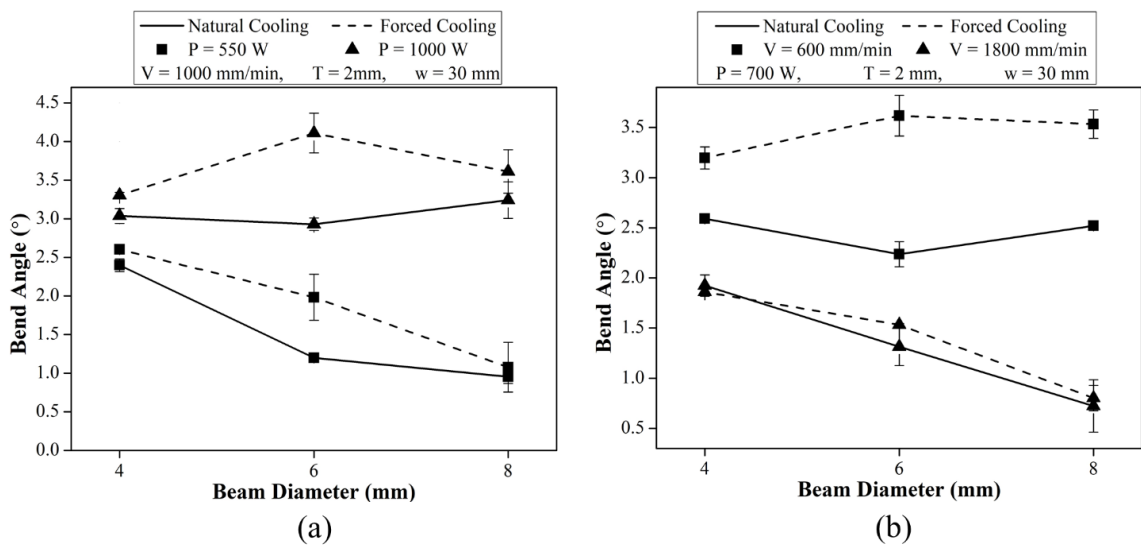


Figure 5-4. Bend angle vs. beam diameter at different (a) laser power (b) scanning speed

Figure 5-5 shows the influence of sheet thickness on bend angle at different powers, scanning speeds, and cooling conditions. The bend angle is decreased with sheet thickness at low laser power in both cooling conditions (Figure 5-5(a)). In contrast, at higher laser power, initially, it increases, reaches to the peak, and reduces with the increase in sheet thickness in natural cooling condition and continuously decreases in forced cooling condition. A similar trend can be seen for low scanning speed in Figure 5-5(b). Whereas, the bend angle is decreased with sheet thickness at high scanning speed in both natural and forced cooling conditions. In general, forced cooling at lower surface is more effective for lower sheet thickness than higher thickness, irrespective of variation in power and scanning speed. The temperature gradient generated in low thickness sheet is less in natural cooling condition, which is increased by applying forced cooling and results in higher bend angle.

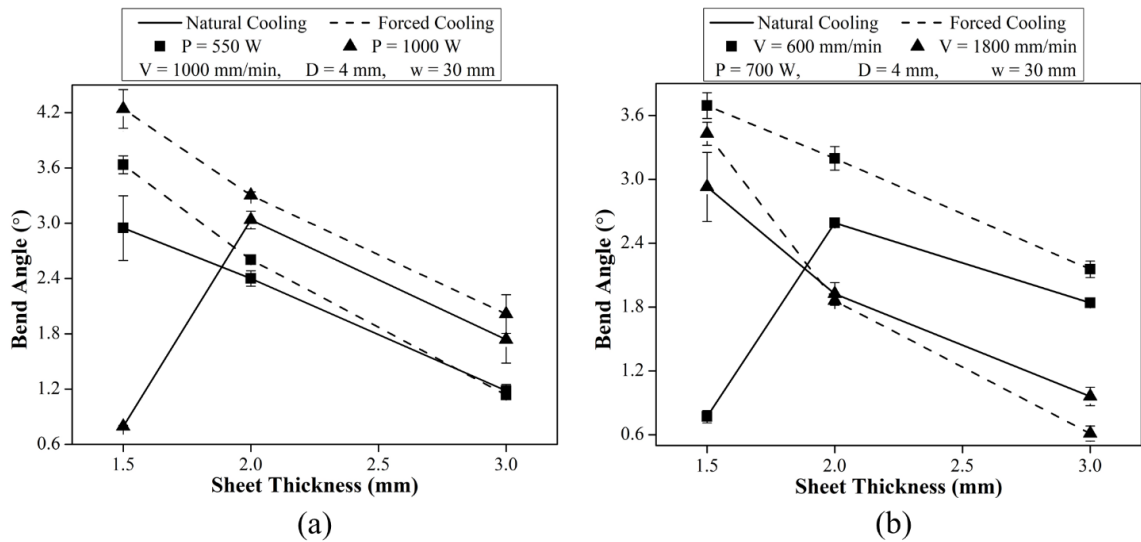


Figure 5-5. Bend angle vs. sheet thickness at different (a) laser power (b) scanning speed

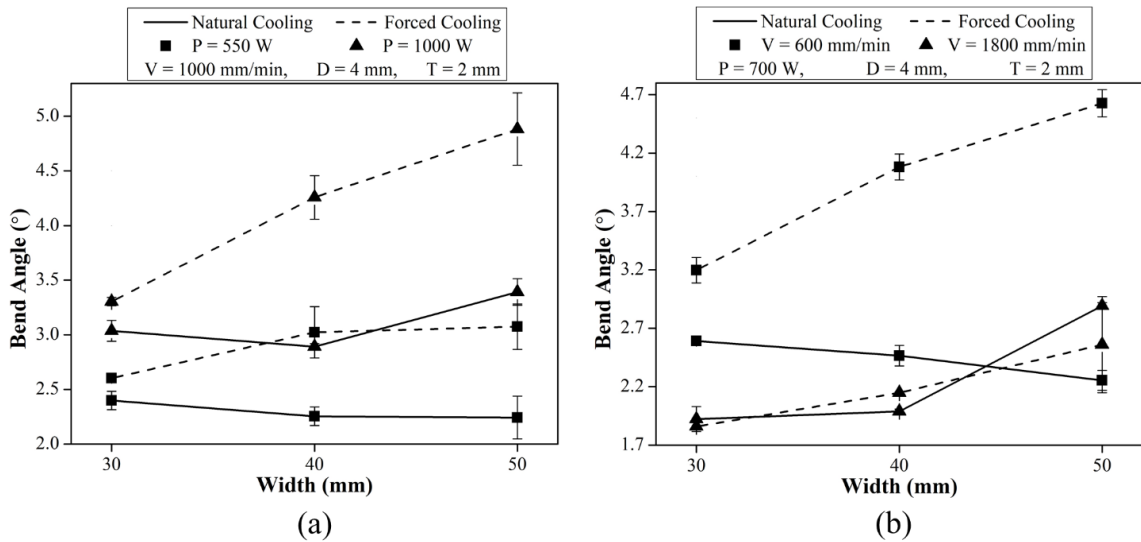


Figure 5-6. Bend angle vs. width of the worksheet at different (a) laser power (b) scanning speed

Figure 5-6(a) shows that in natural cooling condition, the bend angle is nearly constant with the increase in width of the worksheet at low laser power. However, at high laser power, it increases at increased worksheet width. In contrast, the angle continuously increases with the worksheet width in forced cooling condition for both the laser powers. Although, the bend angle is increased drastically at higher laser power in forced cooling condition. The bend angle variation with worksheet width at different scanning speed and cooling conditions is shown in Figure 5-6(b). The bend angle is decreased with the increase in width of the worksheet at low scanning speed during natural cooling condition. Whereas, at high scanning speed, the bend angle is initially nearly constant

but increases at the increased width of the worksheet. In forced cooling condition the bend angle is increased with width of the worksheet at both low and high scanning speeds. Although, increasing rate of bend angle is higher at low scanning speed. In general, the forced cooling is found to be more significant for higher width of the worksheet. The higher width of the worksheet provides more restriction to the expansion of the heating zone, resulting in higher compressive stresses that leads to higher bend angle.

Table 5-3. Bend angle variation with respect to variable cooling water flow rate

Laser Power (W)	Scanning Speed (mm/min)	Beam Diameter (mm)	Bend Angle		
			f = 0 L/min (Natural Cooling)	f = 0.5 L/min (Forced Cooling)	f = 0.85 L/min (Forced Cooling)
550	1000	4	2.40	2.26	2.60
700	1000	4	2.63	2.91	2.85
850	1000	4	2.82	3.16	3.06
1000	1000	4	3.04	3.27	3.30
700	600	4	2.59	3.31	3.20
700	1400	4	2.26	2.16	2.44
700	1800	4	1.92	1.64	1.86

In forced cooling condition the variation of water flow rate is also investigated. The flow rate of cooling water was varied for a particular set of parameters and the respective bend angle achieved is given in Table 5-3.

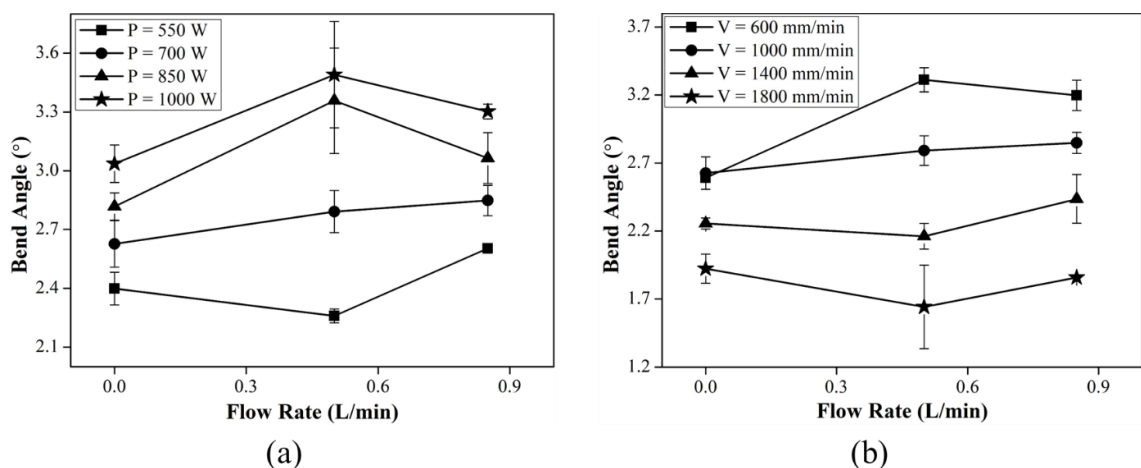


Figure 5-7. Bend angle variation with (a) laser power, and (f) scanning speed at different flow rates

The effect of cooling water flow rate along with laser power and scanning speed, respectively shown in Figure 5-7(a) and (b). At high laser powers, The temperature gradient increased by increasing the cooling flow rate from 0 to 0.5 L/min, which results in higher bend angle(Figure 5-7(a)). Although, on the further increase in the flow rate to 0.85 L/min slight reduction is observed, which may be due to excessive heat carried away by the coolant. At particular laser power of 700 W, the bend angle follows a similar pattern for low scanning speed (Figure 5-7(b)). Whereas, the bend angle is almost constant at high scanning speed and low laser power, because the energy supplied is less and forced cooling further reduces it, and increases the temperature gradient simultaneously.

5.4. Mechanical and Metallurgical analysis

Figure 5-8 shows the tensile test results of base material and bent specimens for both the cooling conditions at different set of parameters. It is found that the tensile strength is almost similar for all the bent specimens with a slight increment (upto 6%) in maximum tensile strength in comparison to the base material. Although, the ductility of the bent specimens is decreased in most of the cases. In forced coolingcondition, the tensile strength is slightly higher and ductility is lower as compared to natural cooling. The hardness of the bent specimen is measured in the scanning region at both upper and lower surfaces for both the cooling conditions at different parameters. The hardness is found to be significantly increased at the upper surface whereas at lower surface, slight increment is observed, as shown in Figure 5-9. This increment is more significant in forced cooling condition (18 to 32 %) in comparison to the natural cooling (10 to 28 %).

The microstructure of the bent specimens is analyzed to explore the possible reason of above-mentioned changes in mechanical properties. The properties of duplex stainless steel depend on the combination of ferrite and austenite phases (Stainless, 2014). The base material has both ferrite (dark) and austenite (bright) phases uniformly distributed along the rolling direction, as shown in Figure 5-10(a). Figure 5-10(b) shows that the distribution of these phases has changed and grain refinement is occurred in the scanning region. At the upper surface, the major portion of the microstructure is ferrite, whereas austenite is present at the grain boundaries of the ferrite matrix, as shown in Figure 5-10 (c). Similar observations are also reported by Odermatt et al. (Odermatt et al., 2021a), where it is observed that the microstructure of melt is fully ferrite, and during cooling,

austenite formation is going to start at the grain boundaries of ferrite. The limited melting and rapid cooling during the forced cooling condition may lead to a relatively higher percentage of austenite with smaller grains. So, the higher ferrite phase and smaller grains of austenite may be the reason behind high strength and hardness and low ductility. At the lower surface, the microstructure is quite similar to the base material but the hardness is increased may be due to the formation of sigma (σ) phase at the boundaries of ferrite and austenite (Dos Santos and Magnabosco, 2016). Literature reports that the sigma phase forms in the temperature range of 500 °C to 850 °C and it dominates at higher cooling rates (Oh et al., 2013; Petrovic et al., 2012; Tehovnik et al., 2016). That may be the reason of higher hardness at low laser powers and high scanning speed and in forced cooling conditions, respectively.

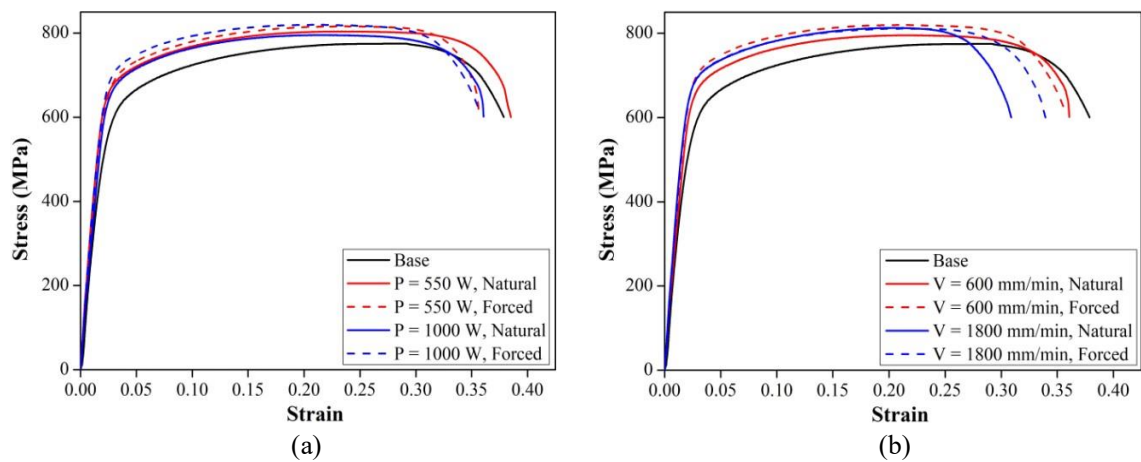


Figure 5-8. Tensile strength analysis at: (a) different laser powers for $V = 600$ mm/min, and (b) different scanning speeds for $P = 1000$ for both natural and forced cooling conditions

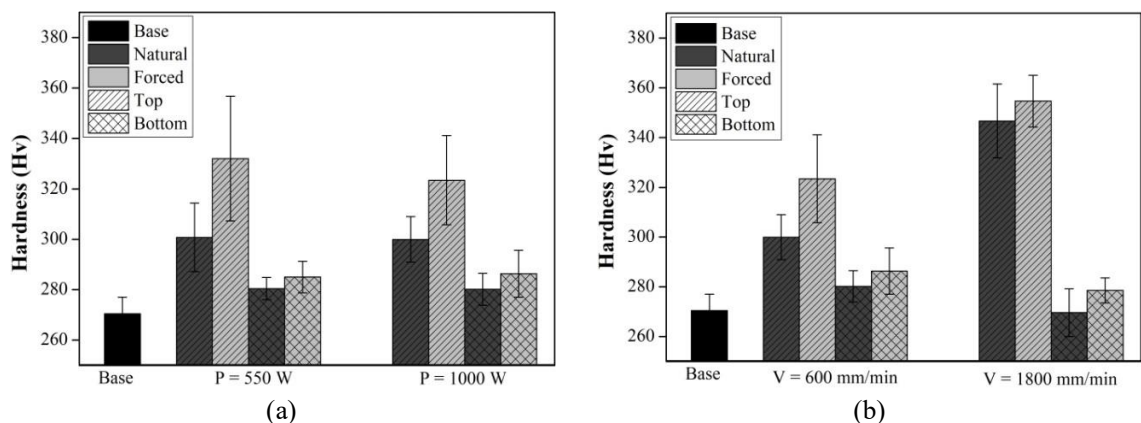


Figure 5-9. Hardness in scanning region at both upper and lower surfaces at: (a) different laser powers for $V = 600$ mm/min, and (b) different scanning speeds for $P = 1000$ W

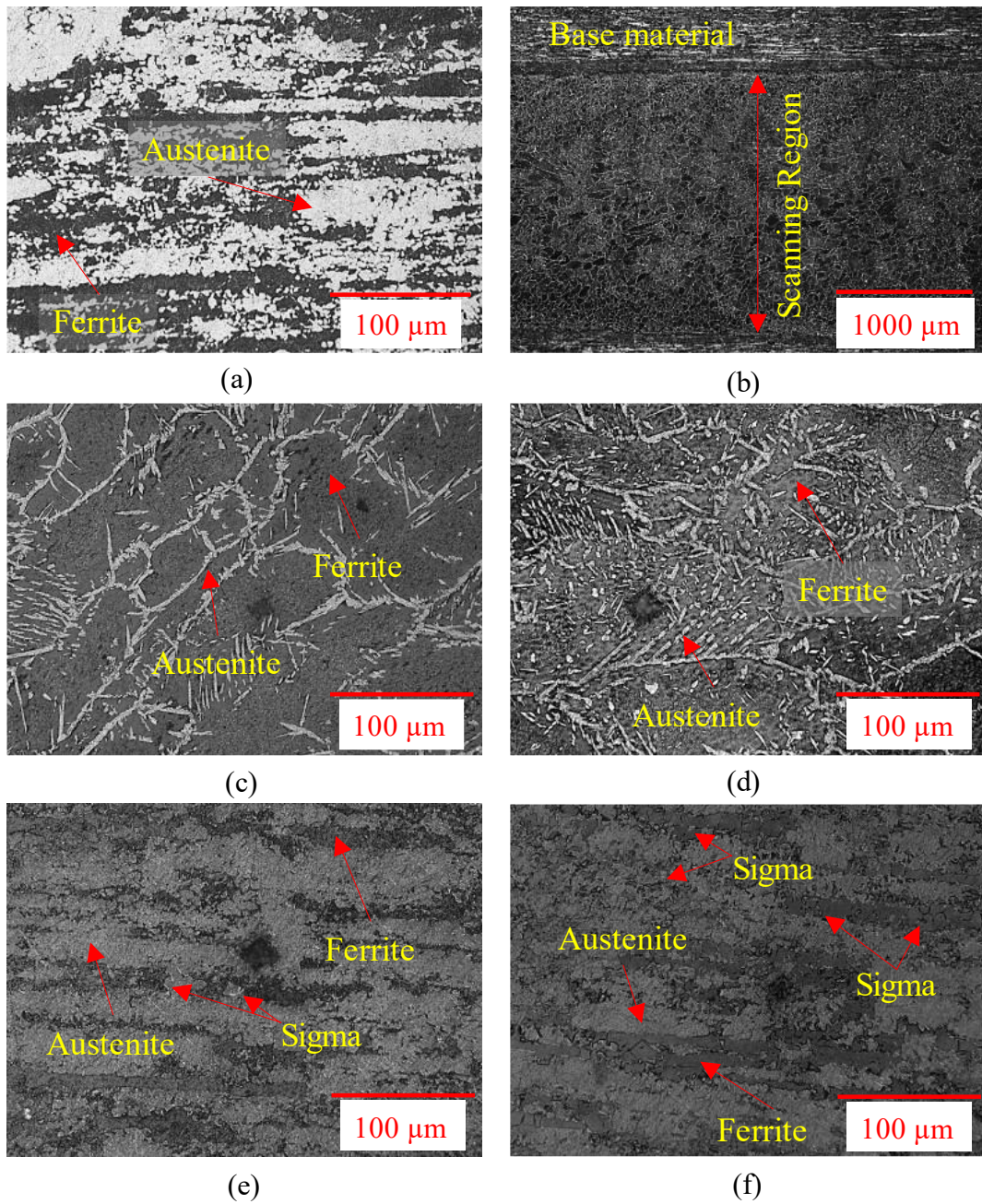


Figure 5-10. Microstructural images of (a) base material, (b) scanning region, (c) upper surface in natural condition and (d) upper surface in forced cooling condition, (e) lower surface in natural condition and (f) lower surface in forced cooling condition

5.5. Optimization

5.5.1. Regression Fit Function

The experimental results discussed above show that for a particular sheet geometry, the bend angle significantly affected by energy parameters (scanning speed, laser power and beam diameter), and cooling conditions. The impact of each parameter is heavily influenced by the other parameters. So, the interaction effect of these process parameters is also investigated by making a fit function (Equation 5-1) that includes all these process parameters using the experimental data. The coefficient of determination (R^2) of the developed empirical model is 87.24%. The P-value shows the significance level of the respective parameter or model. A p-value <0.05 represents that a particular parameter or model significantly affects the response. The P-values of the regression model and process parameters are given in Table 5-4. This function is experimentally validated by comparing the predicted and experimentally achieved bend angle for random values of process parameters. The predicted values align well with the experimental results, with an absolute error of 8.74% as shown in Table 5-5.

$$\begin{aligned}
 \text{Bend Angle} = & 7.036 + 0.798 \times f - 0.006067 \times P \\
 & - 0.001101 \times V - 0.798 \times D \\
 & + 0.000416 \times f \times P - 0.000840 \times f \times V \\
 & + 0.0692 \times f \times D + 0.000002 \times P \times V \\
 & + 0.001205 \times P \times D - 0.000217 \times V \times D
 \end{aligned}
 \tag{5-1}$$

Table 5-4. Results of ANOVA for the regression model of bend angle.

Source	DF	F-Value	P-Value	Significance
Regression	10	84.11	0.000	
Flow Rate	1	3.23	0.075	Non-significant
Laser Power	1	47.22	0.000	Significant
Scanning Speed	1	5.86	0.017	Significant
Beam Diameter	1	58.23	0.000	Significant
Flow Rate*Laser Power	1	1.04	0.310	Non-significant
Flow Rate*Scanning Speed	1	30.08	0.000	Significant
Flow Rate*Beam Diameter	1	3.30	0.072	Non-significant
Laser Power*Scanning Speed	1	18.43	0.000	Significant

Laser Power*Beam Diameter	1	113.80	0.000	Significant
Scanning Speed*Beam Diameter	1	26.11	0.000	Significant
Error	123			
Lack-of-Fit	56	8.08	0.000	
Pure Error	67			
Total	133			

Table 5-5. Experimental validation of fit function at random process parameters.

f	P	V	D	Predicted Bend Angle	Experimental Bend Angle	Standard Deviation	% Error
0.75	620	855	6	2.55	2.66	0.16	4.00
0.21	770	706	5	2.75	2.70	0.02	-1.72
0.85	930	876	4	3.22	3.09	0.35	-3.97
0.85	880	1642	4	2.48	2.19	0.03	-13.46
0	610	679	5	2.37	2.63	0.06	9.74
0.75	700	1065	8	2.2	1.89	0.31	-16.13
0.75	760	1081	5	2.7	2.82	0.04	4.28
0	650	1250	7	1.35	1.67	0.1	19.30
0	820	759	6	2.63	2.59	0.29	-1.59
0.21	960	1755	4	2.59	2.29	0.04	-13.19

5.5.2. Process Parameter Optimization using Pareto optimality and Genetic Algorithm

Table 5-2 present experimental data indicating that similar bend angles can be achieved with different parameters. The process parameters should be selected according to the minimum required energy to achieve a specific bend angle. Therefore, when optimizing these parameters, the objective should not only be to maximize the bend angle but also to maximize the bend angle per unit line energy. Line energy refers to the amount of energy that is delivered to a worksheet per unit length of scanning. This value can be determined by dividing the laser power by the scanning speed. The optimization process should prioritize the first objective outlined in Equation 5-1, which aims to maximize the bend angle, followed by the second objective outlined in Equation 5-2, which aims to maximize the bend angle per unit line energy.

$$\frac{\text{Bend Angle}}{\text{Line Energy}} = \frac{\text{Bend Angle (Equation 1)}}{P/V} \quad 5-2$$

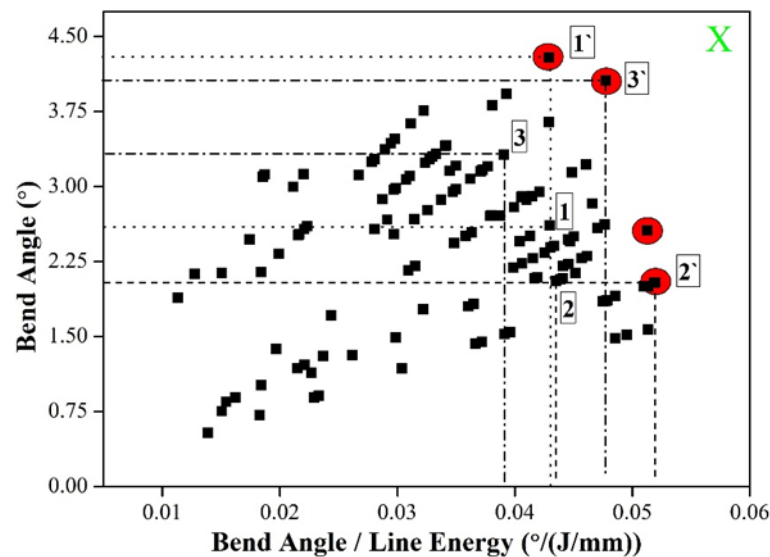


Figure 5-11 Experimental data on the field of both objective functions

Pareto optimization is utilized to tackle the multi-objective optimization problem with the help of Genetic Algorithm, which provides a set of optimal parameters that cannot enhance one objective without compromising the other (Tušar et al., 2015). For a better understanding, the experimental data are plotted on a 2D graph (Figure 5-11), where the axes represent the two objectives of the optimization problem (bend angle and bend angle per line energy). Each black data point represents a unique combination of parameters. It is evident from the figure that every black data point can be enhanced in either of the objectives or both without degrading the other objective. For example, point

1 can be improved to 1' with a higher bend angle without any loss in bend angle per line energy. Similarly, point 2 can upgrade to 2' with higher bend angle per scan without degrading the bend angle. Furthermore, point 3 can improve to 3' by enhancing both the aspects (bend angle and bend angle per scan). Based on the above discussion, it is clear that black data points cannot provide an optimal solution. The optimal solution lies within the Pareto front (red data point), or it may be situated beyond these points and approaching the X, indicated in Figure 5-11. A genetic algorithm is employed to achieve an optimum Pareto front, approaching the X.

The genetic algorithm (GA) is a computational optimization technique that takes inspiration from the process of natural selection as described by Darwin's theory of evolution.. The GA consists of three fundamental genetic operators: selection, crossover, and mutation (Zan et al., 2020). The selection operator is employed to identify the chromosome with the highest fitness value from the population. The chromosomes are then modified through the crossover and mutation operators to achieve the best fit and meet the specific objective. These modified chromosomes are referred to as offspring. The selection operator is subsequently utilized to search for the fittest value from the previous generation and the offspring. The crossover and mutation operators are then applied to develop the new generation (Esfahani et al., 2016; Keshtiara et al., 2021). This process iterates until the best-fit value for the specific objective is attained.

Table 5-6. Optimized Pareto front data set

S.No.	f	P	V	D	Bend angle	Bend angle per line energy
1	0.8498	988.45	1653	7.99	3.08	0.0858
2	0.8499	988.07	1121.9	7.99	3.91	0.074
3	0.85	987.59	673.3	7.99	4.61	0.0524
4	0.8489	988.02	1607.7	7.98	3.15	0.0853
5	0.8469	987.55	791.8	7.98	4.42	0.0591
6	0.8354	987.41	816	7.98	4.37	0.0602
7	0.8477	987.91	1402.9	7.98	3.47	0.082
8	0.8473	987.41	997.2	7.98	4.1	0.069
9	0.8404	987.51	1168.7	7.98	3.83	0.0755

10	0.8498	988.45	1653	7.99	3.08	0.0858
11	0.8459	987.63	1036.2	7.98	4.04	0.0706
12	0.8372	987.47	888.7	7.95	4.25	0.0638
13	0.8497	988.19	1488.9	7.99	3.34	0.0838
14	0.8472	988.14	1555.3	7.98	3.23	0.0847
15	0.8445	987.67	1328.2	7.98	3.58	0.0803
16	0.8427	987.50	712.2	7.98	4.54	0.0546
17	0.8469	987.45	750.9	7.98	4.49	0.0569
18	0.8303	987.23	848.8	7.98	4.31	0.0618

The Pareto optimization with GA gave a set of optimized parameters (Table 5-6). This set of parameters is used to form an optimized Pareto front, shown in Figure 5-12. The maximum optimized bend angle is 4.61° , which is around 7.5% higher than the maximum bend angle achieved in experimental data. The optimum parameters are $f = 0.85$ L/mm, $P = 987.59$ W, $V = 673.3$ mm/min and $D = 7.99$ mm. Furthermore, the bend angle per line energy is also improved by 22.14% from 0.0429 to 0.0529. The optimum parameters are experimentally validated and found in good agreement with error of 2.21%. Overall, in natural cooling condition the maximum bend angle achieved is 3.24° , which enhanced to 4.61° in forced cooling condition. This increment of around 42% in bend angle is achieved with almost same rate of bend angle per line energy.

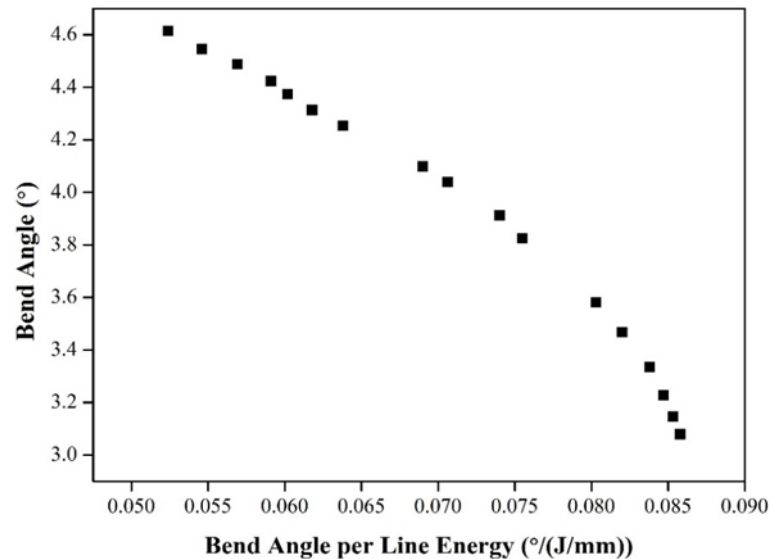


Figure 5-12. Optimized pareto front.

It can also be observed by comparing Figure 5-11 and Figure 5-12 that bend angle per unit line energy has been enhanced significantly after optimization. Even the maximum bend angle per unit line energy (0.05194) achieved in initial experiments is less than that of the minimum in optimized parameters (0.0524), with a higher bend angle.

5.5.3. Mechanical and metallurgical properties at optimum condition

The tensile and hardness test results of the specimens bent with optimum parameters show that the tensile strength of the bend specimen is increased. Although, the ductility is reduced, as shown in Figure 5-13(a). The hardness at both lower and upper surfaces is also increased compared to the base material. However, the hardness at the lower surface is less than the upper surface, as shown in Figure 5-13(b). The microstructure is investigated at both lower and upper surfaces. The etchant (Beraha's solution) reacts with the ferrite phase (dark) only, and the austenite (bright) remains the same (Varbai et al., 2018). Figure 5-13(c) shows that the ferrite and austenite are equally present and arranged in the rolling direction. The laser irradiation has rearranged this distribution. At the upper surface, the austenite accumulates at the ferrite grain boundaries. The high temperature at the upper surface causes melting that results in the complete formation of the ferrite phase, whereas, formation of austenite initiates at the grain boundaries while cooling (Yadav and Kant, 2022). On the other hand, at the lower surface, both phases are distributed uniformly, and grain refinement has occurred.

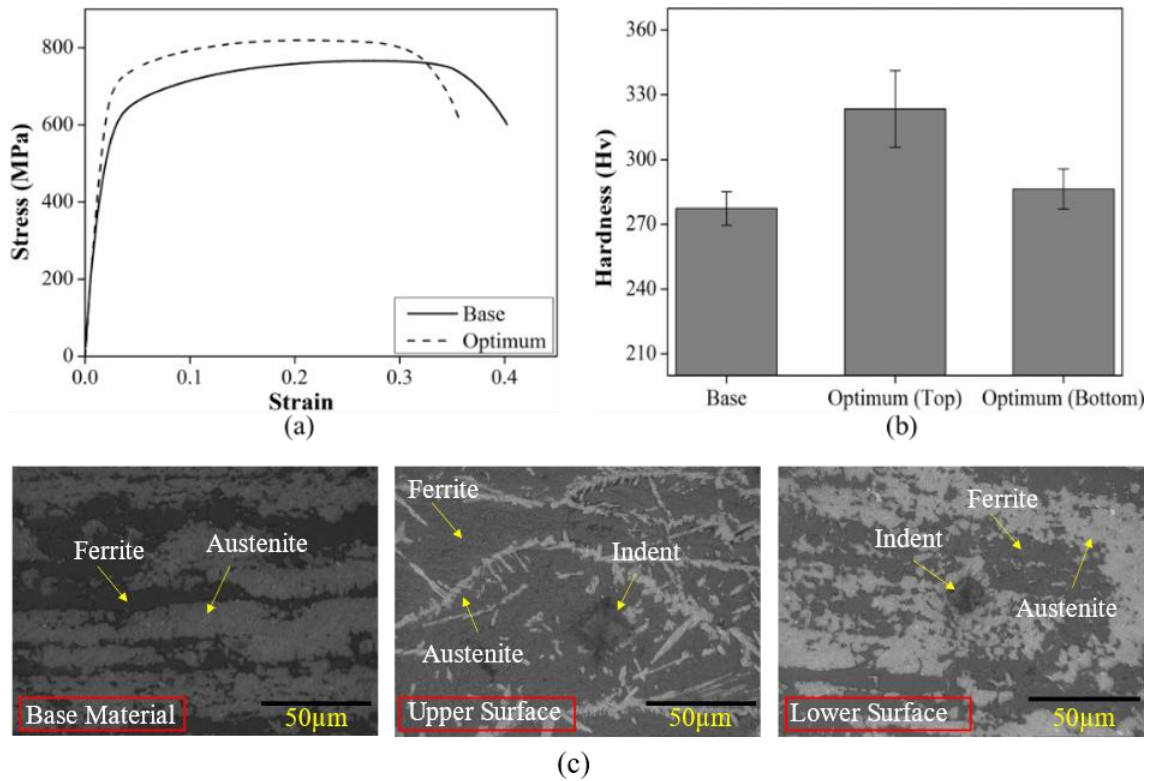


Figure 5-13. Comparison of mechanical properties (a) Tensile (b) hardness and (c) microstructure of the laser bent specimens irradiated with optimum processing condition with respect to the base material

5.6. Summary

The experimental study is conducted on single scan laser bending of duplex-2205 in natural and forced cooling conditions. The temperature profile, bend angle, and mechanical and metallurgical properties in natural and forced cooling conditions are investigated to analyze the effects of worksheet geometry (thickness and width), laser parameters (scanning speed, beam diameter, and power), and cooling conditions (flow rate). These process parameters are optimized using pareto analysis and genetic algorithm in order to achieve higher bend angle with a high rate of bend angle per line energy given to the worksheet. The fit function used for optimization and the optimum parameters are experimentally validated, and the mechanical and metallurgical properties at the optimum condition are also analyzed. The important observations of the study are-

- The maximum temperature at the upper surface is reduced, and the cooling rate is increased with the application of forced cooling, which reduces the material degradation.

- The bend angle is found to be higher in forced cooling at lower scanning speed, intermediate beam diameter, and higher laser power, irrespective of variation in other parameters. Furthermore, the bend angle is observed to be higher in forced cooling for lower thickness and longer width of the worksheet.
- The results of the study indicate that the use of forced cooling on the lower surface can lead to a considerable increase in the bend angle. The maximum bend angle achieved in the natural cooling condition was 3.41° which was enhanced by 35.2 % in the forced cooling condition and reached to 4.61° with almost the same bend angle per line energy rate.
- The tensile strength and hardness of bent specimens are improved at the expense of ductility. Additionally, forced cooling has increased the tensile strength and hardness as compared to natural cooling condition.
- The variation in phase distribution is observed at the upper surface in the scanning region, whereas at the lower surface, the phase distribution is quite similar to base material except for the sigma phase formations at the boundaries of ferrite and austenite.
- The maximum bend angle achieved in the experimental data set was 4.29° , whereas the optimum bend angle is 4.61° , so the bend angle was enhanced by 7.5% only. But the maximum bend angle in initial experiments was achieved at bend angle per line energy of 0.0429 which is enhanced to 0.0524 at optimum condition, so the bend angle per line energy rate is improved by 22.14 %.
- The tensile strength and hardness of the bend specimen at optimum parametric condition were found to be enhanced at the expense of ductility. That was because of the rearrangement of phase distribution in the laser irradiation region.

FORCED COOLING ASSISTED MULTI-SCAN LASER BENDING

This chapter focuses on investigating the potential of forced cooling assisted laser bending with multiple laser irradiations. It consists of two studies that explore the process at different parameter ranges. The first study used the same parameters as the single-scan forced cooling assisted laser bending, which were high-line energy parameters suggested by the pilot study. On the other hand, the second study was performed using low-line energy parameters. Although, the pilot study did not find forced cooling assisted laser bending effective at low line energies in single-scan laser bending. The motivation behind studying low-line energies in a multi-scan approach is based on the idea that the total energy supplied to the worksheet is high due to multiple scans. This approach may potentially yield new information about the process.

6.1. Multi-Scan Forced Cooling assisted Laser Bending at High Line Energy

The present study attempts to enhance the bend angle of duplex stainless steel by applying forced cooling during multi-scan laser bending. It may reduce the number of scans required for achieving a required bend angle which ultimately reduces the time, cost, energy, and material degradation due to excessive heating. The effects of process parameters under natural cooling and forced cooling conditions are analysed in this study, along with the investigation of the metallurgical, mechanical, and corrosion properties of the bent specimens. The process parameters used in this study are identical to those employed in the previous chapter on forced cooling assisted single-scan laser bending, given in Table 5-1. Throughout the study, the number of scans remained constant at five.

6.1.1. Bend angle analysis

The variation in bend angle (after five scans) with laser power for both natural and forced cooling conditions at different scanning speeds is shown in Figure 6-1(a). In natural cooling condition, the bend angle reduces with the increment in laser power for low scanning speeds, while it increases for higher scanning speeds. On the other hand, it is found to be enhanced with laser power in forced cooling condition, although the rate of increment decreases. Figure 6-1(b) reveals that the bend angle is enhanced, attained peak, and then reduced at higher scanning speed for natural conditions. Moreover, the bend angle is minimum and maximum at high and low laser power, respectively, for low scanning speed, whereas this pattern gets reversed at high scanning speed. On the other hand, in forced cooling condition, the bend angle reduces with scanning speed, irrespective of laser power. Additionally, the maximum bend angle is observed at high laser power, irrespective of scanning speed.

The bending by TGM depends on the temperature gradient and the difference in the plastic strain developed between the upper and lower surfaces. The lower scanning speed leads to more laser-worksheet interaction time and results in higher heat transfer to the lower surface, reducing the temperature gradient (Yadav et al., 2022b). The forced cooling helps reduce the temperature at the lower surface, which raises the temperature gradient and enhances the bend angle (Yadav et al., 2022a). Although, the energy absorbed is less at high scanning speed, and forced cooling further takes away a part of the heat, resulting in a lower bend angle, especially at low laser power. Overall, the bend angle is significantly enhanced at low scanning speed and high laser power in forced cooling condition.

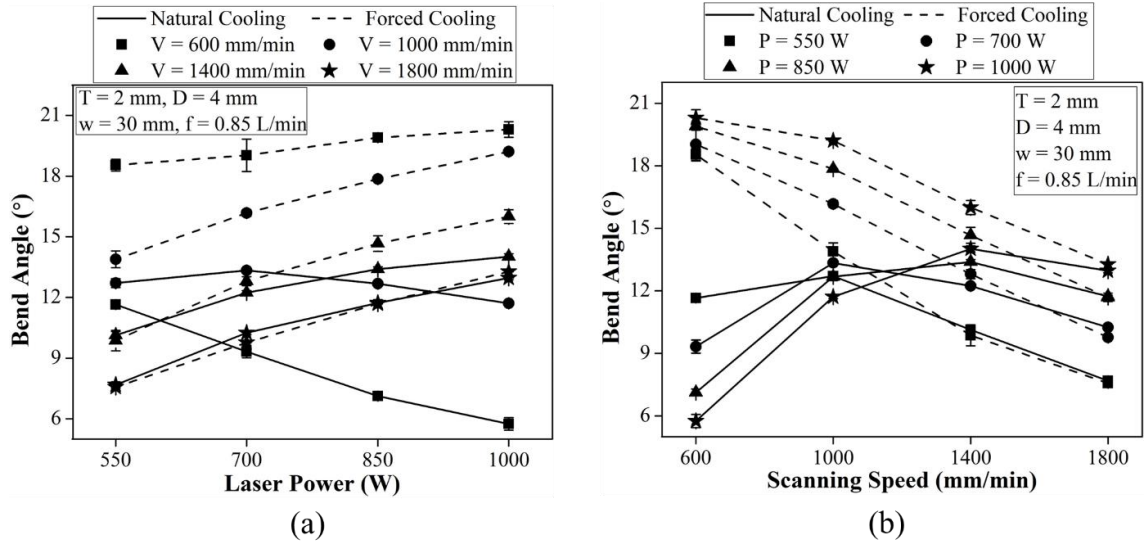


Figure 6-1. Variation in bend angle with (a) laser power at different scanning speed, (b) scanning speed at different laser power for both the cooling conditions

In natural cooling condition, the bend angle decreases with beam diameter at high scanning speed, whereas at low scanning speed, it starts increasing at large beam diameter (Figure 6-2(a)). Similarly, the bend angle decreases with beam diameter in forced cooling condition, although at low scanning speed first it increases and then reduces. In both cooling conditions, the bend angle decreases with beam diameter at low laser power. In contrast, at high laser power, first, it reduces then enhances in the natural cooling condition, and vice-versa in forced cooling condition (Figure 6-2(b)). It may be because, at high laser power and low scanning speed, the compressive stresses at the lower surface are higher at lower beam diameter in natural cooling condition (Ravi Kant and Joshi, 2016b). However, at large beam diameter, these stresses are less due to the reduction in the energy density, which is further reduced by forced cooling. Overall, it is observed that the bend angle is enhanced in forced cooling for a moderate beam diameter.

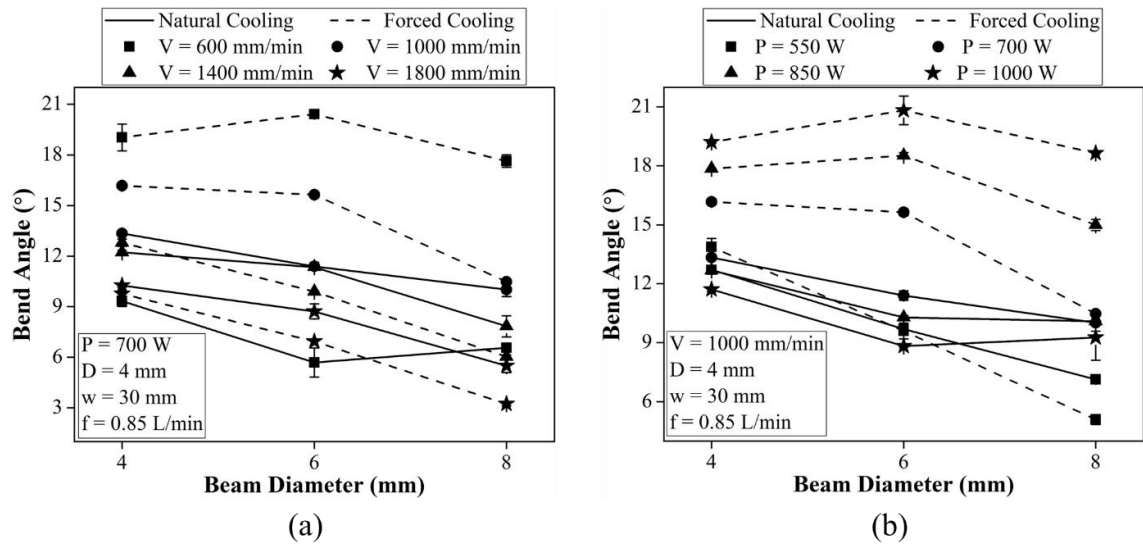


Figure 6-2. The variation in bend angle with beam diameter at various (a) laser power and (b) scanning speed for both the cooling conditions

In natural cooling condition, the bend angle enhances with increment in sheet thickness at 600 mm/min scanning speed, although the rate of increment is reduced at higher sheet thickness (Figure 6-3(a)). At higher scanning speed, it increases and then reduces with the increment sheet thickness. Further increment in scanning speed (1800 mm/min) results in continuous decrement in bend angle. In forced cooling condition, the bend angle is continuously reduced with an increment in the sheet thickness at all sets of scan speed and laser power. Moreover, at low sheet thickness, the angle is maximum and minimum at low and high laser power, respectively, whereas this pattern gets reversed at high sheet thickness (Figure 6-3(b)). The low sheet thickness led to low-temperature gradient in comparison to high sheet thickness for natural cooling condition. Furthermore, the stiffness of the worksheet is also increased with sheet thickness which requires higher energy to get deformed, leading to a low bend angle at high scanning speed and low laser power. The forced cooling raises the temperature gradient in thin sheets at low scanning speed, which enhances the bend angle. Overall, the forced cooling is more significant for low-thickness sheets.

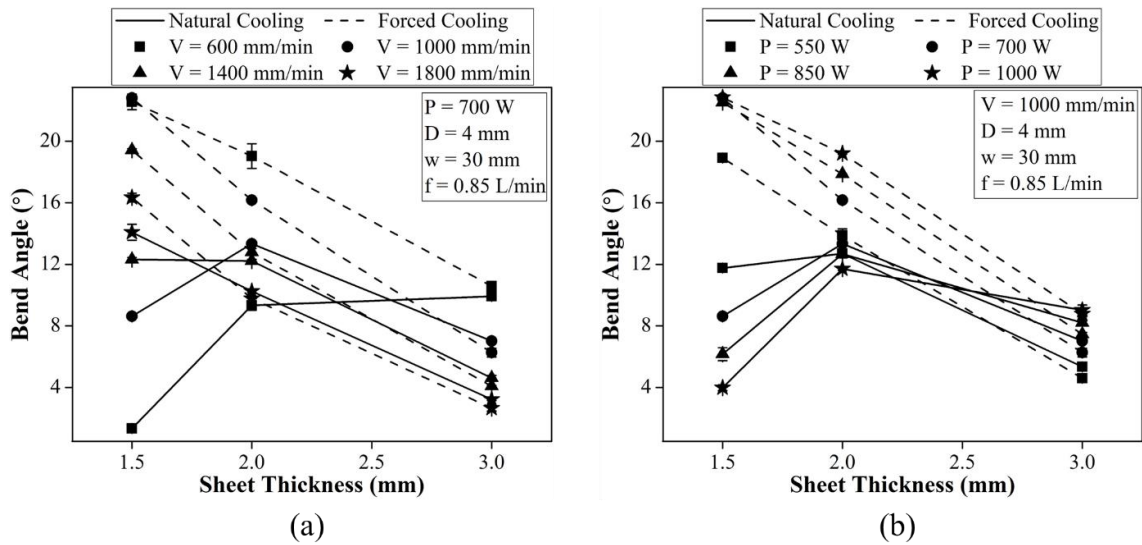


Figure 6-3. The variation in bend angle with sheet thickness at various (a) laser powers and (b) scanning speeds for both the cooling conditions

Figure 6-4(a) & (b) show the effect of worksheet width in natural and forced cooling conditions for various scanning speed and laser power, respectively. The bend angle is enhanced with the worksheet width for all the sets of scanning speed and laser power and in both the cooling conditions. The higher width of the worksheet provides more cooler region, which restricts the thermal expansion, resulting in higher compressive stresses in the heating zone that lead to higher bend angle (Shi et al., 2011).

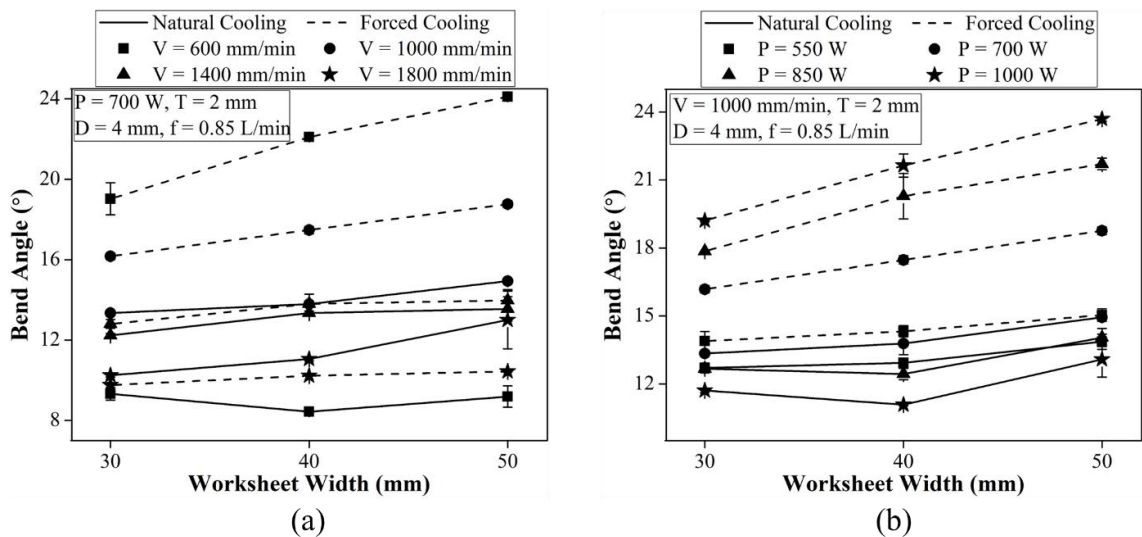


Figure 6-4. The variation in bend angle with worksheet width for both the cooling conditions at various (a) laser powers and (b) scanning speeds

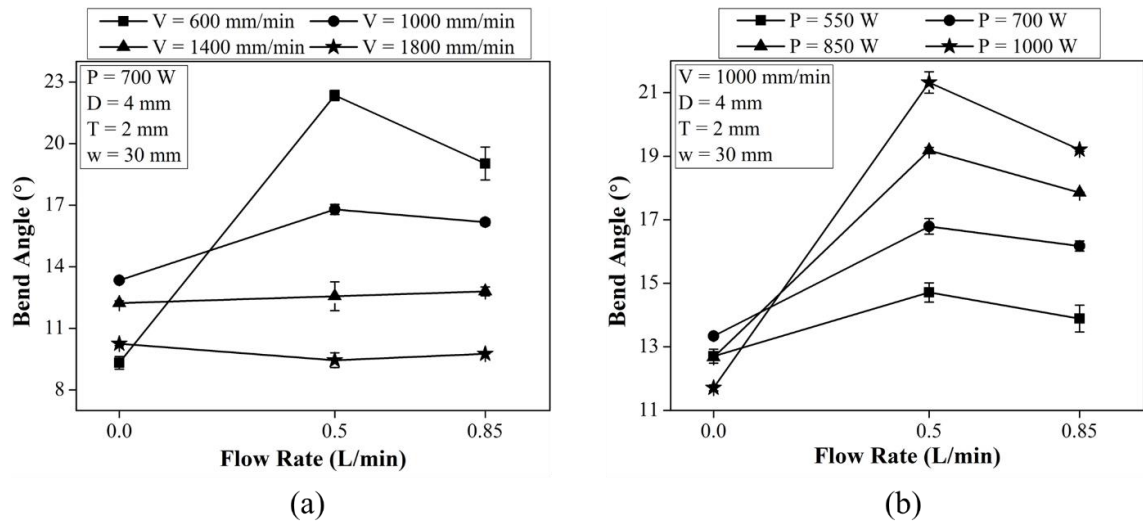


Figure 6-5. The variation in bend angle with flow rate for both the cooling conditions at various (a) laser powers and (b) scanning speeds

The effect of the water flow rate for various scanning speed and laser power are shown in Figure 6-5(a) and (b), respectively. The bend angle is increased with the flow rate moving from 0 (natural cooling) to 0.5 L/min. However, it decreases while further increasing the flow rate. A drastic increment is observed at high laser power and low scanning speed. The increment rate reduces with an increasing scanning speed and with a decreasing laser power. In natural cooling conditions (0 L/min flow rate), the bend angle increases with scanning speed and reduces with laser power. In contrast, in forced cooling condition, the trend gets reversed irrespective of the flow rate. It may be because the temperature gradient reduces with a decrease in scan speed and an increase in laser power, which is significantly enhanced by forced cooling. Although, A higher flow rate of water during forced cooling leads to excessive heat loss resulting in a reduced bend angle.

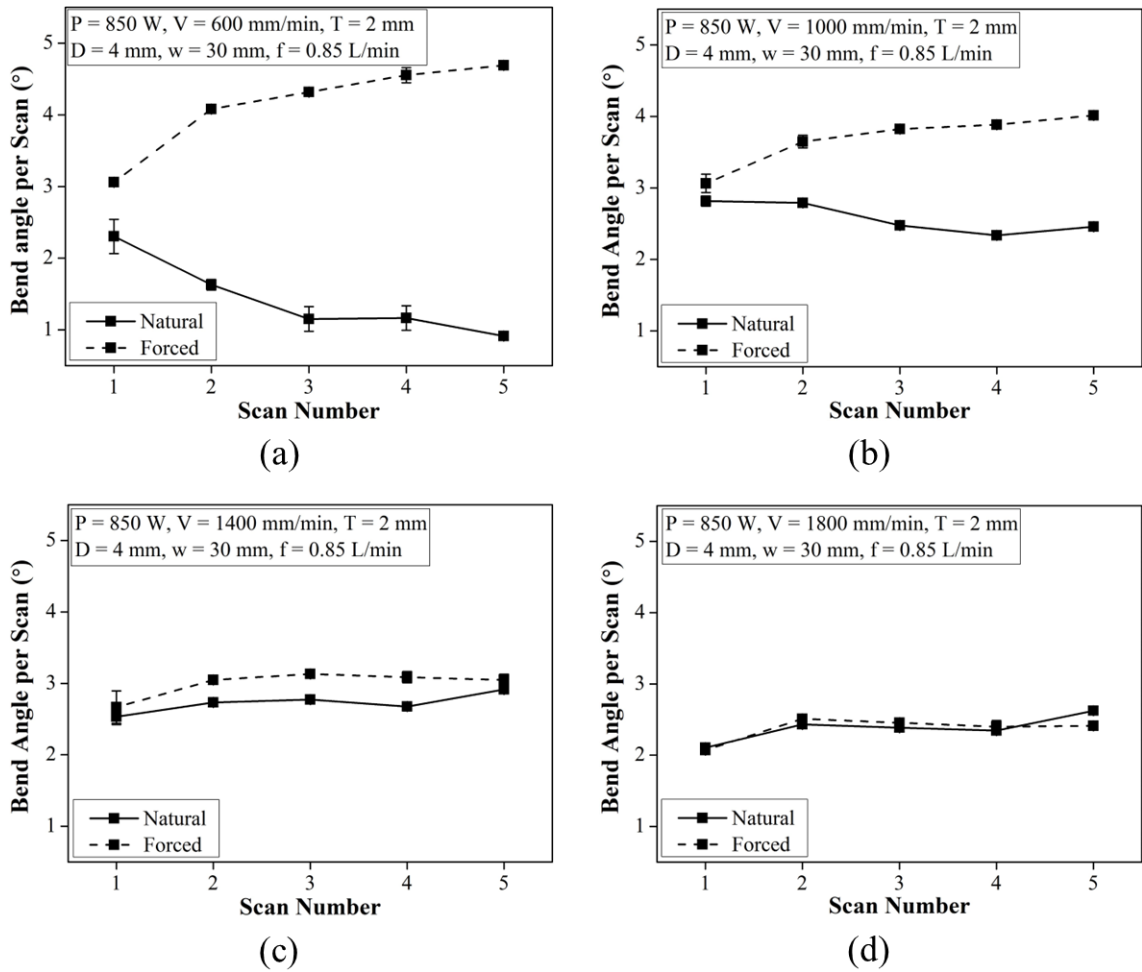


Figure 6-6. Bend angle per scan at constant laser power of 850 W and different scanning speed of (a) 600 mm/min, (b) 1000 mm/min, (c) 1400 mm/min and (d) 1800 mm/min

The bend angle variation with the number of scans in both cooling conditions at different scanning speeds is shown in Figure 6-6. At low scanning speed, the bend angle per scan decreases with an increase in the number of scans for natural cooling condition. On the contrary, in the forced cooling condition, it increases, although the rate of increment decreases with the number of scans, as shown in Figure 6-6(a). A similar pattern is observed at 1000 mm/min scan speed (Figure 6-6(b)) however, the rate of decrement in natural cooling and rate of increment in forced cooling are reduced. The further increment in scanning speed results in a nearly constant bend angle per scan, as shown in Figure 6-6(c) & (d). At lower scanning speed, the temperature gradient is reduced in each subsequent scan for natural cooling condition, whereas forced cooling increases it. The increment in scanning speed raises the temperature gradient, but it also reduces the available energy, and forced cooling further reduces it. Further increment in the

scanning speed results in the reduction of absorbed energy due to less laser and worksheet interaction time, however it increases the temperature gradient. Both these factors counter each other and result in an almost constant bend angle with scan number.

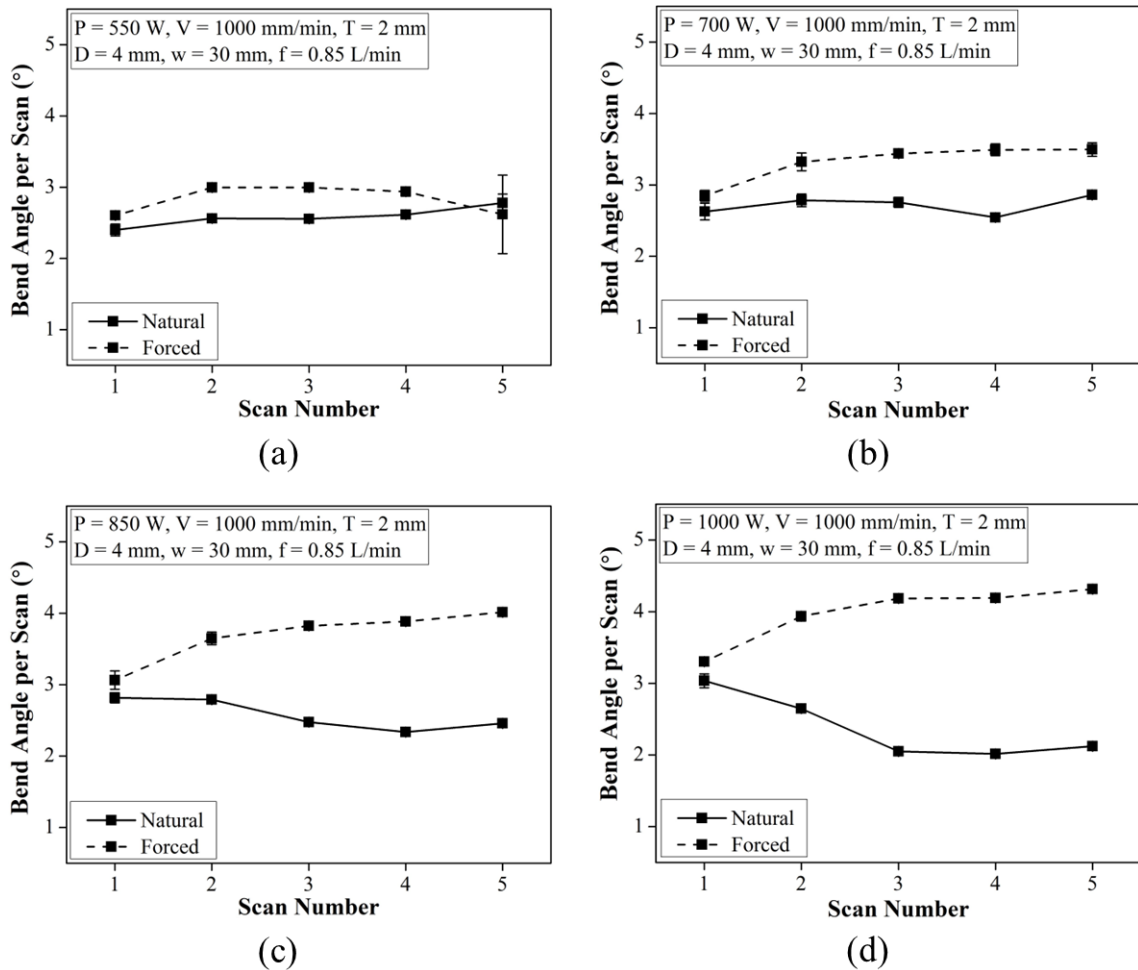


Figure 6-7. Bend angle per scan at a constant scanning speed of 1000 mm/min and different laser power of (a) 550 W, (b) 700 W, (c) 850 W, and (d) 1000 W

The bend angle in each scan is almost same for every scan at low laser powers for both natural and forced cooling conditions (Figure 6-7(a)). It starts to decrease with an increment in power for natural cooling condition, whereas for the forced cooling condition it increases (Figure 6-7(b), (c), & (d)). It may be because, at low laser power, the energy supplied is less which continuously rises with the number of scans, leading to more deformation. Simultaneously, the temperature gradient reduces with the number of scans. In contrast, the energy available rises with laser power, and the temperature gradient reduces with the number of scans in natural cooling conditions. In forced cooling condition, the temperature gradient is higher and the available energy rises with

the number of scans at high power, which leads to lower flow strength and increases bend angle.

6.1.2. Microstructural Analysis

Duplex stainless steel has two phases i.e., hard ferrite phase and soft austenite phase and it is discussed in introduction that percentage of these phases are important in determining the properties. It is recommended to maintain almost equal proportions of these phases to achieve better properties and in general, austenite phase content less than 25% is unacceptable (Hsieh et al., 2001). It is observed from the literature that Nitrogen content and cooling rate are two influential parameters which effect the phase formations thereby properties (Liou et al., 2002). Above 1350°C the whole material converts into complete ferrite phase and during the cooling stage austenite forms at the grain boundaries thereby growing and forming austenite rich grains. Nitrogen needs to be available to form the rich austenite formation as nitrogen is a strong austenite stabilizer (Hsieh et al., 2001). In case of high cooling rate, the available nitrogen forms chromium rich nitrides $\text{Cr}_2\text{N}/\text{CrN}$ precipitates which are preferential sites for pitting corrosion in duplex steel (Hsieh et al., 2001; Liou et al., 2002).

Table 6-1.Set of process parameters and their calculated line energies

S. No.	Laser Power (W)	Scanning speed (mm/min)	Cooling condition	Nomenclature	Line energy (J/mm)
1	550	1000	Natural	N550_1000	33
2	700	600	Natural	N700_600	70
3	700	1800	Natural	N700_1800	23
4	1000	1000	Natural	N1000_1000	60
5	550	1000	Forced	F550_1000	33
6	700	600	Forced	F700_600	70
7	700	1800	Forced	F700_1800	23
8	1000	1000	Forced	F1000_1000	60

There are different ways to decrease the cooling rate like increasing the laser power or decreasing the scanning speed. In the current work, along with the chosen cooling type i.e., forced cooling / natural cooling other process parameters like laser power and scan speed can also affect the cooling rate. The process parameters combinations for which metallurgical and mechanical investigation conducted are given in Table 6-1 along with their nomenclatures and respective line energies. The objective of this section is to

explain the major microstructural changes occurred in the sample. The samples explained in this section are chosen based on the line energies and cooling conditions.

Among the parameters of natural cooling condition, N700_600 have highest line energy which would result in availability of high amount of heat and slowest cooling rate. Figure 6-8(a). shows the microstructure of as received base material which reveals the austenite and ferrite phases identified after etching. Figure 6-8(b) shows the microstructure for the N700_600 bent sample, where it can be observed that Widmanstatten austenite (WA) is formed at the HAZ zone and long elongated austenite in the rest of the scanned area. The WA usually forms from the grain boundary austenite (GBA), which later transforms to austenite (Yang et al., 2011), these GBA, WA and austenite formed from the cooling are known as reformed austenite. The extent of WA in the HAZ is very limited, this indicates that the cooling rate in this condition is enough to form the complete reformed austenite formation. Figure 6-8(c) shows the optical microscopic images for N550_1000 where it showed the indications of WA and ferrite phase with fine grains. The results are in line with the findings of Lacerda et al. (De Lacerda et al., 2015) where they have observed fine ferrite grains with WA with different cooling conditions. This is due to the higher cooling rate in the form of scan speed and lowest laser power (as already mentioned that high power induces slow cooling rate and vice versa) and fine grains are related to sudden cooling and heating of different scans. In Forced cooling condition, F700_1800 which is having a line energy of 23 J/mm have the highest cooling rate in the form of both scan speed and forced cooling from the bottom. Figure 6-8(d) shows the OM image of HAZ and scan area where in the HAZ austenite can be seen and in the scanned area fine ferrite grains are visible owing to the highest cooling rate. Figure 6-8(e) shows the OM images for F550_1000 where it showed the indications of WA and evenly distributed austenite phase in the scan area. This is due to the higher cooling rate in the form of scan speed, lowest laser power and applied forced cooling which limits the extend of temperature raise in HAZ and other places. The EDS image of N700_600 and F700_1800 are shown in Figure 6-9(a) & (b) highlights the distribution of Nitrogen in the scanned area in the bent samples. As it is discussed that nitrogen plays important role in determining the phase fraction and formation of Cr/N based precipitates, it is observed that in N700_600 sample, Nitrogen is more distributed in the scanned area when compared to accumulation happened in F700_1800. This highlights the effect of cooling rate on the

distribution of Nitrogen. This accumulation will lead to the more formation of Cr/N precipitates and less formation of austenite which observed in the OM images as well (Figure 6-8(d)).

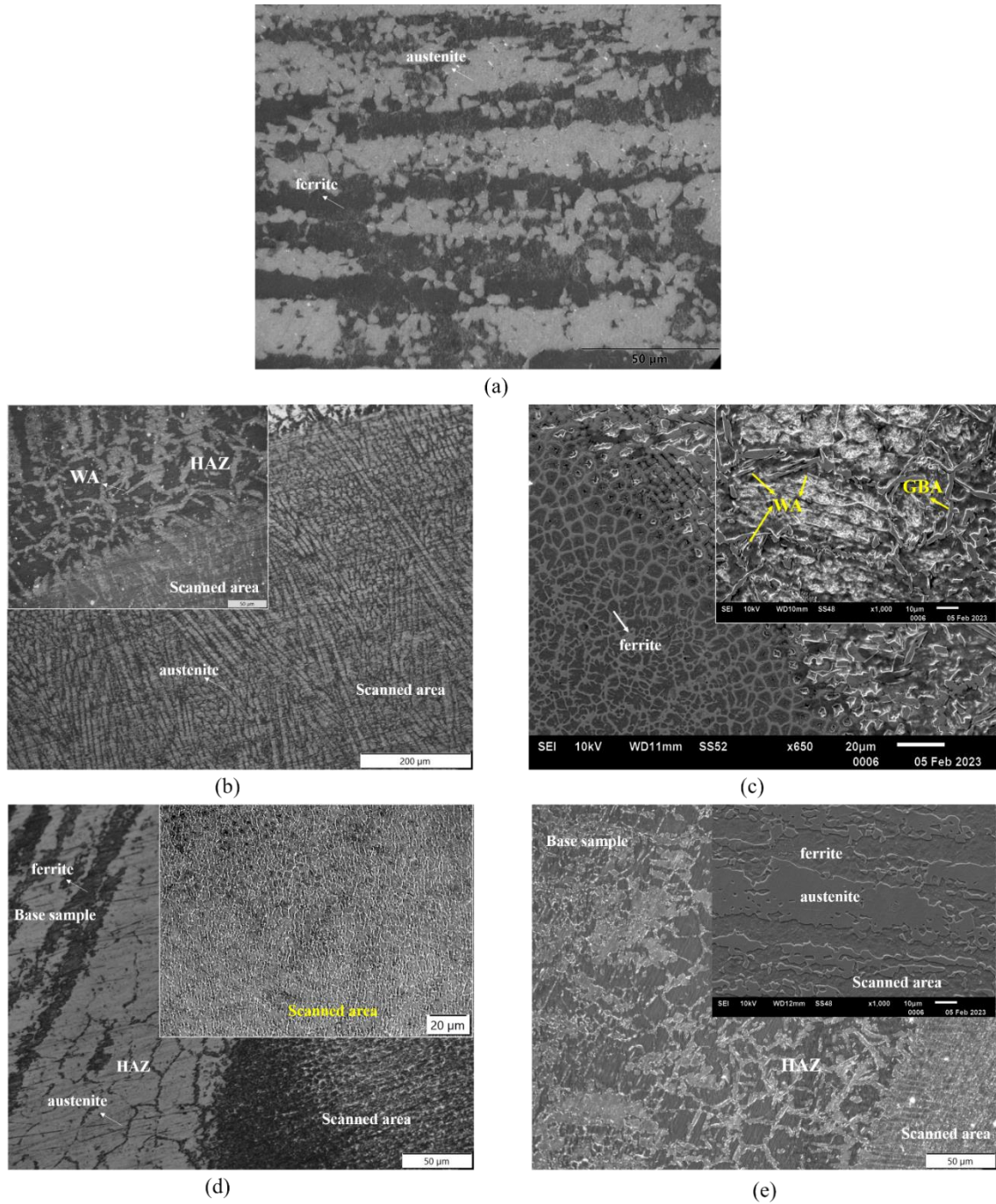


Figure 6-8. Optical & SEM images of selected samples (a) Base material (b) N700_600 (c) N550_1000 (d) F700_1800 (e) F550_1000

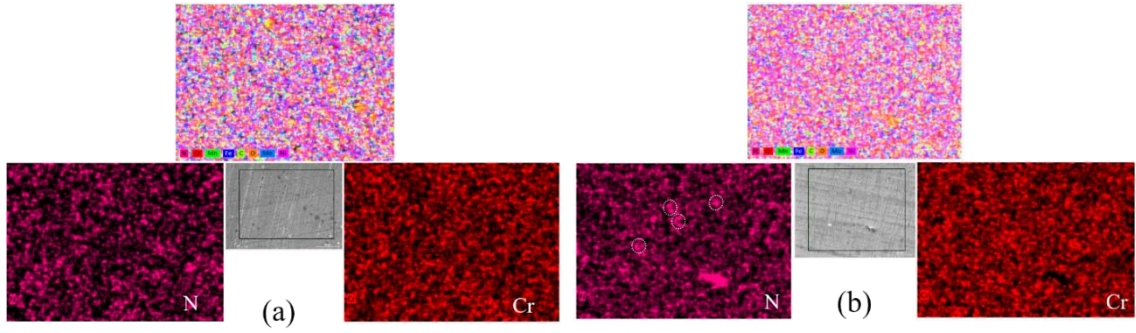


Figure 6-9. EDS mapping and elemental distribution of (a) N700_600 (b) F700_1800

The changes in the cooling rate which results in change in austenite-ferrite phase formation can be observed from XRD plots as well. XRD plots of selected samples are shown in Figure 6-10, where different phases are identified and matched. Among the samples N550_1000 and F550_1000, high cooling rate and low power is associated in F550_1000. This resulted in lower ferrite content in F550_1000 compared with the ferrite content in N550_1000. This can be observed from the peak ratio change at 43.5° and 45.3° which corresponds to austenite and ferrite phases. The same can be inferred for the samples F1000_1000 and N1000_1000 where austenite peaks at 50° is more dominating in N1000_1000 owing to the slow cooling rate which results in more austenite formation.

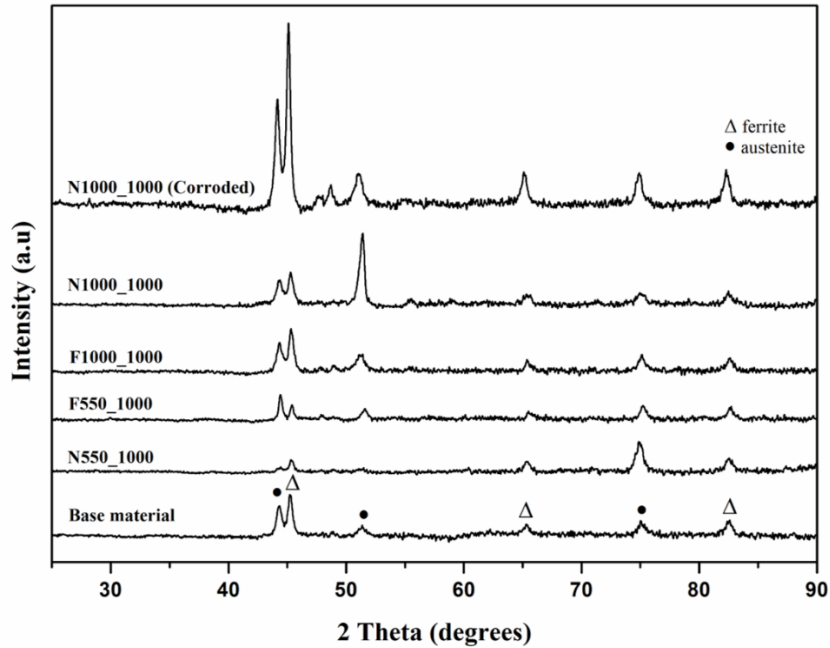


Figure 6-10. XRD plot of samples with different conditions

6.1.3. Mechanical Analysis

Hardness of the bent samples are shown in the Figure 6-11(a). Among all the samples, highest hardness is achieved for F700_1800 owing to the high cooling rate in the form of scan speed as well as forced cooling. This condition should allow to form mostly ferrite with fine grains and Cr/N precipitates as observed in Figure 6-8(d) & 12 (b). The lowest hardness achieved is for N700_600 which is having highest line energy and slowest cooling rate which favors the formation of complete recovery of reformed austenite (Figure 6-9(a)). Among the forced cooling and natural cooling conditions, forced cooling samples exhibited higher hardness in all cases except 500_1000, where N550_1000 exhibited better hardness than the F550_1000. The cooling rate in natural cooling is well enough for the grain formation owing to the less heat while compared with F550_1000 where the laser power used is low and already accompanied with forced cooling thereby limiting the extend of heat transfer. XRD phase analysis of comparison of these samples also indicates the same where the austenite peak at 43° is high when compared with the respective peaks of any other sample. This could be the reason for the drop in hardness as austenite is soft in nature.

The stress-strain plots for the bent samples are shown in Figure 6-11(b). The trend observed in hardness is related to cooling rate which facilitates the formation of soft austenite phase, the same can be observed in tensile test as well. The bent samples have exhibited higher tensile strength, high yield strength and lower fracture strain when compared with the base material. Among the samples, N700_600 which has lowest hardness owing to the high austenite fraction have exhibited highest fracture strain among all the samples. F550_1000 and N700_1800 which have high hardness in their respective sets has showed lower fracture strain. This reduced fracture strain can be attributed to the increase in ferrite content which reduces the ability to accommodate deformation (Odermatt et al., 2021b). Similar kind of findings were observed from Lacerda et al. (De Lacerda et al., 2015) work, where the samples with fine grain size and high ferrite exhibited low yield strength and low ultimate tensile strength.

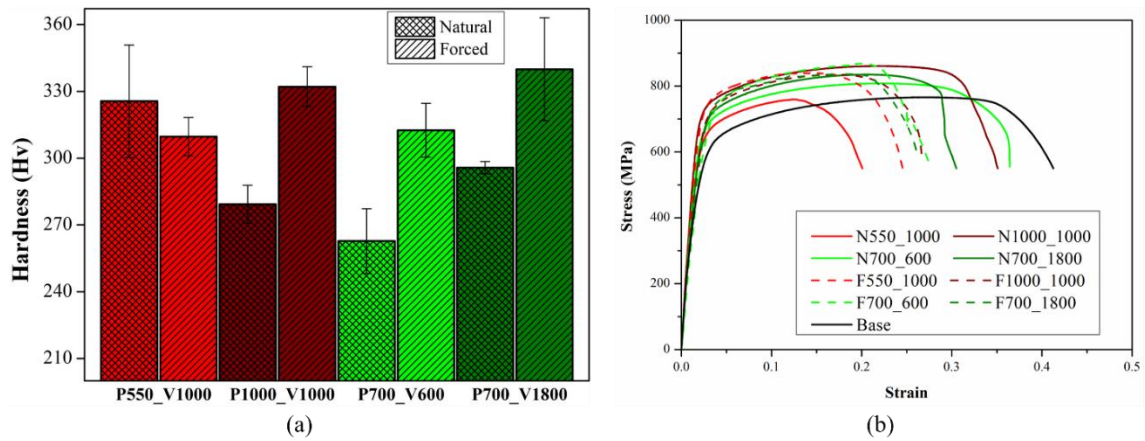


Figure 6-11. Mechanical analysis of bent samples (a) hardness (b) tensile strength

6.1.4. Corrosion Analysis

It is reported in the literature that effect of austenite and ferrite phase percentage on the corrosion resistance is important in deciding the pitting potential and corrosion resistance (Liou et al., 2002). As it is already discussed that cooling rate and nitrogen content highly effects the formation of Cr rich nitrides which are the preferential sites for the pitting corrosion in duplex steels. On the other side, reformed austenite formed from high heat input will result in increasing the pitting potential (Liou et al., 2002). Potentiodynamic plots for the bent samples and base sample are shown in Figure 6-12(a) – (i).

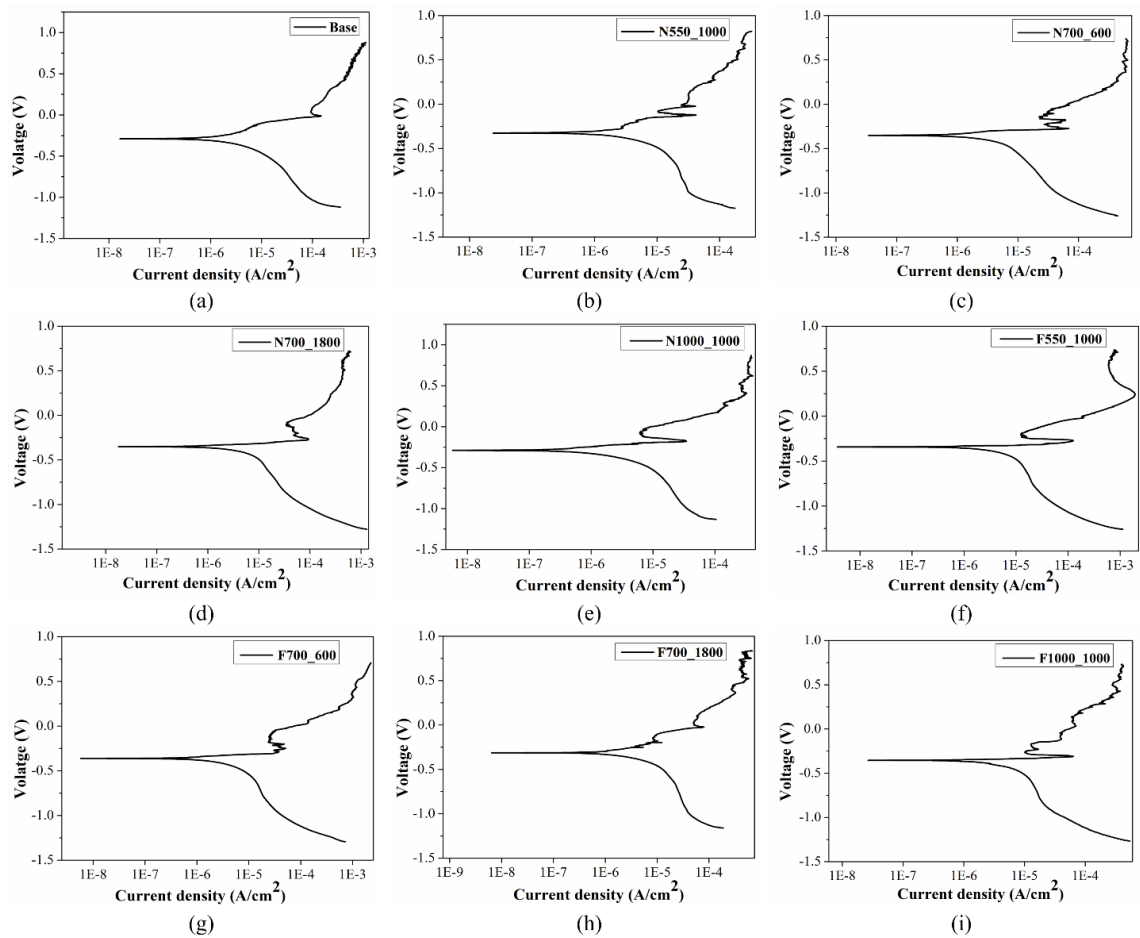


Figure 6-12. Potentiodynamic polarization plots of (a) base material (b) N550_1000 (c) N700_600 (d) N700_1800 (e) N1000_1000 (f) F550_1000 (g) F700_600 (h) F700_1800 (i) F1000_1000

Table 6-2. Electro chemical corrosion results in 3.5% NaCl medium

Material	OCP (V)	E_{corr} (V)	I_{corr} (A/cm ²)	E_{pitt} (V)
Base material	-0.120	-0.285	0.92 E-6	0.11
F550_1000	-0.259	-0.341	1.48 E-6	-0.18
F700_600	-0.294	-0.361	1.13 E-6	-0.11
F700_1800	-0.162	-0.314	1.15 E-6	-0.16
F1000_1000	-0.267	-0.356	1.78 E-6	-0.16
N550_1000	-0.176	-0.324	1.12 E-6	-0.07
N700_600	-0.260	-0.337	1.15 E-6	-0.11
N700_1800	-0.278	-0.348	1.36 E-6	-0.07
N1000_1000	-0.132	-0.266	0.81 E-6	-0.02

E_{corr} is the indication for the corrosion initiation which can be observed from the cathodic to anodic transition, I_{corr} is the corrosion resistance of the material calculated from the slope of cathodic to anodic transition, E_{pitt} is the initiation of the pitting which can be observed from the sudden increase in the current density after a passivation layer. Passivation layer indicates the formation of strong oxide layer on the working electrode upon reacting with the corrosion medium which stops the further corrosion. The I_{corr} , E_{corr} and E_{pitt} are summarized in the Table 6-2. Electro chemical corrosion results in 3.5% NaCl medium. From corrosion results showed in Table 6-2, it can be understood that I_{corr} for all the samples lies between $0.9 \mu\text{A}/\text{cm}^2$ to $1.7 \mu\text{A}/\text{cm}^2$, among which N1000_1000 has exhibited highest corrosion resistance (lower the I_{corr} the higher the corrosion resistance). There observed a change in pitting potential and the passivation current among the samples. Natural cooled samples have showed higher E_{pitt} -0.03V except for N550_1000 sample which E_{pitt} is -0.18V. All Force cooled samples have showed an early-stage pitting between -0.1 to -0.18 V which can be attributed to the rich chromium nitride precipitates. The results of E_{pitt} are in line with the hardness and literature related to effect of cooling rate (Liou et al., 2002; Silva et al., 2021). The E_{pitt} of the bent samples got decreased when compared with the E_{pitt} of the base sample (0.08V) however the metastable pitting is less and the passivation formation after the pitting is observed in all the bent samples. The passive layer is an indication for the formation of protective oxide layer which further stops the corrosion attack. From Figure 6-10 the extra peaks formed in the N1000_1000 sample after the corrosion when compared with the as bent sample which is an indication for oxide formation during corrosion. The EDS analysis of N1000_1000 corroded sample is shown in Figure 6-13 shows a corroded portion in HAZ section with elemental distribution which indicating the oxygen and chromium distribution overlap, which may indicate the formation chromium oxide after reacting with the corrosion medium.

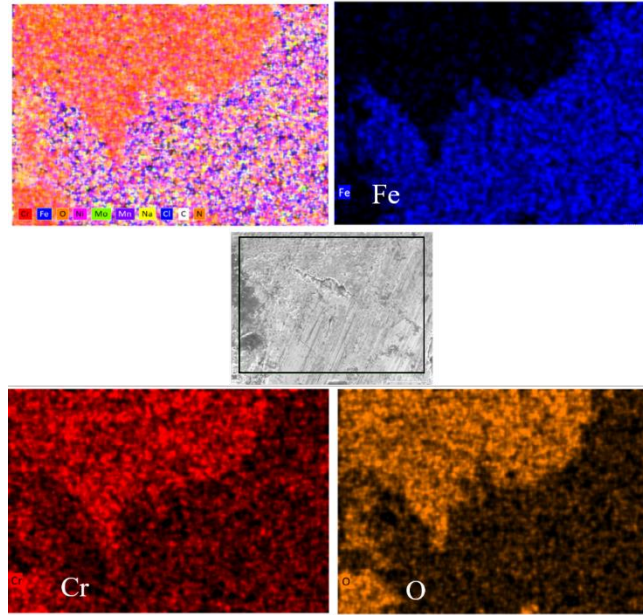


Figure 6-13. EDS mapping and elemental distribution of N1000_1000 after corrosion test

6.2. Multi-Scan Forced Cooling assisted Laser Bending at Low Line Energy

This study investigated the effect of different cooling conditions on multi-scan laser bending at low line energy parameter range. The temperature distribution, bend angle, heat affected zone, time required between the consecutive scans, tensile behaviour, hardness, and microstructure were analyzed experimentally for all cooling conditions with varying line energy.

6.2.1. Input Parameters

In this paper, the experiments are conducted for three different cooling conditions, as mentioned in Table 6-3. The experiments are performed with these three cooling conditions at a range of line energy ($LE = 10 - 25 \text{ J/mm}$), laser power ($P = 250 - 1000 \text{ W}$), and a laser beam of 4 mm diameter. The beam diameter of a defocused laser beam is controlled by adjusting the distance between the focal point of the focusing lens and the worksheet surface (Goyal et al., 2022b; Ravi Kant and Joshi, 2016a). Line energy is the energy supplied to the per unit length, and it is calculated by taking the ratio of laser power to scanning speed. The range of the scanning speed used in this study is 600 to 6000 mm/min. The scanning speed taken with different sets of laser power and line energy is shown in Table 6-4.

Table 6-3. Notation used for three different cooling conditions

Notation	Cooling condition
CC1	Natural cooling, idle time of 2 s between subsequent scans
CC2	Natural cooling, idle time between subsequent scans until the maximum temperature at the top surface reaches below 50 °C
CC3	Forced water cooling at the bottom surface during irradiation and idle time, idle time of 2 s between consecutive scans

Table 6-4. Scanning speed for different sets of laser power and line energy

	<i>P</i> = 250 W	<i>P</i> = 500 W	<i>P</i> = 750 W	<i>P</i> = 1000 W
LE = 10 J/mm	1500 mm/min	3000 mm/min	4500 mm/min	6000 mm/min
LE = 15 J/mm	1000 mm/min	2000 mm/min	3000 mm/min	4000 mm/min
LE = 20 J/mm	750 mm/min	1500 mm/min	2250 mm/min	3000 mm/min
LE = 25 J/mm	600 mm/min	1200 mm/min	1800 mm/min	2400 mm/min

6.2.2. Temperature analysis

Figure 6-14 (a-c) shows T_{avg} in each scan for different cooling conditions at various power at 10 J/mm LE. Unexpectedly, the maximum temperature is obtained during the first scan which is because of higher absorptivity in the first scan due to graphite coating. The temperature is maximum for the lowest laser power and decreases with an increase in laser power. It may be due to constant line energy where a lower laser power leads to a slower scanning speed that leads to a longer interaction time between the laser and the worksheet. The maximum temperature is found to be decreased with number of scans at low laser powers. Whereas at higher laser powers, the temperature decreases for initial scans and increases marginally in later scans. Similar trends are observed at different line energies, as shown in Figure 6-15, Figure 6-16, and Figure 6-17. It is because of decrease in the absorptivity as a result of degradation of graphite coating in the irradiated region (Edwardson et al., 2010b). At higher laser powers, the coating degradation is excessive, and the coating degrades completely in the initial scans. After that, the surface condition is almost similar for further scans, and preheating during the subsequent scans increases the temperature. In CC1, continuous decrement is observed at 250 W laser power only, whereas in CC2 & CC3, it is also observed at 500 W (shown in Figure 6-14 and Figure 6-15). It is due to longer cooling time and high heat transfer rate in CC2 & CC3, respectively. It reduces the maximum temperature and leads to the less coating degradation.

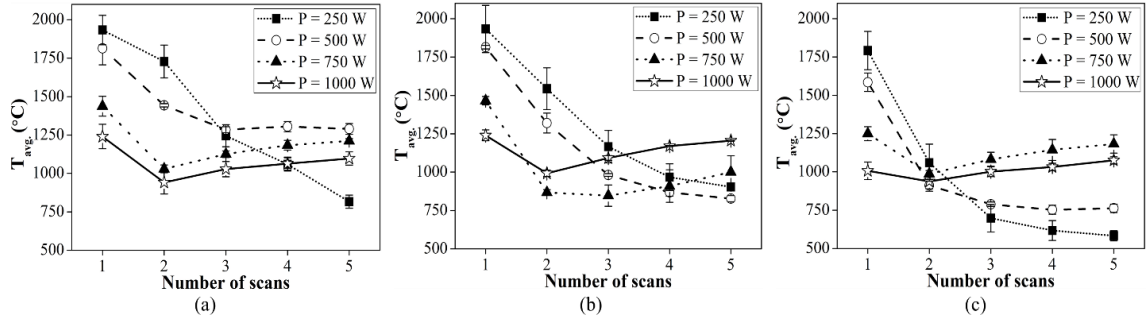


Figure 6-14. T_{avg} . for each scan at various power at 10 J/mm LE for (a) CC1 (b) CC2 (c) CC3

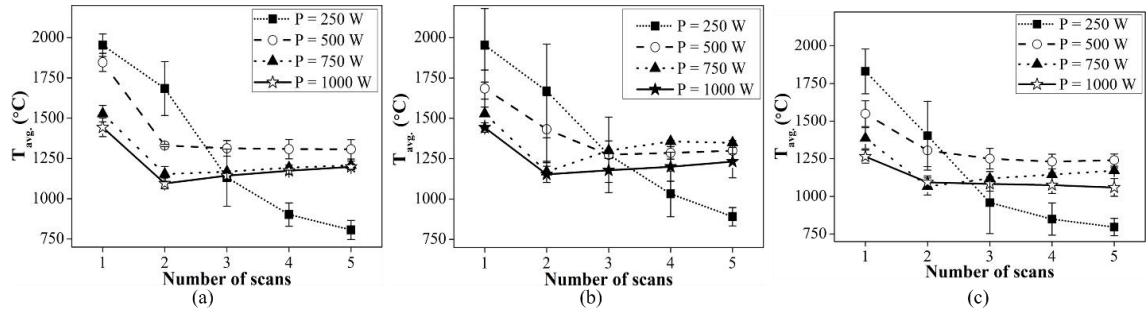


Figure 6-15. T_{avg} . for each scan at various power at 15 J/mm LE for (a) CC1 (b) CC2 (c) CC3

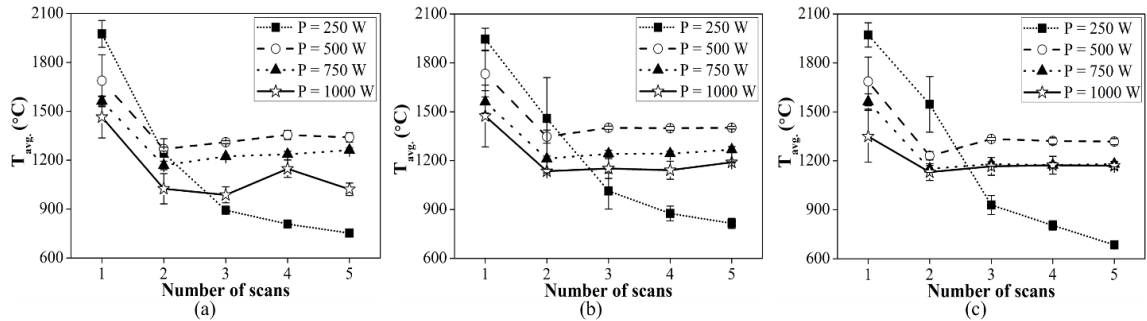


Figure 6-16. T_{avg} . in each scan at various power at 20 J/mm LE for (a) CC1 (b) CC2 (c) CC3

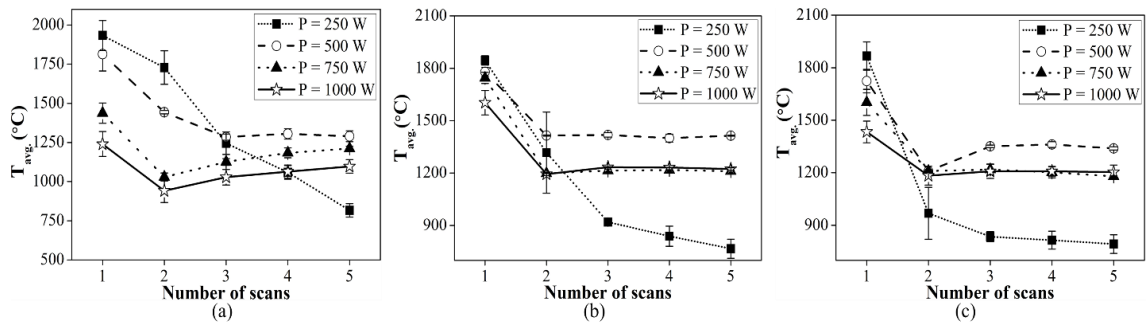


Figure 6-17. T_{avg} . in each scan at various power at 25 J/mm LE for (a) CC1 (b) CC2 (c) CC3

The temperature decreases with the increase in laser power for initial scans, and after that the peak temperature is obtained for 500 W laser power in CC1 (Figure 6-14(a)). Whereas in CC2, at 500 W laser power, the temperature continuously decreases, and the peak temperature is observed for 1000 W for later scans (Figure 6-14(b)). Similarly, the maximum temperature is achieved at 750 W laser power in CC3, as shown in Figure 6-14(c). These maximum temperature peaks shift towards low laser powers with an increase in line energy. Figure 6-15(b) & (c) shows, the maximum temperatures obtained at 750 W and 500 W laser powers in CC2 and CC3, respectively. At line energies 20 and 25 J/mm, except first scan, the peak is observed for 500 W laser power for all cooling conditions, as shown in Figure 6-16 and Figure 6-17. It is because the temperature generation depends on the absorptivity, and on the combination of scanning speed, and laser power. Absorptivity shows its dominance in initial scans due to which temperature is higher in initial scans. After the first scan, at low line energies, laser power dominates because of higher scanning speed. In contrast, at higher line energies the scanning speed is relatively low which becomes a dominating factor for temperature generation because of more interaction time of the laser beam and the worksheet. Due to this at low line energies, the peak temperature is observed at higher laser powers, and with an increase in line energy it shifts towards lower laser powers or scanning speeds.

Figure 6-18 shows the temperature distribution in lateral direction to the scan line in all three cooling conditions. The temperature distribution is drawn by taking one observation point at the center of the scan line and five other points on each side of the scan line for temperature measurement, as shown in Figure 6-18(a). Figure 6-18(b) shows the temperature distribution in the lateral direction during the first scan. The temperature in lateral direction is observed to follow the Gaussian distribution in all three conditions. During the first scan, the temperature is found to be in the same range for all three cooling conditions because of the burning of the graphite coating. In the third scan, the maximum temperature is found to be decreased compared to the first scan for all cooling conditions due to the burnt-out of coating, as shown in Figure 6-18(c). Furthermore, at the center of the scan line (upto 1 mm), the temperature is not varied significantly in different cooling conditions. Whereas moving away from the center line, it is observed to be significantly higher in CC1 than rest two conditions. It is because of the high heat conduction in lateral direction in CC1 in comparison to CC2 and CC3, where the heat losses are enhanced due to longer cooling time and higher convection

rate, respectively. Furthermore, the temperature in CC2 is significantly higher than the CC3. As the heat losses are higher in forced water cooling than natural cooling. Figure 6-18(d) shows the temperature distribution during the fifth scan, which is similar to the third scan. However, the temperature difference between CC1 and other two conditions is increased because of continuous retaining of heat during multi-scans in CC1.

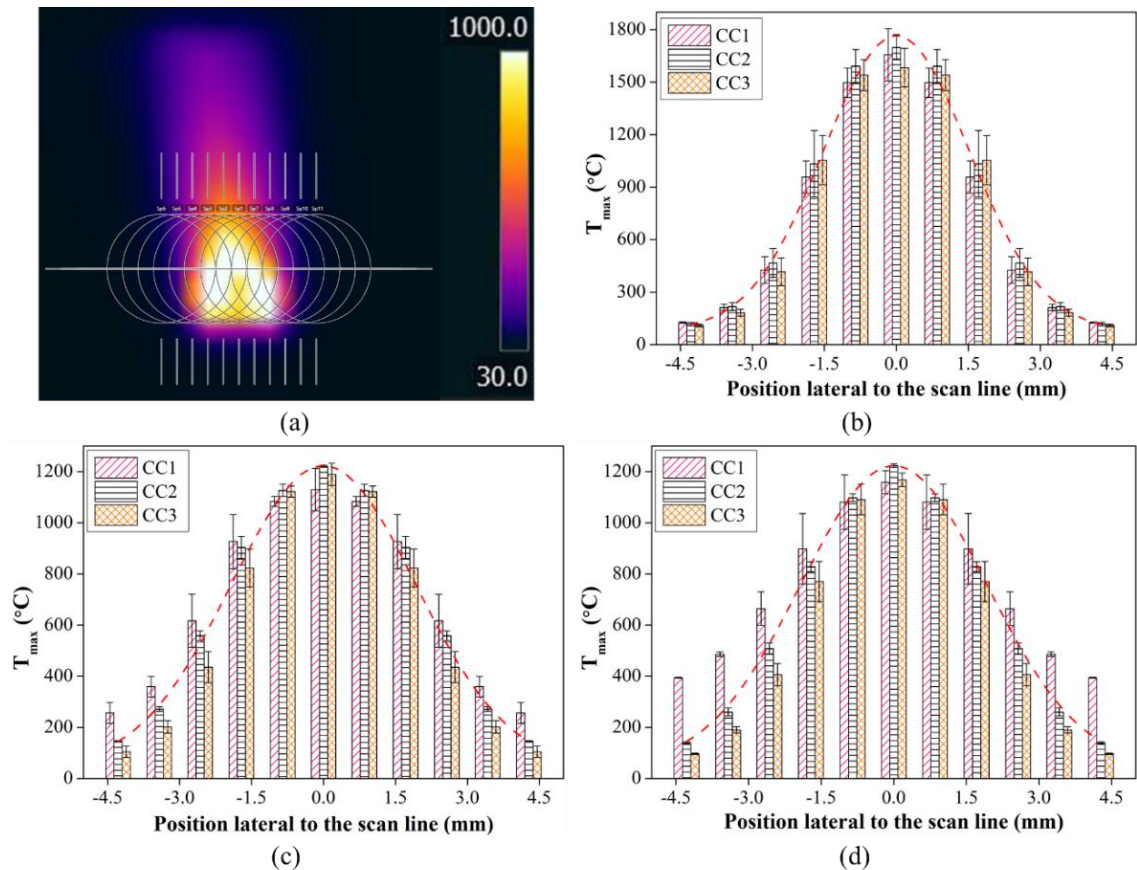


Figure 6-18. Temperature distribution in lateral direction to the scan line at 25 J/mm line energy and 750 W laser power: (a) Observation points considered for temperature measurement and temperature distribution in (b) First scan (c) Third scan and (d) Fifth scan for all three cooling conditions

Figure 6-19 shows the temperature distribution at the top surface along the scan line. The temperature profile is formed by taking the temperature of different points along the scan line as shown in Figure 6-19(a). The temperature profile shows that the temperature is marginally increased along the scan line except at the extreme ends of the sheet (Figure 6-19(b) & (c)). It is because of the preheating of the worksheet due to thermal conduction. At the start of the scan line, the temperature is significantly low as there is no preheating. Whereas, at the end of the scan line a sharp rise in temperature is observed, which is due to the formation of heat sink effect as a result of unavailability

of material ahead. It is also found that during the first scan (Figure 6-19(b)) the temperature in CC1 and CC2 is almost the same and higher than in CC3, although the difference is limited upto 10%. A similar trend is observed during the fifth scan, although the temperature is found to be reduced in all cooling conditions in comparison to the first scan.

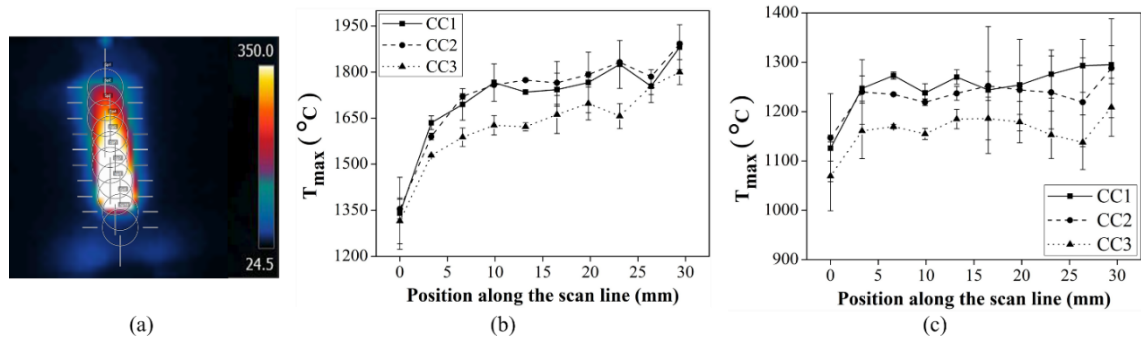


Figure 6-19. Temperature distribution along the scan line at 25 J/mm line energy and 750 W laser power: (a) Observation points considered for temperature measurement and temperature distribution during (b) First scan and (c) fifth scan for all three cooling conditions

6.2.3. Bend angle analysis

The variation of bend angle with the number of scans at different line energies and laser power for all three cooling conditions are discussed in this section. Figure 6-20 to Figure 6-23 show the bend angle increment in each scan at various power and cooling conditions. The bend angle in each scan is found to be decreased with the number of scans, as shown in Figure 6-20. It is because of the graphite coating degradation, strain hardening, and section thickening in the worksheet (Edwardson et al., 2010b, 2006). The rate of decrement in bend angle per scan is higher in CC2. It is because, along with the coating degradation, the long cooling time between the scans further decreases the available energy. However, for CC3, the bend angle initially decreases upto 2nd or 3rd scan and then it increases marginally with the number of scans (Figure 6-20(c)). It may be because the forced cooling at the bottom surface increases the temperature gradient. Figure 6-21, Figure 6-22 and Figure 6-23 show that the bend angle per scan increases with the increase in line energy because, at higher line energies, the scanning speed is low, leading to longer interaction time between the laser and worksheet. At 25 J/mm line energy, in CC1, it is found that the bend angle per scan is nearly constant with the number of scans at higher laser powers (Figure 6-23(a)). In contrast, it increases up to the second scan and then decreases in CC2 & CC3, as shown in Figure 6-23(b & c). In

CC1, due to longer interaction time, the temperature gradient and flow strength of the workpiece material decrease. Whereas, in CC2 and CC3, although the temperature gradient can be maintained by providing longer cooling time and forced cooling, respectively but it decreases the available energy for deformation.

It is also observed in Figure 6-20 - Figure 6-23 that at 250 W laser power, the bend angle generated in the first scan in forced cooling condition (CC3) is higher than other two cases. It is because at lower laser power, the scanning speed is also lower, which reduces the temperature gradient in the first two cases but in CC3, the forced cooling helps in increasing the temperature gradient. Whereas, at higher laser powers, a larger bend angle is achieved in CC1 due to convection loss and less interaction time. In CC1, heat retained from the previous scans, increases the temperature and results in the decrease in flow strength at higher number of scans. Whereas, in CC2 & CC3, a negligible heat is carried from the previous scans, leading to a continuous decrease in bend angle.

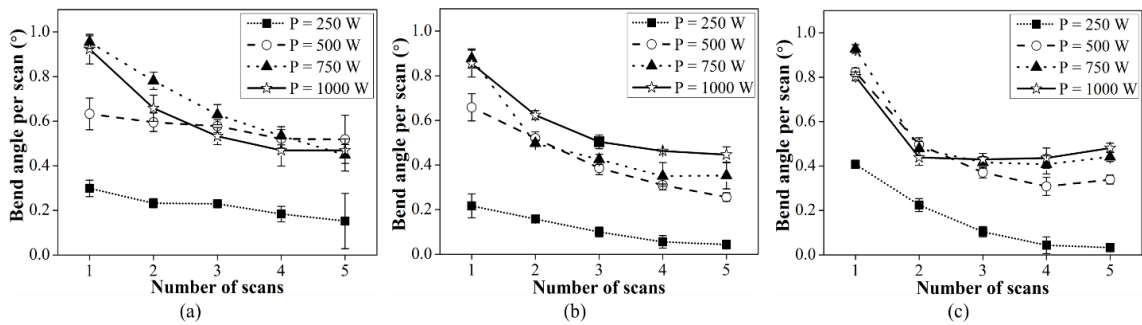


Figure 6-20. Bend angle achieved in each scan at various power and particular line energy of 10 J/mm for (a) CC1 (b) CC2 (c) CC3

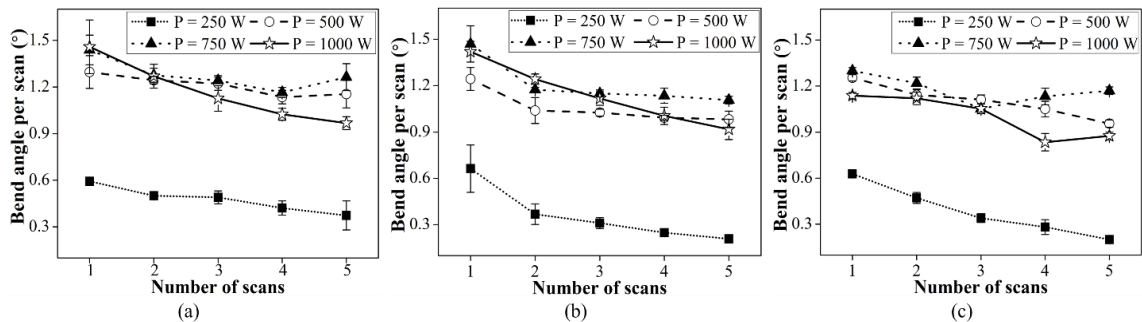


Figure 6-21. Bend angle achieved in each scan at various power and particular line energy of 15 J/mm for (a) CC1 (b) CC2 (c) CC3

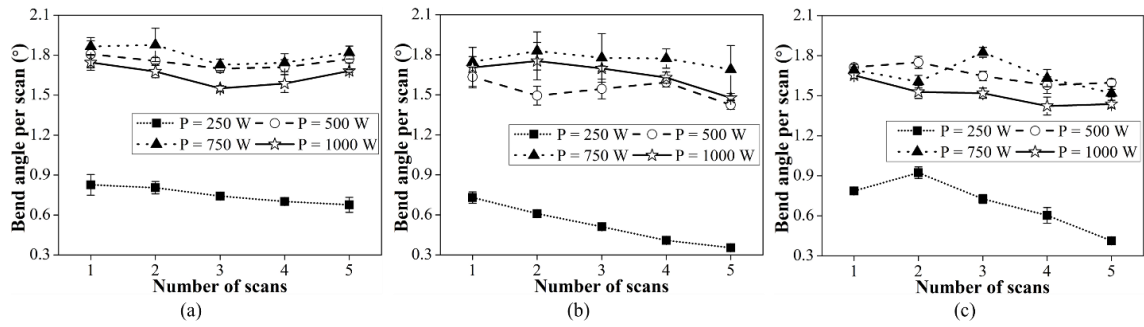


Figure 6-22. Bend angle achieved in each scan at various power and particular line energy of 20 J/mm for (a) CC1 (b) CC2 (c) CC3

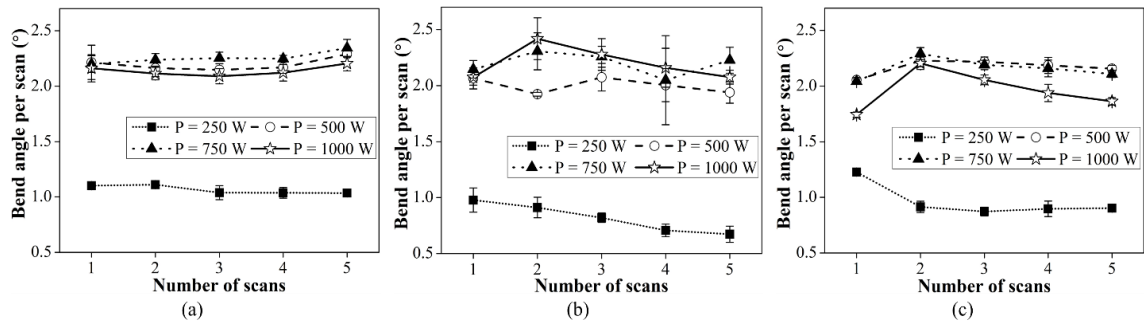


Figure 6-23. Bend angle achieved in each scan at various power and particular line energy of 25 J/mm for (a) CC1 (b) CC2 (c) CC3

Figure 6-24 presents the influence of laser power on the final bend angle achieved after five scans at various LE and cooling conditions. The variation of bend angle with laser power is almost similar in each condition. The bend angle drastically increases with laser power, attains a peak, and then decreases. The initial drastic increase is because the scanning speed increases with an increase in laser power to maintain the constant line energy, leading to a high temperature gradient. Further increase in laser power results into a higher temperature gradient, but the laser-worksheet interaction time is decreased. As soon as the latter one starts dominating, the bend angle decreases at higher laser power. In all three cooling conditions, the bend angle is observed to be increased with an increase in line energy at each laser power.

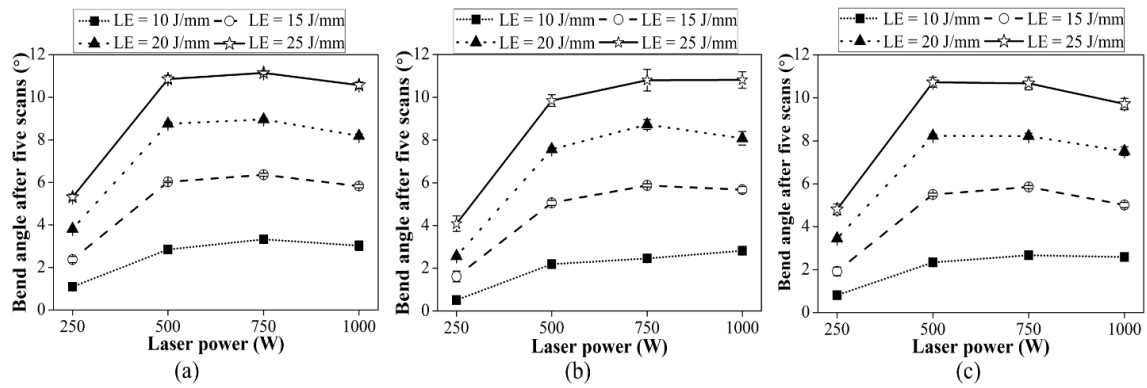


Figure 6-24. Variation in final bend angle after five scans with laser power at various LE for (a) CC1 (b) CC2 (c) CC3

Table 6-5. Bend angle after five scans and percentage change in bend angle for different cooling conditions

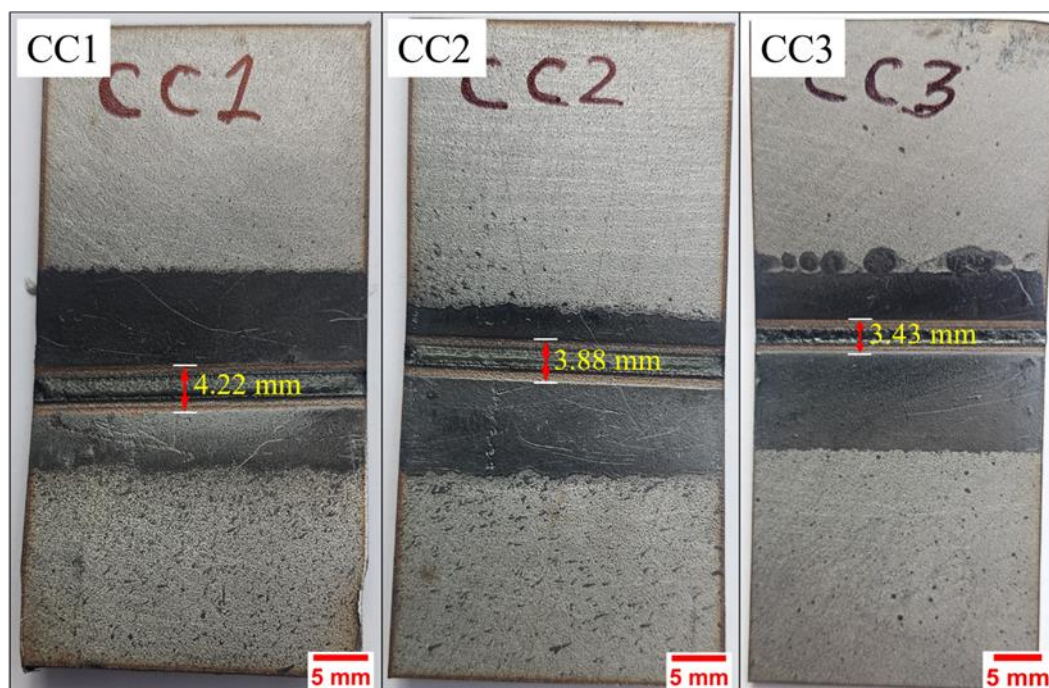
Line Energy	Laser Power	Bend Angle			Percentage change in CC2 w.r.t. CC1	Percentage change in CC3 w.r.t. CC1
		CC1	CC2	CC3		
10	250	1.10	0.51	0.81	-53.08	-25.83
10	500	2.85	2.19	2.34	-22.92	-17.89
10	750	3.32	2.46	2.67	-26.03	-19.61
10	1000	3.02	2.82	2.59	-6.73	-14.44
15	250	2.37	1.62	1.92	-31.84	-19.14
15	500	6.03	5.06	5.50	-16.15	-8.81
15	750	6.36	5.88	5.85	-7.52	-7.95
15	1000	5.83	5.68	5.01	-2.53	-14.06
20	250	3.81	2.56	3.45	-32.76	-9.57
20	500	8.75	7.57	8.23	-13.55	-5.94
20	750	8.96	8.73	8.22	-2.63	-8.26
20	1000	8.19	8.08	7.52	-1.30	-8.18
25	250	5.31	4.08	4.80	-23.06	-9.48
25	500	10.86	9.85	10.72	-9.32	-1.23
25	750	11.15	10.80	10.67	-3.14	-4.24
25	1000	10.57	10.81	9.72	2.24	-8.10

Table 6-5 shows the final bend angle after five scans and the percentage change in bend angle in different cooling conditions. The bend angle achieved in CC1 is larger than the other two cases. The line energy used in this study is low, and CC2 & CC3 further

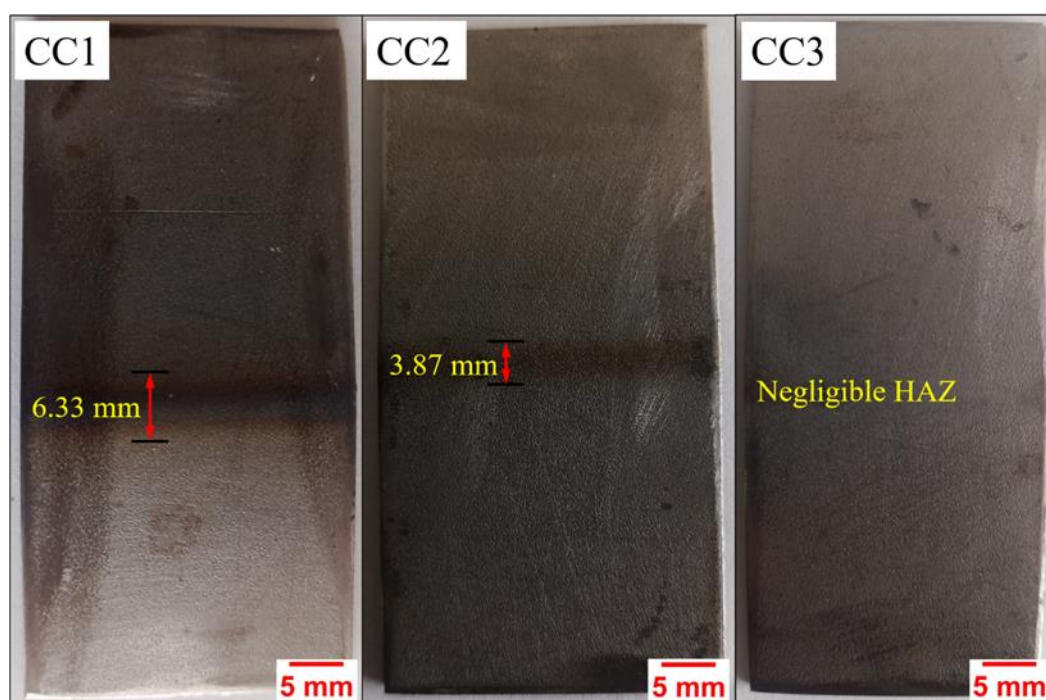
reduce the available energy. Although, at high laser power, the bend angle achieved in CC2 is almost equal to CC1. Due to higher scanning speed, the temperature gradient is increased in CC2, whereas in CC1, it is lower because of the heat retained from previous scans. Similarly, in CC3, the bend angle at high line energy and low laser powers is comparable to CC1, and it is higher than CC2. At high line energy and low laser powers, the scanning speed is low, reducing the temperature gradient in former cases, but in CC3, forced cooling at the bottom surface helps to maintain the higher temperature gradient. It is also observed that at lower line energies, the bend angle in CC2 & CC3 is lower than the CC1, because of the significant loss of energy as compared to the energy supplied in CC2 & CC3.

6.2.4. Mechanical and metallurgical analysis

Figure 6-25 shows the heat-affected zone (HAZ) at the top and bottom surfaces and at the cross-section of the worksheet for all three cooling conditions. The HAZ is measured by image processing software by taking the reference from worksheet dimensions. It is observed that the HAZ at top surface is reduced by 8.06% in CC2 and by 18.72% in CC3 in comparison to CC1. Furthermore, at the bottom surface, it is reduced significantly in CC2 (38.86%), and it becomes negligible in CC3 as compared to CC1. Similarly, the HAZ at cross-section is reduced by 26.17% and 41.5% in CC2 and CC3, respectively. It is because the cooling reduces the bulk heating of the worksheet. So, the cooling reduces the HAZ without any significant change in bend angle. Although the bend angle is comparable in both CC2 & CC3, the heat-affected zone is smaller in CC3, and the production time is also lesser in CC3. The average time required between two consecutive scans is 160 s in CC2, whereas in CC3, it is 2 s.



(a)



(b)

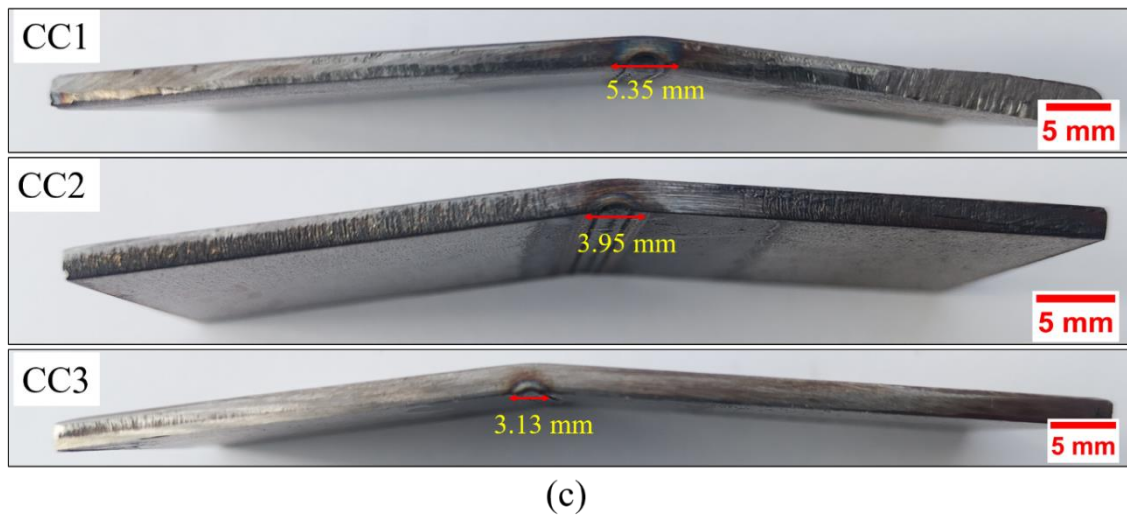


Figure 6-25. HAZ at (a) top surface (b) bottom surface and (c) cross-section of the worksheet in all three cooling conditions at 1000 W power and 25 J/mm LE

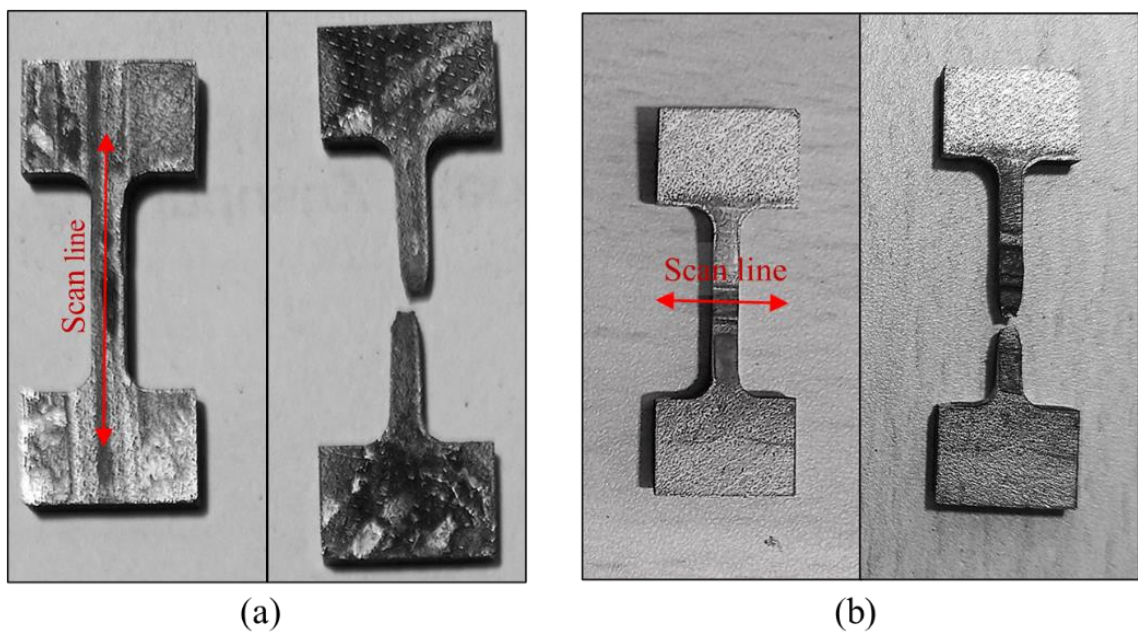


Figure 6-26. Initial and final condition of tensile test specimens (a) along (b) perpendicular to the scan line

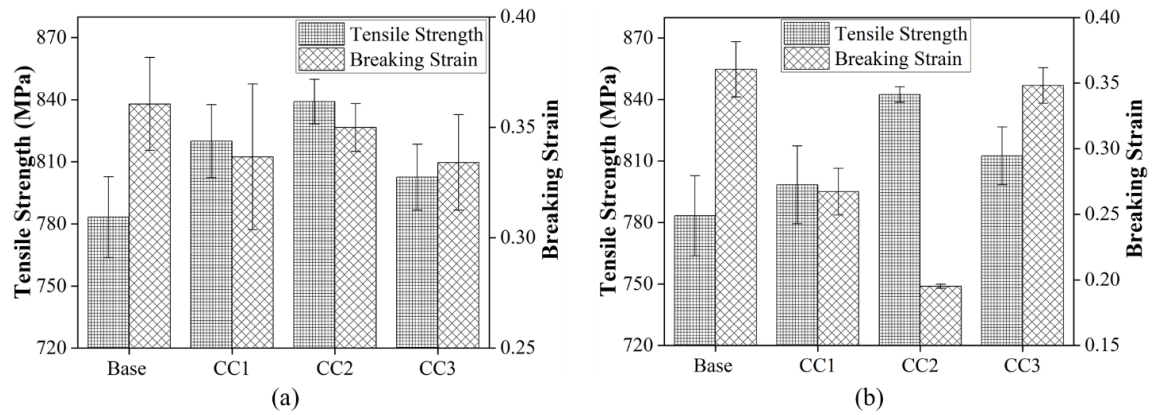


Figure 6-27. Tensile strength and breaking strain along the scanned direction at 750 W power and (a) 10 J/mm (b) 25 J/mm LE

The mechanical properties of the worksheet are analyzed to observe the post-bending effect in all three cooling conditions. The tensile strength is measured along the scan line and perpendicular to the scan line. The specimens used for the micro tensile testing before and after the test are shown in Figure 6-26. The results show that the tensile strength increases and breaking strain decreases in both orientations for all three cooling conditions in comparison with the base material. It may be due to the strain hardening, grain refinement and formation of sigma precipitation. Figure 6-27 shows the variation of tensile strength and breaking strain along the scan line in all cooling conditions. It is observed that while scanning at both 10 J/mm and 25 J/mm line energy the maximum tensile strength is observed in CC2. It may be due to the longer cooling time led to as multiple heat treatment in CC2 whereas in CC1 it is like continuous heating upto five scans and in CC3, the lower heating leads to less deformation which results in lower strain hardening. Wang et. al also reported that strain hardening exponent and hardening capacity increases with an increase in temperature due to increase in difference between ultimate tensile strength and yield strength (Wang et al., 2014). It is also observed that at 10 J/mm the minimum tensile strength out of three cooling conditions is observed in CC3 whereas at 25 J/mm it is in CC1. It may be because at low line energy the heating is quite less in CC3 whereas at high line energy the heating is more and forced cooling led to as multiple heat treatment. Figure 6-28 shows the variation of tensile strength and breaking strain perpendicular the scan line in all cooling conditions. At 10 J/mm LE (Figure 6-28(a)), the tensile strength is maximum in CC1 and minimum in CC3, whereas at 25 J/mm (Figure 6-28(b)) it is maximum in CC3 and minimum in CC1. It may be because in CC1 the heat affected zone is larger which shows that the more area along the gauge length of the tensile test specimen is heat treated whereas in CC2 and CC3 it

is smaller, specially at low line energy. Whereas at high line energies higher heat input and higher cooling rate lead to multiple heat treatment in CC2 and CC3.

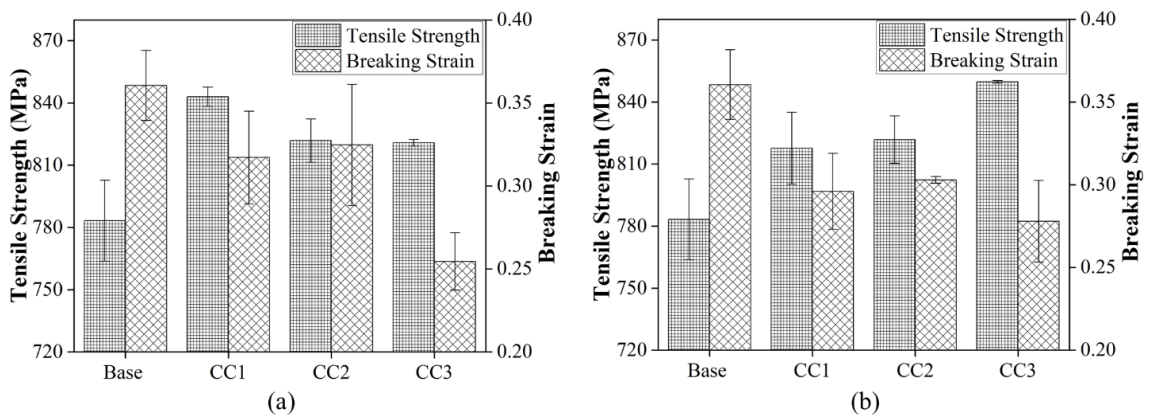


Figure 6-28. Tensile strength and breaking strain perpendicular to the scanned direction at 1000 W power and (a) 10 J/mm (b) 25 J/mm LE

It is also observed that at 10 J/mm, the breaking strain is maximum in CC2, however in CC1, and CC3 it is almost equal (Figure 6-27(a)). Whereas, at 25 J/mm, breaking strain is maximum in CC3 and minimum in CC2 (Figure 6-27(b)). It may be because of the quenching effect in CC3. It is also observed that breaking strain is maximum in CC2 and minimum in CC3 (Figure 6-28(a) & (b)). It is due to the quenching effect and generation of sigma phase, which is brittle in nature. The higher cooling rate increases the formation of sigma phase (Oh et al., 2013).

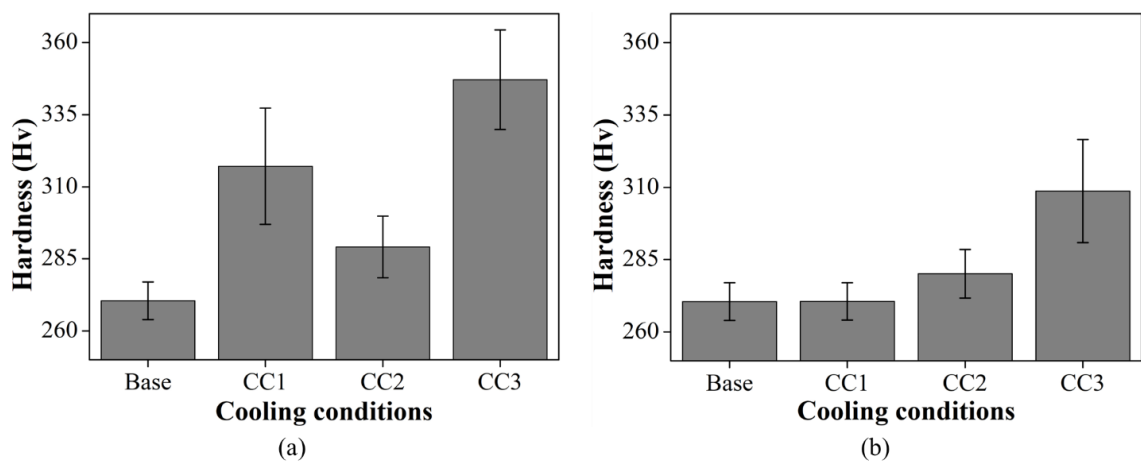


Figure 6-29. Hardness within the scanned region at (a) top surface, (b) bottom surface for different cooling conditions at 15 J/mm line energy, and 1000 W laser power

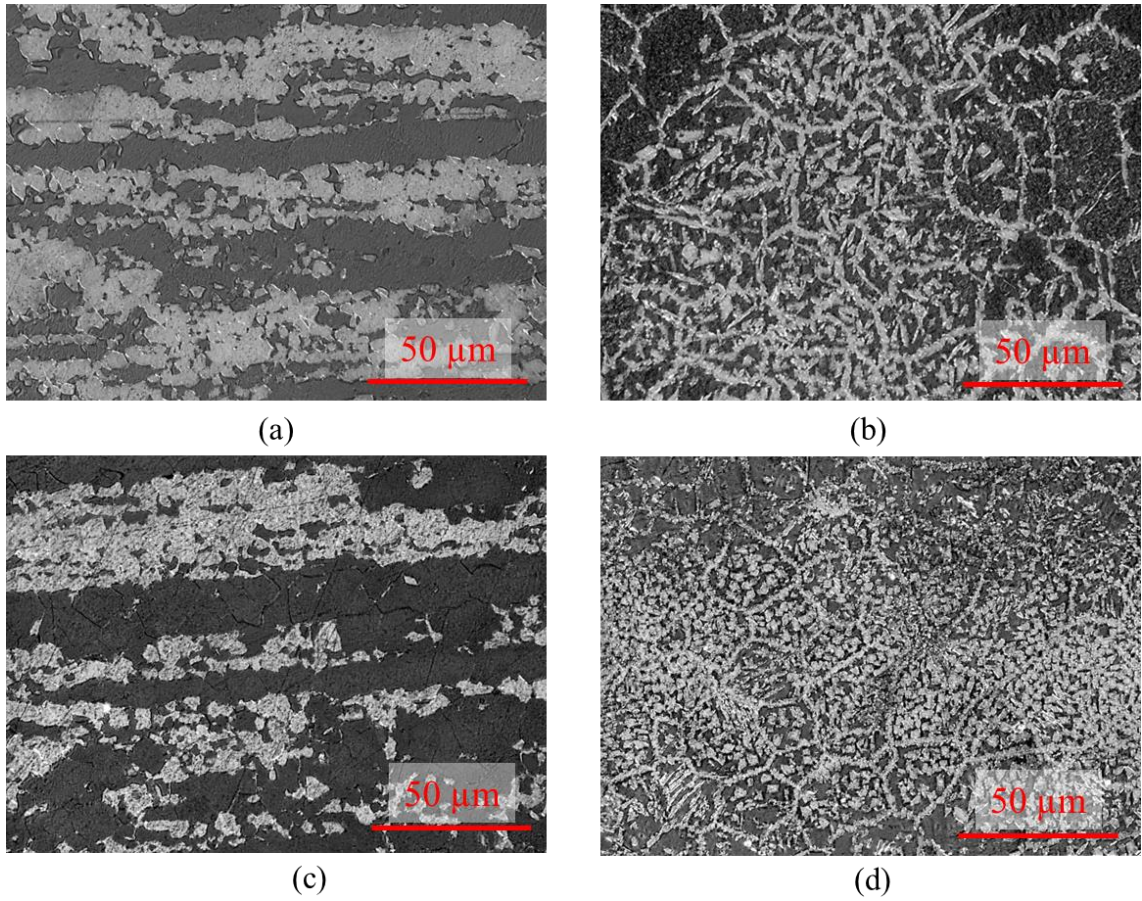


Figure 6-30. Phase analysis of the (a) initial worksheet, and scanned area of the top surface for (b) CC1, (c) CC2, and (d) CC3 at 15 J/mm line energy and 1000 W laser power

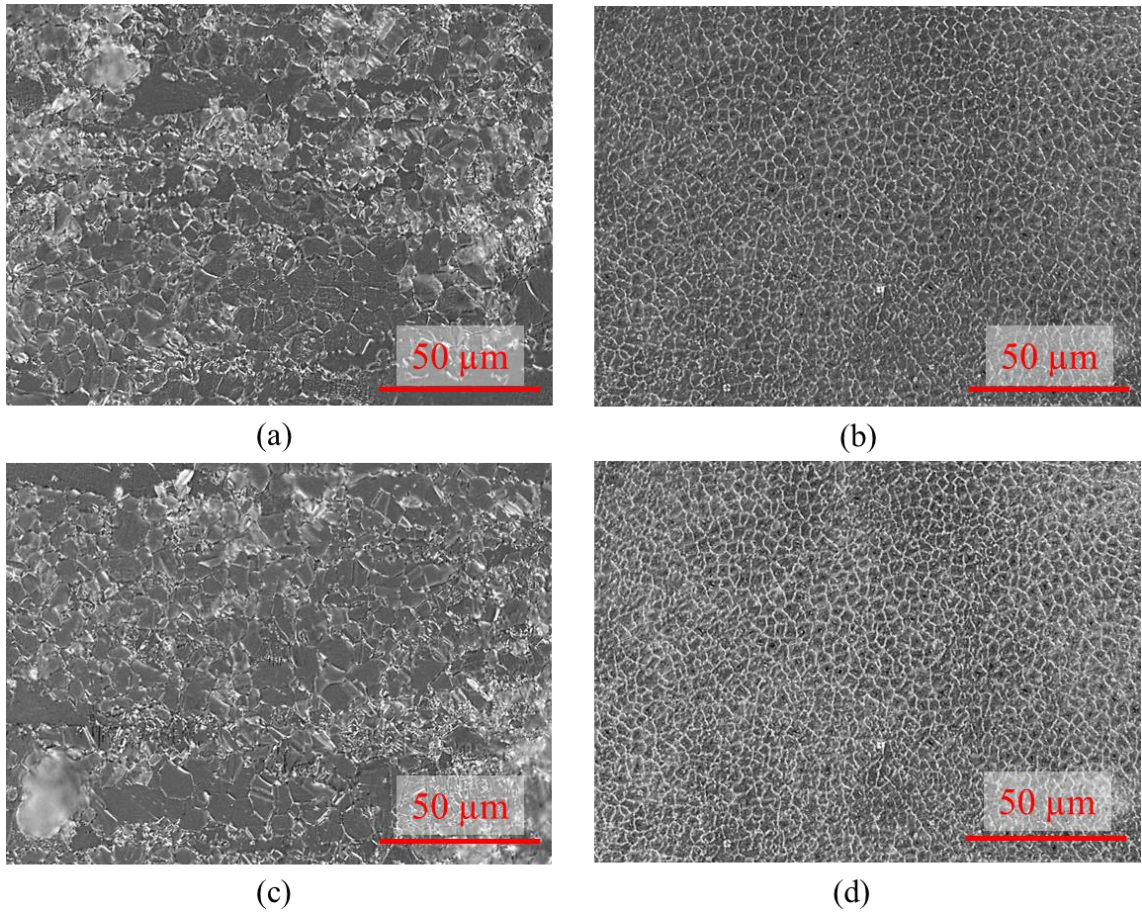


Figure 6-31. Grain size analysis of the (a) initial worksheet, and scanned area of the top surface for (b) CC1 (c) CC2 and (d) CC3 at 15 J/mm line energy and 1000 W laser power

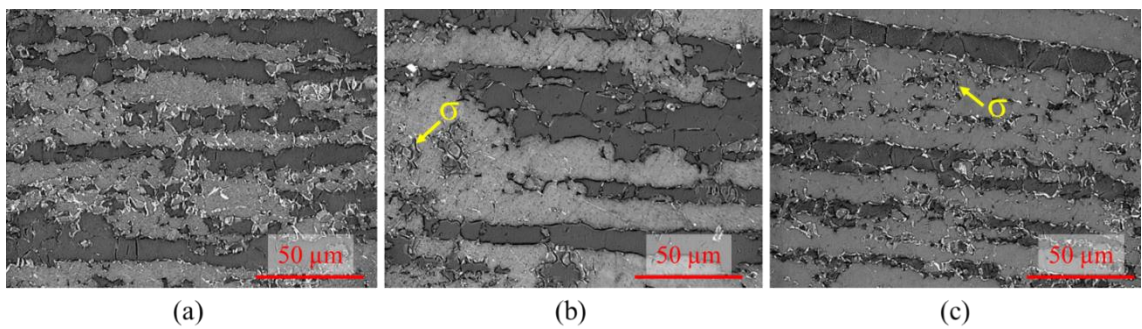


Figure 6-32. Microstructure of the bottom surface in (a) CC1 (b) CC2 (c) CC3 at 15 J/mm line energy and 1000 W laser power

Figure 6-29 shows the hardness in the scanned region on top and bottom surfaces for all three cooling conditions at 15 J/mm line energy and 1000 W laser power. The hardness in the scanned region is found to be increased significantly in CC1 and CC3, whereas in CC2, it is marginal. The properties of duplex stainless steel depend on the combination of ferrite and austenite phases (Stainless, 2014). These phases are identified by etching the specimen with Beraha's solution during microstructural analysis. This

solution reacts with the ferrite and makes it dark, whereas austenite remains brighter (Varbai et al., 2018; Varbai and Májlínger, 2019). It can be observed from Figure 6-30 (a) and (c) that the microstructure of CC2 is quite similar to that of the base material, although the percentage of ferrite content is found to be increased. It may be the possible reason for marginal increase in hardness. In case of CC1, the major portion of the microstructure is ferrite, whereas austenite is present at the grain boundaries of the ferrite matrix with small grains. Similar observations are also reported by Odermatt et al. (Odermatt et al., 2021a), where it is observed that the microstructure of melt is fully ferrite, and during cooling the austenite formation starts at the grain boundaries of ferrite. The limited melting and rapid cooling may lead to a relatively higher percentage of austenite in CC3. The average grain sizes of Base, CC1, CC2, and CC3 are 6.6 μm , 6.1 μm , 4.1 μm , and 3.7 μm , respectively, as shown in Figure 6-31. The fine grain structure of CC1 and CC3 may also be the possible reason for higher hardness. The hardness at the bottom surface in the scanned region increases marginally for CC1 and CC2, whereas it is increased significantly for CC3. It may be due to the formation of sigma (σ) precipitation at the bottom surface shown in Figure 6-32 (a), (b), and (c) (Dos Santos and Magnabosco, 2016). In CC3, the formation of sigma precipitation is dominated because of the higher cooling rate (Oh et al., 2013). The sigma phase is not found at the top surface because it forms in the temperature range of 500 $^{\circ}\text{C}$ to 850 $^{\circ}\text{C}$ (Petrovic et al., 2012) (Tehovnik et al., 2016).

6.3. Summary

This chapter focused on investigating the potential of forced cooling assisted laser bending with multiple laser irradiations. The chapter comprised two comprehensive studies, each exploring the process at different parameter ranges to gain a thorough understanding of the phenomenon.

The first study is focused on enhancing the bend angle of the duplex stainless steel sheet by using forced cooling at the lower surface during the laser bending process. The experiments are conducted for various sets of process conditions in both natural and forced cooling conditions. The influence of different factors, i.e., scan speed, laser power, sheet thickness, worksheet width, beam diameter, and the number of scans, are analyzed in natural and forced cooling conditions. The post-bending effect on mechanical, metallurgical, and corrosion properties are investigated.

- The results showed that the bend angle was enhanced upto 427% due to forced cooling, and it was also affected by the cooling flow rate. The effect of process parameters also exhibited different trends under forced cooling compared to natural cooling.
- Surprisingly, contrary to the literature, the bend angle per scan increased with an increase in the number of scans. Even though the maximum bend angle per scan of 5.8° and 6.8° for 2 mm and 1.5 mm thickness sheets were observed in the fifth scan.
- From the microstructural analysis, it is understood that the cooling rate significantly affects the formation of the austenite phase. The samples with high cooling rate resulted in higher mechanical properties like hardness owing to the high ferrite content. High ferrite content resulted in low fracture strain whereas higher austenite samples have shown fracture strain similar to base material.
- XRD analysis confirmed the variation of austenite and ferrite phases and EDS analysis confirmed the accumulation of Nitrogen in forced cooling conditions. Electrochemical analysis of the bent samples in 3.5% NaCl showed that pitting potential in the forced cooled samples decreased by -0.1 V however the passivation layer is observed in all the samples which should help in stopping further corrosion.

In the second study, the effect of different cooling conditions on multi-scan laser bending at low line energy parameters were investigated. The study analyzed the temperature distribution, bend angle, heat affected zone, time between consecutive scans, tensile behavior, hardness, and microstructure under different cooling conditions. Experiments were conducted with three cooling conditions (natural cooling with idle time, natural cooling with temperature control, and forced water cooling) and varying line energy and laser power. The overall conclusions of the study are as follows:

- The average maximum temperature ($T_{avg.}$) along the scanning line was observed to be decreased during initial scans and becomes stable during further subsequent scans. It was found to be decreased with an increase in laser power at a constant line energy.

- The temperature in lateral direction to the scan line followed the gaussian distribution. The temperature in all three conditions was almost similar within 1 mm of center of the scan line. While moving away from the center the temperature was found in the order of $CC1 > CC2 > CC3$.
- The temperature distribution along the scan line showed that the temperature was minimum at the start of the scan then it marginally increased moving with the scan line and a large increment was found at the end of the scan line
- In-general, the bend angle per scan was found to be decreased with the number of scans in all three cooling conditions. Although in some cases, it was observed to be increased or constant after 3 scans.
- It was observed that the bend angle initially increased with laser power, and then decreased after attaining a peak, whereas, it increased with line energy.
- The bend angle achieved in CC1 was slightly higher than the other two cases at low line energies whereas at higher line energies and low laser power it was almost equal in CC1 and CC3. So, the laser parameters played an important role along with cooling condition.
- The HAZ was observed to be reduced in CC2, compared to the CC1. However, negligible HAZ was observed in CC3 compared to the other two conditions.
- The tensile strength was found to be enhanced and ductility was observed to be decreased for all cooling conditions. The hardness at top and bottom surfaces was improved in all three cooling conditions, but a significant change was observed in CC3.
- The microstructure of top and bottom surfaces in all three-cooling conditions showed that ferrite percentage increased in CC1 and CC2, and grain refinement occurred in CC1 and CC3. Sigma precipitation was formed at the bottom surface.

The chapter concludes that the forced cooling significantly enhanced bend angle at high line energies, without compromising material properties. Although, at low line energies, the bend angle is not significantly influenced by the cooling condition. However, the HAZ, waiting time between the successive scans and the number of scans required for

achieving a required bend angle are reduced in forced cooling condition, which ultimately reduced the time, cost, energy and material degradation due to excessive heating. It highlights the competency of this technique for advancing industrial applications in various sectors, such as microelectronics, aerospace, and marine, where high deformation with good precision is prime requirement.

CONCLUSION AND FUTURE SCOPE

The primary aim of the present research work was to enhance the capabilities of the laser bending process by assisting with the forced cooling and investigate the other performance parameters of the bent specimen. Furthermore, to explore the feasibility of laser bending of high strength dual phase stainless-steel. The following steps were taken during the course of the study-

- Development of a finite element-based 3D numerical model with experimental validation for laser bending of duplex stainless steel.
- Simulations for single scan laser bending of duplex stainless steel under both natural and forced cooling conditions. Analyse the effect of various process parameters for both the cooling conditions. Identify the parametric range for effective forced cooling during laser bending process.
- Experimental feasibility study of forced cooling assisted laser bending with aluminium alloy.
- Development of experimental setup for forced cooling assisted laser bending with real time bend angle and temperature measurement facility.
- Experimental study of single scan forced cooling assisted laser bending of duplex stainless steel for both natural and forced cooling conditions and pre-identified parametric range. Analyse the effect of process parameters on bend angle and examine the post bending effect on material properties.
- Experimental study of multi-scan laser bending of duplex stainless steel for both natural and forced cooling conditions. Analyse the effect of process parameters on bend angle and examine the post bending effect on material properties.

The important observations and research contributions of the present research work are summarized in the subsequent sections.

7.1. Conclusions

Duplex (AISI-2205) is a dual-phase stainless steel consisting of ferrite and austenite, roughly 50% each. Duplex stainless steel is a high-strength (twice the austenite) and corrosion-resistant material used in marine, chemical, oil, and structure industries. Due to its high strength and spring back effect the cold forming of the duplex is difficult. Furthermore, the hot working is also not preferred for duplex-2205 because of the alteration in the material properties due to change in phase percentage. This study explored the feasibility of laser bending of duplex stainless steel and also investigated the post bending effect on material properties.

Literature reports that the applications of the laser bending process in manufacturing industries is limited due to small bend angle per scan and longer production time during multiscan laser bending. Although, researchers have attempted to improve the productivity by applying assisted force, optimizing the process parameters, multiple irradiations, forced cooling, etc., still, the maximum bend angle achieved by laser bending is limited to 2 to 3 degrees per scan. Additionally, limited research has been done on the post-bending effects on microstructure and mechanical properties, whereas, corrosion behavior has not been explored yet. The present study aims to enhance the bend angle per scan during laser bending of duplex stainless steel by applying forced cooling. The study investigates the influence of process parameters on the bend angle (laser power, beam diameter, scan speed, sheet width and thickness, and flow rate of cooling water) for both natural and forced cooling conditions. Moreover, the study comprehensively explores the mechanical properties (hardness and tensile strength), corrosion behavior, and microstructure of the bent specimen for both natural and forced cooling conditions. The stepwise contributions of the research work are presented below.

Pilot Study

- A finite element-based 3D non-linear numerical model was developed with the incorporation of temperature dependent material and surrounding heat loss by convection and radiation. Although, some realistic assumptions were also considered in the model. As laser bending is a thermo-mechanical process, the developed numerical model was experimentally validated with both thermal (top

surface temperature) and mechanical (bend angle) outcomes. The experimental results are found to be in good agreement with the numerical results with an average error of 4.54% and 5.38% in bend angle and temperature respectively.

- Numerical simulations were performed for single-scan laser bending in natural cooling conditions for a wide range of parameters. The underlying bending mechanism was explored with the help of temperature and stress-strain distribution. The effect of line energy, laser power, and scanning speed on bend angle and edge effect were analysed. The mechanical properties of the bent specimen compared with the base material and found that the hardness of the bend specimen increased, and the ductility was reduced, whereas no significant change was observed in the ultimate strength of the material.
- Numerical simulations were performed for single-scan laser bending in forced cooling conditions for a wide range of parameters. The bend angle results were compared with that of natural cooling condition. It was found that the forced cooling significantly increased the bend angle at high line energy parameters and showed a negative effect at low line energy parameters. The underlying phenomenon for this variation was investigated by analysing the temperature and strain distribution during both natural and forced cooling conditions.
- A robust experimental setup was developed, which gave excellent repeatability in the results. The experimental feasibility of forced cooling assisted laser bending was explored with an aluminium alloy sheet. The results show that the temperature of the scanned surface decreases with the number of scans due to coating degradation for both the conditions. The forced cooling reduces the coating degradation up to some extent at low laser powers and results in an increase in temperature. The forced cooling increases the bend angle for most of the parametric conditions except at low laser power and higher scanning speed. The material degradation and excessive melting are reduced with the application of forced cooling condition.

Forced Cooling Assisted Single Scan Laser Bending

- An experimental study is conducted on single scan laser bending of duplex-2205 in natural and forced cooling conditions. The effects of worksheet geometry

(thickness and width), laser parameters (scanning speed, beam diameter, and power) and cooling condition (flow rate) on temperature profile, bend angle, mechanical and metallurgical properties in natural and forced cooling conditions were investigated.

- The maximum temperature at the upper surface is reduced, and the cooling rate is increased with the application of forced cooling which reduces the material degradation.
- A significant increment (35.2%) in bend angle was observed with the application of forced cooling on the bottom surface of the sheet. The process parameter notably affects the effectiveness of forced cooling. The forced cooling was found to be more effective at lower scanning speed, intermediate beam diameter, and higher laser power, irrespective of variation in other parameters. Furthermore, the bend angle is observed to be higher in forced cooling for lower thickness and longer width of the worksheet.
- The hardness and tensile of the bent specimens were found to be improved as compared to the base material. However, the ductility of the bent specimen was reduced. Furthermore, the forced cooling assisted laser bent specimen showed higher strength as compared to the naturally cooled.
- The variation in phase distribution is observed at the upper surface in the scanning region whereas at lower surface the phase distribution is quite similar to base material except the sigma phase formations at boundaries of ferrite and austenite.
- The process parameters were optimized using pareto analysis and genetic algorithm in order to achieve higher bend angle with a high rate of bend angle per line energy given to the worksheet. The optimum parameter was experimentally validated and the properties of the bent specimen were also examined.
- The optimum parameters were $f = 0.85$ L/mm, $P = 987.59$ W, $V = 673.3$ mm/min and $D = 7.99$ mm. Although, the bend angle achieved by optimum parameters was only 7.5% higher than the maximum bend angle in initial experiments but the bend angle per line energy rate is improved by 22.14 %.

- The tensile strength and hardness of the bend specimen at optimum parametric condition were found to be enhanced at the expense of ductility. That was because of the rearrangement of phase distribution in the laser irradiation region.

Forced Cooling Assisted Multi-scan Laser Bending

An experimental study on multi-scan laser bending of duplex stainless steel was performed for both natural and forced cooling conditions. This study was divided into two sections according to the range of line energy provided to the worksheet for deformation. The specific contributions of both sections are presented below.

Multi-Scan Forced Cooling Assisted Laser Bending at High Line Energy

- The experiments were conducted for various set of process conditions i.e., scan speed, laser power, sheet thickness, worksheet width, beam diameter, cooling water flow rate, and the number of scans in both natural and forced cooling conditions. The influence of these factors in both the cooling conditions was analysed. The post-bending effect on mechanical, metallurgical and corrosion properties was also investigated.
- The forced cooling expensively enhanced the bend angle at high line energy. The results showed a maximum increment of 427% in the bend angle. The effect of process parameters also exhibited different trends under forced cooling compared to natural cooling.
- The bend angle per scan was found to be increased with an increase in the number of scans in forced cooling whereas the trend was opposite for natural cooling. Even though, the maximum bend angle per scan of 5.8° and 6.8° for 2 mm and 1.5 mm thickness sheets were observed in the fifth scan which was around 300% higher than that achieved in natural cooling.
- The microstructural analysis revealed that cooling significantly influenced the ratio of ferrite and austenite phases in duplex steel. A higher cooling rate resulted in an increased ferrite content, leading to higher hardness and tensile strength but reduced ductility. Conversely, a higher percentage of austenite showed improved ductility.

- XRD analysis confirmed the variation of austenite and ferrite phases, and EDS analysis confirmed the accumulation of Nitrogen in forced cooling conditions. Electrochemical analysis of the bent samples in 3.5% NaCl showed that pitting potential in the forced cooled samples decreased by -0.1 V however, the passivation layer is observed in all the samples, which should help in stopping further corrosion.

Multi-Scan Forced Cooling Assisted Laser Bending at Low Line Energy

The effect of different cooling conditions on multi-scan laser bending at low line energy parameters were investigated. The study analyzed the temperature distribution, bend angle, heat affected zone, time between consecutive scans, tensile behavior, hardness, and microstructure under different cooling conditions. Experiments were conducted with three cooling conditions (natural cooling with idle time, natural cooling with temperature control, and forced water cooling) and varying line energy and laser power.

- The average maximum temperature ($T_{avg.}$) along the scanning line was observed to be decreased during initial scans and becomes stable during further subsequent scans. It was found to be decreased with an increase in laser power at constant line energy. The temperature in the lateral direction to the scan line followed the Gaussian distribution. The temperature in all three conditions was almost similar within 1 mm of the centre of the scan line. While moving away from the centre, the temperature was found in the order of CC1 > CC2 > CC3. The temperature distribution along the scan line showed that the temperature was minimum at the start of the scan then it marginally increased moving with the scan line and a large increment was found at the end of the scan line.
- It was observed that for low line energy parameters, the bend angle achieved in the forced cooling condition was lower than in the natural cooling condition. The bend angle was found to increase with laser power and then decrease after attaining a peak, whereas it increased with line energy.
- The HAZ was observed to be reduced in CC2, compared to CC1. However, negligible HAZ was observed in CC3 compared to the other two conditions.
- The waiting time between the successive scans and the number of scans required for achieving a required bend angle was reduced in forced cooling conditions,

which ultimately reduced the time, cost, energy and material degradation due to excessive heating.

- The tensile strength and hardness (both top and bottom surfaces) of the bent specimens of all three cooling conditions were improved at the expense of ductility compared to the base material. Furthermore, the forced cooling condition exhibits the highest tensile strength and hardness among all three cooling conditions.
- The microstructure of the bent specimen revealed that the ferrite content increased, and more refined grain structure was observed in forced cooling condition.

In conclusion, this research aimed to enhance laser bending capabilities for high-strength dual-phase stainless steel (duplex-2205) and investigate the post-bending effects on material properties. Forced cooling was explored to increase bend angles, and its effectiveness was examined under different conditions. The investigation into laser bending provided valuable insights into improving bend angles per scan and reducing production time. Through a comprehensive series of experiments and simulations, the influence of various process parameters on bend angles and material properties was studied. The application of forced cooling was explored to increase bend angles, and its effectiveness was examined under different process conditions. The results revealed that forced cooling significantly increased the bend angle during both single and multi-scan laser bending. The cooling process also influenced the microstructural composition, mechanical properties, and corrosion behaviour of the bent specimens. It also reduced the heat effect area and the total production time by reducing the waiting time between successive scans. The findings highlighted the potential of forced cooling to improve the overall productivity of the laser bending process in manufacturing industries.

7.2. Research Contribution

The research contributions of this study can be summarized as follows:

- Development of a 3D numerical model: A finite element-based 3D numerical model was developed and experimentally validated for laser bending of duplex stainless steel. This model serves as a valuable tool for predicting and understanding the behavior of the laser bending process under different conditions.
- Investigation of single-scan laser bending: Simulations and experiments were conducted for single-scan laser bending under both natural and forced cooling conditions. The effect of various process parameters on bend angles was analyzed, and the parametric range for effective forced cooling during laser bending was identified.
- Feasibility study with aluminium alloy: The study explored the feasibility of forced cooling assisted laser bending using an aluminium alloy, providing insights into the effect of forced cooling on temperature and bend angles.
- Development of experimental setup: An experimental setup with real-time bend angle and temperature measurement capability was established for forced cooling assisted laser bending. This setup ensured accurate data collection during the experiments.
- Examination of single and multi-scan laser bending: Experimental studies were conducted on single and multi-scan laser bending of duplex stainless steel under both natural and forced cooling conditions. The effects of process parameters on bend angles and post-bending material properties were thoroughly analyzed.
- Optimization of process parameters: The research work included the optimization of process parameters using pareto analysis and genetic algorithm to achieve higher bend angles per line energy rate. The optimum parameters were experimentally validated to improve bend angles.
- Microstructural and mechanical analysis: The study investigated the microstructure and mechanical properties of the bent specimens, revealing the impact of forced cooling on phase distribution, hardness, and tensile strength.

- Corrosion behavior analysis: The research explored the corrosion behavior of the bent specimens in different cooling conditions, shedding light on potential applications in corrosive environments.

Overall, this research significantly contributes to the advancement of laser bending technology by improving bend angles and understanding the effects of forced cooling on material properties. The findings can potentially lead to more efficient and productive laser bending processes in various manufacturing industries.

7.3. Future directions of the work

The present research work can be extended on the following fronts:

- Development of a numerical model for multi-scan forced cooling assisted laser bending.
- Estimation of heat transfer coefficient for forced cooling and compare different cooling mediums with the same heat transfer coefficient.
- Perform the laser bending in an inert environment and compare the material properties with atmospheric conditions.
- Investigation of post-bending effects after each laser scan and analysis of the alterations in microstructure and mechanical properties following each scan.
- Exploration of forced cooling assisted laser bending for non-linear irradiation paths and complex geometries.
- Development of a feedback-based control system to achieve desired shape of the worksheet.
- Exploration of underwater laser bending.
- Experimental study for controlled thickening and shortening of the sheet by upsetting mechanism.
- Improvement in the controllability of the buckling mechanism.

REFERENCES

- Abazari, H.D., Seyedkashi, S.M.H., Gollo, M.H., Moon, Y.H., 2017. Evolution of microstructure and mechanical properties of SUS430/C11000/SUS430 composites during the laser-forming process. *Met. Mater. Int.* 23, 865–876. <https://doi.org/10.1007/s12540-017-7053-6>
- Abedi, H.R., Gollo, M.H., 2019. An experimental study of the effects of surface roughness and coating of Cr₂O₃ layer on the laser-forming process. *Opt. Laser Technol.* 109, 336–347. <https://doi.org/10.1016/j.optlastec.2018.07.064>
- Abolhasani, D., Seyedkashi, S.M.H., Gollo, M.H., Moon, Y.H., 2019a. Effects of laser beam parameters on bendability and microstructure of stainless steel in three-dimensional laser forming. *Appl. Sci.* 9. <https://doi.org/10.3390/app9204463>
- Abolhasani, D., Seyedkashi, S.M.H., Kim, Y.T., Gollo, M.H., Moon, Y.H., 2019b. A double raster laser scanning strategy for rapid die-less bending of 3D shape. *J. Mater. Res. Technol.* 8, 4741–4756. <https://doi.org/10.1016/j.jmrt.2019.08.021>
- Akinlabi, S., Akinlabi, E., 2018. Laser Beam Forming: A Sustainable Manufacturing Process. *Procedia Manuf.* 21, 76–83. <https://doi.org/10.1016/j.promfg.2018.02.097>
- Akinlabi, S.A., Akinlabi, E., 2017a. Imece2017-72044 Effect of Temperature on the Evolved Microstructure During 1–8.
- Akinlabi, S.A., Akinlabi, E.T., 2017b. Microstructural Evolution during Laser Processing of Titanium Alloy. *Adv. Eng. Res.* 102, 96–101. <https://doi.org/10.2991/icmmse-17.2017.16>
- Akinlabi, S.A., Mashinini, M.P., Fatoba, S.O., Akinlabi, E.T., 2018. Characterization of corrosion behaviour of laser beam formed titanium alloy. *IOP Conf. Ser. Mater. Sci. Eng.* 423. <https://doi.org/10.1088/1757-899X/423/1/012174>
- Akinlabi, S.A., Shukla, M., 2016. Evaluation of the structural integrity of laser formed steel sheets for possible load bearing applications. *Lasers Eng.* 35, 197–216.
- Ames, D.C., Smith, G.L., Lazarus, N., Howell, L.L., Magleby, S.P., 2023. Laser Forming of Compliant Mechanisms. *ASME Open J. Eng.* 2, 021018. <https://doi.org/10.1115/1.4057048>

- Arcella, F.G., Whitney, E.J., Krantz, D., 1995. Laser forming near shapes in titanium 178, 178–183. <https://doi.org/10.2351/1.5058903>
- Arnet, H., Vollertsen, F., 1995. Extending Laser Bending for the Generation of Convex Shapes. *Proc. Inst. Mech. Eng. Part B J. Eng. Manuf.* 209, 433–442. https://doi.org/10.1243/PIME_PROC_1995_209_107_02
- Bachmann, A.L., Dickey, M.D., Lazarus, N., 2020. Making light work of metal bending: Laser forming in rapid prototyping. *Quantum Beam Sci.* 4, 14–17. <https://doi.org/10.3390/qubs4040044>
- Bachmann, A.L., Hanrahan, B., Dickey, M.D., Lazarus, N., 2022. Self-Folding PCB Kirigami: Rapid Prototyping of 3D Electronics via Laser Cutting and Forming. *ACS Appl. Mater. Interfaces* 14, 14774–14782. <https://doi.org/10.1021/acsami.2c01027>
- Banabic, D., 2007. Advanced Methods in Material Forming, *Advanced Methods in Material Forming*. <https://doi.org/10.1007/3-540-69845-0>
- Bao, J., Yao, Y.L., 2001a. Analysis and prediction of edge effects in laser bending. *J. Manuf. Sci. Eng. Trans. ASME* 123, 53–61. <https://doi.org/10.1115/1.1345729>
- Bao, J., Yao, Y.L., 2001b. Analysis and prediction of edge effects in laser bending. *J. Manuf. Sci. Eng. Trans. ASME* 123, 53–61. <https://doi.org/10.1115/1.1345729>
- Biegeleisen, L.K., 1986. Residual stresses and deflection in complex shapes formed by laser bending. Massachusetts Institute of Technology.
- Birnbaum, A.J., Cheng, P., Yao, Y.L., 2007. Effects of clamping on the laser forming process. *J. Manuf. Sci. Eng.* 129, 1035–1044. <https://doi.org/10.1115/1.2375140>
- Blake, R.J., 1996. Laser forming process development 105, E105–E114. <https://doi.org/10.2351/1.5059068>
- Blake, R.J., Pearson, R.M., Revell, A.B., Simon, W.E., 1997. Laser thermal forming of sheet metal parts using desktop laser systems. *Laser Inst. Am. Proc.* 83. <https://doi.org/10.2351/1.5059689>
- Bucher, T., Bolger, C., Zhang, M., Chen, C.J., Yao, Y.L., 2016. Effect of Geometrical Modeling on the Prediction of Laser-Induced Heat Transfer in Metal Foam. *J.*

- Manuf. Sci. Eng. Trans. ASME 138, 1–11. <https://doi.org/10.1115/1.4033927>
- Bucher, T., Cardenas, S., Verma, R., Li, W., Lawrence Yao, Y., 2018a. Laser forming of sandwich panels with metal foam cores. J. Manuf. Sci. Eng. Trans. ASME 140. <https://doi.org/10.1115/1.4040959>
- Bucher, T., Cardenas, S., Verma, R., Li, W., Yao, Y.L., 2019a. Laser forming of sandwich panels with metal foam cores. J. Laser Appl. 31, 022606. <https://doi.org/10.2351/1.5096122>
- Bucher, T., Yao, Y.L., 2018. Advances in laser forming of metal foam: Mechanism, prediction and comparison. Int. J. Mechatronics Manuf. Syst. 11, 250–273. <https://doi.org/10.1504/IJMMS.2018.092877>
- Bucher, T., Young, A., Zhang, M., Chen, C.J., Lawrence Yao, Y., 2018b. Thermally Induced Mechanical Response of Metal Foam During Laser Forming. J. Manuf. Sci. Eng. Trans. ASME 140. <https://doi.org/10.1115/1.4038995>
- Bucher, T., Young, A., Zhang, M., Chen, C.J., Yao, Y.L., 2017. Bending mechanism analysis for laser forming of metal foam. ASME 2017 12th Int. Manuf. Sci. Eng. Conf. MSEC 2017 collocated with JSME/ASME 2017 6th Int. Conf. Mater. Process. 1, 1–11. <https://doi.org/10.1115/MSEC20173026>
- Bucher, T., Zhang, M., Chen, C.J., Verma, R., Li, W., Lawrence Yao, Y., 2019b. Laser Forming of Metal Foam Sandwich Panels: Effect of Panel Manufacturing Method. J. Manuf. Sci. Eng. Trans. ASME 141, 1–11. <https://doi.org/10.1115/1.4043194>
- Castillo, J.I., Celentano, D.J., Cruchaga, M.A., García-Herrera, C.M., 2018. Characterization of strain rate effects in sheet laser forming. Comptes Rendus - Mec. 346, 794–805. <https://doi.org/10.1016/j.crme.2018.05.001>
- Chakraborty, S.S., Maji, K., Racherla, V., Nath, A.K., 2015. Investigation on laser forming of stainless steel sheets under coupling mechanism. Opt. Laser Technol. 71, 29–44. <https://doi.org/10.1016/j.optlastec.2015.02.013>
- Chakraborty, S.S., Maji, K., Racherla, V., Nath, A.K., 2013. Study on the Effect of Fourier Number in Laser Forming of AISI 304 Stainless Steel Sheet under Coupling Mechanism using Finite Element Simulations and, in: International Conference on PRECISION, MESO, MICRO AND NANO ENGINEERING

(COPEN-8: 2013).

- Chakraborty, S.S., More, H., Nath, A.K., 2016. Laser forming of a bowl shaped surface with a stationary laser beam. *Opt. Lasers Eng.* 77, 126–136. <https://doi.org/10.1016/j.optlaseng.2015.08.006>
- Chan, K.C., Liang, J., 2001. Laser bending of a Ti3Al-based intermetallic alloy. *Mater. Lett.* 49, 51–55. [https://doi.org/10.1016/S0167-577X\(01\)00253-1](https://doi.org/10.1016/S0167-577X(01)00253-1)
- Chan, K.C., Liang, J., 2000. Laser bending of an Al6013/SiCp aluminium matrix composite sheet. *J. Mater. Process. Technol.* 100, 214–218. [https://doi.org/10.1016/S0924-0136\(99\)00380-5](https://doi.org/10.1016/S0924-0136(99)00380-5)
- Chan, K.C., Yau, C.L., Lee, W.B., 2000. Laser bending of thin stainless steel sheets. *J. Laser Appl.* 12, 34–40. <https://doi.org/10.2351/1.521911>
- Changdar, A., Chakraborty, S.S., 2021. Laser processing of metal foam - A review. *J. Manuf. Process.* 61, 208–225. <https://doi.org/10.1016/j.jmapro.2020.10.012>
- Che Jamil, M.S., Sheikh, M.A., Li, L., 2011. A finite element study of buckling and upsetting mechanisms in laser forming of plates and tubes. *Int. J. Manuf. Mater. Mech. Eng.* 1, 1–17. <https://doi.org/10.4018/ijmmme.2011010101>
- Chen, D., Wu, S., Li, M., 2004. Deformation behaviours of laser curve bending of sheet metals. *J. Mater. Process. Technol.* 148, 30–34. <https://doi.org/10.1016/j.jmatprotec.2003.12.024>
- Chen, D.J., Xiang, Y.B., Wu, S.C., Li, M.Q., 2002. Application of fuzzy neural network to laser bending process of sheet metal. *Mater. Sci. Technol.* 18, 677–680. <https://doi.org/10.1179/026708302225003569>
- Chen, G., Xu, X., 2001. Experimental and 3d finite element studies of cw laser forming of thin stainless steel sheets. *J. Manuf. Sci. Eng. Trans. ASME* 123, 66–73. <https://doi.org/10.1115/1.1347036>
- Chen, G., Xu, X., 1999. Microscale bending with CW and pulsed laser 167, 167–175. <https://doi.org/10.2351/1.5059299>
- Chen, G., Xu, X., Poon, C.C., Tam, A.C., 1998a. Experimental and 2-D Numerical Studies on Micro-Scale Bending of Stainless Steel With Pulsed Laser. *ASME Int.*

- Mech. Eng. Congr. Expo. Proc. 1998-P, 49–57.
<https://doi.org/10.1115/IMECE1998-0689>
- Chen, G., Xu, X., Poon, C.C., Tam, A.C., 1998b. Laser-assisted microscale deformation of stainless steels and ceramics. *Laser Appl. Microelectron. Optoelectron. Manuf.* III 3274, 133. <https://doi.org/10.1117/12.309504>
- Chen, M.L., Jeswiet, J., Bates, P.J., Zak, G., 2008. Experimental study on sheet metal bending with medium-power diode laser. *Proc. Inst. Mech. Eng. Part B J. Eng. Manuf.* 222, 381–389. <https://doi.org/10.1243/09544054JEM951>
- Cheng, J., Yao, Y.L., 2001. Cooling effects in multiscan laser forming. *J. Manuf. Process.* 3, 60–72. [https://doi.org/10.1016/S1526-6125\(01\)70034-5](https://doi.org/10.1016/S1526-6125(01)70034-5)
- Cheng, P.J., Lin, S.C., 2000. Using neural networks to predict bending angle of sheet metal formed by laser. *Int. J. Mach. Tools Manuf.* 40, 1185–1197. [https://doi.org/10.1016/S0890-6955\(99\)00111-X](https://doi.org/10.1016/S0890-6955(99)00111-X)
- Cheng, S.C., Chen, K.J., Suzuki, Y., Tsuchido, Y., Kuo, T.S., Osakada, K., Horie, M., 2018. Reversible Laser-Induced Bending of Pseudorotaxane Crystals. *J. Am. Chem. Soc.* 140, 90–93. <https://doi.org/10.1021/jacs.7b10998>
- Chinizadeh, M., Kiahosseini, S.R., 2017. Deformation, microstructure, hardness, and pitting corrosion of 316 stainless steel after laser forming: A comparison between natural and forced cooling. *J. Mater. Res.* 32, 3046–3054. <https://doi.org/10.1557/jmr.2017.146>
- Cho, J.R., Tin, S., Reed, R.C., 2004. Measurements of residual strains and stresses in laser formed plates of Ti-6Al-4V using synchrotron X-ray diffraction. *Mater. Sci. Technol.* 20, 465–472. <https://doi.org/10.1179/026708304225010299>
- Choudhary, B.K., Palaparti, D.P.R., Samuel, E.I., 2013. Analysis of tensile stress-strain and work-hardening behavior in 9Cr-1Mo ferritic steel. *Metall. Mater. Trans. A Phys. Metall. Mater. Sci.* 44, 212–223. <https://doi.org/10.1007/s11661-012-1385-0>
- Cook, F., Celentano, D., Ramos-Grez, J., 2016. Experimental-numerical methodology for the manufacturing of cranial prosthesis via laser forming. *Int. J. Adv. Manuf. Technol.* 86, 2187–2196. <https://doi.org/10.1007/s00170-015-8316-3>

- Das, B., Biswas, P., 2018. A review of plate forming by line heating. *J. Sh. Prod. Des.* 34, 155–167. <https://doi.org/10.5957/JSPD.170003>
- Das, B., Biswas, P., 2017. Effect of operating parameters on plate bending by laser line heating. *Proc. Inst. Mech. Eng. Part B J. Eng. Manuf.* 231, 1812–1819. <https://doi.org/10.1177/0954405415612678>
- Davidson, K., Singamneni, S., 2016. Selective Laser Melting of Duplex Stainless Steel Powders: An Investigation. *Mater. Manuf. Process.* 31, 1543–1555. <https://doi.org/10.1080/10426914.2015.1090605>
- Davidson, K.P., Littlefair, G., Singamneni, S., 2021. On the machinability of selective laser melted duplex stainless steels. *Mater. Manuf. Process.* 1–17. <https://doi.org/10.1080/10426914.2021.2001513>
- De Lacerda, J.C., Cândido, L.C., Godefroid, L.B., 2015. Effect of volume fraction of phases and precipitates on the mechanical behavior of UNS S31803 duplex stainless steel. *Int. J. Fatigue* 74, 81–87. <https://doi.org/10.1016/j.ijfatigue.2014.12.015>
- Deacon, D.L., 1984. Material degradation in heavy steel plates caused by bending with a laser. Massachusetts Institute of Technology.
- Dearden, G., Edwardson, S.P., 2003. Some recent developments in two- and three-dimensional laser forming for “macro” and “micro” applications. *J. Opt. A Pure Appl. Opt.* 5. <https://doi.org/10.1088/1464-4258/5/4/352>
- Dehghan, S.H., Loh-Mousavi, M., Farzin, M., Safari, M., 2016. Laser forming of metallic dom shaped parts using spiral and radial-circular scan paths Using Spiral and Radial - Circular Scan Paths. *J. Adv. Manuf. Technol.* 10, 29–44.
- Ding, Y., Zhang, X., Kovacevic, R., 2016. A laser-based machine vision measurement system for laser forming. *Meas. J. Int. Meas. Confed.* 82, 345–354. <https://doi.org/10.1016/j.measurement.2015.10.036>
- Dixit, U.S., Joshi, S.N., Kant, R., 2015. Laser forming systems: a review. *Int. J. Mechatronics Manuf. Syst.* 8, 160–205.
- Dos Santos, D.C., Magnabosco, R., 2016. Kinetic Study to Predict Sigma Phase Formation in Duplex Stainless Steels. *Metall. Mater. Trans. A Phys. Metall. Mater.*

- Sci. 47, 1554–1565. <https://doi.org/10.1007/s11661-016-3323-z>
- Dovč, M., Možina, J., Kosel, F., 1999. Optimizing the final deformation of a circular plate illuminated by a short laser pulse. *J. Phys. D. Appl. Phys.* 32, 644–649. <https://doi.org/10.1088/0022-3727/32/6/008>
- Dutta Majumdar, J., Manna, I., 2011. Laser material processing. *Int. Mater. Rev.* 56, 341–388. <https://doi.org/10.1179/1743280411Y.0000000003>
- Dutta, P.P., Kalita, K., Dixit, U.S., 2018. Electromagnetic-Force-Assisted Bending and Straightening of AH36 Steel Strip by Laser Irradiation. *Lasers Manuf. Mater. Process.* 5, 201–221. <https://doi.org/10.1007/s40516-018-0062-6>
- E. Sobol, V. Bagratashvili, A. Omel'chenko, A.S., 1994. Laser shaping of cartilage, in: *Proc. SPIE 2128, Laser Surgery: Advanced Characterization, Therapeutics, and Systems IV*. SPIE, pp. 43–49. <https://doi.org/https://doi.org/10.1117/12.184919>
- Edwardson, S.P., Abed, E., Bartkowiak, K., Dearden, G., Watkins, K.G., 2006. Geometrical influences on multi-pass laser forming. *J. Phys. D. Appl. Phys.* 39, 382–389. <https://doi.org/10.1088/0022-3727/39/2/021>
- Edwardson, S.P., Abed, E., Carey, C., Edwards, K.R., Bartkowiak, K., Dearden, G., Watkins, K.G., 2007. Key factors influencing the bend per pass in laser forming. *26th Int. Congr. Appl. Lasers Electro-Optics, ICALEO 2007 - Congr. Proc.* 506. <https://doi.org/10.2351/1.5061185>
- Edwardson, S.P., Dearden, G., French, P., Watkins, K.G., Cantwell, W.J., 2003. Laser forming of metal laminate composite materials. *ICALEO 2003 - 22nd Int. Congr. Appl. Laser Electro-Optics, Congr. Proc.* 107. <https://doi.org/10.2351/1.5059977>
- Edwardson, S.P., French, P., Dearden, G., Watkins, K.G., Cantwell, W.J., 2005. Laser forming of fibre metal laminates. *Lasers Eng.* 15, 233–255.
- Edwardson, S.P., Griffiths, J., Dearden, G., Watkins, K.G., 2010a. Temperature Gradient Mechanism: Overview of the multiple pass controlling factors. *Phys. Procedia* 5, 53–63. <https://doi.org/10.1016/j.phpro.2010.08.122>
- Edwardson, S.P., Griffiths, J., Edwards, K.R., Dearden, G., Watkins, K.G., 2010b. Laser forming: Overview of the controlling factors in the temperature gradient mechanism. *Proc. Inst. Mech. Eng. Part C J. Mech. Eng. Sci.* 224, 1031–1040.

<https://doi.org/10.1243/09544062JMES1776>

- Edwardson, S.P., Watkins, K.G., Dearden, G., Magee, J., 2001. Generation of 3D shapes using a laser forming technique, in: International Congress on Applications of Lasers & Electro-Optics. AIP Publishing. pp. 759–768. <https://doi.org/10.2351/1.5059933>
- Els-Botes, A., Mcgrath, P.J., Hattingh, D.G., 2005. The effect of laser deformation on fatigue properties of automotive dual phase steel. WIT Trans. Eng. Sci. 49, 377–386.
- Esfahani, R.T., Golabi, S., Zojaji, Z., 2016. Optimization of finite element model of laser forming in circular path using genetic algorithms and ANFIS. Soft Comput. 20, 2031–2045. <https://doi.org/10.1007/s00500-015-1622-8>
- Esmail Ghadiri Zahrani, A.M., 2013. Experimental investigation of edge effect and longitudinal distortion in laser bending process. Opt. Laser Technol. 45, 301–307. <https://doi.org/10.1016/j.optlastec.2012.06.031>
- Faccoli, M., Roberti, R., 2013. Study of hot deformation behaviour of 2205 duplex stainless steel through hot tension tests. J. Mater. Sci. 48, 5196–5203. <https://doi.org/10.1007/s10853-013-7307-8>
- Fang, Y., Li, P., Zhen, X., Shen, Z., 2022. Modeling of Adjustable Bending Pipe to Compensate for Pipe Assembly Production Errors. Machines 10, 1–15. <https://doi.org/10.3390/machines10060409>
- Fauzi, E.R.I., Jamil, M.S.C., Samad, Z., Sheikh, M.A., Najib, A.M., 2019. Influence of non-conventional beam profile on edge effects in laser forming of AISI 304 stainless steel plate. Int. J. Adv. Manuf. Technol. 104, 1593–1601. <https://doi.org/10.1007/s00170-019-04107-0>
- Fetene, B.N., Dixit, U.S., Davim, J.P., 2017a. Laser-assisted bending by magnetic force. J. Eng. 2017, 343–353. <https://doi.org/10.1049/joe.2017.0145>
- Fetene, B.N., Dixit, U.S., Liao, H., 2017b. Laser bending of friction stir processed and cement-coated sheets. Mater. Manuf. Process. 32, 1628–1634. <https://doi.org/10.1080/10426914.2017.1279321>
- Fetene, B.N., Kumar, V., Dixit, U.S., Echempati, R., 2018a. Numerical and

- experimental study on multi-pass laser bending of AH36 steel strips. *Opt. Laser Technol.* 99, 291–300. <https://doi.org/10.1016/j.optlastec.2017.09.014>
- Fetene, B.N., Kumar, V., Dixit, U.S., Echempati, R., 2018b. Numerical and experimental study on multi-pass laser bending of AH36 steel strips. *Opt. Laser Technol.* 99, 291–300. <https://doi.org/10.1016/j.optlastec.2017.09.014>
- Fetene, B.N., Shufen, R., Dixit, U.S., 2018c. FEM-based neural network modeling of laser-assisted bending. *Neural Comput. Appl.* 29, 69–82. <https://doi.org/10.1007/s00521-016-2544-9>
- Fidder, H., Admiraal, J.P.J., Ocelík, V., De Hosson, J.T.M., 2019. In situ digital image correlation observations of laser forming. *Metals (Basel)*. 10. <https://doi.org/10.3390/met10010017>
- Fidder, H., Ocelík, V., Botes, A., De Hosson, J.T.M., 2018. Response of Ti microstructure in mechanical and laser forming processes. *J. Mater. Sci.* 53, 14713–14728. <https://doi.org/10.1007/s10853-018-2650-4>
- Fidder, H., Ocelik, V., De Hosson, J.T.M., 2017. Microstructure transformation of Alpha-titanium after mechanical and laser forming. *WIT Trans. Eng. Sci.* 116, 215–222. <https://doi.org/10.2495/MC170221>
- Folkersma, K.G.P., Brouwer, D., Römer, G.W., 2016a. Microtube Laser Forming for Precision Component Alignment. *J. Manuf. Sci. Eng. Trans. ASME* 138, 1–6. <https://doi.org/10.1115/1.4033389>
- Folkersma, K.G.P., Brouwer, D.M., Römer, G.R.B.E., Herder, J.L., 2016b. Robust precision alignment algorithm for micro tube laser forming. *Precis. Eng.* 46, 301–308. <https://doi.org/10.1016/j.precisioneng.2016.05.011>
- Folkersma, K.G.P., Römer, G.R.B.E., Brouwer, D.M., Herder, J.L., 2016c. High precision optical fiber alignment using tube laser bending. *Int. J. Adv. Manuf. Technol.* 86, 953–961. <https://doi.org/10.1007/s00170-015-8143-6>
- Frank Hanus, H.H., 1999. Flame Straightening of thermomechanical rolled structural steel. *Steel Res. Int.* 70, 193–197. <https://doi.org/https://doi.org/10.1002/srin.199905625>
- Froend, M., Fomin, F., Riekehr, S., Alvarez, P., Zubiri, F., Bauer, S., Klusemann, B.,

- Kashaev, N., 2017. Fiber laser welding of dissimilar titanium (Ti-6Al-4V/cp-Ti) T-joints and their laser forming process for aircraft application. *Opt. Laser Technol.* 96, 123–131. <https://doi.org/10.1016/j.optlastec.2017.05.017>
- Gao, H., Sheikholeslami, G., Dearden, G., Edwardson, S.P., 2017. Reverse Analysis of Scan Strategies for Controlled 3D Laser Forming of Sheet Metal. *Procedia Eng.* 183, 369–374. <https://doi.org/10.1016/j.proeng.2017.04.054>
- Gao, H., Sheikholeslami, G., Dearden, G., Edwardson, S.P., 2016. Development of scan strategies for controlled 3D laser forming of sheet metal components. *Phys. Procedia* 83, 286–295. <https://doi.org/10.1016/j.phpro.2016.08.027>
- Geiger, M., Huber, A., 1999. Characterization of the Framework Actuator for Laser Adjusting. *J. Manuf. Sci. Prod.* 2, 159–170. <https://doi.org/10.1515/ijmsp.1999.2.3.159>
- Geiger, M., 1994. Synergy of Laser Material Processing and Metal Forming. *CIRP Ann. - Manuf. Technol.* 43, 563–570. [https://doi.org/10.1016/S0007-8506\(07\)60502-2](https://doi.org/10.1016/S0007-8506(07)60502-2)
- Geiger, M., Vollertsen, F., 1993. The Mechanisms of Laser Forming. *CIRP Ann. - Manuf. Technol.* 42, 301–304. [https://doi.org/10.1016/S0007-8506\(07\)62448-2](https://doi.org/10.1016/S0007-8506(07)62448-2)
- Geiger, M., Vollertsen, F., Deinzer, G., 1993. Flexible straightening of car body shells by laser forming. *SAE Tech. Pap.* <https://doi.org/10.4271/930279>
- Geiger, M., Vollertsen, F., Kals, R., 1996. Fundamentals on the Manufacturing of Sheet Metal Microparts. *CIRP Ann. - Manuf. Technol.* 45, 277–282. [https://doi.org/10.1016/S0007-8506\(07\)63063-7](https://doi.org/10.1016/S0007-8506(07)63063-7)
- Ghoreishi, S.R., Mahmoodi, M., 2022. On the laser forming process of copper/aluminum bi-metal sheets with a functional thickness. *Opt. Laser Technol.* 149, 107870. <https://doi.org/10.1016/j.optlastec.2022.107870>
- Ghosh, A., Misra, D., Acharyya, S.K., 2019. Numerical Simulation of the Laser Welding of 2205 Duplex Stainless Steel. *Int. J. laser Sci.* 1, 293–313.
- Giannini, O., Guarino, S., 2016. Fuzzy model for laser assisted bending process. *MATEC Web Conf.* 45, 6–9. <https://doi.org/10.1051/matecconf/20164504010>
- Gisario, A., Barletta, M., 2018. Laser forming of glass laminate aluminium reinforced

- epoxy (GLARE): On the role of mechanical, physical and chemical interactions in the multi-layers material. *Opt. Lasers Eng.* 110, 364–376. <https://doi.org/10.1016/j.optlaseng.2018.06.013>
- Gisario, A., Barletta, M., Venettacci, S., 2016a. Improvements in springback control by external force laser-assisted sheet bending of titanium and aluminum alloys. *Opt. Laser Technol.* 86, 46–53. <https://doi.org/10.1016/j.optlastec.2016.06.013>
- Gisario, A., Mehrpouya, M., Rahimzadeh, A., De Bartolomeis, A., Barletta, M., 2020. Prediction model for determining the optimum operational parameters in laser forming of fiber-reinforced composites. *Adv. Manuf.* 8, 242–251. <https://doi.org/10.1007/s40436-020-00304-3>
- Gisario, A., Mehrpouya, M., Venettacci, S., Barletta, M., 2017. Laser-assisted bending of Titanium Grade-2 sheets: Experimental analysis and numerical simulation. *Opt. Lasers Eng.* 92, 110–119. <https://doi.org/10.1016/j.optlaseng.2016.09.004>
- Gisario, A., Mehrpouya, M., Venettacci, S., Mohammadzadeh, A., Barletta, M., 2016b. LaserOrigami (LO) of three-dimensional (3D) components: Experimental analysis and numerical modelling. *J. Manuf. Process.* 23, 242–248. <https://doi.org/10.1016/j.jmapro.2016.05.005>
- Gollo, M.H., Kalkhoran, S.N.A., 2017. Experimental study on mechanical and chemical behaviors of bi-layer Fe/Al sheet after laser forming. *J. Brazilian Soc. Mech. Sci. Eng.* 39, 1623–1632. <https://doi.org/10.1007/s40430-016-0536-4>
- Gou, R., Dan, W.J., Yu, M., Zhang, W.G., 2018. Effect of laser forming on mechanical properties of multiple-phase steels by using a thermal–microstructure–mechanical model. *Int. J. Mater. Res.* 109, 922–929. <https://doi.org/10.3139/146.111690>
- Goyal, D.K., Yadav, R., Kant, R., 2022a. An integrated hybrid methodology for estimation of absorptivity and interface temperature in laser transmission welding. *Int. J. Adv. Manuf. Technol.* 121, 3771–3786. <https://doi.org/10.1007/s00170-022-09536-y>
- Goyal, D.K., Yadav, R., Kant, R., 2022b. Study of Temperature Field Considering Gradient Volumetric Heat Absorption in Transparent Sheet During Laser Transmission Welding (LTW). *Lasers Eng.* 53, 215–229.

- Guan, Y., Sun, S., Zhao, G., Luan, Y., 2005. Influence of material properties on the laser-forming process of sheet metals. *J. Mater. Process. Technol.* 167, 124–131. <https://doi.org/10.1016/j.jmatprotec.2004.10.003>
- Gudur, S., Simhambhatla, S., 2022. Augmenting wire arc additive manufacturing with laser forming for generative realization of complex geometries. *Optik (Stuttg.)* 262, 169283. <https://doi.org/10.1016/j.ijleo.2022.169283>
- Guglielmotti, A., Quadrini, F., Squeo, E.A., Tagliaferri, V., 2009. Laser bending of Aluminum foam sandwich panels. *Adv. Eng. Mater.* 11, 902–906. <https://doi.org/10.1002/adem.200900111>
- Guo, J., Li, W., Wan, M., Zhao, Y., Li, C., 2021. Design of an innovative laser-assisted four-point bending forming process for high-stiffened structure of aluminum alloy. *Opt. Laser Technol.* 143, 107313. <https://doi.org/10.1016/j.optlastec.2021.107313>
- Guo, Y., Shi, Y., Wang, X., Li, X., Chen, T., 2021a. Angle analysis model of pressure-assisted laser forming and high-precision method. *Opt. Laser Technol.* 142, 107216. <https://doi.org/10.1016/j.optlastec.2021.107216>
- Guo, Y., Shi, Y., Wang, X., Sun, R., Bing, Z., 2020. An analytical model of laser bending angle under preload. *Int. J. Adv. Manuf. Technol.* 108, 2569–2577. <https://doi.org/10.1007/s00170-020-05521-5>
- Guo, Y., Shi, Y., Wang, X., Sun, R., Li, X., 2021b. A method to realize high-precision and large laser thermal bending angle. *J. Manuf. Process.* 62, 168–178. <https://doi.org/10.1016/j.jmapro.2020.12.005>
- Guo, Y., Shi, Y., Wang, X., Zhao, X., 2021c. Preload assisted laser thermoforming at low-temperature. *E3S Web Conf.* 233, 1–5. <https://doi.org/10.1051/e3sconf/202123304043>
- Hao, N., Li, L., 2003a. Finite element analysis of laser tube bending process. *Appl. Surf. Sci.* 208–209, 437–441. [https://doi.org/10.1016/S0169-4332\(02\)01429-0](https://doi.org/10.1016/S0169-4332(02)01429-0)
- Hao, N., Li, L., 2003b. An analytical model for laser tube bending. *Appl. Surf. Sci.* 208–209, 432–436. [https://doi.org/10.1016/S0169-4332\(02\)01428-9](https://doi.org/10.1016/S0169-4332(02)01428-9)
- Hao, Y., Guan, W., Peraza Hernandez, E.A., Lien, J.M., 2021. Planning Laser-Forming Folding Motion with Thermal Simulation. *Proc. - IEEE Int. Conf. Robot. Autom.*

2021-May, 7788–7794. <https://doi.org/10.1109/ICRA48506.2021.9561883>

- Hembram, N., Singh, J.K., Hussain, M., 2016. Optimization of Process Parameters in Laser Bending of Inconel- Optimization of Process Parameters in Laser Bending of Inconel-625 Metal Sheet. *Int. J. Adv. Technol. Eng. Sci.* 4, 108–115.
- Hemmati, S.J., Shin, J.G., 2007. Estimation of flame parameters for flame bending process. *Int. J. Mach. Tools Manuf.* 47, 799–804. <https://doi.org/10.1016/j.ijmachtools.2006.09.005>
- Hennige, T., 2000. Development of irradiation strategies for 3D-laser forming. *J. Mater. Process. Technol.* 103, 102–108. [https://doi.org/10.1016/S0924-0136\(00\)00392-7](https://doi.org/10.1016/S0924-0136(00)00392-7)
- Hennige, T., Holzer, S., Vollertsen, F., Geiger, M., 1997. On the working accuracy of laser bending. *J. Mater. Process. Technol.* 71, 422–432. [https://doi.org/10.1016/S0924-0136\(97\)00108-8](https://doi.org/10.1016/S0924-0136(97)00108-8)
- Hoving, W., 1997. Accurate manipulation using laser technology. *Lasers Mater. Process.* 3097, 284–295.
- Hsiao, Y.C., 1997. Finite Element Analysis of Laser Forming. Massachusetts Institute of Technology.
- Hsiao, Y.C., Shimizu, H., Firth, L., Maher, W., Masubuchi, K., 1997. Finite element modeling of laser forming. *Laser Inst. Am. Proc.* <https://doi.org/10.2351/1.5059621>
- Hsieh, H.S., Lin, J., 2005a. Study of the buckling mechanism in laser tube forming. *Opt. Laser Technol.* 37, 402–409. <https://doi.org/10.1016/j.optlastec.2004.06.004>
- Hsieh, H.S., Lin, J., 2005b. Study of the buckling mechanism in laser tube forming with axial preloads. *Int. J. Mach. Tools Manuf.* 45, 1368–1374. <https://doi.org/10.1016/j.ijmachtools.2005.02.002>
- Hsieh, R.I., Liou, H.Y., Pan, Y.T., 2001. Effects of cooling time and alloying elements on the microstructure of the Gleeble-simulated heat-affected zone of 22% Cr duplex stainless steels. *J. Mater. Eng. Perform.* 10, 526–536. <https://doi.org/10.1361/105994901770344665>
- Hu, Z., Kovacevic, R., Labudovic, M., 2002. Experimental and numerical modeling of

- buckling instability of laser sheet forming. *Int. J. Mach. Tools Manuf.* 42, 1427–1439. [https://doi.org/10.1016/S0890-6955\(02\)00075-5](https://doi.org/10.1016/S0890-6955(02)00075-5)
- Hwang, S.-Y., Park, K.-G., Heo, J., Lee, J.-H., 2021. Thermal Strain-Based Simplified Prediction of Thermal Deformation Caused by Flame Bending. *Appl. Sci.* 11. <https://doi.org/10.3390/app11052011>
- Imhan, K.I., Baharudin, B.T.H.T., Zakaria, A., Ismail, M.I.S.B., Alsabti, N.M.H., Ahmad, A.K., 2018a. Improve the material absorption of light and enhance the laser tube bending process utilizing laser softening heat treatment. *Opt. Laser Technol.* 99, 15–18. <https://doi.org/10.1016/j.optlastec.2017.09.040>
- Imhan, K.I., Baharudin, B.T.H.T., Zakaria, A., Ismail, M.I.S.B., Alsabti, N.M.H., Ahmad, A.K., 2017. Investigation of material specifications changes during laser tube bending and its influence on the modification and optimization of analytical modeling. *Opt. Laser Technol.* 95, 151–156. <https://doi.org/10.1016/j.optlastec.2017.04.030>
- Imhan, K.I., BTHT, B., Zakaria, A., Shah B Ismail, M.I., Hadi Alsabti, N.M., Ahmad, A.K., 2018b. Features of Laser Tube Bending processing based on Laser Forming: A Review. *J. Lasers, Opt. Photonics* 05. <https://doi.org/10.4172/2469-410x.1000174>
- J. Widlaszewski, 1997. Precise laser bending, in: M. Geiger, F.V. (Ed.), *Laser Assisted Net Shape Engineering 2, Proceedings of the LANE'97*. pp. 393–398.
- Jamil, M.S.C., Sheikh, M.A., Li, L., 2011. A study of the effect of laser beam geometries on laser bending of sheet metal by buckling mechanism. *Opt. Laser Technol.* 43, 183–193. <https://doi.org/10.1016/j.optlastec.2010.06.011>
- Jha, G.C., Nath, A.K., Roy, S.K., 2008. Study of edge effect and multi-curvature in laser bending of AISI 304 stainless steel. *J. Mater. Process. Technol.* 197, 434–438. <https://doi.org/10.1016/j.jmatprotec.2007.06.040>
- Ji, Z., Wu, S., 1998. FEM simulation of the temperature field during the laser forming of sheet metal. *J. Mater. Process. Technol.* 74, 89–95. [https://doi.org/10.1016/S0924-0136\(97\)00254-9](https://doi.org/10.1016/S0924-0136(97)00254-9)
- Jorge, A.M., Reis, G.S., Balancin, O., 2011. Influence of the microstructure on the

- plastic behaviour of duplex stainless steels. *Mater. Sci. Eng. A* 528, 2259–2264.
<https://doi.org/10.1016/j.msea.2010.11.087>
- Jović, S., Makragić, S., Jovanović, M., 2017. Parameters influence of laser forming on shaped surface by soft computing technique. *Optik (Stuttg)*. 142, 451–454.
<https://doi.org/10.1016/j.ijleo.2017.04.089>
- K. Paramasivan, S. Das, S. marimuthu and D. misra, 2019. Numerical Study of the Mechanism of Laser Forming Process. *Int. J. laser Sci.* 1, 347–382.
- Kaglyak, O., Romanov, B., Romanova, K., Myrgorod, O., Ruban, A., Shvedun, V., 2021. Repeatability of sheet material formation results and interchangeability of processing modes at multi-pass laser formation. *Mater. Sci. Forum* 1038 MSF, 15–24. <https://doi.org/10.4028/www.scientific.net/MSF.1038.15>
- Kant, R., 2016. Assessment of Feasibility, Productivity and Product Quality during Laser Based Bending of Magnesium Alloy Sheets. *Indian institute of technology Guwahati*.
- Kant, R., Joshi, S.N., 2018. Numerical investigations into influence of scanning path curvature on deformation behavior during curvilinear laser bending of magnesium sheets. *J. Therm. Stress.* 41, 313–330.
<https://doi.org/10.1080/01495739.2017.1403298>
- Kant, R., Joshi, S.N., 2016. Numerical and experimental studies on the laser bending of magnesium M1A alloy. *Lasers Eng.* 35, 39–62.
- Kant, Ravi, Joshi, S.N., 2016a. Numerical and experimental studies on the laser bending of magnesium M1A alloy. *Lasers Eng.* 35, 39–62.
- Kant, Ravi, Joshi, S.N., 2016b. Thermo-mechanical studies on bending mechanism, bend angle and edge effect during multi-scan laser bending of magnesium M1A alloy sheets. *J. Manuf. Process.* 23, 135–148.
<https://doi.org/10.1016/j.jmapro.2016.05.017>
- Kant, R., Joshi, S.N., 2013. Finite element simulation of laser assisted bending with moving mechanical load. *Int. J. Mechatronics Manuf. Syst.* 6, 351–366.
<https://doi.org/10.1504/IJMMS.2013.057128>
- Kant, R., Joshi, S.N., 2012. Analysis of Sheet-Holding Methods in Laser Bending

- Process, in: 3rd Asian Symposium on Materials & Processing (ASMP 2012).
- Kant, R., Joshi, S.N., Dixit, U.S., 2016. Research issues in the laser sheet bending process, in: *Materials Forming and Machining*. Woodhead Publishing, pp. 73–97. <https://doi.org/10.1016/B978-0-85709-483-4.00004-1>
- Kant, R., Joshi, S.N., Dixit, U.S., 2015. An integrated FEM-ANN model for laser bending process with inverse estimation of absorptivity. *Mech. Adv. Mater. Mod. Process.* 1, 1–12. <https://doi.org/10.1186/s40759-015-0006-1>
- Kant, Ravi, Sunny, A.P., Gurung, H., 2016. Investigation on Importance of Absorptivity during Laser Bending Process, in: *6th International & 27th All India Manufacturing Technology, Design and Research (AIMTDR 2016)*. pp. 1193–1197.
- Keshtiara, M., Golabi, S., Tarkesh Esfahani, R., 2021. Multi-objective optimization of stainless steel 304 tube laser forming process using GA. *Eng. Comput.* 37, 155–171. <https://doi.org/10.1007/s00366-019-00814-0>
- Khandandel, S.E., Hossein Seyedkashi, S.M., Moradi, M., 2021. Numerical and experimental analysis of the effect of forced cooling on laser tube forming. *J. Brazilian Soc. Mech. Sci. Eng.* 43, 1–11. <https://doi.org/10.1007/s40430-021-03063-9>
- Khandandel, S.E., Seyedkashi, S.M.H., Moradi, M., 2020. A novel path strategy design for precise 2D and 3D laser tube forming process; experimental and numerical investigation. *Optik (Stuttg.)* 206, 164302. <https://doi.org/10.1016/j.ijleo.2020.164302>
- Kim, S.K., Kang, K.Y., Kim, M.S., Lee, J.M., 2015. Low-temperature mechanical behavior of super duplex stainless steel with sigma precipitation. *Metals (Basel)*. 5, 1732–1745. <https://doi.org/10.3390/met5031732>
- Klocke, F., 2008. *Manufacturing Processes 4*. Springer Heidelberg New York. <https://doi.org/10.1007/978-3-642-36772-4>
- Knupfer, S.M., Moore, A.J., 2010. The effects of laser forming on the mechanical and metallurgical properties of low carbon steel and aluminium alloy samples. *Mater. Sci. Eng. A* 527, 4347–4359. <https://doi.org/10.1016/j.msea.2010.03.069>

- Kotobi, M., Honarpisheh, M., 2018. Through-depth residual stress measurement of laser bent steel–titanium bimetal sheets. *J. Strain Anal. Eng. Des.* 53, 130–140. <https://doi.org/10.1177/0309324717753212>
- Kotobi, M., Honarpisheh, M., 2017. Experimental and numerical investigation of through-thickness residual stress of laser-bent Ti samples. *J. Strain Anal. Eng. Des.* 52, 347–355. <https://doi.org/10.1177/0309324717719212>
- Kotobi, M., Mansouri, H., Honarpisheh, M., 2019. Investigation of laser bending parameters on the residual stress and bending angle of St-Ti bimetal using FEM and neural network. *Opt. Laser Technol.* 116, 265–275. <https://doi.org/10.1016/j.optlastec.2019.03.030>
- Kumar, V., Dixit, U.S., 2018. A model for the estimation of hardness of laser bent strips. *Opt. Laser Technol.* 107, 491–499. <https://doi.org/10.1016/j.optlastec.2018.06.029>
- Kurp, P., Mucha, Z., Tofil, S., Mulczyk, K., 2016. The influence of treatment parameters on the microstructure, properties and bend angle of laser formed construction bars. *Arch. Metall. Mater.* 61, 1151–1156. <https://doi.org/10.1515/amm-2016-0192>
- Lambiase, F., Di Ilio, A., Paoletti, A., 2016. Productivity in multi-pass laser forming of thin AISI 304 stainless steel sheets. *Int. J. Adv. Manuf. Technol.* 86, 259–268. <https://doi.org/10.1007/s00170-015-8150-7>
- Lambiase, F., Di Ilio, A., Paoletti, A., 2013. An experimental investigation on passive water cooling in laser forming process. *Int. J. Adv. Manuf. Technol.* 64, 829–840. <https://doi.org/10.1007/s00170-012-4072-9>
- Lambiase, F., Paoletti, A., Di Ilio, A., 2011. Experimental investigation of parameters effect on laser forming productiveness. *Key Eng. Mater.* 473, 791–798. <https://doi.org/10.4028/www.scientific.net/KEM.473.791>
- Lang, X., Weidong, L., Xiufeng, W., Mingong, W., 2017. Analysis on Process Parameters of Laser Bending of Preloaded metal plate. *J. Beijing Univ. Aeronaut. Astronaut.* 43, 1149–1154.
- Lawrence, J., Schmidt, M.J.J., Li, L., 2001. The forming of mild steel plates with a 2.5 kW high power diode laser. *Int. J. Mach. Tools Manuf.* 41, 967–977. [https://doi.org/10.1016/S0890-6955\(00\)00117-6](https://doi.org/10.1016/S0890-6955(00)00117-6)

- Lazarus, N., Smith, G.L., 2018. Laser Folding in a Roll-to-Roll Manufacturing Process. *Lasers Manuf. Mater. Process.* 5, 237–247. <https://doi.org/10.1007/s40516-018-0064-4>
- Lazarus, N., Smith, G.L., 2017. Laser Forming for Complex 3D Folding. *Adv. Mater. Technol.* 2, 1–6. <https://doi.org/10.1002/admt.201700109>
- Li, Q., Lin, X., Wang, X., Yang, H., Song, M., Huang, W., 2016. Research on the grain boundary liquation mechanism in heat affected zones of laser forming repaired K465 nickel-based superalloy. *Metals* (Basel). 6. <https://doi.org/10.3390/met6030064>
- Li, W., Yao, Y.L., 2001. Laser bending of tubes: Mechanism, analysis, and prediction. *J. Manuf. Sci. Eng. Trans. ASME* 123, 674–681. <https://doi.org/10.1115/1.1392992>
- Li, W., Yao, Y.L., 2000. Buckling based laser forming process: Concave or convex, in: *International Congress on Applications of Lasers & Electro-Optics*. AIP Publishing, pp. D220–D229. <https://doi.org/10.2351/1.5059467>
- Li, Z., Wang, X., 2019a. Numerical simulation of stainless steel-carbon steel laminated plate considering interface in pulsed laser bending. *Materials* (Basel). 12, 1410. <https://doi.org/10.3390/ma12091410>
- Li, Z., Wang, X., 2019b. Analytical model for estimating bending angle in laser bending of 304 stainless steel/Q235 carbon steel laminated plate. *J. Laser Appl.* 31, 042012. <https://doi.org/10.2351/1.5116729>
- Liou, H.Y., Hsieh, R.I., Tsai, W.T., 2002. Microstructure and pitting corrosion in simulated heat-affected zones of duplex stainless steels. *Mater. Chem. Phys.* 74, 33–42. [https://doi.org/10.1016/S0254-0584\(01\)00409-6](https://doi.org/10.1016/S0254-0584(01)00409-6)
- Liu, H., Zhang, W., Gau, J.T., Shen, Z., Zhang, G., Ma, Y., Wang, X., 2018. Microscale laser flexible dynamic forming of Cu/Ni laminated composite metal sheets. *J. Manuf. Process.* 35, 51–60. <https://doi.org/10.1016/j.jmapro.2018.07.013>
- Liu, J., Sun, S., Guan, Y., Ji, Z., 2010. Experimental study on negative laser bending process of steel foils. *Opt. Lasers Eng.* 48, 83–88. <https://doi.org/10.1016/j.optlaseng.2009.07.019>

- Lubiano, Gi., Ramos, jorge A., Magee, J., 2000. Laser Bending of Thin Metal Sheets by Means of a Low Power CO2 Laser, in: 11th International Solid Freeform Fabrication Symposium.
- Luo, M., Hu, Y., Hu, L., Yao, Z., 2020. Efficient process planning of laser peen forming for complex shaping with distributed eigen-moment. *J. Mater. Process. Technol.* 279, 116588. <https://doi.org/10.1016/j.jmatprotec.2020.116588>
- Magee, J., Watkins, K.G., Steen, W.M., 1998a. Advances in laser forming. *J. Laser Appl.* 10, 235–246. <https://doi.org/10.2351/1.521859>
- Magee, J., Watkins, K.G., Steen, W.M., 1997. Laser forming of aerospace alloys. *Laser Inst. Am. Proc.* 83. <https://doi.org/10.2351/1.5059678>
- Magee, J., Watkins, K.G., Steen, W.M., Calder, N.J., Sidhu, J., Kirby, J., 1998b. Laser bending of high strength alloys. *J. Laser Appl.* 10, 149–155. <https://doi.org/10.2351/1.521844>
- Magee, J., Watkins, K.G., Steen, W.M., Cooke, R.L., Sidhu, J., 1998c. Development of an integrated laser forming demonstrator system for the aerospace industry 141, E141–E150. <https://doi.org/10.2351/1.5059141>
- Maher, W., Tong, K.-O., Bampton, C., Bright, M., Wooten, J., Rhodes, C., 1998. Laser forming of titanium and other metals is useable within metallurgical constraints 121, E121–E130. <https://doi.org/10.2351/1.5059139>
- Maji, K., 2019a. Parametric study and optimization of pulsed laser thermal micro-forming of thin sheets. *Int. J. Manuf. Mater. Mech. Eng.* 9, 47–61. <https://doi.org/10.4018/IJMMME.2019040103>
- Maji, K., 2019b. Prediction and optimization of deformations in coupling mechanism based laser forming of sheet metals. *Mater. Sci. Forum* 969 MSF, 552–557. <https://doi.org/10.4028/www.scientific.net/MSF.969.552>
- Maji, K., Chakraborty, S.S., Pratihari, D.K., Nath, A.K., 2020. Inverse analysis and multi-objective optimization of coupling mechanism based laser forming process. *Sadhana - Acad. Proc. Eng. Sci.* 45, 1–16. <https://doi.org/10.1007/s12046-019-1245-3>
- Maji, K., Pratihari, D.K., Nath, A.K., 2018. Forward and inverse predictions of

- deformations in laser forming of shaped surfaces under coupling mechanism. *J. Laser Appl.* 30, 032011. <https://doi.org/10.2351/1.5033450>
- Maji, K., Pratihari, D.K., Nath, A.K., 2016. Experimental investigations, modeling, and optimization of multi-scan laser forming of AISI 304 stainless steel sheet. *Int. J. Adv. Manuf. Technol.* 83, 1441–1455. <https://doi.org/10.1007/s00170-015-7675-0>
- Majumdar, J.D., Nath, A.K., Manna, I., 2004. Studies on laser bending of stainless steel. *Mater. Sci. Eng. A* 385, 113–122. <https://doi.org/10.1016/j.msea.2004.06.009>
- Marya, M., Edwards, G.R., 2000. Factors affecting the laser bending of Ti–6Al–2Sn–4Zr–2Mo. *J. Laser Appl.* 12, 149–159. <https://doi.org/10.2351/1.521926>
- Masoudi Nejad, R., Hoseini Shojaati, Z.S., Wheatley, G., Ghahremani Moghadam, D., 2021. On the bending angle of aluminum-copper two-layer sheets in laser forming process. *Opt. Laser Technol.* 142, 107233. <https://doi.org/10.1016/j.optlastec.2021.107233>
- Merklein, M., Hennige, T., Geiger, M., 2001. Laser forming of aluminium and aluminium alloys - Microstructural investigation. *J. Mater. Process. Technol.* 115, 159–165. [https://doi.org/10.1016/S0924-0136\(01\)00759-2](https://doi.org/10.1016/S0924-0136(01)00759-2)
- Mjali, K.V., Botes, A., 2018. The influence of the concept of “line energy” on the mechanical properties of laser formed commercially pure grade 2 titanium alloy plates. *Procedia Manuf.* 26, 267–275. <https://doi.org/10.1016/j.promfg.2018.07.035>
- Mjali, K. V., Els-Botes, A., Mashinini, P.M., 2018. Residual Stress Distribution and the Concept of Total Fatigue Stress in Laser and Mechanically Formed Commercially Pure Grade 2 Titanium Alloy Plates. *J. Manuf. Sci. Eng. Trans. ASME* 140. <https://doi.org/10.1115/1.4037438>
- Mjali, K. V., Els-Botes, A., Mashinini, P.M., 2017. The effects of laser and mechanical forming on the hardness and microstructural layout of commercially pure grade 2 titanium alloy plates, in: *ASME 2017 12th International Manufacturing Science and Engineering Conference, MSEC 2017 Collocated with the JSME/ASME 2017 6th International Conference on Materials and Processing.* pp. 1–9. <https://doi.org/10.1115/MSEC2017-2603>

- Moshaiov, A., Latorre, R., 1985. Temperature Distribution During Plate Bending By Torch Flame Heating. *J. Sh. Res.* 29, 1–11. <https://doi.org/10.5957/jsr.1985.29.1.1>
- Moshaiov, A., Vorus, W.S., 1987. Mechanics of the Flame Bending Process: Theory and Applications. *J. Sh. Res.* 31, 269–281. <https://doi.org/10.5957/jsr.1987.31.4.269>
- Mucha, Z., Hoffman, J., Kalita, W., Mucha, S., 1997. Laser forming of thick free plates. *Laser Assist. Net Shape Eng. 2, Proc. LANE'97* 383–393.
- Mucha, Z., Widłaszewski, J., Kurp, P., Mulczyk, K., 2016. Mechanically assisted laser forming of thin beams, in: *Laser Technology 2016: Progress and Applications of Lasers*. p. 101590U. <https://doi.org/10.1117/12.2262114>
- Mulay, S., Paliwal, V., Babu, N.R., 2021. Analytical approach to predict the bend angle of sheet formed by multiple laser scans. *Procedia CIRP* 99, 272–277. <https://doi.org/10.1016/j.procir.2021.03.040>
- Mulay, S., Paliwal, V., Babu, N.R., 2020. Analytical model for prediction of bend angle in laser forming of sheets. *Int. J. Adv. Manuf. Technol.* 109, 699–715. <https://doi.org/10.1007/s00170-020-05643-w>
- N. Kitamura, 1983. Technical report of joint project on materials processing by high power laser. *JWES-TP 8302*, 359–371.
- Nath, U., Yadav, V., 2022. Analytical modeling of temperature evolution and bend angle in laser forming of Al 6061-T6 sheets and its experimental analysis. *Opt. Laser Technol.* 154, 108307. <https://doi.org/10.1016/j.optlastec.2022.108307>
- Nath, U., Yadav, V., Purohit, R., 2021. Finite element analysis of AM30 magnesium alloy sheet in the laser bending process. *Adv. Mater. Process. Technol.* 1–13. <https://doi.org/10.1080/2374068X.2021.1878699>
- Navarrete, Á., Celentano, D., 2018. Effect of workpiece geometry using circular scan patterns in sheet laser forming processes. *Int. J. Adv. Manuf. Technol.* 96, 1835–1846. <https://doi.org/10.1007/s00170-018-1628-3>
- Navarrete, Á., Cook, F., Celentano, D., Cruchaga, M., García-Herrera, C., 2018. Numerical simulation and experimental validation of sheet laser forming processes using general scanning paths. *Materials (Basel)*. 11.

<https://doi.org/10.3390/MA11071262>

- Nejati, M.R., Gollo, M.H., Tajdari, M., Ghaffarian, H., 2018. Input value prediction of parameters in laser bending using Fuzzy and PSO. *Soft Comput.* 22, 2189–2203. <https://doi.org/10.1007/s00500-016-2479-1>
- Nomani, J., Pramanik, A., Hilditch, T., Littlefair, G., 2017. Stagnation zone during the turning of Duplex SAF 2205 stainless steels alloy. *Mater. Manuf. Process.* 32, 1486–1489. <https://doi.org/10.1080/10426914.2017.1279289>
- Odermatt, A.E., Ventzke, V., Dorn, F., Dinsé, R., Merhof, P., Kashaev, N., 2021a. Effect of laser beam welding on microstructure, tensile strength and fatigue behaviour of duplex stainless steel 2205. *J. Manuf. Process.* 72, 148–158. <https://doi.org/10.1016/j.jmapro.2021.10.020>
- Odermatt, A.E., Ventzke, V., Dorn, F., Dinsé, R., Merhof, P., Kashaev, N., 2021b. Effect of laser beam welding on microstructure, tensile strength and fatigue behaviour of duplex stainless steel 2205. *J. Manuf. Process.* 72, 148–158. <https://doi.org/10.1016/j.jmapro.2021.10.020>
- Odumodu, K., Das, S., 1997. A Numerical and Experimental Analysis of Forceless Forming Using Lasers. *Comput. Model. Simul. Eng.* 2, 243–266.
- Oh, Y.J., Yang, W.J., Lee, J.H., Kim, D.H., Yoo, W.D., Lee, J.H., 2013. Effect of Cooling Rate on Microstructural and Mechanical Properties of SAF 2205 Duplex Stainless Steel. *J. Korean Soc. Heat Treat.* 14–20.
- Olowinsky, A., Gillner, A., Poprawe, R., 1998. Laser beam micro-forming – A new technology 89, E89–E97. <https://doi.org/10.2351/1.5059156>
- Padmanabham, G., Bathe, R., 2018. Laser Materials Processing for Industrial Applications. *Proc. Natl. Acad. Sci. India Sect. A - Phys. Sci.* 88, 359–374. <https://doi.org/10.1007/s40010-018-0523-5>
- Paramasivan, K., Das, S., Marimuthu, S., Misra, D., 2018a. Experimental and Numerical Investigation on Micro-Bending of AISI 304 Sheet Metal Using a Low Power Nanosecond Laser. *Lasers Manuf. Mater. Process.* 5, 95–112. <https://doi.org/10.1007/s40516-018-0056-4>
- Paramasivan, K., Das, S., Marimuthu, S., Misra, D., 2018b. Increment in laser bending

- angle by forced bottom cooling. *Int. J. Adv. Manuf. Technol.* 94, 2137–2147.
<https://doi.org/10.1007/s00170-017-1035-1>
- Paramasivan, K., Das, S., Sundar, M., Misra, D., 2017. Numerical simulation of laser bending of AISI 304 plate with a rectangular cut out. *Int. J. Eng. Sci. Technol.* 9, 1–15.
- Petrovic, D.S., Klancnik, G., Medved, J., 2012. The effect of cooling rate on the solidification and microstructure evolution in duplex stainless steel A DSC study.
<https://doi.org/10.1007/s10973-012-2370-y>
- Pohl, M., Storz, O., Glogowski, T., 2007. Effect of intermetallic precipitations on the properties of duplex stainless steel. *Mater. Charact.* 58, 65–71.
<https://doi.org/10.1016/j.matchar.2006.03.015>
- Ponticelli, G.S., Guarino, S., Giannini, O., 2018. A fuzzy logic-based model in laser-assisted bending springback control. *Int. J. Adv. Manuf. Technol.* 95, 3887–3898.
<https://doi.org/10.1007/s00170-017-1482-8>
- Pramanik, A., Basak, A.K., Dixit, A.R., Chattopadhyaya, S., 2018. Processing of duplex stainless steel by WEDM. *Mater. Manuf. Process.* 33, 1559–1567.
<https://doi.org/10.1080/10426914.2018.1453165>
- Pridham, M., Thomson, G., 1994. Production of Metal Prototypes Using a High Powered Laser Machining Centre. *Solid Free. Fabr. Symp.*
- Quadrini, F., Guglielmotti, A., Squeo, E.A., Tagliaferri, V., 2010. Laser forming of open-cell aluminium foams. *J. Mater. Process. Technol.* 210, 1517–1522.
<https://doi.org/10.1016/j.jmatprotec.2010.04.010>
- Ramos-Moore, E., Hoffmann, J., Siqueira, R.H.M., de Carvalho, S.M., de Lima, M.S.F., Celentano, D.J., 2021. Experimental and simulation analysis of effects of laser bending on microstructures applied to advanced metallic alloys. *Metals (Basel)*. 11, 1–12. <https://doi.org/10.3390/met11020362>
- Ramos, J.A., Magee, J., Watkins, K., Steen, W.M., Noble, F., 1998. Microstructure of laser bent aluminium alloy Alclad 2024-T3 178, E178–E185.
<https://doi.org/10.2351/1.5059146>
- Rattan, A., Jasra, Y., Saxena, R.K., 2020. Prediction of bending behavior for laser

- forming of lime coated plain carbon steel using finite element method. *Mater. Today Proc.* 28, 1943–1950. <https://doi.org/10.1016/j.matpr.2020.05.411>
- Raza, M.S., Datta, S., Gopinath, M., Saha, P., 2021. Monitoring and analysis of melt-assisted deformation behavior of 304L stainless steel during multipass laser forming process using IR pyrometer and laser-based displacement sensor. *Opt. Laser Technol.* 135, 106718. <https://doi.org/10.1016/j.optlastec.2020.106718>
- Roohi, A.H., Gollo, M.H., Naeini, H.M., 2012. External force-assisted laser forming process for gaining high bending angles. *J. Manuf. Process.* 14, 269–276. <https://doi.org/10.1016/j.jmapro.2012.07.004>
- Roohi, A.H., Moslemi Naeini, H., Hoseinpour Gollo, M., 2017. An experimental investigation of parameters effect on laser forming of Al6061-T6 sheets. *Proc. Inst. Mech. Eng. Part L J. Mater. Des. Appl.* 231, 433–442. <https://doi.org/10.1177/1464420715599181>
- Roohi, A.H., Moslemi Naeini, H., Hoseinpour Gollo, M., Soltanpour, M., Bruschi, S., Ghiotti, A., 2018. Forming of closed-cell aluminum foams under thermal loadings: experimental investigation. *Int. J. Adv. Manuf. Technol.* 95, 3919–3928. <https://doi.org/10.1007/s00170-017-1501-9>
- Safari, M., 2022. A comparative study on laser bending process with linear and curved irradiating schemes. *Optik (Stuttg.)* 264, 169426. <https://doi.org/10.1016/j.ijleo.2022.169426>
- Safari, M., Alves de Sousa, R.J., Joudaki, J., 2021. Experimental investigation of the effects of irradiating schemes in laser tube bending process. *Metals (Basel)*. 11. <https://doi.org/10.3390/met11071123>
- Safari, M., de Sousa, R.A., Joudaki, J., 2020a. Recent advances in the laser forming process: A review. *Metals (Basel)*. 10, 1–19. <https://doi.org/10.3390/met10111472>
- Safari, M., de Sousa, R.A., Joudaki, J., 2020b. Fabrication of saddle-shaped surfaces by a laser forming process: An experimental and statistical investigation. *Metals (Basel)*. 10, 1–13. <https://doi.org/10.3390/met10070883>
- Safari, M., Joudaki, J., 2018. Prediction of Bending Angle for Laser Forming of Tailor Machined Blanks by Neural Network. *Iran. J. Mater. Form.* 5, 45–57.

- Safari, M., Mostaan, H., 2016. Experimental and numerical investigation of laser forming of cylindrical surfaces with arbitrary radius of curvature. *Alexandria Eng. J.* 55, 1941–1949. <https://doi.org/10.1016/j.aej.2016.07.033>
- Sala, S.T., Keller, S., Chupakhin, S., Pörtl, D., Klusemann, B., Kashaev, N., 2022. Effect of laser peen forming process parameters on bending and surface quality of Ti-6Al-4V sheets. *J. Mater. Process. Technol.* 305. <https://doi.org/10.1016/j.jmatprotec.2022.117578>
- Scully, K., 1987. Laser Line Heating. *J. Sh. Prod.* 3, 237–246. <https://doi.org/10.5957/jsp.1987.3.4.237>
- Seyedkashi, S.M.H., Abazari, H.D., Gollo, M.H., Woo, Y.Y., Moon, Y.H., 2019. Characterization of laser bending of SUS304L/C11000 clad sheets. *J. Mech. Sci. Technol.* 33, 3223–3230. <https://doi.org/10.1007/s12206-019-0617-2>
- Seyedkashi, S.M.H., Cho, J.R., Lee, S.H., Moon, Y.H., 2018. Feasibility of underwater laser forming of laminated metal composites. *Mater. Manuf. Process.* 33, 546–551. <https://doi.org/10.1080/10426914.2017.1376075>
- Seyedkashi, S.M.H., Gollo, M.H., Biao, J., Moon, Y.H., 2016. Laser bendability of SUS430/C11000/SUS430 laminated composite and its constituent layers. *Met. Mater. Int.* 22, 527–534. <https://doi.org/10.1007/s12540-016-5711-8>
- Shahabad, S.I., Naeini, H.M., Roohi, A.H., Soltanpour, M., Tavakoli, A., 2017a. Height prediction of dome-shaped products in laser forming process. *Int. J. Adv. Manuf. Technol.* 88, 2227–2236. <https://doi.org/10.1007/s00170-016-8946-0>
- Shahabad, S.I., Naeini, H.M., Roohi, A.H., Tavakoli, A., Nasrollahzade, M., 2017b. Experimental investigation of laser forming process to produce dome-shaped products. *Int. J. Adv. Manuf. Technol.* 90, 1051–1057. <https://doi.org/10.1007/s00170-016-9437-z>
- Sharma, A., Mani Prabu, S.S., Palani, I.A., Hosmani, S.S., Patil, R., 2018. Formability studies on Ni-Ti shape memory alloy using laser forming technology, in: *IOP Conference Series: Materials Science and Engineering*. <https://doi.org/10.1088/1757-899X/390/1/012053>
- Sharma, Y.P., Sidhu, B.S., Kant, R., Yadav, R., 2023. Enhancing the bend angle and

- mechanical properties of mild steel using fiber laser bending technique under the influence of electromagnetic force. *Opt. Lasers Eng.* 168, 107631. <https://doi.org/10.1016/j.optlaseng.2023.107631>
- Shen, H., 2008. Mechanism of laser micro-adjustment. *J. Phys. D. Appl. Phys.* 41. <https://doi.org/10.1088/0022-3727/41/24/245106>
- Shen, H., Hu, J., 2013. Controlling edge effects in laser bending. *Appl. Mech. Mater.* 272, 1521–1525. <https://doi.org/10.4028/www.scientific.net/AMM.271-272.1521>
- Shen, H., Hu, J., Yao, Z., 2011. Cooling effects in laser forming. *Mater. Sci. Forum* 663–665, 58–63. <https://doi.org/10.4028/www.scientific.net/MSF.663-665.58>
- Shen, H., Hu, J., Yao, Z., 2010. Analysis and control of edge effects in laser bending. *Opt. Lasers Eng.* 48, 305–315. <https://doi.org/10.1016/j.optlaseng.2009.11.005>
- Shen, H., Wang, H., Zhou, W., 2018a. Process modelling in laser forming of doubly-curved sheets from cylinder shapes. *J. Manuf. Process.* 35, 373–381. <https://doi.org/10.1016/j.jmapro.2018.08.027>
- Shen, H., Yao, Z., Hu, J., 2008. An analytical model for bending angle in metal/ceramic bilayer system of laser forming. *J. Appl. Phys.* 104. <https://doi.org/10.1063/1.3041478>
- Shen, H., Zhou, J., Shi, Y.J., Yao, Z.Q., Hu, J., 2007. Varying velocity scan in laser forming of plates. *Mater. Sci. Technol.* 23, 483–486. <https://doi.org/10.1179/174328407X179548>
- Shen, H., Zhou, W., Wang, H., 2018b. Laser forming of doubly curved plates using minimum energy principle and comprehensive strain control. *Int. J. Mech. Sci.* 145, 42–52. <https://doi.org/10.1016/j.ijmecsci.2018.07.005>
- Shi, Y., Hu, J., Dong, C., 2011. Analysis of the geometric effect on the forming accuracy in laser forming. *Proc. Inst. Mech. Eng. Part B J. Eng. Manuf.* 225, 1792–1800. <https://doi.org/10.1177/0954405411414341>
- Shi, Y., Liu, Y., Yi, P., Hu, J., 2012a. Effect of different heating methods on deformation of metal plate under upsetting mechanism in laser forming. *Opt. Laser Technol.* 44, 486–491. <https://doi.org/10.1016/j.optlastec.2011.08.019>

- Shi, Y., Yao, Z., Shen, H., Hu, J., 2006. Research on the mechanisms of laser forming for the metal plate. *Int. J. Mach. Tools Manuf.* 46, 1689–1697. <https://doi.org/10.1016/j.ijmachtools.2005.09.016>
- Shi, Y., Yi, P., Liu, Y., 2012b. Numerical investigation of temperature field of different mechanisms in laser forming. *Proc. Inst. Mech. Eng. Part C J. Mech. Eng. Sci.* 226, 2118–2125. <https://doi.org/10.1177/0954406211430884>
- Shi, Y., Zhang, C., Sun, G., Li, C., 2016. Study on reducing edge effects by using assistant force in laser forming. *J. Mater. Process. Technol.* 227, 169–177. <https://doi.org/10.1016/j.jmatprotec.2015.08.018>
- Shimizu, H., 1997. A Heating Process Algorithm for Metal Forming by a MOving heat source. Massachusetts Institute of Technology.
- Silva, D.D.S., Simões, T.A., Macedo, D.A., Bueno, A.H.S., Torres, S.M., Gomes, R.M., 2021. Microstructural influence of sigma phase on pitting corrosion behavior of duplex stainless steel/NaCl electrolyte couple. *Mater. Chem. Phys.* 259. <https://doi.org/10.1016/j.matchemphys.2020.124056>
- Silve, B.S., Zhao, H., 2004. Laser Forming As a Method of Producing Designed Objects, in: *The 18th Santa Fe Symposium on Jewellery Manufacturing Technology*. pp. 1–34.
- Silve, S., 2006. A synthesis of programming techniques for laser forming. *Digit. Creat.* 17, 100–112. <https://doi.org/10.1080/14626260600787696>
- Siqueira, R.H.M., Carvalho, S.M., Kam, I.K.L., Riva, R., Lima, M.S.F., 2016. Non-contact sheet forming using lasers applied to a high strength aluminum alloy. *J. Mater. Res. Technol.* 5, 275–281. <https://doi.org/10.1016/j.jmrt.2016.02.002>
- Smith, G.L., Lazarus, N., McCormick, S., 2018. Laser Folded Antenna, in: *2018 IEEE MTT-S International Microwave Workshop Series on Advanced Materials and Processes for RF and THz Applications, IMWS-AMP 2018*. IEEE, pp. 1–3. <https://doi.org/10.1109/IMWS-AMP.2018.8457156>
- Stainless, T., 2014. Practical Guidelines for the Fabrication of Duplex Stainless Steels, International Molybdenum Association.
- Steen, W.M., 2003. Laser material processing - An overview. *J. Opt. A Pure Appl. Opt.*

5. <https://doi.org/10.1088/1464-4258/5/4/351>

- Sun, H., 1998. Thin lens equation for a real laser beam with weak lens aperture truncation. *Opt. Eng.* 37, 2906. <https://doi.org/10.1117/1.601877>
- Tathgir, S., Rathod, D.W., Batish, A., 2020. Process enhancement using hydrogen-induced shielding: H₂-induced A-TIG welding process. *Mater. Manuf. Process.* 35, 1084–1095. <https://doi.org/10.1080/10426914.2020.1765251>
- Tathgir, S., Rathod, D.W., Batish, A., 2019. A-TIG welding process for enhanced-penetration in Duplex stainless-steel: effect of activated fluxes. *Mater. Manuf. Process.* 34, 1659–1670. <https://doi.org/10.1080/10426914.2019.1666990>
- Tavakoli, A., Moslemi Naeini, H., Roohi, A.H., Hoseinpour Gollo, M., Imani Shahabad, S., 2017a. Optimization of circular scan path to produce bowl shapes in 3D laser forming process. *J. Laser Appl.* 29, 042001. <https://doi.org/10.2351/1.5000128>
- Tavakoli, A., Moslemi Naeini, H., Roohi, A.H., Hoseinpour Gollo, M., Shahabad, S.I., 2017b. Determining optimized radial scan path in 3D laser forming of steel AISI 304 plates to produce bowl shapes. *Int. J. Adv. Manuf. Technol.* 91, 3457–3465. <https://doi.org/10.1007/s00170-017-9985-x>
- Tavakoli, A., Naeini, H.M., Roohi, A.H., Gollo, M.H., Shahabad, S.I., 2018. Codification of scan path parameters and development of perimeter scan strategies for 3D bowl-shaped laser forming. *Opt. Laser Technol.* 98, 121–133. <https://doi.org/10.1016/j.optlastec.2017.07.046>
- Tavares, S.S.M., Pardal, J.M., De Abreu, H.F.G., Dos Santos Nunes, C., Da Silva, M.R., 2012. Tensile properties of duplex UNS S32205 and lean duplex UNS S32304 steels and the influence of short duration 475 °C aging. *Mater. Res.* 15, 859–864. <https://doi.org/10.1590/S1516-14392012005000116>
- Tehovnik, F., Arzenšek, B., Arh, B., Skobir, D., Pirnar, B., Žužek, B., 2011. Microstructure evolution in SAF 2507 super duplex stainless steel. *Mater. Tehnol.* 45, 339–345.
- Tehovnik, F., Žužek, B., Burja, J., 2016. Hot tensile testing of SAF 2205 duplex stainless steel. *Mater. Tehnol.* 50, 989–993. <https://doi.org/10.17222/mit.2016.242>
- Th. B. Kermanidis, An. K. Kyrsanidi, S.G.P., 1997. Numerical simulation of the laser

- forming process in metallic plates. *WIT Trans. Eng. Sci.* 17, 589–598.
- Thomsen, A.N., Endelt, B., Kristiansen, M., 2019a. Feedback control of laser forming using flattening simulations for error determination. *IOP Conf. Ser. Mater. Sci. Eng.* 651. <https://doi.org/10.1088/1757-899X/651/1/012093>
- Thomsen, A.N., Endelt, B., Kristiansen, M., 2017. A New Method for Calculating the Error Term Used in 2D Feedback Control of Laser Forming. *Phys. Procedia* 89, 148–155. <https://doi.org/10.1016/j.phpro.2017.08.003>
- Thomsen, A.N., Kristiansen, E., Kristiansen, M., Endelt, B., 2019b. Investigation of the profile of laser bends with variable scan distance. *Procedia Manuf.* 36, 192–199. <https://doi.org/10.1016/j.promfg.2019.08.025>
- Thomsen, A.N., Kristiansen, E., Kristiansen, M., Endelt, B., 2018. Influence of cooling on edge effects in laser forming. *Procedia CIRP* 74, 394–397. <https://doi.org/10.1016/j.procir.2018.08.155>
- Thomson, G., Pridham, M., 2001. Material property changes associated with laser forming of mild steel components. *J. Mater. Process. Technol.* 118, 40–44. [https://doi.org/10.1016/S0924-0136\(01\)00859-7](https://doi.org/10.1016/S0924-0136(01)00859-7)
- Thomson, G., Pridham, M., 1998. Improvements to laser forming through process control refinements. *Opt. Laser Technol.* 30, 141–146. [https://doi.org/10.1016/S0030-3992\(98\)00037-1](https://doi.org/10.1016/S0030-3992(98)00037-1)
- Thomson, G., Pridham, M., 1997a. A feedback control system for laser forming. *Mechatronics* 7, 429–441. [https://doi.org/10.1016/s0957-4158\(97\)00014-7](https://doi.org/10.1016/s0957-4158(97)00014-7)
- Thomson, G., Pridham, M.S., 1997b. Controlled laser forming for rapid prototyping. *Rapid Prototyp. J.* 3, 137–143. <https://doi.org/10.1108/13552549710191845>
- Tong, K.-O., 1998. A numerical study on laser forming of titanium plates 131, E131–E140. <https://doi.org/10.2351/1.5059140>
- Tušar, T., Member, S., Filipi, B., 2015. Visualization of Pareto Front Approximations in Evolutionary Multiobjective Optimization: A Critical Review and the Prosecution Method. *IEEE Trans. Evol. Comput.* 19, 225–245. <https://doi.org/10.1109/TEVC.2014.2313407>

- Varbai, B., Májlínger, K., 2019. Optimal etching sequence for austenite to ferrite ratio evaluation of two lean duplex stainless steel weldments. *Meas. J. Int. Meas. Confed.* 147, 1–5. <https://doi.org/10.1016/j.measurement.2019.07.060>
- Varbai, B., Pickle, T., Májlínger, K., 2018. Development and comparison of quantitative phase analysis for duplex stainless steel weld. *Period. Polytech. Mech. Eng.* 62, 247–253. <https://doi.org/10.3311/PPme.12234>
- Vollertsen, F., 1994. Mechanisms and models for laser Forming, in: *Proceeding of the LANE'94*. p. 345. <https://doi.org/10.1017/CCOL9780521851282.008>
- Vollertsen, F., Komel, I., Kals, R., 1995. The laser bending of steel foils for microparts by the buckling mechanism-a model. *Model. Simul. Mater. Sci. Eng.* 3, 107–119. <https://doi.org/10.1088/0965-0393/3/1/009>
- W. M. Steen, 1997. Current trends in laser material processing. *Lasers Mater. Process.* 3097, 2–7.
- Wang, S.Q., Liu, J.H., Chen, D.L., 2014. Effect of strain rate and temperature on strain hardening behavior of a dissimilar joint between Ti-6Al-4V and Ti17 alloys. *Mater. Des.* 56, 174–184. <https://doi.org/10.1016/j.matdes.2013.11.003>
- Wang, X., Liu, D., Li, W., Xu, L., Dong, Y., 2015. Study of laser bending of a preloaded Titanium alloy sheet. *Manuf. Rev.* 1, 1–6. <https://doi.org/10.1051/mfreview/2015002>
- Wang, X., Shi, Y., Guo, Y., Li, X., Zhao, X., 2021a. Laser forming process of complex surface on Al7075. *Int. J. Adv. Manuf. Technol.* 116, 2975–2988. <https://doi.org/10.1007/s00170-021-07407-6>
- Wang, X., Shi, Y., Guo, Y., Sun, R., Li, X., Zhou, X., 2020. Laser curve scanning forming process of laminated metal composite plate. *Mater. Des.* 191, 108614. <https://doi.org/10.1016/j.matdes.2020.108614>
- Wang, X., Shi, Y., Guo, Y., Wang, Q., 2022a. Bowl surface laser forming process of stainless steel composite plate. *Int. J. Adv. Manuf. Technol.* 118, 3819–3831. <https://doi.org/10.1007/s00170-021-08098-9>
- Wang, X., Shi, Y., Guo, Y., Wang, Q., 2022b. Design of 3D surface laser forming process. *J. Manuf. Process.* 73, 306–315.

<https://doi.org/10.1016/j.jmapro.2021.11.019>

- Wang, X., Shi, Y., Guo, Y., Wang, Q., Fan, K., 2021b. Influence of laser scanning times on the mechanical properties of laminated composite plates. *Opt. Laser Technol.* 144, 107442. <https://doi.org/10.1016/j.optlastec.2021.107442>
- Widłaszewski, J., Nowak, M., Nowak, Z., Kurp, P., 2022. Curvature Change in Laser-Assisted Bending of Inconel 718 26. <https://doi.org/10.3390/psf2022004026>
- Widłaszewski, J., Nowak, Z., Kurp, P., 2021. Effect of pre-stress on laser-induced thermoplastic deformation of inconel 718 beams. *Materials (Basel)*. 14, 1–18. <https://doi.org/10.3390/ma14081847>
- Woizeschke, P., Heinrich, L., Eichner, P., 2018. Laser edge forming to increase the bending radius in hemming. *MATEC Web Conf.* 190, 1–6. <https://doi.org/10.1051/matecconf/201819002002>
- Wu, D., Ma, G.Y., Liu, S., Wang, X.Y., Guo, D.M., 2010a. Experiments and simulation on laser bending of silicon sheet with different thicknesses. *Appl. Phys. A Mater. Sci. Process.* 101, 517–521. <https://doi.org/10.1007/s00339-010-5889-4>
- Wu, D., Zhang, Q., Guo, D., 2009. Experiments on laser bending of brittle materials. *Opt. InfoBase Conf. Pap.* 5–6.
- Wu, D., Zhang, Q., Ma, G., Guo, Y., Guo, D., 2010b. Laser bending of brittle materials. *Opt. Lasers Eng.* 48, 405–410. <https://doi.org/10.1016/j.optlaseng.2009.09.009>
- Xavier, C.R., Junior, H.G.D., De Castro, J.A., 2015. An experimental and numerical approach for the welding effects on the duplex stainless steel microstructure. *Mater. Res.* 18, 489–502. <https://doi.org/10.1590/1516-1439.302014>
- Xu, L., Li, W., Wan, M., Wang, X., Dong, Y., 2015. Laser bending process of preloaded sheet metal. *MATEC Web Conf.* 21, 1–7. <https://doi.org/10.1051/matecconf/20152104004>
- Xu, W., Zhang, L.C., Wang, X., 2013. Laser bending of silicon sheet: Absorption factor and mechanisms. *J. Manuf. Sci. Eng. Trans. ASME* 135, 061005. <https://doi.org/10.1115/1.4025579>
- Yadav, R., Goyal, D.K., Kant, R., 2022a. Enhancing process competency by forced

- cooling in laser bending process. *J. Therm. Stress.* 45, 617–629.
<https://doi.org/10.1080/01495739.2022.2103057>
- Yadav, R., Goyal, D.K., Kant, R., 2022b. A comprehensive study on the effect of line energy during laser bending of duplex stainless steel. *Opt. Laser Technol.* 151, 108025. <https://doi.org/10.1016/j.optlastec.2022.108025>
- Yadav, R., Kant, R., 2022. Effectiveness of forced cooling during laser bending of duplex-2205. *Mater. Manuf. Process.* 38, 598–607.
<https://doi.org/10.1080/10426914.2022.2146717>
- Yang, L.J., Wang, Y., Djendel, M., Qi, L.T., 2004. Experimental investigation on 3D laser forming of metal sheet. *Mater. Sci. Forum* 471–472, 568–572.
<https://doi.org/10.4028/www.scientific.net/msf.471-472.568>
- Yang, Y., Yan, B., Li, J., Wang, J., 2011. The effect of large heat input on the microstructure and corrosion behaviour of simulated heat affected zone in 2205 duplex stainless steel. *Corros. Sci.* 53, 3756–3763.
<https://doi.org/10.1016/j.corsci.2011.07.022>
- Yau, C.L., Chan, K.C., Lee, W.B., 1998. Laser bending of leadframe materials. *J. Mater. Process. Technol.* 82, 117–121. [https://doi.org/10.1016/S0924-0136\(98\)00012-0](https://doi.org/10.1016/S0924-0136(98)00012-0)
- Yau, C.L., Chan, K.C., Lee, W.B., 1996. Laser bending of Al-based metal matrix composites sheets 124, E124–E131. <https://doi.org/10.2351/1.5059071>
- Ye, Y., Nie, Z., Huang, X., Ren, X., Li, L., 2021. An analytical model for estimating the bending curvatures of metal sheets in laser peen forming. *Materials (Basel)*. 14, 1–14. <https://doi.org/10.3390/ma14020462>
- Ye, Y., Zeng, R., Nie, Z., Ren, Y., Ren, X., 2020. Researches on the curvature adjustment of metal sheet induced by laser shock forming through experiments and simulations. *Int. J. Adv. Manuf. Technol.* 108, 2791–2802.
<https://doi.org/10.1007/s00170-020-05469-6>
- Yocom, C.J., Zhang, X., Liao, Y., 2018. Research and development status of laser peen forming: A review. *Opt. Laser Technol.* 108, 32–45.
<https://doi.org/10.1016/j.optlastec.2018.06.032>
- Yoshigai, N., Kudo, K., Tsumori, F., Osada, T., Miura, H., 2016. Anisotropic

- mechanical properties of ni-base superalloy compacts by direct laser forming technology. *Funtai Oyobi Fummatsu Yakin/Journal Japan Soc. Powder Powder Metall.* 63, 427–433. <https://doi.org/10.2497/jjspm.63.427>
- Yoshioka, S., Miyazaki, T., Imai, M., Shirai, Y., Misu, T., 1998. Bending of fine metal wire and foil with YAG laser beam 161, E161–E169. <https://doi.org/10.2351/1.5059144>
- Zahrani, E.G., Marasi, A., 2013. Experimental investigation of edge effect and longitudinal distortion in laser bending process. *Opt. Laser Technol.* 45, 301–307. <https://doi.org/10.1016/j.optlastec.2012.06.031>
- Zan, X., Wu, Z., Guo, C., Yu, Z., 2020. A Pareto-based genetic algorithm for multi-objective scheduling of automated manufacturing systems. *Adv. Mech. Eng.* 12, 1–15. <https://doi.org/10.1177/1687814019885294>
- Zhang, M., Chen, C.J., Huang, Y., Zou, T., 2018. Bending processing and mechanism of laser forming pure aluminum metal foam. *Int. J. Adv. Manuf. Technol.* 94, 1849–1856. <https://doi.org/10.1007/s00170-017-0976-8>
- Zhang, T., Liu, Y., Ashmore, N., Li, W., Lawrence Yao, Y., 2022. Effect of Laser Forming on the Energy Absorbing Behavior of Metal Foams. *J. Manuf. Sci. Eng. Trans. ASME* 144, 1–12. <https://doi.org/10.1115/1.4051285>
- Zhang, T., Yao, Y.L., 2022. Effect of Laser Forming on the Fatigue Behavior of Metal Foams. *J. Manuf. Sci. Eng.* 144, 1–10. <https://doi.org/10.1115/1.4054454>
- Zhang, Y., Dong, W., Qiao, Y., Zhang, C., 2019. Edge Effect Investigation of DP980 Steel Sheet in Multiple Laser Scanning Process. *Int. J. Precis. Eng. Manuf.* 20, 319–326. <https://doi.org/10.1007/s12541-019-00086-0>

APPENDIX

Appendix 2.1

PERMISSIONS FOR FIGURE 2.3 (First 2 Pages of The License Agreement)

7/21/23, 5:13 PM

RightsLink Printable License

SPRINGER NATURE LICENSE TERMS AND CONDITIONS

Jul 21, 2023

This Agreement between Indian Institute of Technology Ropar -- Ramsingh Yadav ("You") and Springer Nature ("Springer Nature") consists of your license details and the terms and conditions provided by Springer Nature and Copyright Clearance Center.

License Number	5593610391755
License date	Jul 21, 2023
Licensed Content Publisher	Springer Nature
Licensed Content Publication	The International Journal of Advanced Manufacturing Technology
Licensed Content Title	Influence of non-conventional beam profile on edge effects in laser forming of AISI 304 stainless steel plate
Licensed Content Author	E. R. Imam Fauzi et al
Licensed Content Date	Jul 30, 2019
Type of Use	Thesis/Dissertation
Requestor type	academic/university or research institute
Format	print and electronic
Portion	figures/tables/illustrations
Number of figures/tables/illustrations	1
Will you be translating?	no

Circulation/distribution	50000 or greater
Author of this Springer Nature content	no
Title	Improving Process Competency of Laser Bending of Duplex Stainless-Steel Sheet by Applying Forced Cooling
Institution name	Indian Institute of Technology Ropar
Expected presentation date	Oct 2023
Portions	Figure 2
Requestor Location	Indian Institute of Technology Ropar RL- 103, SATISH DHAWAN BLOCK, IIT Ropar, Rupnagar, Punjab Rupnagar, Punjab 140001 India Attn: Indian Institute of Technology Ropar
Total	0.00 USD

Terms and Conditions

Springer Nature Customer Service Centre GmbH Terms and Conditions

The following terms and conditions ("Terms and Conditions") together with the terms specified in your [RightsLink] constitute the License ("License") between you as Licensee and Springer Nature Customer Service Centre GmbH as Licensor. By clicking 'accept' and completing the transaction for your use of the material ("Licensed Material"), you confirm your acceptance of and obligation to be bound by these Terms and Conditions.

1. Grant and Scope of License

1. 1. The Licensor grants you a personal, non-exclusive, non-transferable, non-sublicensable, revocable, world-wide License to reproduce, distribute, communicate to the public, make available, broadcast, electronically transmit or create derivative works using the Licensed Material for the purpose(s) specified in your RightsLink Licence Details only. Licenses are granted for the specific use requested in the order and for no other use, subject to these Terms and Conditions. You acknowledge and agree that the rights granted to you under this License do not include the right to modify, edit, translate, include in collective works, or create derivative works of the Licensed Material in whole or in part unless expressly stated in your RightsLink Licence Details. You may use the Licensed Material only as permitted under this

Appendix 2.2

PERMISSIONS FOR FIGURE 2.6 (First 2 Pages of The License Agreement)

7/21/23, 5:21 PM

RightsLink Printable License

ELSEVIER LICENSE TERMS AND CONDITIONS

Jul 21, 2023

This Agreement between Indian Institute of Technology Ropar -- Ramsingh Yadav ("You") and Elsevier ("Elsevier") consists of your license details and the terms and conditions provided by Elsevier and Copyright Clearance Center.

License Number	5593610829395
License date	Jul 21, 2023
Licensed Content Publisher	Elsevier
Licensed Content Publication	Optics & Laser Technology
Licensed Content Title	An experimental study of the effects of surface roughness and coating of Cr ₂ O ₃ layer on the laser-forming process
Licensed Content Author	Hamid Reza Abedi, Mohammad Hoseinpour Gollo
Licensed Content Date	Jan 1, 2019
Licensed Content Volume	109
Licensed Content Issue	n/a
Licensed Content Pages	12
Start Page	336
End Page	347
Type of Use	reuse in a thesis/dissertation
Portion	figures/tables/illustrations

<https://s100.copyright.com/AppDispatchServlet>

1/7

Number of figures/tables/illustrations 2

Format both print and electronic

Are you the author of this Elsevier article? No

Will you be translating? No

Title Improving Process Competency of Laser Bending of Duplex Stainless-Steel Sheet by Applying Forced Cooling

Institution name Indian Institute of Technology Ropar

Expected presentation date Oct 2023

Portions Figure 9 and Figure 17

Requestor Location Indian Institute of Technology Ropar
RL- 103, SATISH DHAWAN BLOCK,
IIT Ropar,
Rupnagar, Punjab
Rupnagar, Punjab 140001
India
Attn: Indian Institute of Technology Ropar

Publisher Tax ID GB 494 6272 12

Total 0.00 USD

Terms and Conditions

INTRODUCTION

1. The publisher for this copyrighted material is Elsevier. By clicking "accept" in connection with completing this licensing transaction, you agree that the following terms and conditions apply to this transaction (along with the Billing and Payment terms and conditions established by Copyright Clearance Center, Inc. ("CCC"), at the time that you opened your RightsLink account and that are available at any time at <https://myaccount.copyright.com>).

GENERAL TERMS

2. Elsevier hereby grants you permission to reproduce the aforementioned material subject to the terms and conditions indicated.

Appendix 2.3

PERMISSIONS FOR FIGURE 2.7 (First 2 Pages of The License Agreement)

7/21/23, 5:24 PM

RightsLink Printable License

ELSEVIER LICENSE TERMS AND CONDITIONS

Jul 21, 2023

This Agreement between Indian Institute of Technology Ropar -- Ramsingh Yadav ("You") and Elsevier ("Elsevier") consists of your license details and the terms and conditions provided by Elsevier and Copyright Clearance Center.

License Number	5593610995722
License date	Jul 21, 2023
Licensed Content Publisher	Elsevier
Licensed Content Publication	Journal of Manufacturing Processes
Licensed Content Title	External force-assisted LaserOrigami (LO) bending: Shaping of 3D cubes and edge design of stainless steel chairs
Licensed Content Author	Annamaria Gisario,Massimiliano Barletta,Simone Venettacci,Francesco Veniali
Licensed Content Date	Apr 1, 2015
Licensed Content Volume	18
Licensed Content Issue	n/a
Licensed Content Pages	8
Start Page	159
End Page	166
Type of Use	reuse in a thesis/dissertation

<https://s100.copyright.com/AppDispatchServlet>

1/7

Portion	figures/tables/illustrations
Number of figures/tables/illustrations	1
Format	both print and electronic
Are you the author of this Elsevier article?	No
Will you be translating?	No
Title	Improving Process Competency of Laser Bending of Duplex Stainless-Steel Sheet by Applying Forced Cooling
Institution name	Indian Institute of Technology Ropar
Expected presentation date	Oct 2023
Portions	Figure 9
Requestor Location	Indian Institute of Technology Ropar RL- 103, SATISH DHAWAN BLOCK, IIT Ropar, Rupnagar, Punjab Rupnagar, Punjab 140001 India Attn: Indian Institute of Technology Ropar
Publisher Tax ID	GB 494 6272 12
Total	0.00 USD
Terms and Conditions	

INTRODUCTION

1. The publisher for this copyrighted material is Elsevier. By clicking "accept" in connection with completing this licensing transaction, you agree that the following terms and conditions apply to this transaction (along with the Billing and Payment terms and conditions established by Copyright Clearance Center, Inc. ("CCC"), at the time that you opened your RightsLink account and that are available at any time at <https://myaccount.copyright.com>).

Appendix 2.4

PERMISSIONS FOR FIGURE 2.10 (First 2 Pages of The License Agreement)

Laser Institute of America ORDER DETAILS

Jul 21, 2023

Order Number	501831894
Order date	Jul 21, 2023
Licensed Content Publisher	Laser Institute of America
Licensed Content Publication	Journal of Laser Applications
Licensed Content Title	Factors affecting the laser bending of Ti-6Al-2Sn-4Zr-2Mo
Licensed Content Author	Marya, M.; Edwards, G. R.
Licensed Content Date	Aug 1, 2000
Licensed Content Volume	12
Licensed Content Issue	4
Type of Use	Thesis/Dissertation
Requestor type	Student
Format	Print and electronic
Portion	Figure/Table
Number of figures/tables	4

Will you be translating?	No
Title	Improving Process Competency of Laser Bending of Duplex Stainless-Steel Sheet by Applying Forced Cooling
Institution name	Indian Institute of technology Ropar
Expected presentation date	Oct 2023
Portions	Figure 4, Figure 5, Figure 6, Figure 8
	IIT Ropar IIT Ropar
Requestor Location	Rupnagar, 140001 India Attn: IIT Ropar
Total	Not Available

Appendix 2.5

PERMISSIONS FOR FIGURE 2.11 (First 2 Pages of The License Agreement)

SPRINGER NATURE LICENSE TERMS AND CONDITIONS

Jul 21, 2023

This Agreement between Indian Institute of Technology Ropar -- Ramsingh Yadav ("You") and Springer Nature ("Springer Nature") consists of your license details and the terms and conditions provided by Springer Nature and Copyright Clearance Center.

License Number	5593651216816
License date	Jul 21, 2023
Licensed Content Publisher	Springer Nature
Licensed Content Publication	The International Journal of Advanced Manufacturing Technology
Licensed Content Title	An experimental investigation on passive water cooling in laser forming process
Licensed Content Author	F. Lambiase et al
Licensed Content Date	Apr 5, 2012
Type of Use	Thesis/Dissertation
Requestor type	academic/university or research institute
Format	print and electronic
Portion	figures/tables/illustrations
Number of figures/tables/illustrations	1
Will you be translating?	no

Circulation/distribution	50000 or greater
Author of this Springer Nature content	no
Title	Improving Process Competency of Laser Bending of Duplex Stainless-Steel Sheet by Applying Forced Cooling
Institution name	Indian Institute of Technology Ropar
Expected presentation date	Oct 2023
Portions	Figure 2
Requestor Location	Indian Institute of Technology Ropar RL- 103, SATISH DHAWAN BLOCK, IIT Ropar, Rupnagar, Punjab Rupnagar, Punjab 140001 India Attn: Indian Institute of Technology Ropar
Total	0.00 USD

Terms and Conditions

Springer Nature Customer Service Centre GmbH Terms and Conditions

The following terms and conditions ("Terms and Conditions") together with the terms specified in your [RightsLink] constitute the License ("License") between you as Licensee and Springer Nature Customer Service Centre GmbH as Licensor. By clicking 'accept' and completing the transaction for your use of the material ("Licensed Material"), you confirm your acceptance of and obligation to be bound by these Terms and Conditions.

1. Grant and Scope of License

1. 1. The Licensor grants you a personal, non-exclusive, non-transferable, non-sublicensable, revocable, world-wide License to reproduce, distribute, communicate to the public, make available, broadcast, electronically transmit or create derivative works using the Licensed Material for the purpose(s) specified in your RightsLink Licence Details only. Licenses are granted for the specific use requested in the order and for no other use, subject to these Terms and Conditions. You acknowledge and agree that the rights granted to you under this License do not include the right to modify, edit, translate, include in collective works, or create derivative works of the Licensed Material in whole or in part unless expressly stated in your RightsLink Licence Details. You may use the Licensed Material only as permitted under this

Appendix 2.6

PERMISSIONS FOR FIGURE 2.12 (First 2 Pages of The License Agreement)

SPRINGER NATURE LICENSE TERMS AND CONDITIONS

Jul 21, 2023

This Agreement between Indian Institute of Technology Ropar -- Ramsingh Yadav ("You") and Springer Nature ("Springer Nature") consists of your license details and the terms and conditions provided by Springer Nature and Copyright Clearance Center.

License Number	5593660099382
License date	Jul 21, 2023
Licensed Content Publisher	Springer Nature
Licensed Content Publication	Journal of Materials Research
Licensed Content Title	Deformation, microstructure, hardness, and pitting corrosion of 316 stainless steel after laser forming: A comparison between natural and forced cooling
Licensed Content Author	Morteza Chinizadeh et al
Licensed Content Date	Aug 1, 2017
Type of Use	Thesis/Dissertation
Requestor type	academic/university or research institute
Format	print and electronic
Portion	figures/tables/illustrations
Number of figures/tables/illustrations	1
Will you be translating?	no

Circulation/distribution	50000 or greater
Author of this Springer Nature content	no
Title	Improving Process Competency of Laser Bending of Duplex Stainless-Steel Sheet by Applying Forced Cooling
Institution name	Indian Institute of Technology Ropar
Expected presentation date	Oct 2023
Portions	Figure 1
Requestor Location	Indian Institute of Technology Ropar RL- 103, SATISH DHAWAN BLOCK, IIT Ropar, Rupnagar, Punjab Rupnagar, Punjab 140001 India Attn: Indian Institute of Technology Ropar
Total	0.00 USD

Terms and Conditions

Springer Nature Customer Service Centre GmbH Terms and Conditions

The following terms and conditions ("Terms and Conditions") together with the terms specified in your [RightsLink] constitute the License ("License") between you as Licensee and Springer Nature Customer Service Centre GmbH as Licensor. By clicking 'accept' and completing the transaction for your use of the material ("Licensed Material"), you confirm your acceptance of and obligation to be bound by these Terms and Conditions.

1. Grant and Scope of License

1.1. The Licensor grants you a personal, non-exclusive, non-transferable, non-sublicensable, revocable, world-wide License to reproduce, distribute, communicate to the public, make available, broadcast, electronically transmit or create derivative works using the Licensed Material for the purpose(s) specified in your RightsLink Licence Details only. Licenses are granted for the specific use requested in the order and for no other use, subject to these Terms and Conditions. You acknowledge and agree that the rights granted to you under this License do not include the right to modify, edit, translate, include in collective works, or create derivative works of the Licensed Material in whole or in part unless expressly stated in your RightsLink Licence Details. You may use the Licensed Material only as permitted under this

Appendix 2.7

PERMISSIONS FOR FIGURE 2.13 (First 2 Pages of The License Agreement)

ELSEVIER LICENSE TERMS AND CONDITIONS

Jul 21, 2023

This Agreement between Indian Institute of Technology Ropar -- Ramsingh Yadav ("You") and Elsevier ("Elsevier") consists of your license details and the terms and conditions provided by Elsevier and Copyright Clearance Center.

License Number	5593660344831
License date	Jul 21, 2023
Licensed Content Publisher	Elsevier
Licensed Content Publication	Journal of Manufacturing Processes
Licensed Content Title	LaserOrigami (LO) of three-dimensional (3D) components: Experimental analysis and numerical modelling
Licensed Content Author	A. Gisario,M. Mehrpouya,S. Venettacci,A. Mohammadzadeh,M. Barletta
Licensed Content Date	Aug 1, 2016
Licensed Content Volume	23
Licensed Content Issue	n/a
Licensed Content Pages	7
Start Page	242
End Page	248
Type of Use	reuse in a thesis/dissertation

Portion	figures/tables/illustrations
Number of figures/tables/illustrations	1
Format	both print and electronic
Are you the author of this Elsevier article?	No
Will you be translating?	No
Title	Improving Process Competency of Laser Bending of Duplex Stainless-Steel Sheet by Applying Forced Cooling
Institution name	Indian Institute of Technology Ropar
Expected presentation date	Oct 2023
Portions	Figure 9
Requestor Location	Indian Institute of Technology Ropar RL- 103, SATISH DHAWAN BLOCK, IIT Ropar, Rupnagar, Punjab Rupnagar, Punjab 140001 India Attn: Indian Institute of Technology Ropar
Publisher Tax ID	GB 494 6272 12
Total	0.00 USD
Terms and Conditions	

INTRODUCTION

1. The publisher for this copyrighted material is Elsevier. By clicking "accept" in connection with completing this licensing transaction, you agree that the following terms and conditions apply to this transaction (along with the Billing and Payment terms and conditions established by Copyright Clearance Center, Inc. ("CCC"), at the time that you opened your RightsLink account and that are available at any time at <https://myaccount.copyright.com>).

GENERAL TERMS

Appendix 2.8

PERMISSIONS FOR FIGURE 2.14 (First 2 Pages of The License Agreement)

JOHN WILEY AND SONS LICENSE TERMS AND CONDITIONS

Jul 21, 2023

This Agreement between Indian Institute of Technology Ropar -- Ramsingh Yadav ("You") and John Wiley and Sons ("John Wiley and Sons") consists of your license details and the terms and conditions provided by John Wiley and Sons and Copyright Clearance Center.

License Number 5593660862261

License date Jul 21, 2023

Licensed Content
Publisher John Wiley and Sons

Licensed Content
Publication Advanced Materials Technologies

Licensed Content Title Laser Forming for Complex 3D Folding

Licensed Content Author Gabriel L. Smith, Nathan Lazarus

Licensed Content Date Aug 10, 2017

Licensed Content
Volume 2

Licensed Content Issue 10

Licensed Content Pages 6

Type of use Dissertation/Thesis

Requestor type University/Academic

Format Print and electronic

Portion	Figure/table
Number of figures/tables	1
Will you be translating?	No
Title	Improving Process Competency of Laser Bending of Duplex Stainless-Steel Sheet by Applying Forced Cooling
Institution name	Indian Institute of Technology Ropar
Expected presentation date	Oct 2023
Portions	Figure 3
Requestor Location	Indian Institute of Technology Ropar RL- 103, SATISH DHAWAN BLOCK, IIT Ropar, Rupnagar, Punjab Rupnagar, Punjab 140001 India Attn: Indian Institute of Technology Ropar
Publisher Tax ID	EU826007151
Total	0.00 USD
Terms and Conditions	

TERMS AND CONDITIONS

This copyrighted material is owned by or exclusively licensed to John Wiley & Sons, Inc. or one of its group companies (each a "Wiley Company") or handled on behalf of a society with which a Wiley Company has exclusive publishing rights in relation to a particular work (collectively "WILEY"). By clicking "accept" in connection with completing this licensing transaction, you agree that the following terms and conditions apply to this transaction (along with the billing and payment terms and conditions established by the Copyright Clearance Center Inc., ("CCC's Billing and Payment terms and conditions"), at the time that you opened your RightsLink account (these are available at any time at <http://myaccount.copyright.com>).

Terms and Conditions

Appendix 2.9

PERMISSIONS FOR FIGURE 2.15 (First 2 Pages of The License Agreement)

SPRINGER NATURE LICENSE TERMS AND CONDITIONS

Jul 21, 2023

This Agreement between Indian Institute of Technology Ropar -- Ramsingh Yadav ("You") and Springer Nature ("Springer Nature") consists of your license details and the terms and conditions provided by Springer Nature and Copyright Clearance Center.

License Number	5593661097110
License date	Jul 21, 2023
Licensed Content Publisher	Springer Nature
Licensed Content Publication	The International Journal of Advanced Manufacturing Technology
Licensed Content Title	Experimental-numerical methodology for the manufacturing of cranial prosthesis via laser forming
Licensed Content Author	Felipe Cook et al
Licensed Content Date	Jan 19, 2016
Type of Use	Thesis/Dissertation
Requestor type	academic/university or research institute
Format	print and electronic
Portion	figures/tables/illustrations
Number of figures/tables/illustrations	2
Will you be translating?	no

Circulation/distribution	50000 or greater
Author of this Springer Nature content	no
Title	Improving Process Competency of Laser Bending of Duplex Stainless-Steel Sheet by Applying Forced Cooling
Institution name	Indian Institute of Technology Ropar
Expected presentation date	Oct 2023
Portions	Figure 11 and Figure 13
Requestor Location	Indian Institute of Technology Ropar RL- 103, SATISH DHAWAN BLOCK, IIT Ropar, Rupnagar, Punjab Rupnagar, Punjab 140001 India Attn: Indian Institute of Technology Ropar
Total	0.00 USD

Terms and Conditions

Springer Nature Customer Service Centre GmbH Terms and Conditions

The following terms and conditions ("Terms and Conditions") together with the terms specified in your [RightsLink] constitute the License ("License") between you as Licensee and Springer Nature Customer Service Centre GmbH as Licensor. By clicking 'accept' and completing the transaction for your use of the material ("Licensed Material"), you confirm your acceptance of and obligation to be bound by these Terms and Conditions.

1. Grant and Scope of License

1. 1. The Licensor grants you a personal, non-exclusive, non-transferable, non-sublicensable, revocable, world-wide License to reproduce, distribute, communicate to the public, make available, broadcast, electronically transmit or create derivative works using the Licensed Material for the purpose(s) specified in your RightsLink Licence Details only. Licenses are granted for the specific use requested in the order and for no other use, subject to these Terms and Conditions. You acknowledge and agree that the rights granted to you under this License do not include the right to modify, edit, translate, include in collective works, or create derivative works of the Licensed Material in whole or in part unless expressly stated in your RightsLink Licence Details. You may use the Licensed Material only as permitted under this

Appendix 2.10

PERMISSIONS FOR FIGURE 2.16 (First 2 Pages of The License Agreement)

SPRINGER NATURE ORDER DETAILS

Jul 21, 2023

Order Number	501831911
Order date	Jul 21, 2023
Licensed Content Publisher	Springer Nature
Licensed Content Publication	The International Journal of Advanced Manufacturing Technology
Licensed Content Title	Determining optimized radial scan path in 3D laser forming of steelAISI 304 plates to produce bowl shapes
Licensed Content Author	A. Tavakoli et al
Licensed Content Date	Jan 24, 2017
Type of Use	Thesis/Dissertation
Requestor type	academic/university or research institute
Format	print and electronic
Portion	figures/tables/illustrations
Number of figures/tables/illustrations	6
Will you be translating?	no
Circulation/distribution	50000 or greater
Author of this Springer Nature content	no

Title	Improving Process Competency of Laser Bending of Duplex Stainless-Steel Sheet by Applying Forced Cooling
Institution name	Indian Institute of Technology Ropar
Expected presentation date	Oct 2023
Portions	Figure 6, Figure 7, Figure 8, Figure 9, Figure 10, Figure 11
Requestor Location	Indian Institute of Technology Ropar RL- 103, SATISH DHAWAN BLOCK, IIT Ropar, Rupnagar, Punjab Rupnagar, Punjab 140001 India Attn: Indian Institute of Technology Ropar
Total	Not Available

Appendix 2.11

PERMISSIONS FOR FIGURE 2.18 (First 2 Pages of The License Agreement)

ELSEVIER LICENSE TERMS AND CONDITIONS

Jul 21, 2023

This Agreement between Indian Institute of Technology Ropar -- Ramsingh Yadav ("You") and Elsevier ("Elsevier") consists of your license details and the terms and conditions provided by Elsevier and Copyright Clearance Center.

License Number	5593671372166
License date	Jul 21, 2023
Licensed Content Publisher	Elsevier
Licensed Content Publication	Optik - International Journal for Light and Electron Optics
Licensed Content Title	Augmenting wire arc additive manufacturing with laser forming for generative realization of complex geometries
Licensed Content Author	Srinath Gudur,Suryakumar Simhambhatla
Licensed Content Date	Jul 1, 2022
Licensed Content Volume	262
Licensed Content Issue	n/a
Licensed Content Pages	1
Start Page	169283
End Page	0
Type of Use	reuse in a thesis/dissertation

Portion	figures/tables/illustrations
Number of figures/tables/illustrations	1
Format	both print and electronic
Are you the author of this Elsevier article?	No
Will you be translating?	No
Title	Improving Process Competency of Laser Bending of Duplex Stainless-Steel Sheet by Applying Forced Cooling
Institution name	Indian Institute of Technology Ropar
Expected presentation date	Oct 2023
Portions	Figure 8
Requestor Location	Indian Institute of Technology Ropar RL- 103, SATISH DHAWAN BLOCK, IIT Ropar, Rupnagar, Punjab Rupnagar, Punjab 140001 India Attn: Indian Institute of Technology Ropar
Publisher Tax ID	GB 494 6272 12
Total	0.00 USD
Terms and Conditions	

INTRODUCTION

1. The publisher for this copyrighted material is Elsevier. By clicking "accept" in connection with completing this licensing transaction, you agree that the following terms and conditions apply to this transaction (along with the Billing and Payment terms and conditions established by Copyright Clearance Center, Inc. ("CCC"), at the time that you opened your RightsLink account and that are available at any time at <https://myaccount.copyright.com>).

GENERAL TERMS

Appendix 3.1

DEFLUX SUBROUTINE TO DEFINE INPUT PARAMETERS (Laser Power, Beam Diameter, Scanning Speed, Beam Shape, Heat Flux Distribution, And Position of Laser Scan)

```
SUBROUTINE DFLUX(FLUX,SOL,JSTEP,JINC,TIME,NOEL,NPT,COORDS,JLTYP,
! TEMP,PRESS,SNAME)
C
  INCLUDE 'ABA_PARAM.INC'
C
  DIMENSION COORDS(3),FLUX(2),TIME(2)
  CHARACTER*80 SNAME
C
! Type declarations
  REAL P
  REAL R
  REAL Q
  REAL V
  REAL X
  REAL Y
  REAL D
  REAL U
C
! Executable statements
  P=600          !LASER POWER [W]s
  R=0.002        !BEAM RADIUS [m][0.004/2]
  Q=0.8*P/(3.14*R*R)      !BODY FLUX [W/m^2]
  V=0.015        !1/60 SCANNING SPEED [m/s] or 1000mm/min
  X=0.050        !STARTING COORDINATE OF THE LASER BEAM
!   Y=0.040      !STARTING COORDINATE OF THE LASER BEAM
!   Z=0
  Y=(0-R)+(V*TIME(1))
  X=COORDS(1)-X
  Y=COORDS(2)-Y
  D=sqrt(X**2+Y**2)
  U=2*Q*exp(-2*(X**2+Y**2)/R**2)  !Actual flux
C
! Heat flux for surface cases
  IF(D.LE.R) THEN
    FLUX(1)=U
    !Flux(1)=2*Q*exp(-D*2/R**2)
  END IF
  FLUX(2)=0
C
  RETURN
END
```

COMPOSITION TEST REPORT OF THE MATERIAL USED

**Stainless Steel Duplex Steel Nickel & Titanium,
Brass Alloys, Carbon Steel, Alloy Steel Etc.**

Room no 30 1st floor Radha krishna society
4th khitwadi lane mumbai 400 004
E-mail : rotanjat91@gmail.com
Mob.: 99679 53013 / 95948 70199



LAXMI
PMI TESTING SERVICE

TEST REPORTS

[illegible]

→ The above test reports relate only to the sample submitted.
→ The above sample is not drawn by the laboratory.

Appendix 4.2

SPECIFICATIONS OF LASER CUTTING MACHINE

Make	: Abro Technologies Pvt. Ltd
Model	: L3015
Working Area	: 1500 × 3000 mm
Axis travel X-axis	: 3000 mm
Axis travel Y-axis	: 1500 mm
Axis travel Z-axis	: 150 mm
Maximum positioning speed of X and Y-axis	: 70 m/min
Maximum positioning speed of Z-axis	: 20 m/min
Positioning Accuracy	: ±0.1 mm/m
Power supply	: 380 V, 50/60 Hz
Laser cutting control Software	: CypOne- 6.1.723
Assisted gas	: Oxygen/Nitrogen/Air

Appendix 4.3

SPECIFICATIONS OF FIBER LASER SOURCE

Make	: Max Photonics
Model	: MFSC-1000W
Type	: Fiber Laser
Capacity	: 1kW
Tuning range of output power	: 10-100%
Wavelength	: 1080±10 nm
Laser switching ON time	: 50-100 μ s
Laser switching OFF time	: 50-100 μ s
Spectrum width	: 3-5 nm
Beam quality (M^2)	: 1.3
Red guide laser power	: 150 μ W
Maximum modulation rate	: 20 kHz
Feeding fiber cable length	: 15 m
Feeding fiber core size	: 50 μ m
Feeding fiber cable bending radius	: 200 mm
Cooling method	: Water cooling

Appendix 4.4

LASER DISPLACEMENT SENSOR SPECIFICATIONS

Make	: ILD1320-50 from Micro-Epsilon
Measuring range	: 50 mm
Start of measuring range	: 35 mm
End of measuring range	: 85 mm
Measuring rate	: 2 kHz
Repeatability	: 5 μ m
Temperature stability	: \pm 0.015 % FSO/ K
Light source	: Semiconductor laser < 1 mW, 670 nm (red)
Laser safety class	: Class 2 in accordance with IEC 60825-1: 2014
Supply voltage	: 11-30 VDC
Power consumption	: < 2 W (24 V)
Signal input input:	: 1 \times HTL laser on/off; 1 \times HTL multifunction trigger in, zero setting, mastering, teach
Digital interface	: RS 422 (16 bit)/ PROFINET/ EtherNet/IP
Analog output measuring	: 4 to 20 mA (12 bit; freely scalable within the range)
Switching output	: 1 \times error output: npn, pnp, push pull
Connection bending	: Integrated cable 3 m, open ends, minimum radius 30 mm (fixed installation)
Mounting	: Screw connection via two mounting holes
Operation temperature range	: 0 to + 50 °C (non-condensing)
Material	: Aluminium housing
Weight (including	: Approx. 30 g (without cable), approx. 145 g cable)

Appendix 4.5

THERMAL IMAGING CAMERA SPECIFICATIONS

Make : FLIR

Model : A315

Imaging and optical data

Field of view (FOV)/ Minimum focus distance : $25^{\circ} \times 18.8^{\circ}$ / 0.4 m (1.31 ft.)

Spatial resolution (IFOV) : 1.36 mrad

Focal length : 18 mm (0.7 in.)

F-number : 1.3

Image frequency : 60 Hz

Lens identification : Automatic

Thermal sensitivity/NETD : $< 0.05^{\circ}\text{C}$ @ $+30^{\circ}\text{C}$ (86°F) / 50 mK

Focus : Automatic or manual (built in motor)

Detector data

Focal plane array (FPA)/ Spectral range : Uncooled microbolometer / 7.5-13 μm

IR resolution : 320×240 pixels

Detector pitch : 25 μm

Detector time constant : Typical 12 ms

Measurement

Object temperature range : -20 to $+120^{\circ}\text{C}$, 0 to 500°C , 0 to 2000°C

Accuracy : $\pm 2^{\circ}\text{C}$ or $\pm 2\%$ of reading

Measurement analysis

Atmospheric transmission correction distance, and relative	: Automatic, based on inputs for atmospheric temperature humidity
Optics transmission correction	: Automatic, based on signals from internal sensors
Emissivity correction	: Variable from 0.01 to 1.0
Reflected apparent temperature correction reflected	: Automatic, based on input of temperature
External optics/windows correction transmission and	: Automatic, based on input of optics/window temperature
Measurement corrections	: Global object parameters
Ethernet	
Ethernet	: Control and image
Ethernet, image streaming	: 16-bit 320 × 240 pixels at 60 Hz,
Signal	linear, Temperature linear,
Radiometric, compatible	GigE Vision and GenICam
Ethernet, standard	: IEEE 802.3
Ethernet, connector type	: RJ-45
Ethernet, type	: Gigabit ethernet
Ethernet, communication proprietary	: TCP/IP socket-based FLIR and GenICam protocol
Ethernet, protocols	: TCP, UDP, SNTP, RTSP, RTP,
HTTP,	ICMP, IGMP, ftp, SMTP,
SMB (CIFS),	DHCP, MDNS (Bonjour),
uPnP	
Digital input/output	
Digital input	: 2 opto-isolated, 10-30 VDC

Digital output, purpose set)	: Output to ext. device (programmatically set)
Digital output mA	: 2 opto-isolated, 10-30 VDC, max 100 mA
Digital I/O, isolation voltage	: 500 VRMS
Digital I/O, supply voltage	: 12/24 VDC, max 200 mA
Digital I/O, connector type	: 6-pole jackable screw terminal
Digital input, purpose flow ctrl.	: Image tag (start, stop, general), Image (Stream on/off), Input ext. device (programmatically read)

Power system

External power operation	: 12/24 VDC, 24 W absolute max
External power, connector type	: 2-pole jackable screw terminal
Voltage	: Allowed range 10-30 VDC

Environmental data

Storage temperature range	: -40°C to +70°C
Humidity (operating and storage) humidity	: IEC 60068-2-30/24 h 95%, relative +25°C to +40°C
EMC	: EN 61000-6-2:2001 (Immunity) EN 61000-6-3:2001 (Emission) FCC 47 CFR Part 15 Class B (Emission)
Vibration	: 2 g (IEC 60068-2-6)

Appendix 4.6

MICROHARDNESS SPECIFICATIONS

Make	: 402 MVD from Wilson
Hardness scales	: Vickers and Knoop
Test load	: 10, 25, 50, 100, 200, 300, 500, 1000, 2000 gf
Test load selection	: Dial
Accuracy	: Conforms to EN-ISO 6507, ASTM E384 and E92
Load control	: Automatic (loading/dwell/unloading)
Load duration (dwell time)	: 5-99 seconds
Turret	: Automatic
Eyepiece magnification	: 10X
Digital encoder resolution	: 0.1 μm
Objectives	: 10X, 40X
Total magnification	: 400X (for measurement)
Measuring range	: 100X (for observation), 200 μm
Optical path	: 2-way switchable- eyepiece/camera
Light filter	: Green and blue
Light source	: Halogen lamp
Display test force	: Length of diagonal, hardness converted value,
Hardness value	: 5-digit
Diagonal length	: 4-digit (D1, D2)
Data output	: Built-in printer, RS232
Statistics	: Number, average, standard deviation, range

Conversion strength	: Brinell, rockwell, superficial rockwell, tensile
Maximum specimen height	: 85 mm (2.55 in)
Depth from the centerline	: 120 mm (3.35 in)
XY-stage dimensions	: 100 × 100 mm
XY-stage travel range	: 25 × 25 mm
Minimum reading	: 0.01 mm
Operating temperature range	: 10° to 38° C
Humidity	: 10% -90% non-condensing
Dimensions	: 513 × 320 × 470 mm
Weight	: 36 kg
Power supply	: 110-220 V AC, 60/50 Hz

Appendix 4.7

AUTOLAB WORKSTATION SPECIFICATIONS

Make	: Multi Autolab/M204
Electrode connections	: 2,3, and 4
Potential range	: +/- 10 V
Compliance voltage	: +/- 20 V
Maximum current	: +/- 400 mA
Current ranges	: 100 mA to 10 nA
Potential accuracy	: +/- 0.2%
Potential resolution	: 3 μ V
Current accuracy	: +/- 0.2%
Current resolution	: 0.0003 % (of current range)
Input impedance	: > 100GOhm
Potentiostat bandwidth	: 1 MHz
Computer interface	: USB
Control software	: NOVA

Appendix 4.8

OPTICAL MICROSCOPE SPECIFICATIONS

Make	: Inverted metallurgical microscope GX53 from Olympus
Optical system	: UIS2 optical system (infinity-corrected)
Reflected light illumination unit	: Manual brightfield/darkfield selection by mirror unit
Light source 100 W source	: White LED (with light intensity manager)/ 12 V, halogen lamp/ 100 W mercury lamp/light guide
Observation mode contrast,	: brightfield, darkfield, differential interface simple polarizing, mix observation
Imprinting of scale observation	: All ports reversed positions (up/down) from positions seen through the eyepiece
Electrical system	: Built-in LED power supply for reflected light illumination
Focus	: Rack and pinion with roller guide
Focus stroke surface)	: 9 mm (2 mm above and 7 mm below the stage surface)
Fine handle stroke per rotation	: 100 μm (minimum scale: 1 μm)
Coarse handle stroke per rotation	: 7 mm
Tubes U- binocular (U-	: Widefield (FN 22), Inverted- binocular (U-BI90, BI90CT), trinocular (U-TR30H-2), tilting TBI90)
Stage for GX	: X/Y stroke- 50 \times 50 mm, max. load 5 kg
Weight	: Approx. 25 kg (microscope frame 20 kg)

Appendix 4.9

SCANNING ELECTRON MICROSCOPE SPECIFICATIONS

Make	: JSM-6610LV from JEOL
Resolution HV mode	: 3 nm (30 kV), 8 nm (3 kV), 15 nm (1 kV)
LV mode	: 4 nm (30 kV)
Magnification size)	: $\times 5$ to $\times 300000$ (on 128 mm \times 96 mm image
Preset magnifications	: 5 step, user selectable
Standard recipe	: Built in
Custom recipe pressure)	: Operation conditions (optics, image mode, LV specimen stage
Image mode Composition,	: Secondary electron image, REF image, Topography, Shadowed
Accelerating voltage	: 0.3 kV to 30 kV
Filament	: Factory pre-centered filament
Electron gun	: Fully automated, manual override
Condenser lens	: Zoom condenser lens
Objective lens	: Super conical objective lens
Objective lens apertures	: 3 stages, XY fine adjustable
Stigmator memory	: Built in
Electrical image shift	: $\pm 50 \mu\text{m}$ (WD = 10 mm)
Auto functions	: Focus, brightness, contrast, stigmator
Specimen stage	: Eucentric large-specimen stage axes motorized-
X: 125 -10° to 90°,	mm, Y: 100 mm, Z: 5 mm to 80 mm, Tilt: Rotation: 360°

Reference image (Navigator)	: 4 images
Specimen exchange	: Draw out the stage
Maximum specimen	: 200 mm diameter
Measurement	: Built in
Image format	: bmp, tiff, jpeg
Auto image archiving	: Built in
Pumping system	: Fully automated, DP: 1, RP: 1 or 2
Switching vacuum mode	: Through the menu, less than 1 minute
LV Pressure	: 10 to 270 Pa
JED-2300 EDS	: Built in

Appendix 4.10

X-RAY DIFFRACTION SPECIFICATIONS

Make	: X'Pert PRO from PANalytical
X-Ray source	: Cu K α radiation (K α = 1.54187 Å)
Goniometer radius	: 240 mm
Geometry (goniometer)	: Bragg-Brentano (θ - θ system, vertical)
Scan range of 2θ	: 3°-150°
Minimum-Maximum step size	: 0.001°-1.27°
Divergence slits	: 1/2° to 1/32°
Automatic sample changer	: 15 samples
Incident PreFIX Module mirror for	: Fixed divergence slit holder, Focussing X-Ray Cu K α
Diffracted PreFIX Module	: X'Celerator lineal detector
Available software	: X'pert data collector, X'pert data viewer, X'pert highscore

